

University of Alberta

Structural and Inhibitory Studies of LL-Diaminopimelate Aminotransferase and Investigation of Methods for Small Peptide Crystallization

by

Chenguang Fan

A thesis submitted to the Faculty of Graduate Studies and Research
in partial fulfillment of the requirements for the degree of

Doctor of Philosophy

Department of Chemistry

©Chenguang Fan
Fall, 2012
Edmonton, Alberta

Permission is hereby granted to the University of Alberta Libraries to reproduce single copies of this thesis and to lend or sell such copies for private, scholarly or scientific research purposes only. Where the thesis is converted to, or otherwise made available in digital form, the University of Alberta will advise potential users of the thesis of these terms.

The author reserves all other publication and other rights in association with the copyright in the thesis and, except as herein before provided, neither the thesis nor any substantial portion thereof may be printed or otherwise reproduced in any material form whatsoever without the author's prior written permission.

Abstract

The pyridoxal-5'-phosphate (PLP)-dependent enzyme LL-diaminopimelate aminotransferase (LL-DAP-AT) catalyzes a key step in the biosynthesis of L-lysine in plants and *Chlamydia*. In this thesis, studies of mechanistic and inhibitory aspects of LL-DAP-AT are described.

Two LL-DAP-ATs from *Arabidopsis thaliana* and *Chlamydia trachomatis* were studied using X-ray crystallography. Furthermore, synthetic analogues of PLP-glutamate adduct **87**, PLP-LL-diaminopimelate adduct **89**, and pyridoxamine-5'-phosphate-tetrahydrodipicolinate (THDP) adduct **91** were co-crystallized with LL-DAP-AT. It was found that the hydrolysis product of THDP is the true substrate for this enzymatic transamination reaction. Crystallographic studies provide insights regarding the broader substrate specificity of *Chlamydia* LL-DAP-AT compared to the *Arabidopsis* enzyme.

Since mammals require lysine from their diet, specific inhibitors of LL-DAP-AT could potentially serve as non-toxic antibiotics. A high-throughput screening study has been performed on a 29,201-compound library. *N*-(3-(Hydrazinecarbonyl)naphthalen-2-yl)benzenesulfonamide (**122**) was identified as the best hit ($IC_{50} \sim 5 \mu M$). In addition, three potential pharmacophores (derivatives of rhodanine, barbiturate, and thiobarbiturate) were identified. Structure-activity relationship (SAR) studies were conducted based on lead compound **122** and rhodanine derivatives. *N*-(5-Fluoro-2-(hydrazinecarbonyl)phenyl)benzenesulfonamide (**155**) was identified as a two-fold better inhibitor compared to the lead compound. It was found that a free

hydrazide and a phenylsulfonamide were essential for inhibition. These two moieties needed to be attached to an aryl system, but further substitution of the aryl group was tolerated. These results may provide insight for future inhibitor design.

In the second portion of this thesis, efforts toward development of methods for small peptide (< 5 kDa) crystallization are described. A co-crystallization approach was investigated, which involves linking a small peptide to a small molecule inhibitor to a readily crystallizable enzyme. Upon mixing, the small peptide may be co-crystallized with the enzyme. Subtilisin A (SubA, **191**), a 35-amino acid circular bacteriocin, was selected for this co-crystallization study. Two bioconjugates, *N*-acetyl glucosamine (GlcNAc)-SubA and *N,N,N'*-triacetylchitotriose ((GlcNAc)₃)-SubA, were prepared toward co-crystallization with lysozyme. A bioconjugate of arylsulfonamide-SubA was also synthesized for co-crystallization with carbonic anhydrase II (CAII). Current attempts towards co-crystallization were unsuccessful, likely due to the poor solubility of these bioconjugates. Efforts are underway towards co-crystallization by potentially improving the solubility of the bioconjugates.

Acknowledgements

I would like first thank my supervisor, Professor. John C. Vederas, for his continuous guidance, encouragement, and support throughout my PhD studies. As an excellent teacher and mentor, he has provided a stimulating learning environment. I have been really inspired by his enthusiastic and rigorous attitude towards science. I am grateful for working in such an influential and inspiring research group. It has been a pleasurable experience to work with everyone in the Vederas group, both past and current members; I have learned a lot from all of them. All of these people truly helped me to grow as a better scientist and a better individual.

I would like to thank Dr. David Dietrich and Dr. Jennifer Chaytor for proofreading my thesis, and providing very useful suggestions regarding various research topics. I would also like to thank Christopher Lohans and Shaun McKinnie for proofreading parts of this thesis. Improvements were made based on their help and suggestions.

I especially want to thank Dr. Marco van Belkum and Dr. Matthew Clay for the assistance on my research project. I have learned a lot of biological knowledge and techniques from them.

I would like to thank my collaborators, Dr. Michael James, Dr. M. Joanne Lemieux, Dr. Cory Brooks, Dr. Nobuhiko Watanabe, and Dr. Michael K. Deyholos. Their excellent collaboration and support provided enormous impact on my research projects.

The Department of Chemistry at the University of Alberta has excellent support from all of its service labs. I would like to thank all the support staff from the NMR Facility, Mass Spectrometry Laboratory, Analytical and Instrumental Laboratory and X-ray crystallography facility. Dr. Randy Whittal, Dr. Angie Morales-Izquierdo, Jing Zheng, and Mark Miskolzie provided tremendous help.

Last but not least, the support from all my family and friends carried me through the years of my graduate studies. Especially, I am grateful to my wife and parents, without whose understanding and support this thesis would not have taken shape. Thanks to all of you for always believing in me and helping me realize my goals.

Table of Contents

Chapter 1. Structural and inhibitory studies of LL-diaminopimelate aminotrasferase	1
1.1 Introduction	1
1.1.1 An overview of lysine biosynthesis	1
1.1.1.1 α-Aminoadipic acid (AAA) pathway	1
1.1.1.2 Diaminopimelate (DAP) pathway.....	5
1.1.2 Discovery of LL-DAP-AT	9
1.1.3 Inhibitory studies of DAP pathways	12
1.1.3.1 Potential target for the development of new antibiotics.....	12
1.1.3.2 Recent inhibitory studies of DAP enzymes.....	14
1.1.3.2.1 Inhibitory studies on DHDP synthase.....	14
1.1.3.2.2 Inhibitory studies on DHDP reductase	17
1.1.3.2.3 THDP <i>N</i>-acyltransferase, <i>N</i>-acyl-LL-DAP aminotransferase, and <i>N</i>-acyl-LL-DAP deacylase.....	19
1.1.3.2.4 Inhibitory studies of DAP epimerase	23
1.1.3.2.5 Inhibitory studies of <i>meso</i>-DAP D-dehydrogenase.....	26
1.1.3.2.6 Inhibitory studies of <i>meso</i>-DAP decarboxylase.....	28
1.1.3.3 LL-DAP-AT as a target for potential antibiotics or herbicides	29
1.2 Project objectives	31
1.3 Results and discussion	32
1.3.1 Expression and purification of LL-DAP-AT	32
1.3.2 X-ray crystallographic studies on LL-DAP-AT	32

1.3.2.1 First crystal structure of LL-DAP-AT from <i>Arabidopsis thaliana</i>.....	32
1.3.2.2 Mechanism of catalysis of LL-DAP-AT from <i>A. thaliana</i>.....	36
1.3.2.2.1 Crystallographic study of the PLP-Glu analogue bound enzyme.....	39
1.3.2.2.2 Crystallographic studies of LL-DAP-AT bound to the PLP-DAP analogue	42
1.3.2.2.3 Crystallographic studies of mutant enzymes (K270N and K270Q).....	44
1.3.2.3 X-ray crystallographic study of LL-DAP-AT from <i>Chlamydia trachomatis</i>	46
1.3.3 High-throughput screening of a 29,201 compound library against LL-DAP-AT.....	52
1.3.4 SAR studies on the lead compounds	58
1.3.4.1 Aryl-hydrazide derivatives as inhibitors of LL-DAP-AT	58
1.3.4.1.1 Modifications of hydrazide moiety of the lead arylhydrazide.....	59
1.3.4.1.2 Modifications of the naphthalene moiety of the lead arylhydrazide.....	60
1.3.4.1.3 Modifications of the phenylsulfonamide moiety of the lead arylhydrazide.....	63
1.3.4.1.4 Preliminary study on the mode of action of the aryl-hydrazide derivatives as inhibitors to LL-DAP-AT	65

1.3.4.2 Rhodanine derivatives as inhibitors of LL-DAP-AT	67
1.3.4.2.1 Inhibitory studies of rhodanine-based analogues against LL-DAP-AT.....	69
1.3.4.2.2 <i>N</i> -Ethyl-rhodanine-based analogues	70
1.3.4.2.3 <i>N</i> -Amino-rhodanine-based analogues	71
1.3.4.2.4 <i>N</i> -Aminoacetyl-rhodanine based analogues	72
1.3.4.2.5 Overall analysis of the SAR studies based on rhodanine- based analogues.....	73
1.4 Conclusion and future direction.....	74
 Chapter 2. Investigation of methods for crystallization of small peptides	77
2.1 Introduction	77
2.1.1 Potential approaches for crystallization of small peptides.....	77
2.1.1.1 Racemic peptide crystallization	77
2.1.1.2 Co-crystallization method for protein crystallization	78
2.1.2 Subtilisin A (SubA) as a target for development of method for crystallization of small peptides.....	81
2.1.2.1 Subtilisin A as a bacteriocin.....	81
2.1.2.2 General background of bacteriocin.....	82
2.1.2.2.1 Classification of bacteriocins	82
2.1.2.2.2 Application of bacteriocins as antibiotics and food preservative	83

2.1.2.3 Structure elucidation of Subtilisin A.....	84
2.2 Project goal.....	89
2.3 Results and discussion	90
2.3.1 Glucosamine and chitotriose as lysozyme inhibitors	90
2.3.1.1 Previous crystallographic studies on lysozyme	90
2.3.1.2 Bioconjugation of <i>N</i> -acetylglucosamine to SubA.....	93
2.3.1.2.1 Squarate as linker in the bioconjugation of <i>N</i> - acetylglucosamine to SubA.....	94
2.3.1.2.2 Preparation of bioconjugate of <i>N</i> -acetylglucosamine-SubA via click chemistry.....	96
2.3.1.3 Bioconjugate of <i>N,N',N''</i> -triacetylchitotriose (GlcNAc) ₃ -SubA	104
2.3.2 Benzenesulfonamide-SubA bioconjugates as inhibitors of carbonic anhydrase II (CAII).	106
2.3.2.1 Click chemistry as a linking approach between benzenesulfonamide and SubA.....	106
2.3.2.1.1 Copper (I) catalyzed click chemistry between benzenesulfonamide and SubA.....	106
2.3.2.1.2 Copper-free click chemistry between benzenesulfonamide and SubA	107
2.3.2.2 Ureido-containing arylsulfonamide coupled SubA bioconjugate	113

2.3.2.2.1 Literature precedent for ureido-containing arylsulfonamide inhibitors to CAII.....	113
2.3.2.2.2 Synthesis of the ureido-containing arylsulfonamide compounds.....	115
2.3.2.2.3 Inhibitory activity testing of ureido-containing benzenesulfonamide inhibitors against CAII.....	117
2.3.2.2.4 Coupling between the ureido-containing benzenesulfonamide and SubA.....	118
2.4 Conclusion and future directions	119
Chapter 3. Experimental Procedures.....	121
3.1 General Information.....	121
3.1.1 Reagents, solvents and purifications	121
3.1.2 Characterization	123
3.2 Substrate mimic 88 and 90 into LL-DAP-AT	125
3.2.1 Synthesis of substrate-PLP imine adduct mimic.....	125
(<i>S</i>)-2-((3-Hydroxy-2-methyl-5-(phosphonooxymethyl)pyridin-4-yl)methylamino)pentanedioic acid (88).....	125
(2 <i>S</i> ,6 <i>S</i>)-2-Amino-6-(2-hydroxy-3-methyl-6-(phosphonooxymethyl)benzylamino)heptanedioic acid (90)	126
3.2.2 Incorporation of PLP-Glu and PLP-DAP into LL-DAP-AT	127
3.3 General procedure for high-throughput screening of LL-DAP-AT inhibitors.....	128

3.4 General procedure for determination of IC₅₀ values of inhibitors of LL-DAP-AT	130
3.5 General procedure for time dependence testing of inhibitors of LL-DAP-AT	131
3.6 Sulfonamido-arylhydrazide derived inhibitors of LL-DAP-AT	132
3.6.1 Preparation of the hydrazide-modified analogues (144 and 147)	132
3-(Phenylsulfonamido)-2-naphthoic acid (141).....	132
3-(Phenylsulfonamido)- <i>N</i> -(piperidin-1-yl)-2-naphthamide (144)	133
<i>N</i> -(3-(2-Acetylhydrazinecarbonyl)naphthalen-2-yl)benzenesulfonamide (147).....	134
3.6.2 Preparation of naphthalene and sulfonamide modified sulfonamide-arylhydrazide analogues	135
3.6.2.1 General procedure for synthesis of sulfonamide - carboxylic acid intermediate (148a-163a).....	135
3.6.2.2 General procedure for synthesis of naphthalene and sulfonamide modified sulfonamide – hydrazide analogues (148b-163b) using sulfonamide – carboxylic acid intermediate.....	136
3.6.2.3 Characterization data of sulfonamide – carboxylic acid intermediates and sulfonamide – hydrazide analogues.....	136
3-(Phenylsulfonamido)propanoic acid (148a)	137
<i>N</i> -(3-Hydrazinyl-3-oxopropyl)benzenesulfonamide (148b).....	137
(<i>S</i>)-1-(Phenylsulfonyl)pyrrolidine-2-carbohydrazide (149b)	138
(<i>R</i>)-1-(Phenylsulfonyl)pyrrolidine-2-carbohydrazide (150b).....	138

2-(Phenylsulfonamido)benzoic acid (151a) ¹⁸⁶	139
<i>N</i> -(2-(Hydrazinecarbonyl)phenyl)benzenesulfonamide (151b).....	139
4-Chloro-2-(phenylsulfonamido)benzoic acid (152a)	140
<i>N</i> -(5-Chloro-2-(hydrazinecarbonyl)phenyl)benzenesulfonamide (152b)	140
4-Methoxy-2-(phenylsulfonamido)benzoic acid (153a).....	141
<i>N</i> -(2-(Hydrazinecarbonyl)-5-methoxyphenyl)benzenesulfonamide (153b).....	142
4,5-Dimethoxy-2-(phenylsulfonamido)benzoic acid (154a)	142
<i>N</i> -(2-(Hydrazinecarbonyl)-4,5-dimethoxyphenyl)benzenesulfonamide (154b).....	143
4-Fluoro-2-(phenylsulfonamido)benzoic acid (155a) ¹⁸⁷	144
<i>N</i> -(5-Fluoro-2-(hydrazinecarbonyl)phenyl)benzenesulfonamide (155b)	144
4,5-Difluoro-2-(phenylsulfonamido)benzoic acid (156a)	145
<i>N</i> -(4,5-Difluoro-2-(hydrazinecarbonyl)phenyl)benzenesulfonamide (156b).....	146
4-Methyl-2-(phenylsulfonamido)benzoic acid (157a).....	146
<i>N</i> -(2-(Hydrazinecarbonyl)-5-methylphenyl)benzenesulfonamide (157b)	147
2-(Phenylsulfonamido)-4-(trifluoromethyl)benzoic acid (158a) ¹⁸⁸	148
<i>N</i> -(2-(Hydrazinecarbonyl)-5-(trifluoromethyl)phenyl)benzenesulfonamide (158b)	149

2-(4-Chlorophenylsulfonamido)-4-fluorobenzoic acid (159a)	150
4-Chloro- <i>N</i> -(5-fluoro-2-(hydrazinecarbonyl)phenyl)benzenesulfonamide (159b)	151
4-Fluoro-2-(4-methoxyphenylsulfonamido)benzoic acid (160a)	152
<i>N</i> -(5-Fluoro-2-(hydrazinecarbonyl)phenyl)-4-methoxybenzenesulfonamide (160b)	153
4-Fluoro-2-(4-fluorophenylsulfonamido)benzoic acid (161a)	154
4-Fluoro- <i>N</i> -(5-fluoro-2-(hydrazinecarbonyl)phenyl)benzenesulfonamide (161b)	155
4-Fluoro-2-(4-methylphenylsulfonamido)benzoic acid (162a) ¹⁸⁹	156
<i>N</i> -(5-Fluoro-2-(hydrazinecarbonyl)phenyl)-4-methylbenzenesulfonamide (162b)	157
4-Fluoro-2-(methylsulfonamido)benzoic acid (163a)	158
<i>N</i> -(5-Fluoro-2-(hydrazinecarbonyl)phenyl)methanesulfonamide (163b)	158
(<i>E</i>)-4-((2-(4-Fluoro-2-(phenylsulfonamido)benzoyl)hydrazono)methyl)-5-hydroxy-6-methylpyridin-3-yl)methyl dihydrogen phosphate (164)	159

3.7 Synthesis of Rhodanine derived inhibitors of LL-DAP-AT 160

3.7.1 General procedure for synthesis of rhodanine-based analogues

(170-190)..... 160

3.7.2 Characterization data for rhodanine-based analogues 161

(*Z*)-5-Benzylidene-2-thioxothiazolidin-4-one (170)^{191, 192} 161

(Z)-5-(4-Chlorobenzylidene)-2-thioxothiazolidin-4-one (171) ¹⁹¹	161
(Z)-5-(4-(Dimethylamino)benzylidene)-2-thioxothiazolidin-4-one (172) ¹⁹¹	162
(Z)-5-(4-Methoxybenzylidene)-2-thioxothiazolidin-4-one (173) ¹⁹¹ ...	162
(Z)-5-(Naphthalen-1-ylmethylene)-2-thioxothiazolidin-4-one (174) ¹⁹²	163
(Z)-5-(2-Nitrobenzylidene)-2-thioxothiazolidin-4-one (175) ¹⁹³	163
(Z)-5-(2-Hydroxybenzylidene)-2-thioxothiazolidin-4-one (176) ¹⁹¹ ...	164
(Z)-5-Benzylidene-3-ethyl-2-thioxothiazolidin-4-one (177) ¹⁹⁴	164
(Z)-3-Ethyl-5-(2-hydroxybenzylidene)-2-thioxothiazolidin-4-one (178)	165
(Z)-3-Ethyl-5-(4-methoxybenzylidene)-2-thioxothiazolidin-4-one (179) ¹⁹⁴	165
(Z)-5-(4-Chlorobenzylidene)-3-ethyl-2-thioxothiazolidin-4-one (180) ¹⁹⁵	166
(Z)-3-Ethyl-5-(naphthalen-1-ylmethylene)-2-thioxothiazolidin-4-one (181) ¹⁹⁶	167
(Z)-3-Ethyl-5-(quinolin-5-ylmethylene)-2-thioxothiazolidin-4-one (182) ¹⁹⁷	167
(Z)-3-Amino-5-benzylidene-2-thioxothiazolidin-4-one (183) ¹⁹⁸	168
(Z)-3-Amino-5-(4-methoxybenzylidene)-2-thioxothiazolidin-4-one (184) ¹⁹⁵	168

(<i>Z</i>)-3-Amino-5-(4-chlorobenzylidene)-2-thioxothiazolidin-4-one (185) ¹⁹⁵	169
(<i>Z</i>)- <i>N</i> -(5-Benzylidene-4-oxo-2-thioxothiazolidin-3-yl)acetamide (186) ¹⁹⁹	169
(<i>Z</i>)- <i>N</i> -(5-(4-Methoxybenzylidene)-4-oxo-2-thioxothiazolidin-3-yl)acetamide (187)	170
(<i>Z</i>)- <i>N</i> -(5-(4-Chlorobenzylidene)-4-oxo-2-thioxothiazolidin-3-yl)acetamide (188)	171
(<i>Z</i>)- <i>N</i> -(5-((5-(4-Nitrophenyl)furan-2-yl)methylene)-4-oxo-2-thioxothiazolidin-3-yl) acetamide (189)	172

3.8 Preparation of glucosamine linked to SubA..... 173

3.8.1 Using squarate as the linker..... 173

<i>tert</i> -Butyl 2,2'-disulfanediybis(ethane-2,1-diyl)dicarbamate (203) ²⁰⁰	173
(1 <i>S</i> ,2 <i>R</i> ,3 <i>R</i> ,4 <i>S</i> ,5 <i>R</i>)-2-Acetamido-5-(acetoxymethyl)-1-(2-(<i>tert</i> -butoxycarbonylamino)ethylthio)tetrahydro-2 <i>H</i> -pyran-3,4-diyl diacetate (206)	173
(1 <i>S</i> ,2 <i>R</i> ,3 <i>R</i> ,4 <i>S</i> ,5 <i>R</i>)-2-Acetamido-5-(acetoxymethyl)-1-(2-(2-methoxy-3,4-dioxocyclobut-1-enylamino)ethylthio)tetrahydro-2 <i>H</i> -pyran-3,4-diyl diacetate and (6 <i>S</i> ,2 <i>R</i> ,3 <i>R</i> ,4 <i>S</i> ,5 <i>R</i>)-2-acetamido-5-(acetoxymethyl)-1-(2-((<i>Z</i>)-3-hydroxy-2-methoxy-4-oxocyclobut-2-enylideneamino)ethylthio)tetrahydro-2 <i>H</i> -pyran-3,4-diyl diacetate (208)	175

<i>N</i> -((1 <i>S</i> ,2 <i>R</i> ,3 <i>R</i> ,4 <i>S</i> ,5 <i>R</i>)-3,4-Dihydroxy-5-(hydroxymethyl)-1-(2-(2-methoxy-3,4-dioxocyclobut-1-enylamino)ethylthio)tetrahydro-2 <i>H</i> -pyran-2-yl)acetamide (209)	176
3.8.2 Click chemistry used in linking glucosamine and SubA	177
(1 <i>R</i> ,2 <i>R</i> ,3 <i>R</i> ,4 <i>S</i> ,5 <i>R</i>)-2-Acetamido-5-(acetoxymethyl)-1-azidotetrahydro-2 <i>H</i> -pyran-3,4-diyl diacetate (210) ²⁰¹	177
4-(1-((2 <i>R</i> ,3 <i>R</i> ,4 <i>R</i> ,5 <i>S</i> ,6 <i>R</i>)-3-Acetamido-4,5-diacetoxy-6-(acetoxymethyl)tetrahydro-2 <i>H</i> -pyran-2-yl)-1 <i>H</i> -1,2,3-triazol-4-yl)butanoic acid (212)	178
Subtilisin A-lysine- ϵ -amido-5-hexyne (215)	179
Alkynyl-SubA digestion product (216 & 217) using endoproteinase Asp-N	181
MS/MS analysis of alkynyl-SubA digestion product (218)	182
<i>N</i> -((1 <i>R</i> ,2 <i>R</i> ,3 <i>R</i> ,4 <i>S</i> ,5 <i>R</i>)-1-azido-3,4-dihydroxy-5-(hydroxymethyl)tetrahydro-2 <i>H</i> -pyran-2-yl)acetamide (219) ²⁰¹	183
GlcNAc – SubA click chemistry adduct (220)	184
3.9 Click chemistry used in linking chitotriose to SubA	185
<i>N</i> -((2 <i>S</i> ,3 <i>R</i> ,5 <i>S</i> ,6 <i>R</i>)-5-((2 <i>S</i> ,3 <i>R</i> ,4 <i>R</i> ,5 <i>S</i> ,6 <i>R</i>)-3-Acetamido-4,5-dihydroxy-6-(hydroxymethyl)tetrahydro-2 <i>H</i> -pyran-2-yloxy)-2-((2 <i>R</i> ,3 <i>S</i> ,5 <i>R</i> ,6 <i>R</i>)-5-acetamido-6-azido-4-hydroxy-2-(hydroxymethyl)tetrahydro-2 <i>H</i> -pyran-3-yloxy)-4-hydroxy-6-(hydroxymethyl)tetrahydro-2 <i>H</i> -pyran-3-yl)acetamide (224) ¹⁷⁷	185
(GlcNAc) ₃ – SubA click chemistry adduct (225)	186

3.10 Linking benzenesulfonamides to SubA as CAII inhibitors	187
3.10.1 Purification of CAII.....	187
3.10.2 Inhibitor testing against CAII	191
3.10.3 Benzenesulfonamide derivatives – SubA linkage.....	192
Imidazole-1-sulfonyl azide (226) ¹⁷⁸	192
4-(2-Azidoethyl)benzenesulfonamide (227) ¹³³	193
1-Fluorocyclooct-2-ynecarboxylic acid (231) ¹⁸¹	194
Ethyl 2-oxocyclooctanecarboxylate and (<i>Z</i>)-ethyl 2-hydroxycyclooct-1-enecarboxylate (234 and 235) ²⁰²	195
Ethyl 1-fluoro-2-oxocyclooctanecarboxylate (237) ¹⁸¹	196
Ethyl 1-fluorocyclooct-2-ynecarboxylate (238) ¹⁸¹	197
Ethyl 9-fluoro-1-(4-sulfamoylphenethyl)-4,5,6,7,8,9-hexahydro-1 <i>H</i> -cycloocta- [<i>d</i>][1,2,3]triazole-9-carboxylate (239).....	198
Ethyl 4-fluoro-1-(4-sulfamoylphenethyl)-4,5,6,7,8,9-hexahydro-1 <i>H</i> -cycloocta- [<i>d</i>][1,2,3]triazole-4-carboxylate (240).....	199
3-methyl-4-(3-(4-sulfamoylphenyl)ureido)benzoic acid (243).....	200
Ethyl 4-(3-(4-sulfamoylphenyl)ureido)benzoate (246) ^{185, 203}	201
Ethyl 4-amino-3-methylbenzoate (248) ²⁰⁴	201
Ethyl 3-methyl-4-(3-(4-sulfamoylphenyl)ureido)benzoate (250) ^{185, 203, 205}	202
Ureido-containing sulfonamide 243– SubA coupling adduct (251)...	204

Appendix: X-ray crystal structure of compound 239 ... 205

References..... 219

List of Figures

Figure 1-1. The first steps in the AAA pathway for the formation of α -aminoadipic acid. i) Homocitrate synthase; ii) Homoaconitase; iii) Homoaconitase; iv) Homoisocitrate dehydrogenase; v) L- α -Aminoadipate aminotransferase	2
Figure 1-2. Second half of fungal AAA pathway. i) L- α -Aminoadipate semialdehyde dehydrogenase; ii) L- α -Aminoadipate semialdehyde dehydrogenase; iii) Saccharopine reductase; iv) Saccharopine reductase; v) Saccharopine dehydrogenase	3
Figure 1-3. A variant of the second half of putative AAA pathway from <i>T. thermophilus</i> . i) LysX; ii) LysZ; iii) LysY; iv) LysJ; v) LysK.....	5
Figure 1-4. The most common bacterial DAP pathway. i) DHDP synthase; ii) DHDP reductase; iii) THDP acyltransferase; iv) <i>N</i> -acyl-DAP aminotransferase; v) <i>N</i> -acyl-DAP deacylase; vi) DAP epimerase; vii) DAP decarboxylase.....	7
Figure 1-5. The <i>meso</i> -DAP formation in <i>B. sphaericus</i> catalyzed by <i>meso</i> -DAP D-dehydrogenase (coloured in blue)	8
Figure 1-6. LL-DAP-AT-catalyzed transamination (coloured in blue) to form LL-DAP	9
Figure 1-7. Catalytic mechanism of DHDP synthase	15
Figure 1-8. Analogues of HTHDP and their ability to inhibit DHDP synthase...	16
Figure 1-9. 4-Oxo-heptenedioic acid derivatives and the proposed mode of inhibition of DHDP synthase	17

Figure 1-10. DHDP reductase-catalyzed dehydration and reduction to form L-THDP	17
Figure 1-11. Inhibitors of DHDP reductase developed by the Merck research laboratory ⁶⁷	18
Figure 1-12. Inhibitors of DHDP reductase optimized by bi-ligand approach....	19
Figure 1-13. The three enzymatic steps convert L-THDP to LL-DAP that catalyzed by THDP <i>N</i> -acyltransferase, <i>N</i> -acyl-LL-DAP aminotransferase, and <i>N</i> -acyl-LL-DAP deacylase	20
Figure 1-14. a) Inhibitor 47 of THDP <i>N</i> -succinyltransferase. b) Mechanism of THDP <i>N</i> -succinyltransferase	21
Figure 1-15. Studies on <i>N</i> -succinyl DAP aminotransferase. a) Compounds used in substrate specificity study; b) Substrate analogues as inhibitors; c) A separate inhibitory study	22
Figure 1-16. Inhibitors of <i>N</i> -succinyl DAP desuccinylase	23
Figure 1-17. Proposed transition state of DAP epimerase-catalyzed step	24
Figure 1-18. The irreversible inhibitors of DAP epimerase. a) Design of initial inhibitor 64 ; b) Mode of action of pure stereoisomeric inhibitors 65 and 66	25
Figure 1-19. 3-substituted analogues of DAP studied by Gelb <i>et al.</i> ⁹¹ as inhibitors of DAP epimerase	26
Figure 1-20. Inhibitors of <i>meso</i> -DAP D-dehydrogenase and their measured K_i values	27
Figure 1-21. Inhibitors of <i>meso</i> -DAP decarboxylase.....	29
Figure 1-22. The enzymatic assay used in the inhibitory study of LL-DAP-AT ²⁴	31

Figure 1-23. Overall structure of the LL-DAP-AT homodimer in a cartoon representation. Subunit A is labelled in blue and B is labelled in yellow. PLP, sulfate, and glycerol are shown in stick form ⁴⁰	34
Figure 1-24. The stereo diagram of PLP binding site of LL-DAP-AT. The active site residues' side chains, PLP, and a sulfate ion are shown in stick form, the residues coloured in grey are from the neighbouring subunit, the red spheres represent water molecules, and the hydrogen bonds are shown as yellow dotted lines. This picture was adopted from Watanabe <i>et al.</i> ⁴⁰	35
Figure 1-25. Typical proposed mechanism of PLP-dependent transamination reactions	37
Figure 1-26. a) Substrate-PLP adducts; b) Analogues of substrate-PLP adducts	38
Figure 1-27. The stereo diagram of the structures of the PLP-Glu analogue bound to LL-DAP-AT. a) Active site residues and analogue 88 are shown in stick form. Residues from subunit A and B, and analogue 88 are coloured in green, grey, and yellow, respectively. b) Overlaid structure, residues from the native enzyme and the enzyme bound to the PLP-Glu analogue are coloured in yellow and light blue, respectively ¹¹²	41
Figure 1-28. The stereo diagram of the structure of the PLP-DAP analogue bound to LL-DAP-AT. a) Active site residues and the PLP-DAP analogue are shown in stick form. Residues from subunit A, B, and the analogue are coloured green, grey, and yellow, respectively. b) Overlaid structure; residues from native enzyme, PLP-Glu analogue, and PLP-DAP bound	

enzymes are coloured in yellow, light blue, and emerald green,
respectively¹¹² 43

Figure 1-29. K270N mutant of LL-DAP-AT complexed with Glu (left) and LL-DAP (right). a) Active site structure of K270N complexed to Glu (left) and LL-DAP (right); b) Structures of the true external aldimines 45

Figure 1-30. Stereo diagram of apo-LL-DAP-AT from *Chlamydia trachomatis*. The large domains (LDs) of each subunit are coloured blue and yellow, and the small domains (SDs) are coloured grey and green⁴³ 47

Figure 1-31. Stereo diagram of the structure of the PLP binding site of *Chlamydia* LL-DAP-AT⁴³ 48

Figure 1-32. The domain alignment structures between *Chlamydia* and *Arabidopsis* LL-DAP-AT. a) Superposition of the large domains (LDs) (*Chlamydia* enzyme in orange; *Arabidopsis* enzyme in grey); b) Superposition of the small domains (SDs) (*Chlamydia* enzyme in orange; *Arabidopsis* enzyme in grey). The flexible loops (A, B, and C) of *Chlamydia* LL-DAP-AT are coloured magenta⁴³ 49

Figure 1-33. The superposition of the structures of LL-DAP-AT from *C. trachomatis* and *A. thaliana*. a) Displacement of the SD (9.5 Å) of LL-DAP-AT from *C. trachomatis* is indicated by the black arrow. The LDs of the *Chlamydia* and *Arabidopsis* enzymes are coloured gray and orange, respectively. The SDs of the *Chlamydia* and *Arabidopsis* enzymes are coloured magenta and green, respectively. b) The overlaid active site structures of *Chlamydia* (green) and *Arabidopsis* (yellow) enzymes. Residue

names in brackets are from *Arabidopsis* LL-DAP-AT. Residues from loops A and B of the *Chlamydia* enzyme are not shown, as they are disordered⁴³ 51

Figure 1-34. The three potential pharmacophore structures identified from the HTS..... 57

Figure 2-1. D- and L-BmBKTx1 were crystallization by racemic crystallization¹²⁶ 78

Figure 2-2. The extracellular domains of interleukin-1 receptor type 1 (IL-1R1, in green, blue, and orange) bound to an IL-1 antagonist peptide (AF10847, in red).¹³¹ PDB code: 1G0Y 79

Figure 2-3. ¹²⁹Xe-cryptophane biosensor (**190**) complexed with CAII. The Xe-cryptophane complex is shown on the left, and the co-crystal structure is shown on the right¹³³ 80

Figure 2-4. Amino acid sequence of subtilisin A showing the three crosslinking thioether bridges..... 81

Figure 2-5. Model compounds for the fully substituted phenylalanine and threonine to confirm sulfur-carbon linkage of SubA 86

Figure 2-6. a) Desulfurization using nickel boride reduction. b) Conversion between free amino acid to the corresponding pentafluoropropanamide isopropyl esters 87

Figure 2-7. Structure of SubA with proposed stereochemistry of sulfur- α -carbon crosslinks labelled in magenta 88

Figure 2-8. A) Superposition of the backbone of residues of the eight lowest energy structures of SubA. B) Representative conformer of SubA with

indication of stereochemistry of the modified residues. C) Coil representation of the backbone of SubA, the break shown is at the position of C- and N-terminal cyclization. (This figure adopted Kawulka et al. ¹⁴⁰)	89
Figure 2-9. Compounds used in the co-crystallography studies of lysozyme by Phillips and co-workers ¹⁶⁷	91
Figure 2-10. 4-Methylumbelliferyl β -glycosides used in the co-crystallization of lysozyme ¹⁶⁸	92
Figure 2-11. Crystal structure of lysozyme complex with 4MeU-(GlcNAc) ₃ (199) PDB code: 1BB6.....	93
Figure 2-12. MS/MS analysis of enzymatic digested alkynyl-SubA. a) b-ion labeled in red; b) y-ion labeled in blue	100
Figure 2-13. Spot on lawn antimicrobial activity testing results of SubA and alkynyl-SubA against <i>L. lactis</i> subsp. <i>cremoris</i> HP. The spots labelled C1, T1, and T2 were used for a separate study, and should be ignored. The spot labelled C2 was used as a negative control (spotted with 10 μ L of 1:1 mixture of acetonitrile and water). The spots labelled as A1, A2, and A3 correspond to SubA at 200 μ M, 100 μ M, and 50 μ M concentrations, respectively. The spots labelled as A'1, A'2, and A'3 correspond to alkynyl-SubA at 200 μ M, 100 μ M, and 50 μ M concentrations, respectively	101
Figure 2-14. Literature examples of cyclooctyne derivatives 229 , 230 , and 231 used in copper-free click chemistry ¹⁷⁹⁻¹⁸²	108
Figure 2-15. <i>p</i> -Nitrophenol acetate assay for activity testing of CAII.....	111

Figure 2-16. Inhibitory activity testing of the sulfonamide inhibitors against CAII as tested using <i>p</i> -nitrophenol acetate assay.....	112
Figure 2-17. Examples of ureido-containing arylsulfonamides reported in the literature as inhibitors of CAII ¹⁸⁵	114
Figure 2-18. Crystal structure of CAII with overlays of various ureido-containing arylsulfonamides, 241a-e , labeled in orange, pink, yellow, grey, and cyan, respectively ¹⁸⁵ Reproduced with permission from Pacchiano et al. ¹⁸⁵	115
Figure 2-19. Proposed ureido-containing benzenesulfonamide inhibitors to CAII	116
Figure 2-20. Results of activity testing of the ureido-containing benzene-sulfonamide inhibitors against CAII.....	118
Figure 3-1. Purification of CAII using SP Sepharose Fast Flow resin	189
Figure 3-2. SDS-PAGE gel showing the CAII purification. From right to left, lane 1 to lane 10	190

List of Tables

Table 1-1. Inhibition results of the top 46 compounds against LL-DAP-AT from HTS study	54
Table 1-2. The inhibitory effects of the aryl-hydrazide analogues obtained from modification of naphthalene moiety against LL-DAP-AT	62
Table 1-3. The inhibitory effects of the aryl-hydrazide analogues obtained from modification of phenylsulfonamide moiety against LL-DAP-AT.....	64
Table 1-4. Inhibitory effects of <i>N</i> -unsubstituted rhodanine analogues against LL-DAP-AT	70
Table 1-5. The inhibitory effect of <i>N</i> -ethyl-rhodanine analogues against LL-DAP-AT	71
Table 1-6. The inhibitory effects of <i>N</i> -amino-rhodanine analogues against LL-DAP-AT	72
Table 1-7. The inhibitory effects of <i>N</i> -aminoacetyl-rhodanine analogues against LL-DAP-AT	73
Table 2-1. Classification of bacteriocins produced by Gram-positive bacteria ...	83

List of Schemes

Scheme 1-1. The preparation of hydrazide analogues (144 and 147) of the lead arylhydrazide 122	60
Scheme 1-2. The general synthetic route for preparation of hydrazide analogues	61
Scheme 1-3. Hydrazone formation between the hydrazide group of inhibitor 155 and the aldehyde group of PLP	65
Scheme 1-4. Hydrazone formation between the hydrazine group of isoniazid and the aldehyde group of PLP	67
Scheme 1-5. General synthetic route for rhodanine-derived inhibitors for LL-DAP-AT	69
Scheme 2-1. Synthetic approach towards GlcNAc-squarate-SubA bioconjugate	95
Scheme 2-2. Model click chemistry reaction on glucosamine derivative	96
Scheme 2-3. Preparation of alkynyl-SubA	97
Scheme 2-4. Enzymatic digestion of alkynyl-SubA by endoproteinase Asp-N...	99
Scheme 2-5. Preparation of GlcNAc-SubA bioconjugate (220) using click chemistry	103
Scheme 2-6. Preparation of (GlcNAc) ₃ -SubA bioconjugate 225 using click chemistry	105
Scheme 2-7. Preparation of azido-benzenesulfonamide 228	107
Scheme 2-8. Preparation of the monofluorinated cyclooctyne 231	110
Scheme 2-9. Click chemistry with monofluorinated cyclooctyne derivative and azido-benzenesulfonamide derivative affords isomers 239 and 240	111

Scheme 2-10. Preparation of ureido-containing benzenesulfonamide 246	116
Scheme 2-11. Preparation of 243 , the second ureido-containing benzene- sulfonamide inhibitor	117
Scheme 2-12. Preparation of ureido-benzenesulfonamide-SubA bioconjugate.	119

List of Abbreviations

$[\alpha]_D$	specific rotation
AAA	α -aminoadipic acid
Ac	acetyl
AcCl	acetyl chloride
ACS	American Chemical Society
Ala or A	alanine
AMP	adenosine monophosphate
aq.	aqueous
Arg or R	arginine
ASA	aspartate semialdehyde
Asn or N	asparagine
Asp or D	aspartic acid
AT	aminotransferase
ATP	adenosine triphosphate
Boc	<i>tert</i> -butyloxycarbonyl
Bn	benzyl
br	broad
Bu	butyl
<i>c</i>	concentration
CAII	carbonic anhydrase II
CHCA	α -cyano-4-hydroxy cinnamic acid
CoA	coenzyme A

conc.	concentration
CRAA	catechol-rhodanine acetic acid
C-terminal	carboxy terminal
Cys or C	cysteine
δ	chemical shift
d	doublet
DAP	diaminopimelic acid
DHDP	dihydrodipicolinate
DMC	2-chloro-1,3-dimethylimidazolium chloride
DMF	dimethylformamide
DMSO	dimethylsulfoxide
equiv	equivalents
EI	electron ionization
ESI	electrospray ionization
Et	ethyl
Et ₂ O	diethylether
Et ₃ N	triethylamine
EtOAc	ethyl acetate
FT	Fourier transform
Gly or G	glycine
Gln or Q	glutamine
Glu or E	glutamic acid
GlcNAc	<i>N</i> -acetylglucosamine

(GlcNAc) ₃	N,N',N''-triacetylchitotriose
HEPES	4-(2-hydroxyethyl)-1-piperazineethanesulfonic acid
HOBt	1-hydroxybenzotriazole
HPLC	high performance liquid chromatography
HRMS	high resolution mass spectrometry
HTHDP	4-hydroxytetrahydrodipicolinate
HTS	high-throughput screening
IL-1	interleukin-1
IL-1R1	interleukin-1 receptor type 1
Ile or I	isoleucine
IR	infrared
<i>J</i>	coupling constant
α-Kg	α-ketoglutarate
LAB	lactic acid bacteria
LD	large domain
Leu or L	leucine
Lys or K	lysine
m	multiplet
MALDI	matrix assisted laser desorption ionization
Me	methyl
MeOH	methanol
4MeU	4-methylumbelliferyl
MHz	megahertz

MS	mass spectrometry
MS/MS	tandem mass spectrometry
NaAsc	sodium ascorbate
NAD	nicotinamide adenine dinucleotide
NADP	nicotinamide adenine dinucleotide phosphate
<i>N</i> -terminal	amino terminal
NMR	nuclear magnetic resonance
OAB	<i>o</i> -aminobenzaldehyde
2,6-PDC	2,6-pyridinedicarboxylic acid
Ph	phenyl
Phe or F	phenylalanine
PLP	pyridoxal-5'-phosphate
PMP	pyridoxamine-5'-phosphate
PP _i	pyrophosphate
ppm	part per million
PyBOP	benzotriazole-1-yl-oxy-tris-pyrrolidino-phosphonium hexafluorophosphate
q	quartet
RP	reversed phase
rpm	revolutions per minute
s	singlet
SAR	structure activity relationship
SD	small domain

Ser or S	serine
sp.	species
spp.	multiple species
STI	sexually transmitted infections
SubA	subtilosin A
subsp.	subspecies
t	triplet
<i>t</i> Bu	<i>tertiary</i> -butyl
TCA	tricarboxylic acid
TFA	trifluoroacetic acid
TFFH	tetramethylfluoroformamidinium hexafluorophosphate
THDP	tetrahydrodipicolinate
THF	tetrahydrofuran
Thr or T	threonine
TLC	thin layer chromatography
TOF	time of flight
t_R	retention time
Tyr or Y	tyrosine
UV-Vis	ultra violet visible
ZBG	zinc-binding groups

Chapter 1. Structural and inhibitory studies of LL-diaminopimelate aminotransferase

1.1 Introduction

1.1.1 An overview of lysine biosynthesis

Lysine is an essential amino acid, as its biosynthetic pathway is absent in animals. Therefore animals have to acquire this amino acid from their diet. However, lysine biosynthesis does occur in plants, bacteria, and fungi.¹

Lysine is perhaps the only known proteinogenic amino acid to have two distinctive biosynthetic pathways. In most fungi, lysine is biosynthesized by the α -aminoadipic acid (AAA) pathway.^{2,3} However, in plants and most bacteria, the biosynthesis of lysine proceeds through diaminopimelate (DAP) intermediates. Both of these pathways will be discussed in the next sections.

1.1.1.1 α -Aminoadipic acid (AAA) pathway

The AAA pathway occurs mostly in fungi, as well as some bacteria (e.g., *Thermus* spp.^{2,3}). There are two known variants of this pathway, but both involve the formation of α -aminoadipic acid as a key intermediate (**Figure 1-1**). The formation of α -aminoadipic acid begins with acetyl-CoA (**1**) and α -ketoglutaric acid (α -Kg, **2**). The enzyme homocitrate synthase catalyzes a condensation reaction between **1** and **2** to form homocitrate (**3**). Homocitrate (**3**) is converted to homoisocitrate (**5**) by homoaconitase, which belongs to the aconitase super family of enzymes. The homoaconitase-catalyzed reaction is proposed to be a two-step

process: first, homocitrate is dehydrated to form *cis*-homoaconitate (**4**), which is then hydrated to form homoisocitrate (**5**). This is analogous to the aconitase-catalyzed step in the tricarboxylic acid (TCA) cycle. Homoisocitrate dehydrogenase then oxidizes homoisocitrate to oxo-homocitrate (**6**), which undergoes decarboxylation to form α -ketoadipic acid (**7**). α -Ketoadipic acid (**7**) is then converted to L- α -aminoadipic acid (**8**) by L- α -aminoadipate aminotransferase. This aminotransferase is a pyridoxal-5'-phosphate (PLP) dependent enzyme that uses L-glutamate as the amino donor.

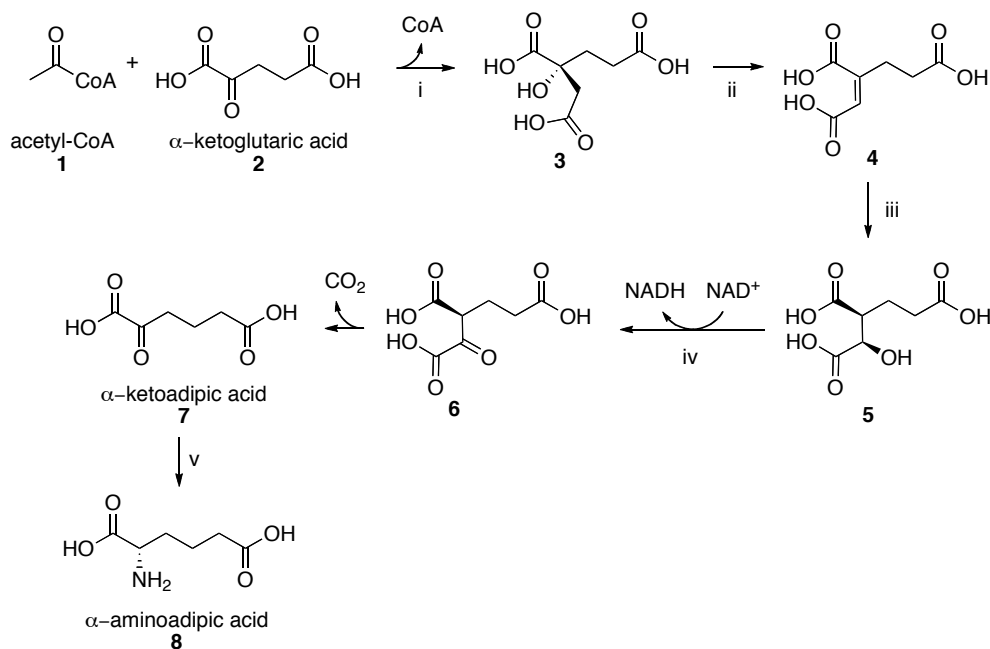


Figure 1-1. The first steps in the AAA pathway for the formation of α -aminoadipic acid. i) Homocitrate synthase; ii) Homoaconitase; iii) Homoaconitase; iv) Homoisocitrate dehydrogenase; v) L- α -Aminoadipate aminotransferase

The rest of the biosynthesis, which requires the conversion of L- α -aminoadipic acid (**8**) to lysine can then follow two different pathways. For the fungal AAA pathway, the remaining biosynthetic steps are shown in **Figure 1-2**. In the second half, L- α -aminoadipic acid (**8**) is first adenylated by adenosine triphosphate (ATP) to L- α -aminoadipate adenyl monophosphate (**9**), releasing pyrophosphate. Subsequently, reduction by L- α -aminoadipate semialdehyde dehydrogenase gives L- α -aminoadipate 6-semialdehyde (**10**). The L- α -aminoadipate 6-semialdehyde (**10**) reacts with L-glutamate (**11**) to form an imine adduct (**12**), which is then reduced by saccharopine reductase to form saccharopine (**13**). Finally, lysine is formed by the action of saccharopine dehydrogenase with the release of α -Kg (**2**).

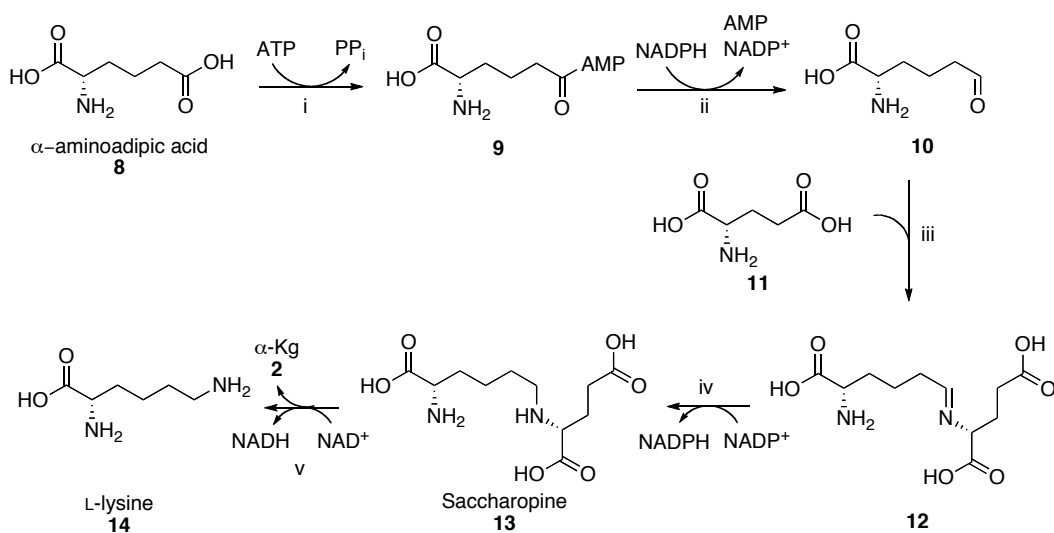


Figure 1-2. Second half of fungal AAA pathway. i) L- α -Aminoadipate semialdehyde dehydrogenase; ii) L- α -Aminoadipate semialdehyde dehydrogenase; iii) Saccharopine reductase; iv) Saccharopine reductase; v) Saccharopine dehydrogenase

The AAA pathway also occurs in some archaea, such as *Thermoproteus* and *Sulfolobus*.⁴ In the late 1990s, a variant of the AAA pathway was observed in the thermophilic bacterium, *Thermus thermophilus*.^{5, 6} The first half of this pathway, formation of L- α -aminoadipate, is the same as the fungal AAA pathway. In the second half of this putative pathway (**Figure 1-3**), L- α -aminoadipate (**8**) is first acetylated on the amino group to give *N*²-acetyl- α -aminoadipate (**15**).⁷ The ϵ -carboxylate is then phosphorylated to **16** by LysZ, which is an *N*²-acetylglutamate kinase (ArgB) homolog.⁸ Reduction of **16** catalyzed by LysY, yields *N*²-acetyl- α -aminoadipate 6-semialdehyde (**17**). This enzyme is an *N*²-acetylglutamate 5-semialdehyde dehydrogenase (ArgC) homolog.⁸ The last two steps are catalyzed by LysJ and LysK. LysJ is a PLP-dependent aminotransferase that uses L-glutamate as the amino donor and is an *N*²-acetylornithine aminotransferase (ArgD) homolog.⁹ Deacetylation, catalyzed by LysK, an *N*²-acetylornithine deacetylase (ArgE) homolog, forms lysine.¹⁰ From these studies and DNA sequences, a hypothesis can be made that the *T. thermophilus* AAA pathway and arginine biosynthetic pathway (via ArgB, ArgC, ArgD, and ArgE) may share a common evolutionary origin.

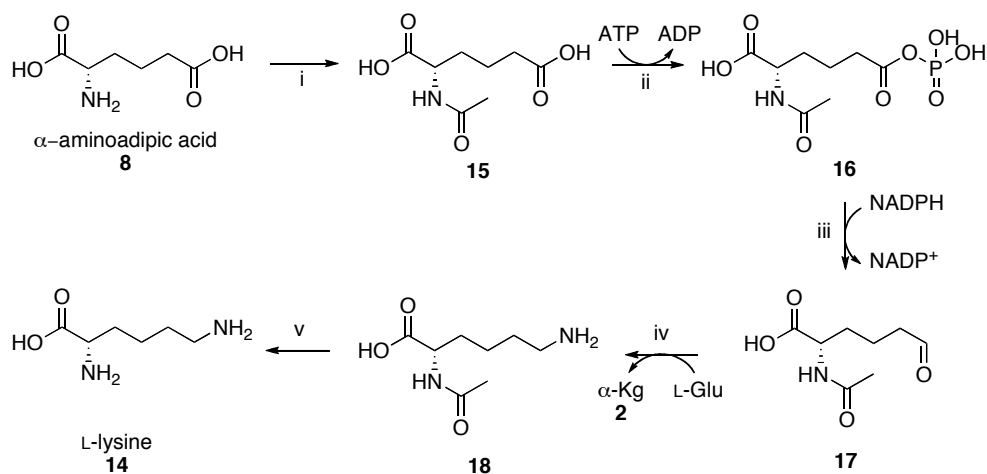


Figure 1-3. A variant of the second half of putative AAA pathway from *T. thermophilus*. i) LysX; ii) LysZ; iii) LysY; iv) LysJ; v) LysK

1.1.1.2 Diaminopimelate (DAP) pathway

In addition to the AAA pathway described in the previous section, there is another mechanism for lysine biosynthesis. Most bacteria and plants use the diaminopimelate (DAP) pathway to synthesize lysine. Unlike the AAA metabolic route, the DAP pathway has several variants found in different organisms. In this section, a general overview of all of the known variants of the DAP pathway will be discussed.

The most well studied bacterial DAP pathway is shown in **Figure 1-4**. The biosynthetic route starts with pyruvate (**19**) and L-aspartate semialdehyde (ASA, **20**). Glucose catabolism forms pyruvate, whereas ASA is formed from L-aspartate via enzymatic phosphorylation and reduction, catalyzed by L-aspartate kinase and ASA dehydrogenase, respectively. ASA is also an intermediate involved in threonine, isoleucine, and methionine biosynthesis.^{11, 12} The condensation reaction

between pyruvate and ASA is the first committed step in lysine biosynthesis via DAP. This step is catalyzed by L-dihydrodipicolinate synthase, and forms L-dihydrodipicolinate (L-DHDP, **21**).¹³ The L-DHDP is then reduced to tetrahydrodipicolinate (L-THDP, **22**) by DHDP reductase. An *N*-acyltransferase-catalyzed step generates L- α -keto- ϵ -(*N*-acylamino)pimelate (**23/24**). Depending on the species, the acyl group can either be a succinyl or an acetyl group. In most bacteria, a succinyl group is used, although acetyl groups are used by some *Bacillus* spp., such as *B. megaterium*.^{2, 14} L- α -Keto- ϵ -(*N*-acylamino)pimelate (**23/24**) is further converted to *N*- α -acyl-LL-DAP (**25** a or b) by *N*- α -acyl-DAP aminotransferase, which is a PLP-dependent aminotransferase. Deacylation then forms LL-DAP (**26**) as the next intermediate.¹⁵ LL-DAP (**26**) is epimerized to *meso*-DAP (**27**) by DAP epimerase, a PLP-independent racemase.^{1, 16, 17} Finally, *meso*-DAP (**27**) is converted to L-lysine (**14**) by DAP decarboxylase, another PLP dependent enzyme.¹⁸

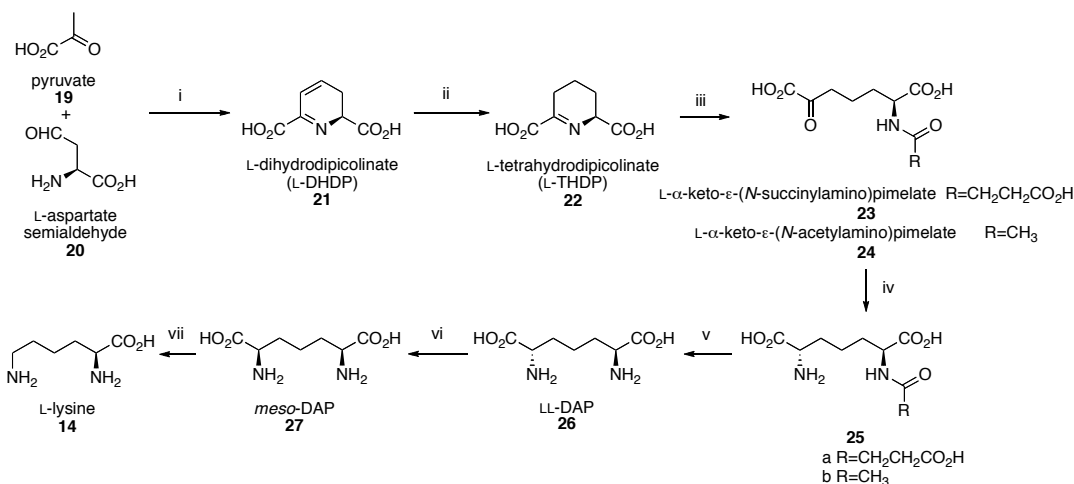


Figure 1-4. The most common bacterial DAP pathway. i) DHDP synthase; ii) DHDP reductase; iii) THDP acyltransferase; iv) *N*-acyl-DAP aminotransferase; v) *N*-acyl-DAP deacylase; vi) DAP epimerase; vii) DAP decarboxylase

Although the majority of bacteria use the route shown above, there are other variations. The first variant is shown in **Figure 1-5**. This is a shorter biosynthesis that converts L-THDP (**22**) directly to *meso*-DAP by the enzyme *meso*-DAP D-dehydrogenase. This variant of the DAP pathway occurs in a relatively small number of bacteria, such as *Bacillus*, *Sphaericus*,^{19, 20} *Corynebacterium glutamicum*, and *Brevibacterium* sp.^{21, 22} A recent phylogenomic analysis of the microbial genome database reveals that 77% of microorganisms containing the *meso*-DAP D-dehydrogenase ortholog also have a second DAP pathway to synthesize lysine.²³

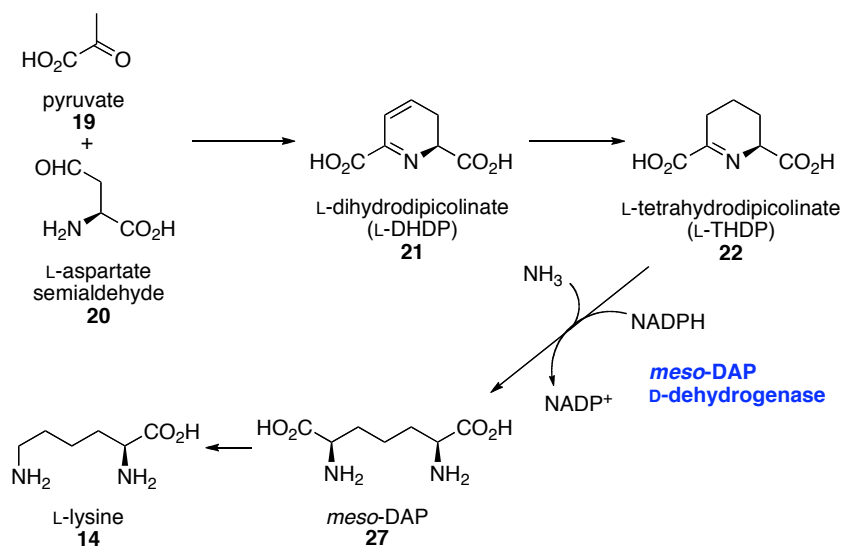


Figure 1-5. The *meso*-DAP formation in *B. sphaericus* catalyzed by *meso*-DAP D-dehydrogenase (coloured in blue)

It has been thought for decades that plants use the DAP pathway to synthesize lysine in the same way as bacteria. Recently a newly discovered aminotransferase enzyme was isolated that converts L-THDP directly to LL-DAP.²⁴ As shown in **Figure 1-6**, this single enzyme replaces three enzymes (an acylase, an aminotransferase, and a deacylase) in the common bacterial DAP pathway (**Figure 1-4**). This enzyme has been named LL-DAP aminotransferase (LL-DAP-AT), and is a PLP dependent aminotransferase that uses L-glutamate as the amino donor.²⁵ Studies of this enzyme are a primary focus of this thesis, and a more detailed description of LL-DAP-AT will be provided in later sections.

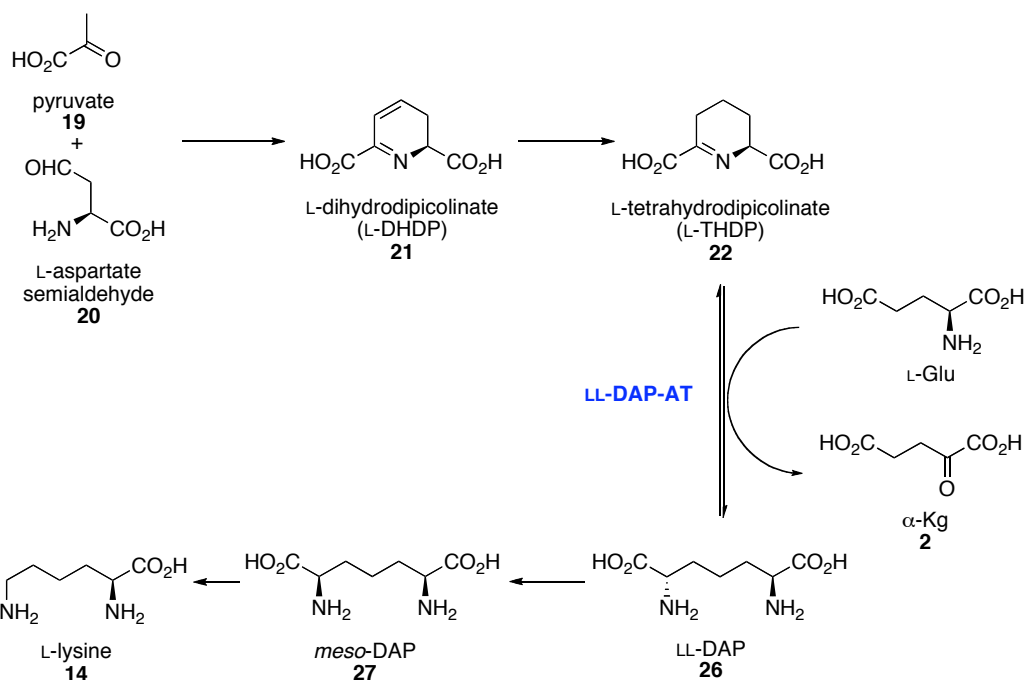


Figure 1-6. LL-DAP-AT-catalyzed transamination (coloured in blue) to form LL-DAP

1.1.2 Discovery of LL-DAP-AT

It had been thought that lysine biosynthesis in plants occurs via one of the bacterial DAP pathways.^{26, 27} This incorrect hypothesis was due to the identification of particular enzymatic steps of the bacterial DAP pathway in plants.^{25, 28} It has been known for a long time that lysine biosynthesis in plants begins with aspartic acid. One of the key intermediates, ASA, is formed by the enzymes L-aspartate kinase and ASA dehydrogenase. These two enzymes from plants have been studied extensively.^{29, 30} DHDP synthase-catalyzed condensation reactions in plants have also been studied by feeding synthetic ASA to the enzyme.^{31, 32} DHDP reductase is the next enzyme in the bacterial DAP pathway. The enzyme from maize has been partially purified, and its activity has been

measured.^{22,33} More recently, the gene encoding plant DHDP reductase has been detected in *Arabidopsis* spp.³⁴ The next three enzymes (an acylase, an aminotransferase, and a deacylase) of the standard DAP pathway have not been detected in plants.²⁸ The last two enzymatic steps catalyzed by DAP epimerase and meso-DAP decarboxylase were detected from plant extracts prior to the discovery of LL-DAP-AT.^{22,35-37} Recently, a crystal structure of DAP epimerase from *A. thaliana* was obtained and characterized by our group.³⁸ These enzymatic steps suggests that lysine biosynthesis in plants occurs via one of the bacterial DAP pathways.

In 2000, the first complete genome sequence from a plant species, that of *Arabidopsis thaliana*, was obtained and analyzed.³⁹ This milestone event in biology made it possible for researchers to identify potential enzymes involved in different biological pathways in this model plant. In 2005, the Leustek group searched the genome of *A. thaliana* for the enzymes involved in lysine biosynthesis.²⁸ Among the DAP pathway enzymes identified, the genome contained orthologs of DHDP synthase, DHDP reductase, DAP epimerase, and meso-DAP decarboxylase. However, THDP acyltransferase, *N*- α -acyl-DAP aminotransferase, and *N*- α -acyl-DAP deacylase were not identified in the *A. thaliana* genome. Beyond the search of biosynthetic genes, activity tests using plant extracts also suggested that this plant species lacks these three enzymes. These studies indicated that lysine is made by a DAP pathway similar in some aspects to the bacterial DAP route, but with some variations.²⁸ Another study

showed that *meso*-DAP D-dehydrogenase, is also absent from this plant species.²² These results suggest that a previously unknown DAP pathway exists in plants.

Not long after, a novel aminotransferase was identified from *A. thaliana*, which represents a new DAP pathway variant.²⁴ As mentioned earlier, this plant enzyme was shown to catalyze the conversion of THDP to LL-DAP, which normally requires three enzymes in the bacterial DAP pathway.¹¹ LL-DAP-AT was predicted to be a typical PLP-dependent aminotransferase that uses glutamate as the amino donor.²⁴ This was later confirmed based on an X-ray crystal structure obtained by our group.⁴⁰ The detailed X-ray crystallographic study will be discussed in the later sections of this thesis.

This shorter route (**Figure 1-6**) appears to be the general lysine biosynthetic pathway in plants and is also found in cyanobacteria.²⁴ The phylogenetic distribution of LL-DAP-AT may be due to cyanobacteria and plant chloroplasts sharing a similar evolutionary pathway.⁴¹ LL-DAP-AT is also found in *Chlamydia* species, and has thus been identified as a trans-kingdom enzyme.⁴² Recently, the X-ray crystal structure of LL-DAP-AT from *Chlamydia trachomatis* was also obtained and analyzed by our group,⁴³ and will be discussed in greater detail in subsequent sections of this thesis. Systematic biochemical and phylogenetic characterization indicates that the occurrence of LL-DAP-AT is limited to specific lineages of eubacteria, e.g., *Cyanobacteria*, *Desulfuromonadales*, *Firmicutes*, *Bacteroidetes*, *Chlamydiae*, *Spirochaeta*, and *Chloroflexi* and two archaeal groups, *Methanobacteriaceae* and *Archaeoglobaceae*.^{23, 44} More recently, two bacterial species, *Bacteroides fragilis* and *Clostridium thermocellum*, were found

to use dual DAP pathways (LL-DAP-AT and *meso*-DAP D-dehydrogenase) to synthesize lysine.⁴⁵

1.1.3 Inhibitory studies of DAP pathways

1.1.3.1 Potential target for the development of new antibiotics

For decades, lysine biosynthesis in bacteria and plants has been considered a target for the development of new antibiotics and herbicides. Mammals do not biosynthesize lysine, and so they have to acquire this essential amino acid from their diet. On the other hand, fungi, bacteria, and plants are all able to synthesize lysine. Thus, if the biosynthetic route is inhibited, and the organism is unable to produce lysine, it may result in the death of the organism. Because lysine biosynthesis is absent in mammals, specific inhibitors of the enzymes involved in lysine biosynthesis may be expected to show low or no toxicity towards mammals. All of these facts make the lysine biosynthetic pathway an attractive target to develop new antibiotics or herbicides. However, to date there are no clinically used antibiotics or commercially used herbicides specifically targeting lysine biosynthetic pathways.¹² In addition, a complete understanding of its biosynthetic route may assist in the engineering of plants with increased lysine content for better nutrition.⁴⁶

Recently, the rapid emergence of antibiotic-resistant bacteria has drawn enormous attention from researchers.⁴⁷ Historically, bacterial infections by *Mycobacterium tuberculosis* and *Staphylococcus aureus* were successfully treated through the use of a number of existing antibiotics. Recent occurrence of multidrug-resistant strains of these bacteria has made these infections difficult to

treat.⁴⁸ *Chlamydia* is another infectious bacterial strain that has started to show drug resistance in hospitals.⁴⁹ Significant numbers of severe human infections are caused by bacterial species within the genus *Chlamydia*, especially sexually transmitted infections (STI).^{43, 50} Studies have shown that over 90 million people are infected with chlamydia worldwide, and there are approximately five million new cases of chlamydial infection each year in the USA alone.⁵¹ Chlamydial infections can cause various associated diseases, such as pelvic inflammatory disease, with potential development of infertility in certain women.⁵⁰ In addition to the STI caused by *Chlamydia*, it can also cause trachoma, which is a common cause of blindness.⁵¹ Due to the increase in the number of drug-resistant bacterial infections, there is a great demand for development of new antibiotics in health care research.

Currently, most of the clinically used antibiotics are derived from the scaffolds of older generation antibiotics that were discovered between the mid-1930s and 1960s.⁵² Development of new generations of older antibiotics is one of the commonly used solutions to fight against the rise of resistant pathogens.⁵³ The tailoring and modification of the older generation of antibiotics will most likely continue to be effective to counter drug resistance. However, an important alternative approach is to find new targets that have not yet been explored.

Bacterial lysine biosynthetic pathways are valid targets for potential antibiotics development. As mentioned above, lysine biosynthesis is absent in mammals, which may allow for the preparation of novel antibiotics with minimal human toxicity.¹ L-Lysine is one of the major components used by Gram-positive

bacteria to synthesize the peptidoglycan found in the cell wall. The direct precursor of lysine in the bacterial DAP pathways, *meso*-DAP, is involved in the construction of Gram-negative bacterial cell walls. The cross-links between *meso*-DAP/L-lysine and peptidoglycan amino acids play a significant role in strengthening the bacterial cell walls.^{54, 55} If the lysine biosynthetic pathway is inhibited, the construction of bacterial cell walls may be disrupted, which would lead to cell death. Thus, the enzymes involved in these pathways represent important targets with the potential for activity against multidrug-resistant bacteria.

1.1.3.2 Recent inhibitory studies of DAP enzymes

The DAP pathways have been the subject of study for several decades, and have prompted numerous reviews in the literature^{1, 12, 15, 56} in addition to continuing studies on the design of inhibitors⁵⁷⁻⁶⁰ since the 1980s.⁶¹ In the following sections, inhibitory studies of each of the key enzymes in the various DAP pathways will be discussed, in order of their appearance in DAP biosynthetic pathway.

1.1.3.2.1 Inhibitory studies on DHDP synthase

DHDP synthase is the first enzyme in the DAP pathway committed to lysine biosynthesis. As mentioned previously, this enzyme catalyzes the condensation reaction between pyruvate (**19**) and ASA (**20**). The proposed mechanism^{13, 62} is shown in **Figure 1-7**. Pyruvate is first bound in the enzyme active site, and a condensation reaction with an active site lysine residue forms an

enamine (**27**). This enamine attacks the aldehyde moiety of the ASA (**20**) to form enzyme-bound intermediate **28**. A transamination reaction forms 4-hydroxytetrahydrodipicolinate (HTHDP, **29**), with the release of the active site lysine residue. Finally, dehydration gives DHDP (**21**). It was questioned whether the dehydration of HTHDP is catalyzed by DHDP synthase or is a spontaneous process. A recent report suggests that the true substrate for DHDP reductase, the next enzyme in the pathway, is HTHDP (**29**) rather than DHDP (**21**).⁶³ Thus, the dehydration of HTHDP appears to be an enzymatic process; DHDP reductase is likely also acting as a dehydratase.⁶³

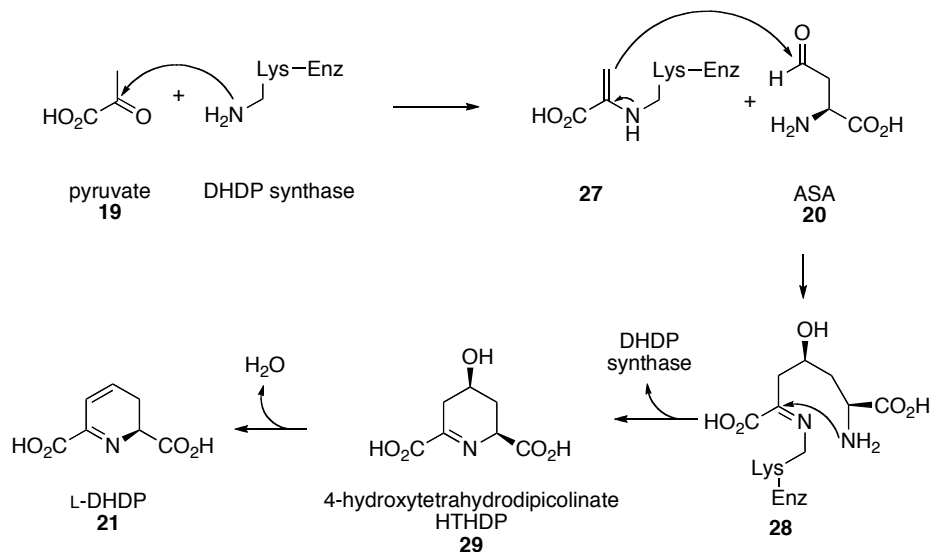


Figure 1-7. Catalytic mechanism of DHDP synthase

Efforts have been previously made toward designing DHDP synthase inhibitors. In one of these studies, a series of analogues of HTHDP (**Figure 1-8**) were chosen as inhibitors of DHDP synthase.^{64,65} Although these inhibitors only

showed poor inhibition, they are still the most potent reversible inhibitors that have been developed for DHDP synthase.¹²

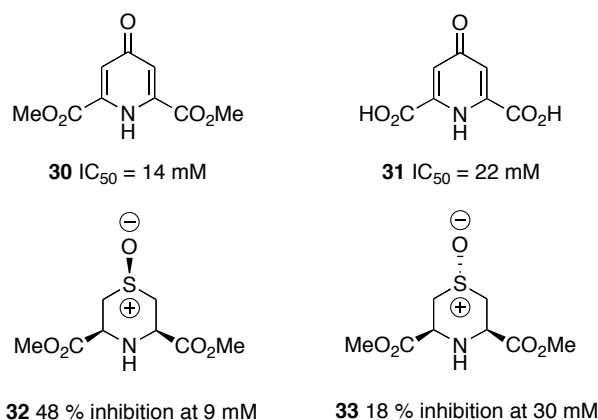


Figure 1-8. Analogues of HTHDP and their ability to inhibit DHDP synthase

In a different study,^{59, 66} two 4-oxo-heptenedioic acid derivatives were designed as irreversible inhibitors. The structures and the proposed mechanism of inhibition are shown in **Figure 1-9**. The dieneone **34** was the best inhibitor in this study with an inactivation rate of $5.4 \text{ M}^{-1}\text{s}^{-1}$ against DHDP synthase.¹² These inhibitors may be quite effective against this enzyme, but these molecules are extremely reactive irreversible inhibitors, and may not be suitable as pharmaceuticals. Since compounds **34** and **35** are good Michael acceptors, they can react with nucleophilic residues under physiological conditions, such as cysteine. This could lead to non-specific interactions with different enzymes that are not targeted for inhibition, resulting in inhibitors which may show high levels of toxicity.

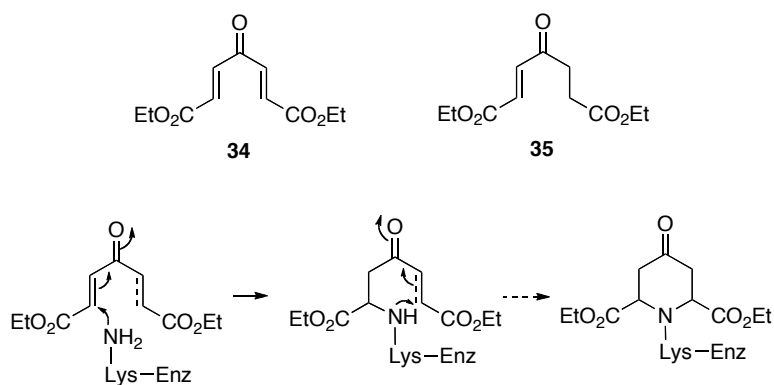


Figure 1-9. 4-Oxo-heptenedioic acid derivatives and the proposed mode of inhibition of DHDP synthase

1.1.3.2.2 Inhibitory studies on DHDP reductase

Similar to DHDP synthase, DHDP reductase is also a common enzyme found in all of the known species that utilize the DAP pathway for *meso*-DAP and lysine biosynthesis (**Figure 1-10**). This enzyme is also considered a target for the development of broad-spectrum antibiotics and herbicides.

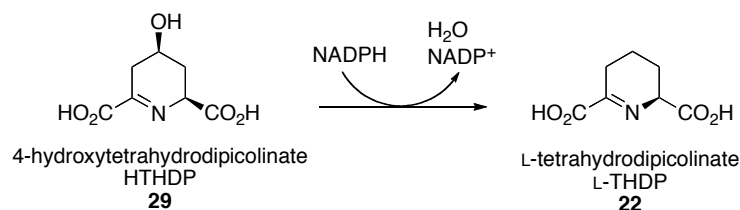


Figure 1-10. DHDP reductase-catalyzed dehydration and reduction to form L-THDP

In the early 2000s, a group from the Merck research laboratory⁶⁷ used a combined approach of molecular modelling and conventional screening to identify several potent inhibitors of DHDP reductase. A group of sulfonamide

derivatives (**Figure 1-11a**) showed good to moderate inhibition against the target enzyme. However, this group of compounds was not found to possess any antimicrobial activity in a whole cell agar diffusion assay. From the screening of the Merck Chemical Collection, a number of other lead compounds were identified in addition to the sulfonamide derivatives, three of which are shown in **Figure 1-11b**. This study could lead to the discovery of better inhibitors, based on the lead compounds identified.

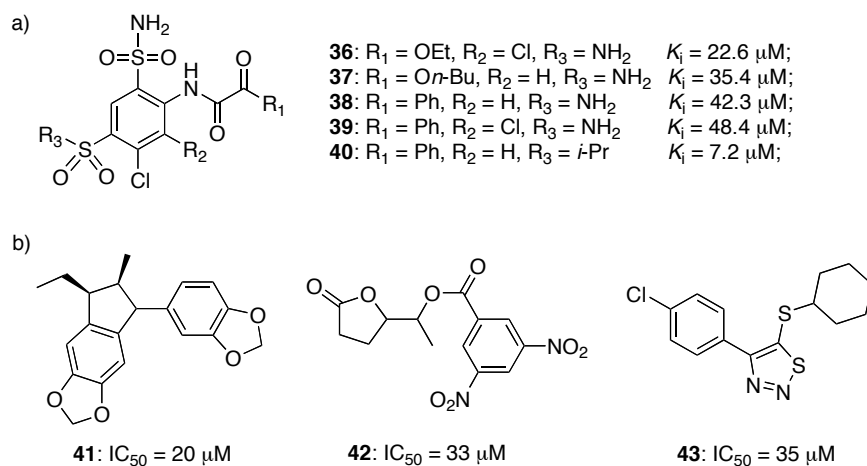


Figure 1-11. Inhibitors of DHDP reductase developed by the Merck research laboratory⁶⁷

Researchers have also gained a better understanding of the structural features of DHDP reductase.⁶⁸⁻⁷¹ In 2003, the enzyme was co-crystallized with the inhibitor 2,6-pyridinedicarboxylic acid (2,6-PDC, **44**).⁷⁰ Electron density corresponding to 2,6-PDC was found in the DHDP binding site. As mentioned previously, DHDP reductase is a NAD(P)H-dependent enzyme. Catechol-rhodanine acetic acid (CRAA, **45**) is a well known inhibitor of NAD(P)H binding

proteins.⁷² Recently, based on this knowledge, a bi-ligand strategy was used to develop inhibitors to DHDP reductase.⁷²⁻⁷⁴ Upon linking of 2,6-PDC (**44**) to CRAA (**45**) with a short tether, the resulting complex **46** (**Figure 1-12**) showed fairly potent inhibition, with an inhibition constant (K_i) of 100 nM.⁷³ As mentioned in the previous section, DHDP reductase likely also acts as a dehydratase. Thus the true substrate may be HTHDP (**29**) rather than THDP,⁶³ and future rational design of inhibitors could be based on the structure of HTHDP.

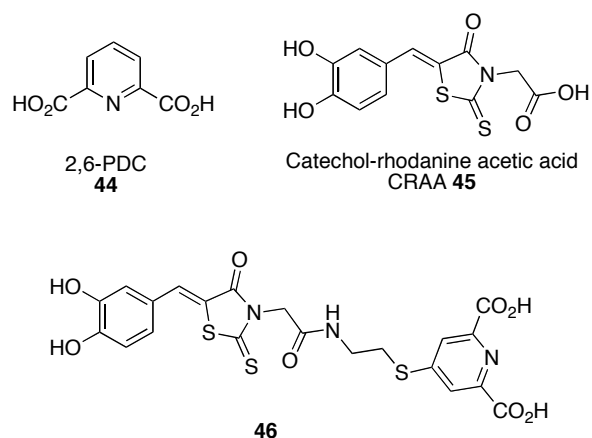


Figure 1-12. Inhibitors of DHDP reductase optimized by bi-ligand approach

1.1.3.2.3 THDP *N*-acyltransferase, *N*-acyl-LL-DAP aminotransferase, and *N*-acyl-LL-DAP deacylase

The three enzymes involved in conversion between L-THDP and LL-DAP (**Figure 1-13**) continue to draw much attention, via structural and mechanistic studies.⁷⁵⁻⁷⁷ However, the development of inhibitors of these enzymes has not

been extensively studied. Some of the early attempts towards the development of inhibitors will be discussed in this section.

There are two variants of these three enzymatic steps, which utilize substrates with either a succinyl group or an acetyl group. As most bacteria use a succinyl group, most of focus on the development of inhibitors has targeted the succinyl pathway.

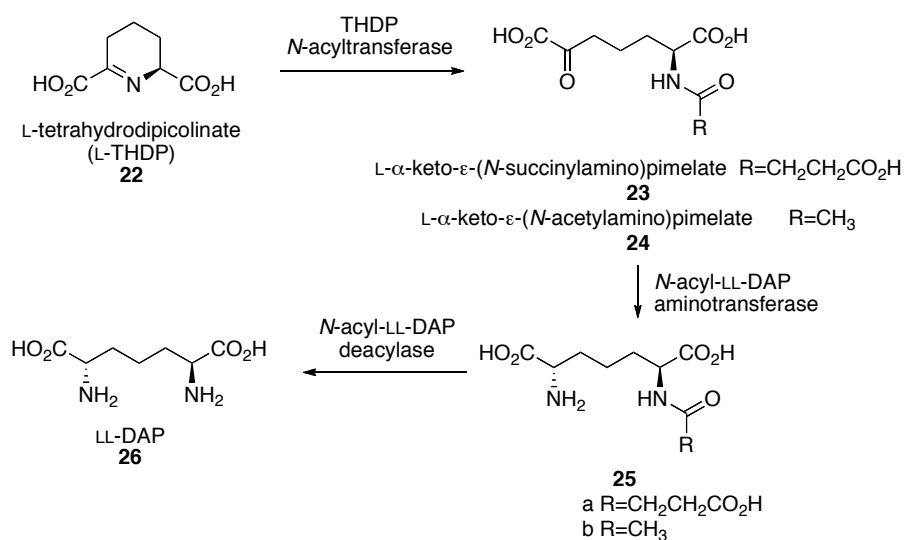


Figure 1-13. The three enzymatic steps convert L-THDP to LL-DAP that catalyzed by THDP *N*-acyltransferase, *N*-acyl-LL-DAP aminotransferase, and *N*-acyl-LL-DAP deacylase

In the late 1980s, the rational design of inhibitors of THDP *N*-succinyltransferase was reported.⁷⁸ The authors used THDP analogues as inhibitors of the enzyme, and the best inhibitor is shown in **Figure 1-14a**. The inhibitor is thought to equilibrate between two configurations (**47** and **48**) in solution. A later study showed that the first step in the enzymatic process is a ring

opening hydrolysis, as shown in **Figure 1-14b**.^{79, 80} Thus the inhibitor likely acts as an analogue of the intermediates of **49** and **50**.

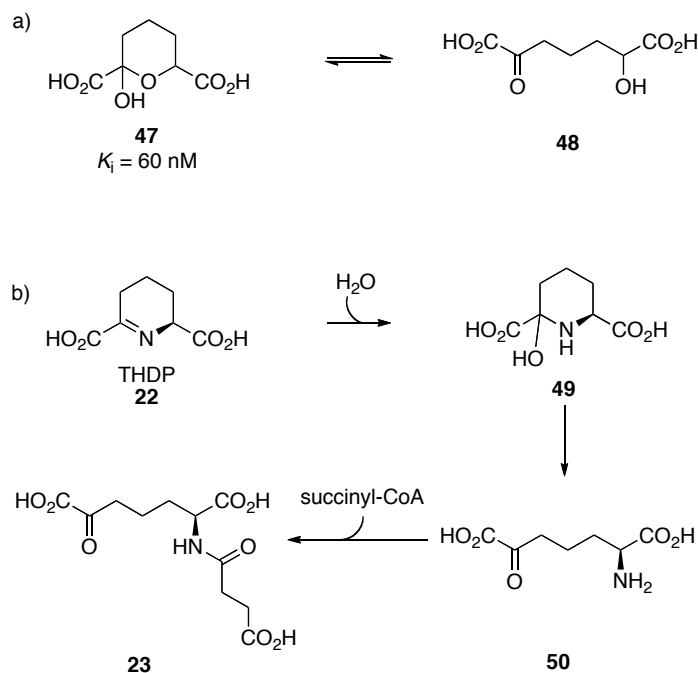


Figure 1-14. a) Inhibitor **47** of THDP *N*-succinyltransferase. b) Mechanism of THDP *N*-succinyltransferase

Inhibitory studies of *N*-succinyl DAP aminotransferase, a PLP-dependent enzyme, have been reported both by our group as well as Cox and co-workers.^{56, 81-84} Previously, we reported numerous substrate analogues that acted as potent inhibitors.⁸³ In the same report, the substrate specificity of this aminotransferase was discussed. In fact, the enzyme was found to tolerate the presence of different acyl groups (**23**, **24**, **51-53**) as shown in **Figure 1-15a**. In a subsequent study, a few corresponding hydrazine derivatives of the substrate were found to be potent reversible slow-binding inhibitors.^{81, 84} The two best inhibitors (**54** and **55**) are

shown in **Figure 1-15b**. In a separate report, the aza-, thia-, and oxa-analogues of the substrate were designed as mechanism-based irreversible inhibitors, but only the aza-analogue (**56**) showed weak inhibition against the enzyme.

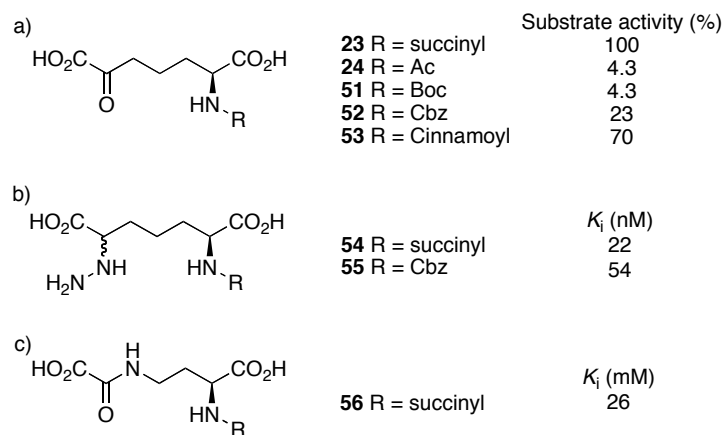


Figure 1-15. Studies on *N*-succinyl DAP aminotransferase. a) Compounds used in substrate specificity study; b) Substrate analogues as inhibitors; c) A separate inhibitory study

N-succinyl-LL-DAP desuccinylase was found to be a metallo-amidase that uses zinc ions in the active site.⁸⁵ A recent report⁵⁷ described an inhibitory screening of molecules containing zinc-binding groups (ZBG). In this study, ZBGs included thiols, carboxylic acids, boronic acids, phosphonates and hydroxamates. Some examples of the inhibitors are shown in **Figure 1-16**. The best inhibitor was found to be L-captopril (**57**), a clinically used antihypertensive agent developed in the 1970s,⁸⁶ with an inhibition constant of 1.8 μ M. L-penicillamine (**58**), a penicillin metabolite, was also found to be active against this metallo-enzyme. However, L-penicillamine is not an ideal drug candidate as it is known to be toxic.⁸⁷ Beyond these well-studied drug-like compounds, relatively

simple compounds like 4-mercaptobutanoic acid (**59**) showed moderate inhibition. Similarly, compounds containing boronic acids (**60** and **61**) or phosphonic acids (**62**) are reasonable inhibitors of this enzyme.

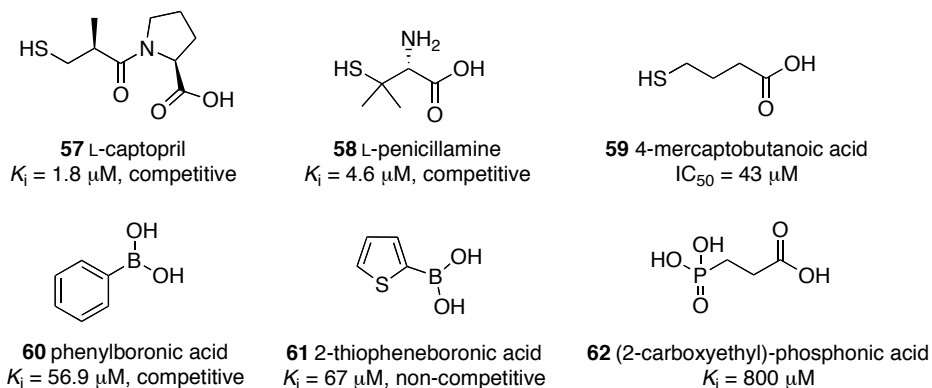


Figure 1-16. Inhibitors of *N*-succinyl DAP desuccinylase

1.1.3.2.4 Inhibitory studies of DAP epimerase

The final step in the biosynthesis of *meso*-DAP in the DAP pathway is accomplished by DAP epimerase which converts LL-DAP to *meso*-DAP. This enzymatic reaction proceeds through a two-base mechanism (**Figure 1-17**).^{16, 17} This was confirmed by X-ray crystallographic studies of the enzyme complexed with two stereoisomers of irreversible inhibitors.^{16, 17} There are two cysteine residues in the active site which act as a base (thiolate) and acid (thiol). In the forward reaction from LL-DAP to *meso*-DAP, thiolate Cys73 first acts as a base to remove the α -proton. The resulting anion is then protonated by abstracting the proton from the Cys217.

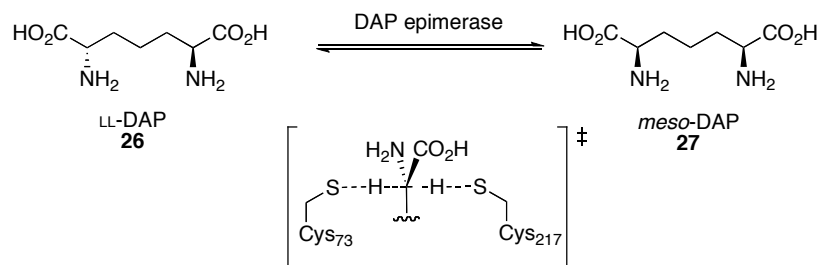


Figure 1-17. Proposed transition state of DAP epimerase-catalyzed step

The irreversible inhibitors used in the mechanistic studies are shown in **Figure 1-18**. Initially, Higgins and co-workers⁸⁸ designed α -(halomethyl)-DAP (**63 a - c**) as inhibitors of DAP epimerase. They realized that the active compound was in fact an aziridine-containing compound (**64**), formed by spontaneous ring closing. Since inactivation of the enzyme was extremely fast, the authors were unable to measure the inhibition constant.⁸⁸ Subsequently, additional studies have been done both by our group and by Cox and co-workers. Our group reported the synthesis of the pure diastereomers of aziridine-containing DAP, LL-azi-DAP (**65**), and DL-azi-DAP (**66**)^{89, 90} The X-ray crystal structures were then obtained of the complex formed between DAP epimerase and these inhibitors.¹⁶ The mode of action of these inhibitors was proposed as shown in **Figure 1-18b**. The structure of LL-azi-DAP resembles LL-DAP, the substrate of the forward reaction. Cys73 attacks the aziridine ring to yield covalent adduct **67**, which inactivates the enzyme. Similarly, DL-azi-DAP resembles *meso*-DAP, which would be considered to be the substrate of the reverse reaction. These studies have provided further support for the two-base mechanism.

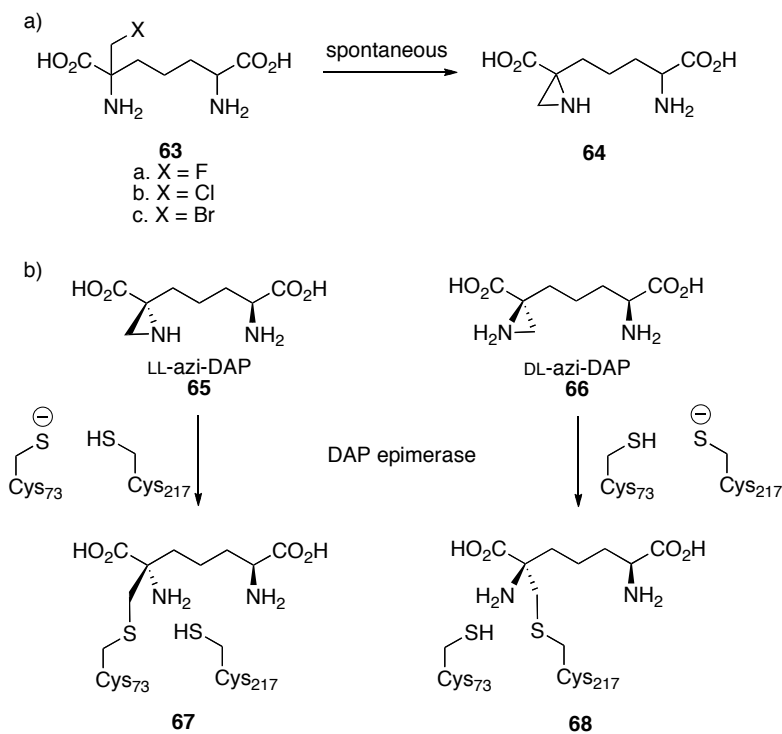


Figure 1-18. The irreversible inhibitors of DAP epimerase. a) Design of initial inhibitor **64**; b) Mode of action of pure stereoisomeric inhibitors **65** and **66**

Besides the aziridine analogues, some other inhibitory studies on DAP epimerase have been done by our research group.⁹¹ A series of 3-substituted LL-DAP and *meso*-DAP analogues were synthesized in a stereocontrolled manner. The 3-hydroxyl-LL-DAP (**69a**) and 3-hydroxyl-*meso*-DAP (**69b**) were found to be weak inhibitors of DAP epimerase with 50% inhibition observed at 2.5 mM and 4 mM, respectively. In the cases of the 3-fluoro-DAP analogues, the four compounds (**70a, b** and **71a, b**) were found to be potent inhibitors with IC_{50} values of 4 – 25 μ M. Interestingly, when the configuration of C3 is *S* (**70a** and **70b**), extensive epimerization occurs at C2. Conversely, 3*R*-configuration

analogues (**71a** and **71b**) undergo rapid elimination of hydrogen fluoride catalyzed by DAP epimerase to form THDP.

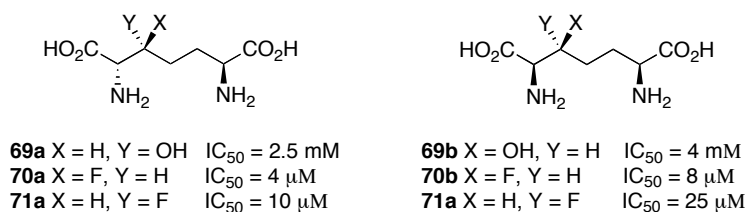


Figure 1-19. 3-substituted analogues of DAP studied by Gelb *et al.*⁹¹ as inhibitors of DAP epimerase

1.1.3.2.5 Inhibitory studies of *meso*-DAP D-dehydrogenase

In a small number of bacterial species, *meso*-DAP can be synthesized via an alternative route by the direct transformation of THDP to *meso*-DAP catalyzed by *meso*-DAP D-dehydrogenase. Although this enzyme was first isolated from *Bacillus sphaericus*,^{19,21} most of the research has been conducted on the enzyme from *Corynebacterium glutamicum*.⁹² The initial inhibitory studies have focused on analogues of DAP as enzyme inhibitors. As shown in **Figure 1-20**, compound **72** showed inhibition on both the forward ($K_i = 4.2 \mu\text{M}$ vs THDP) and reverse ($K_i = 23 \mu\text{M}$ vs *meso*-DAP) reactions.⁹³ Interestingly, compound **73**, the diastereomer of **72**, exhibited only weak inhibition against the enzyme. The detailed enzyme kinetics have also revealed that inhibitor **72** only binds to the THDP binding site, as **72** showed competitive inhibition versus THDP and uncompetitive inhibition versus NADP ($K_i = 9.2 \mu\text{M}$).⁹³ Later, the co-crystal structure of the enzyme with **72** in the active site was obtained.⁹⁴ However, the orientation of the inhibitor in

the active site was reversed, with the L-amino acid center located at the distal position, where the D-amino acid would normally be presented.⁹⁴ In a separate study,⁹⁵ two other inhibitors (**74** and **75**) were found to be active against *meso*-DAP D-dehydrogenase. Enzyme kinetic studies indicated that compound **74** was a competitive inhibitor of *meso*-DAP whereas **72** showed non-competitive inhibition to *meso*-DAP.⁹⁵ The other unsaturated analogue **75** showed non-competitive inhibition versus *meso*-DAP. This suggests that **74** may be the true mimic to the imine intermediate.⁹⁵ The X-ray crystallography studies⁹⁶ of the enzyme complexed with **74** revealed a more detailed binding feature of this enzymatic step.

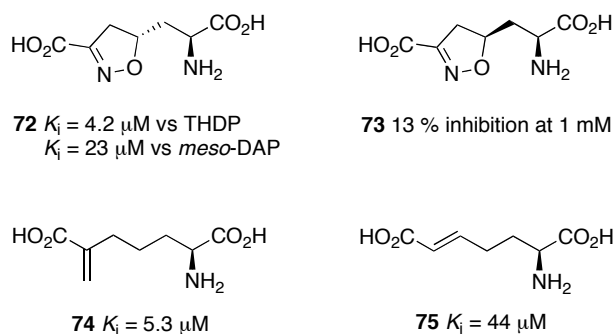


Figure 1-20. Inhibitors of *meso*-DAP D-dehydrogenase and their measured K_i values

Many previous inhibitory studies have focused on *meso*-DAP D-dehydrogenase.^{93, 95, 97-99} However, the potential antibacterial uses of these inhibitors are limited, as only a small number of bacterial species use *meso*-DAP D-dehydrogenase for the biosynthesis of lysine.¹⁰⁰

1.1.3.2.6 Inhibitory studies of *meso*-DAP decarboxylase

The last step of lysine biosynthesis requires the enzyme *meso*-DAP decarboxylase, which converts *meso*-DAP to L-lysine. This enzymatic step is a PLP-dependent process that stereospecifically targets the D-amino acid moiety of *meso*-DAP.¹⁰¹ This decarboxylation reaction has been shown to proceed with an inversion of configuration, whereas most PLP-dependent decarboxylases operate with retention of configuration.¹⁰² Recently, X-ray crystallographic studies^{18, 103} have provided a better understanding of the structural and mechanistic aspects of this enzyme. As *meso*-DAP decarboxylase is essential for most of the bacteria utilizing the DAP pathway, this enzyme is an attractive target for the development of antibacterial drugs.^{18, 104}

Similar to the studies of the other DAP enzymes, inhibitory studies of *meso*-DAP decarboxylase were also focused on the design of substrate analogues. In the mid 1980s, a number of DAP analogues were prepared and tested against this decarboxylase.⁶¹ Our group found the racemic hydrazine DAP analogue (**76**) to be the most potent inhibitor in this series of analogues, which showed 93% inhibition against the *meso*-DAP decarboxylase from *Bacillus sphaericus* at 0.4 mM.⁶¹ In another study, several unsaturated DAP analogues were synthesized and their biological effects were evaluated against both the enzyme and bacterial indicator strains.¹⁰⁵ Based on the inhibition studies of these analogues, racemic compound **77** showed the greatest potency (65% inhibition at 1 mM), but this compound lacks *in vivo* antibacterial activity. Analogues **78** (mixture of stereoisomers, *meso* and the racemate) did not show potent inhibition against

meso-DAP decarboxylase, but they showed good antibacterial activity with a minimum inhibitory concentration (MIC) of 2 $\mu\text{g/mL}$ and 4 $\mu\text{g/mL}$ against *Escherichia coli* and *Pseudomonas aeruginosa*, respectively.¹⁰⁵ These results indicate that the *meso*-DAP decarboxylase may not be the target for **78**. Subsequently, stereospecific syntheses of phosphonate analogues of DAP (**79**) have been achieved by our group.¹⁰⁶ Although they are weak inhibitors of *meso*-DAP decarboxylase, with the best reported IC_{50} value being 320 μM , they may lead to the design of better inhibitors in the future.

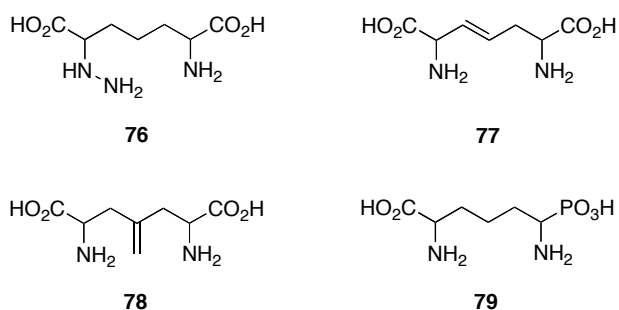


Figure 1-21. Inhibitors of *meso*-DAP decarboxylase

1.1.3.3 LL-DAP-AT as a target for potential antibiotics or herbicides

As mentioned previously, there is an urgent need for the development of new antibiotics against *Chlamydia*. Recently, it has been found that *Chlamydia* use LL-DAP-AT as a key enzyme in lysine biosynthesis. Thus, LL-DAP-AT may represent a good target for the development of novel antibiotics to specifically counter *Chlamydia*.⁴³ In certain cases, inhibitors of the enzymes involved in the DAP pathway have already shown promising antimicrobial activity.^{56, 57, 82} Thus,

the inhibitors directly targeting LL-DAP-AT could be used as antibiotics that are specific to *Chlamydia* infections,⁴² or used as algacides¹⁰⁷, or herbicides.⁶⁰ Substrate-based inhibitor design can be very effective, as shown in previous sections, but their *in vivo* antibiotic activity is often limited by their poor uptake into bacterial cells.⁵⁶ As an alternative approach to inhibitor discovery, a robotic high-throughput screening (HTS) approach was used in this study.

HTS has been widely used in the field of drug discovery in the last few decades.¹⁰⁸ Modern robotic technology can be used to identify potential drug leads from large libraries of drug-like compounds with great structural diversity in a short period of time. In general, to set up a HTS experiment, the important aspects are the development of a rapid and reliable assay platform, and obtaining a library of structurally diverse drug-like compounds. In this current study, an established enzymatic assay was adopted from an earlier study of LL-DAP-AT,²⁴ and a library of 29,201 drug-like compounds were obtained from a commercial source (ChemBridge Corporation).

The enzymatic assay used in this study is shown in **Figure 1-22**. Briefly, the assay involves monitoring the reverse of the transamination process, with α -ketoglutarate (**2**) used as an amino acceptor. Introduction of *o*-aminobenzaldehyde (OAB) (**80**) to the assay allows for the product (L-THDP, **22**) to be converted into a conveniently monitored chromophore **81**. By adding inhibitors to the assay, the rate of formation of **81** is expected to decrease. Based on these data, the evaluation of the potency of inhibitors against this target enzyme can be achieved.

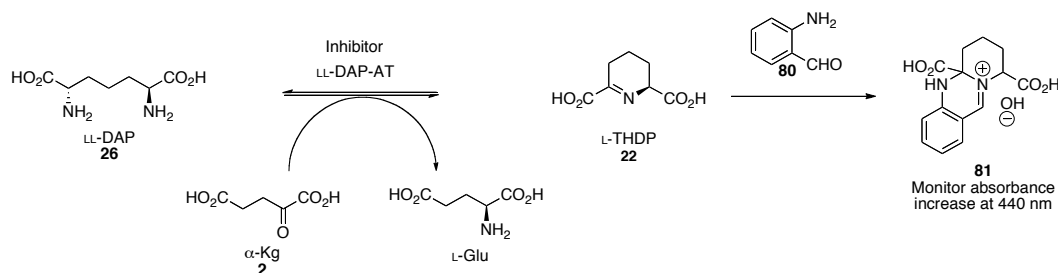


Figure 1-22. The enzymatic assay used in the inhibitory study of LL-DAP-AT²⁴

1.2 Project objectives

In the first part of this project, the structural features and mechanism of catalysis of LL-DAP-AT were studied by X-ray crystallography. The enzyme from *Arabidopsis thaliana* was cloned and overexpressed in *E. coli* with a C-terminal hexahistidine tag to aid in protein purification. The purified enzyme was then crystallized to obtain the X-ray crystal structure, allowing for the examination of the structural features of the enzyme. To further study the mechanism of this enzymatic transamination reaction, several analogues of intermediates were synthesized to trap the enzyme in a stable form to allow for study by X-ray crystallography.

The second part included inhibitory studies on LL-DAP-AT. Initially, a HTS approach was used to explore potential inhibitors to the target enzyme. After identifying lead compounds and potential pharmacophores, structure-activity relationship (SAR) studies of the hits were performed.

1.3 Results and discussion

1.3.1 Expression and purification of LL-DAP-AT

The cloning, overexpression, and purification of LL-DAP-AT was done by Dr. Marco J. van Belkum and Dr. Matthew D. Clay in our group.⁴⁰ The sequence of LL-DAP-AT from *A. thaliana* was used and the gene was optimized for bacterial codon usage. The vector pQE60 was used to overexpress LL-DAP-AT with a C-terminal hexa-histidine tag in *E. coli* at 25 °C. In a typical purification process, 5-10 mg of active LL-DAP-AT can be obtained from 1 L of culture.

The LL-DAP-AT from *Chlamydia trachomatis* was cloned, expressed, and purified in a very similar manner as the *A. thaliana* enzyme, also done by Dr. Marco J. van Belkum and Dr. Matthew D. Clay in our group.⁴³

1.3.2 X-ray crystallographic studies on LL-DAP-AT

1.3.2.1 First crystal structure of LL-DAP-AT from *Arabidopsis thaliana*

The first X-ray crystal structure of LL-DAP-AT from *A. thaliana* was obtained in collaboration with the research group of Dr. Michael James in the Department of Biochemistry at the University of Alberta.⁴⁰ The majority of the crystallization and crystal analysis was done by Dr. Nobuhiko Watanabe in the James group. The detailed crystallographic information can be found in a research paper published in the *Journal of Molecular Biology* in 2007.⁴⁰ In this section, only the overall significance of the crystallographic work will be discussed.

The overall structure of LL-DAP-AT is shown in **Figure 1-23**. The enzyme is a homodimer, and the two subunits are related by a non-crystallographic 2-fold

axis. Upon analysis of the crystal structure, LL-DAP-AT was found to belong to the type I fold PLP-dependent aminotransferases.^{109, 110} The two subunits interact tightly to form two active sites in the interfacial area, and each of the active sites is formed by residues from both subunits. In general, a large interacting area between the two subunits is expected for type I fold PLP-dependent aminotransferases,¹⁰⁹ and LL-DAP-AT is no exception. 21% of the total solvent accessible surface is involved in subunit interactions.⁴⁰ Within the interfacial surface, 65% of residues are non-polar and the remaining 35% of residues are polar, which indicates that the monomers interact mainly through hydrophobic interactions.⁴⁰ However, electrostatic interactions also play a significant role in the dimer interactions. In total, 54 hydrogen bonds and 15 salt bridges are observed in the crystal structure.⁴⁰ Furthermore, the *N*-terminal “arm” also contributes significantly to the dimer stability, forming 14 hydrogen bonds and two salt bridges with the neighbouring subunit.⁴⁰

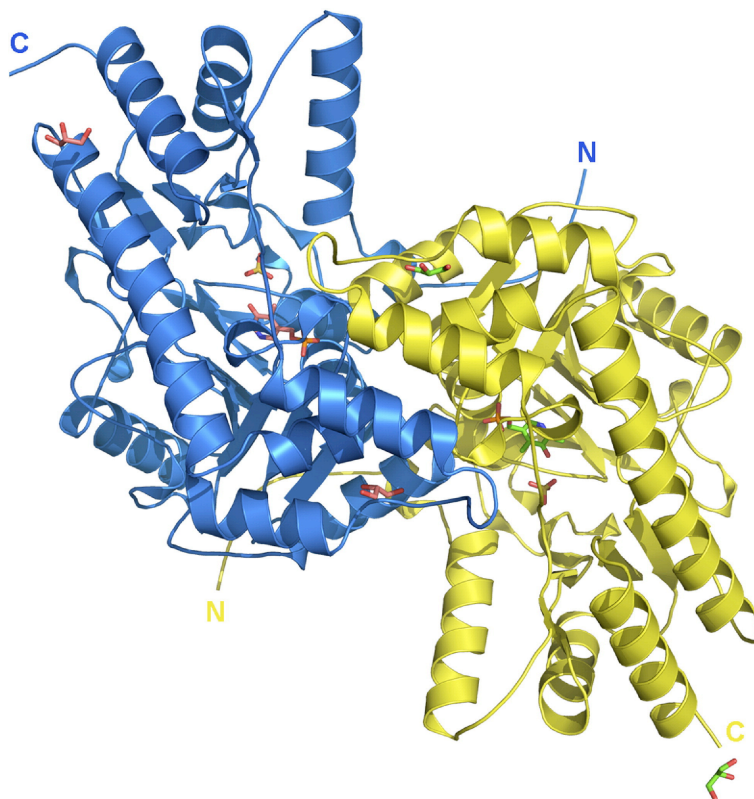


Figure 1-23. Overall structure of the LL-DAP-AT homodimer in a cartoon representation. Subunit A is labelled in blue and B is labelled in yellow. PLP, sulfate, and glycerol are shown in stick form⁴⁰

This X-ray crystallographic study confirmed that LL-DAP-AT is a PLP-dependent aminotransferase,⁴⁰ which had been proposed in earlier studies based on gene sequencing.²⁴ Stereo diagrams of the PLP binding site are shown in **Figure 1-24.**⁴⁰

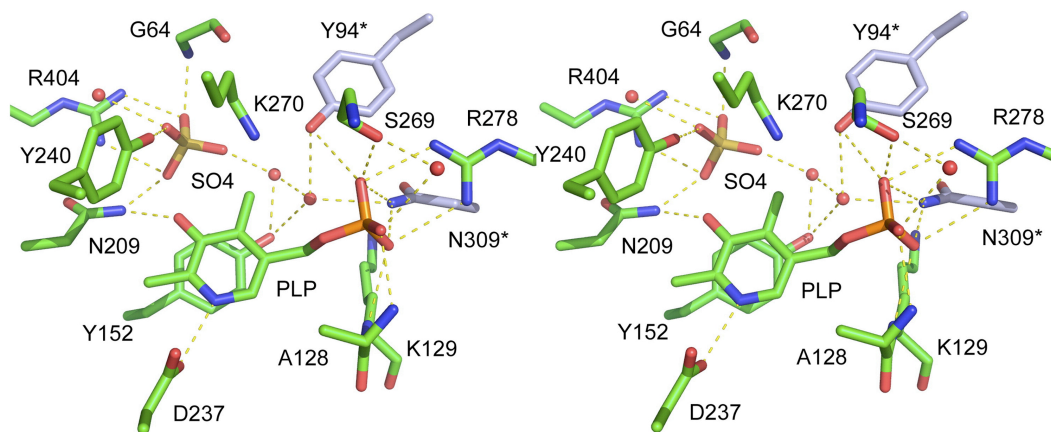


Figure 1-24. The stereo diagram of PLP binding site of LL-DAP-AT. The active site residues' side chains, PLP, and a sulfate ion are shown in stick form, the residues coloured in grey are from the neighbouring subunit, the red spheres represent water molecules, and the hydrogen bonds are shown as yellow dotted lines. This picture was adopted from Watanabe *et al.*⁴⁰

As shown in the active site diagram, the PLP molecule is extensively bound in the active site by hydrogen bonds and salt bridges, in addition to the aromatic π -stacking interaction between the pyridine ring of PLP and Tyr152. The hydroxyl group of PLP forms hydrogen bonds to Asn209, Tyr240, and the sulfate ion. The side chain carboxylate of Asp237 forms a hydrogen bond to the positively charged nitrogen in the pyridinium ring of PLP. Furthermore, the phosphate moiety of PLP interacts with residues in the active site via hydrogen bonds (one water molecule, Ala128, Lys129, Ser269, Tyr94*, and Asn309*) and a salt bridge to Arg278. Notably, Tyr94* and Asn309* are from the neighbouring subunit. The sulfate ion (from the buffer used in crystallization) shown in yellow is bound by a salt bridge to Arg404, in addition to hydrogen bonds with several residues and two water molecules. The sulfate ion is likely mimicking an LL-

DAP-AT substrate, either DAP or glutamate, which will be discussed in later sections of this thesis.

Interestingly, the PLP molecule was expected to form an internal aldimine with Lys270. However, the covalent bond of the Schiff base is not observed in the crystal structure. A potential reason is that the high dosage of radiation could damage the Schiff base imine bond as has been seen previously.¹¹¹ Nevertheless, the side chain amino group of Lys270 is pointing towards the C4' position of PLP, which suggests the existence of a formal imine bond.

1.3.2.2 Mechanism of catalysis of LL-DAP-AT from *A. thaliana*

In order to study the mechanism of this enzymatic transamination reaction, an X-ray crystallographic approach was used. As confirmed in the earlier study,⁴⁰ this transamination reaction is a PLP-dependent process, and it has been suggested that the enzyme uses glutamate as an amino donor.²⁴ To trap the enzyme during catalysis, a substrate mimic was used.

The typical reaction mechanism of PLP-dependent transamination reactions is shown in **Figure 1-25**. Initially, PLP forms an internal aldimine (**81**) with a lysine residue in the active site of the aminotransferase. Upon binding with the amino donor, normally L-glutamate, L-aspartic acid, or L-alanine, an external aldimine (**82**) is formed. Proton transfer leads to another imine intermediate (**83**), followed by hydrolysis, which forms pyridoxamine-5'-phosphate (PMP, **84**) with the release of the keto side product (*e.g.*, α -ketoglutarate). Upon binding of the substrates, which acts as an amino acceptor, PMP attacks the substrate to form another imine intermediate (**85**). Tautomerization gives the external aldimine **86**.

After transamination, the internal aldimine is formed again with the release of the amino product.

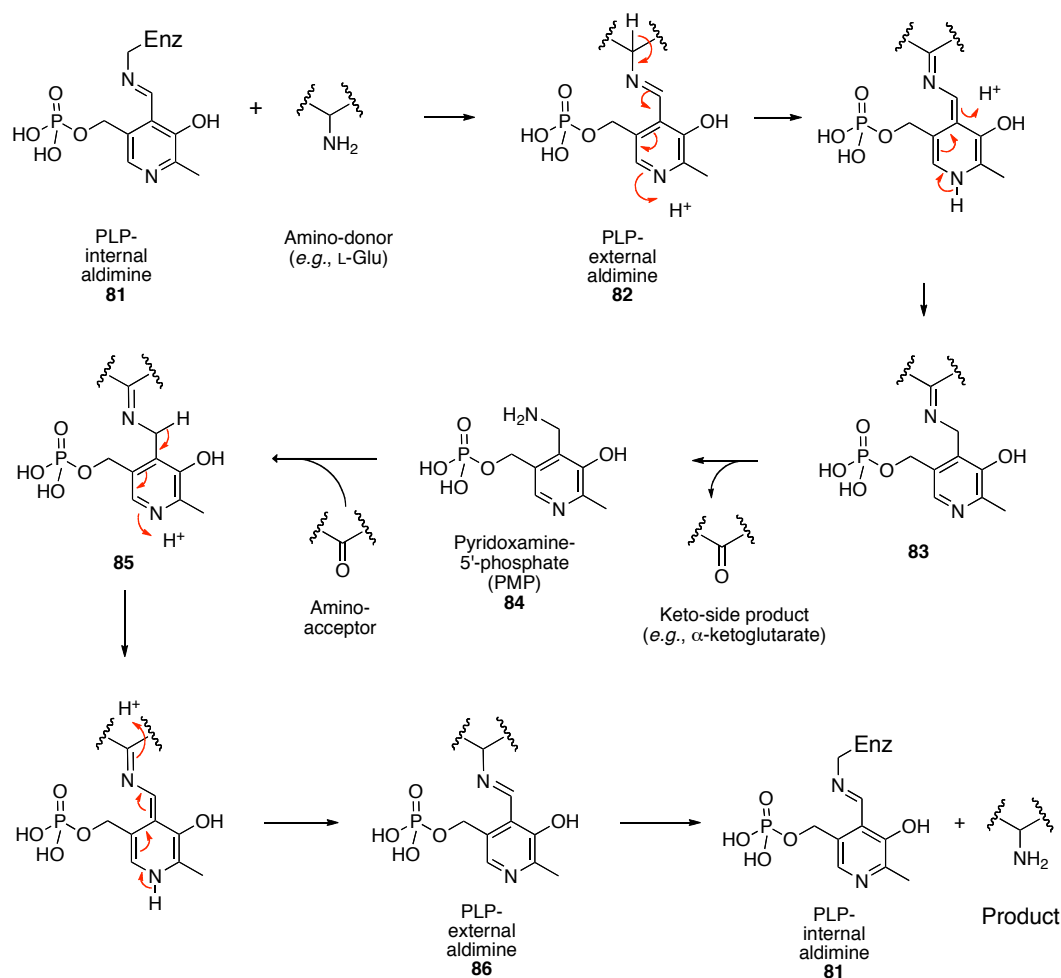


Figure 1-25. Typical proposed mechanism of PLP-dependent transamination reactions

With this knowledge of the transamination reaction mechanism, several analogues that mimic intermediates were designed and prepared by former postdoctoral fellow in our group, Dr. Matthew D. Clay.¹¹² As mentioned previously, L-glutamate has to bind to the enzyme and react with the internal PLP-

enzyme aldimine (**81**) to form the first external aldimine (**87**). To observe binding, a mimic of this intermediate may be used to trap the enzyme. Reducing the imine bond of **87** to a C-N single bond, compound **88** would closely resemble intermediate **87** while preventing any further transformation. Similarly, to mimic the external PLP-LL-DAP aldimine **89**, analogue **90** was prepared. Another interesting question is whether THDP or its ring open form is the true substrate of this enzymatic transamination process. Assuming that THDP is the true substrate, then PMP should react directly with THDP to form adduct **91**. Removing the ring nitrogen, as in analogue **92**, closely resembles the adduct **91**, while preventing any further transformations.

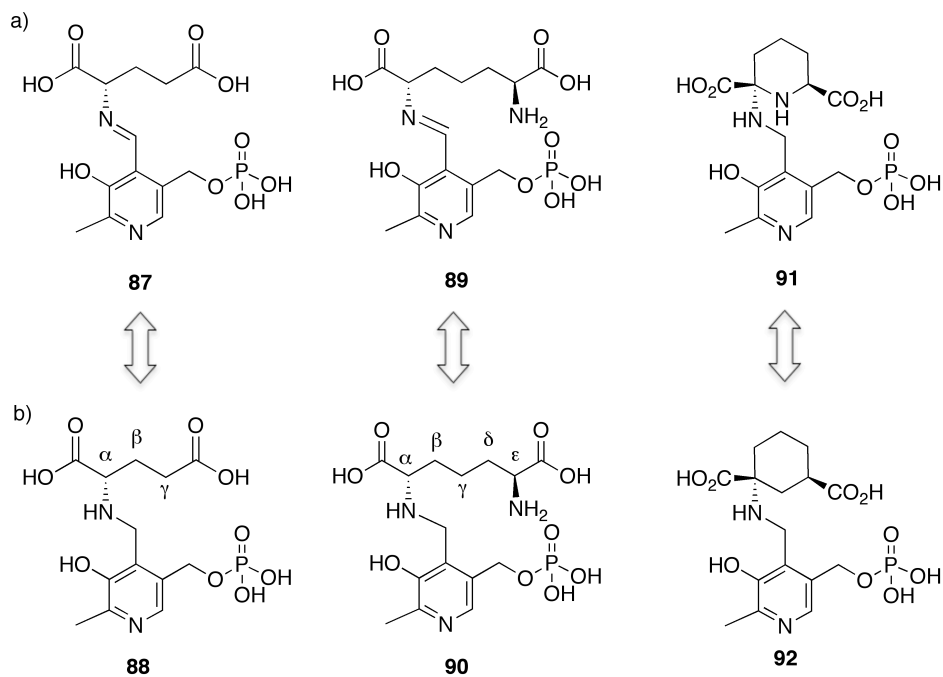


Figure 1-26. a) Substrate-PLP adducts; b) Analogues of substrate-PLP adducts

These analogues (**88**, **90**, and **92**) were initially prepared by Dr. Matthew D. Clay,¹¹² and **88** and **90** were resynthesized for the present study. Detailed procedures for the preparation of **88** and **90** by reductive amination are described in **Chapter 3**.

After synthesis of intermediate analogues, they were incorporated into the enzyme. First, PLP was removed from the enzyme by addition of phenylhydrazine, followed by dialysis to obtain the apo-enzyme. The analogues were then introduced to the apo-enzyme and purified by dialysis. Following incorporation of the analogues, the enzyme was crystallized by the hanging-drop vapour-diffusion method. Enzyme crystals were obtained and analyzed by Dr. Nobuhiko Watanabe in the group of Dr. Michael James.¹¹² Crystal structures of LL-DAP-AT bound to the analogues PLP-Glu (**88**) and PLP-DAP (**90**) were obtained. No significant conformational changes of the enzyme upon binding of the analogues were observed, which indicates that the analogues indeed resemble the intermediates. In the case of analogue **92**, only the apo-enzyme was crystallized suggesting that analogue **92** is unable to bind to the enzyme active site.

1.3.2.2.1 Crystallographic study of the PLP-Glu analogue bound enzyme

The active site structure of PLP-Glu analogue (**88**) bound to LL-DAP-AT is shown in **Figure 1-27**. Compared to the native LL-DAP-AT structure, the PLP portion of the analogue is essentially bound in the active site in the same way as free PLP is bound. The α -carboxylate group of glutamate occupies the position where the sulfate ion is located in the native enzyme structure. The α -carboxylate

group of glutamate is bound to the active site primarily through a salt bridge to the guanidinium group of Arg404, in addition to hydrogen bonds with Asn209, and Gly64. The distal carboxylate of the glutamate is recognized by three well-conserved residues, Tyr37, Tyr152, and Lys129, through hydrogen bonding. Lys270 points towards the reduced imine bond. As the imine bond has been reduced to a single bond, the enzyme is unable to catalyze the transamination.

Although binding of intermediate analogue **88** did not result in any significant backbone conformational changes, there were some conformational changes in the active site residues to accommodate the glutamate moiety. An overlaid diagram of the native enzyme and the enzyme-bound PLP-Glu analogue is shown in **Figure 1-27b**. Tyrosine residues Tyr152 and Tyr364 show the most significant conformational changes. Tyr152 shifts toward the active site to form a hydrogen bond with the distal carboxylate group of the glutamate. Movement also allows for a better aromatic π -stacking interaction between the phenol group of Tyr152 and the pyridine ring of PLP. Tyr364 was pointing away from the active site in the native enzyme structure, but in the bound structure, the side chain shifts about 90° toward the active site.

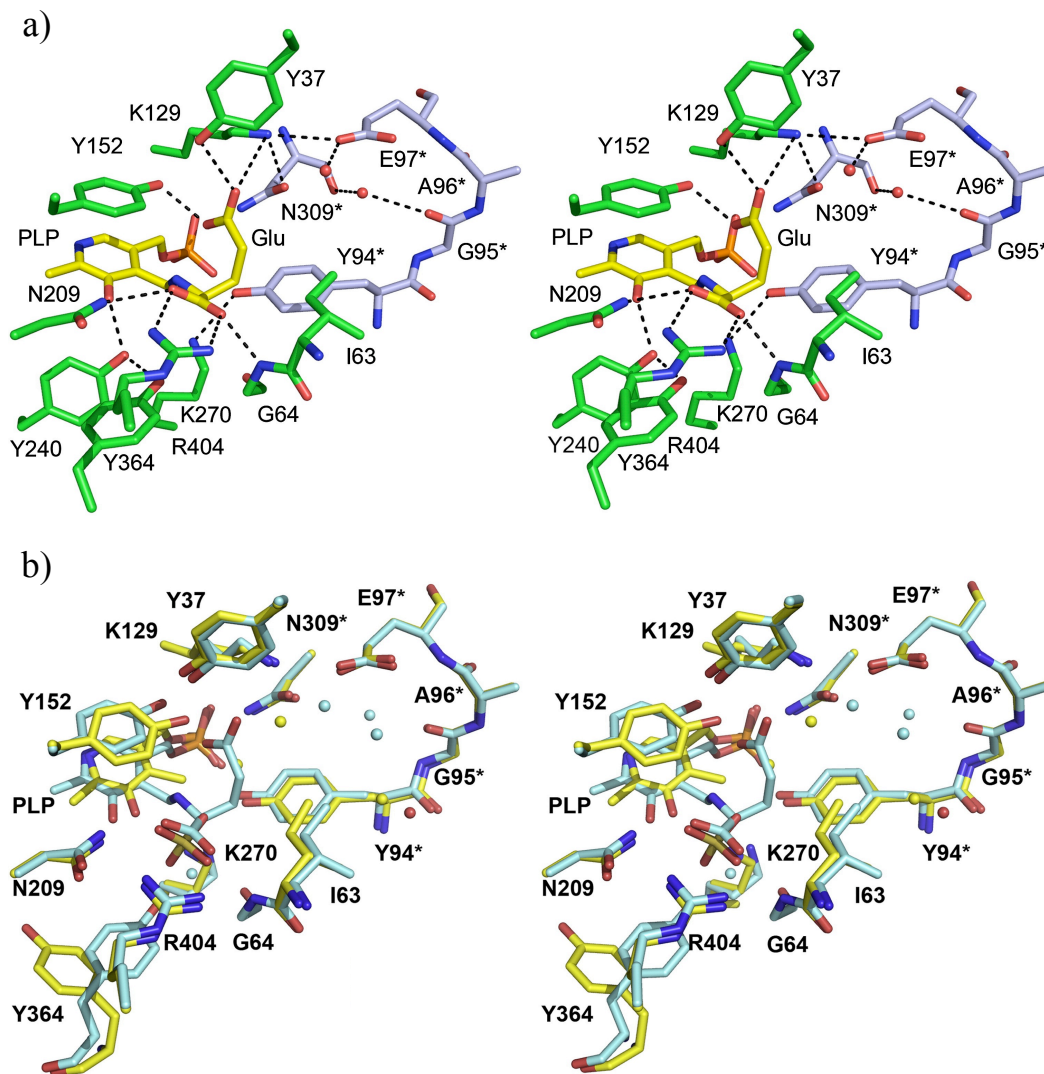


Figure 1-27. The stereo diagram of the structures of the PLP-Glu analogue bound to LL-DAP-AT. a) Active site residues and analogue **88** are shown in stick form. Residues from subunit A and B, and analogue **88** are coloured in green, grey, and yellow, respectively. b) Overlaid structure, residues from the native enzyme and the enzyme bound to the PLP-Glu analogue are coloured in yellow and light blue, respectively¹¹²

1.3.2.2.2 Crystallographic studies of LL-DAP-AT bound to the PLP-DAP analogue

The PLP-DAP analogue **90** bound to the enzyme active site in a very similar fashion as PLP-Glu (**Figure 1-28**). The PLP portion of the analogue is recognized in a nearly identical way as is the PLP-Glu analogue complex. Interestingly, carboxylate groups are also recognized in a very similar way, even though the backbone of DAP is two carbon atoms longer than glutamate. The α -carboxylate of the DAP moiety binds in nearly the same way as the α -carboxylate of the PLP-Glu analogue, via a salt bridge to Arg404 and hydrogen bonds to Asn209 and Gly64. The ϵ -carboxylate is stabilized by hydrogen bonds to Tyr37, Tyr152, and Lys129. The ϵ -amino group is stereospecifically held in place by a direct hydrogen bond to Asn309*, as well as water mediated hydrogen bonds to Glu97*, Gly95*, and Asn309*. The LL-DAP-AT from *A. thaliana* is stereospecific for LL-DAP, while the corresponding enzyme from *Chlamydia*, can also accept *meso*-DAP as substrate. This stereospecific recognition is partly accomplished by the side chain Tyr94*, which is located near the ϵ -amino group to provide additional stability through an electrostatic interaction between the positively charged amino group of DAP and the aromatic ring of Tyr94*. Such an interaction would be unfavourable in the case of *meso*-DAP.

In **Figure 1-28b**, an overlaid diagram of native LL-DAP-AT, LL-DAP-AT bound to the PLP-Glu analogue, and LL-DAP-AT bound to the PLP-DAP analogue is shown. The structure of LL-DAP-AT bound to the PLP-Glu analogue and the PLP-DAP analogue are very similar, and both analogues adopt a V-

shaped backbone configuration to accommodate the analogues into the active site. The only difference is the side chain of Ile63, which shifts away from the active site in the PLP-DAP bound enzyme, resulting in a larger pocket to accommodate the DAP moiety.

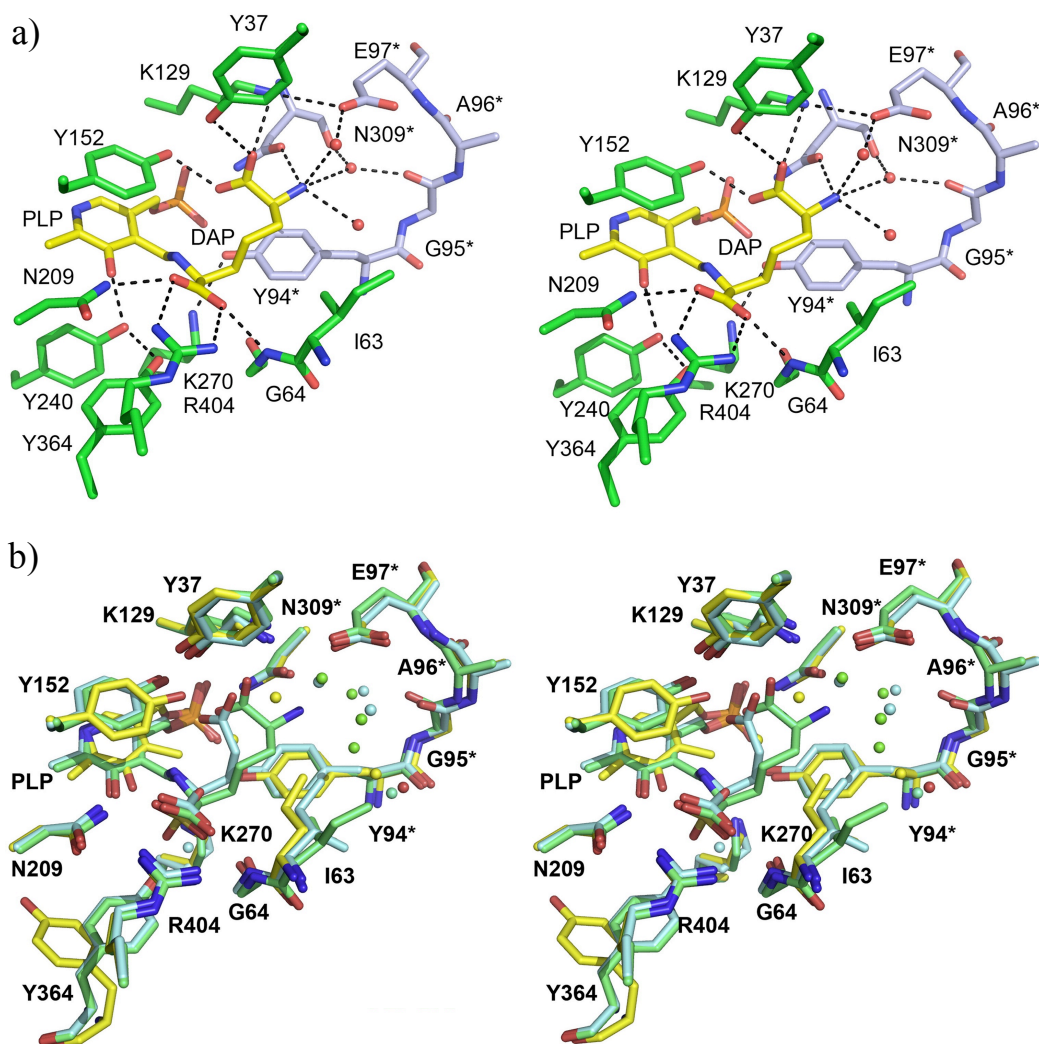


Figure 1-28. The stereo diagram of the structure of the PLP-DAP analogue bound to LL-DAP-AT. a) Active site residues and the PLP-DAP analogue are shown in stick form. Residues from subunit A, B, and the analogue are coloured green, grey, and yellow, respectively. b) Overlaid structure; residues from native enzyme, PLP-Glu analogue, and PLP-DAP bound enzymes are coloured in yellow, light blue, and emerald green, respectively¹¹²

1.3.2.2.3 Crystallographic studies of mutant enzymes (K270N and K270Q)

The intermediate analogues **88** and **90** are stable towards enzymatic transformations and closely resemble the binding properties of the intermediates. However, they are not fully representative of the true intermediate in the enzymatic process. For instance, the imine bonds have been reduced, which leads to a greater mobility of the molecule, and may cause conformational changes in the active site. To address this, a mutagenesis approach was used to obtain a catalytically inactive enzyme. As mentioned previously, Lys270 was believed to be the residue that forms an internal aldimine with PLP. This lysine residue was mutated to asparagine or glutamine. With these mutants, natural substrates glutamate and LL-DAP can form the true external aldimine with PLP (**87** and **89**) in the active site. Following crystallization, structures were obtained of the K270N mutant with PLP (holo-enzyme) and glutamate. Additionally, crystals of the K270Q mutant bound to LL-DAP and glutamate were also obtained. The crystallization and crystal structure analysis was again performed by Dr. Nobuhiko Watanabe.¹¹² Examining the crystal structures, the mutant enzymes are shown to be very structurally similar to the wild-type enzyme. The structure of the K270N mutant complexed with glutamate and LL-DAP is shown in **Figure 1-29a**, with the structure of the external aldimine shown in **Figure 1-29b**. The binding properties of natural substrates are shown to be very similar to that of substrate analogues, despite the replacement of Lys270 with an asparagine residue and the double bond between the C4' of PLP and the nitrogen of the α -amino group of glutamate or LL-DAP.

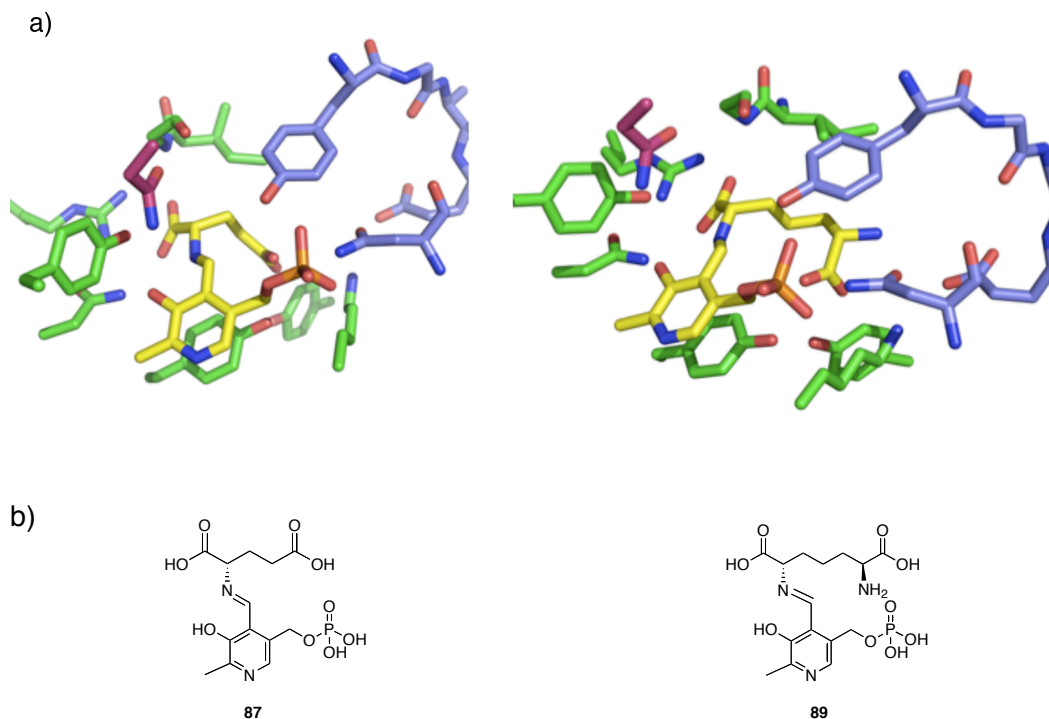


Figure 1-29. K270N mutant of LL-DAP-AT complexed with Glu (left) and LL-DAP (right). a) Active site structure of K270N complexed to Glu (left) and LL-DAP (right); b) Structures of the true external aldimines

Based on X-ray crystallography, the proposed mechanism of LL-DAP-AT most likely follows the general mechanism shown in **Figure 1-25**. Specifically, PLP first forms an internal aldimine with Lys270, glutamate then forms an external aldimine **87** with PLP, which then forms PMP (**84**) following release of α -ketoglutarate (**2**). Substrate THDP is then likely to be hydrolyzed to give the open form, which then binds to the enzyme and reacts with PMP. Tautomerization gives the other external aldimine **89**. Transamination with the active site Lys270 reforms the internal aldimine with the release of the product LL-DAP-AT, allowing for the catalytic cycle to continue.

1.3.2.3 X-ray crystallographic study of LL-DAP-AT from *Chlamydia trachomatis*

In a separate study, LL-DAP-AT from *Chlamydia trachomatis* was cloned, overexpressed, and purified by our group. The isolation of the enzyme was done by Dr. Marco J. van Belkum and Dr. Matthew D. Clay.⁴³ The crystallization and analysis of the diffraction pattern were done by Dr. Nobuhiko Watanabe. A similar approach was used, and we prepared substrate analogues and attempted to incorporate them into the enzyme. At this point, only the apo-enzyme and holo-enzyme have been crystallized.

Based on comparison of the primary sequences of the *Arabidopsis* enzyme with the *Chlamydia* enzyme, more than 40% of their amino acid residues are identical. The catalytic mechanism and the active site residues are highly conserved between these enzymes. However, the substrate recognition appears to be somewhat different.⁴² The *Arabidopsis* enzyme has very strict substrate specificity; in the reverse reaction, only LL-DAP can be recognized as an amino donor. When *meso*-DAP is fed to the enzyme, no turnover is observed. In contrast, the *Chlamydia* enzyme is able to catalyze the transamination reaction using *meso*-DAP as a substrate almost as efficiently as LL-DAP.^{42, 43} To explore this difference in substrate recognition between the two enzymes, X-ray crystallography was applied.

A stereo diagram of the crystal structure of apo-LL-DAP-AT from *Chlamydia trachomatis* is shown in **Figure 1-30**. The enzyme has a similar three-dimensional structure compared to the *Arabidopsis* LL-DAP-AT, with both

existing as homodimers. In each monomer, there is a large domain (LD) and a small domain (SD). The two LDs make up the PLP binding moiety, which forms two active sites for catalysis of the transamination reaction. This enzyme is also a typical type I fold PLP-dependent aminotransferase.⁴³

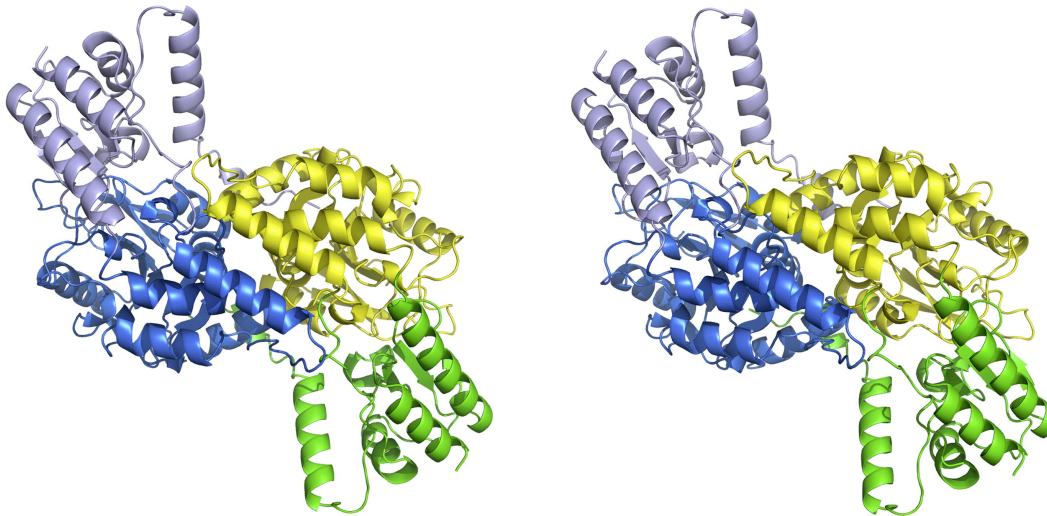


Figure 1-30. Stereo diagram of apo-LL-DAP-AT from *Chlamydia trachomatis*. The large domains (LDs) of each subunit are coloured blue and yellow, and the small domains (SDs) are coloured grey and green⁴³

In order to better understand the PLP-binding properties, PLP-bound holo-LL-DAP-AT was also crystallized. The active site structure is shown in **Figure 1-31**. In this crystal structure, it is clear that PLP is bound to Lys236 through a covalent bond via a Schiff base linkage.⁴³ Very similar to *Arabidopsis* LL-DAP-AT, the pyridine ring of PLP is stabilized by aromatic stacking with Tyr128 and hydrogen bonding to Tyr205, Asn174, and Asp202. The phosphate group of PLP is stabilized by hydrogen-bonding interactions with Ser233, Ser235, Asn275*, Ala104, and Lys105. There is a significant difference in the PLP binding in

Arabidopsis LL-DAP-AT. In this case, phosphate moiety forms a salt bridge with the guanidinium group of Arg278.⁴⁰ In the *Chlamydia* enzyme, Arg244 is not pointing toward the phosphate group of PLP. Instead, it forms hydrogen bonds with the neighbouring subunit residue Asn275*, which provides a contribution to the dimeric interactions between the subunits.⁴³

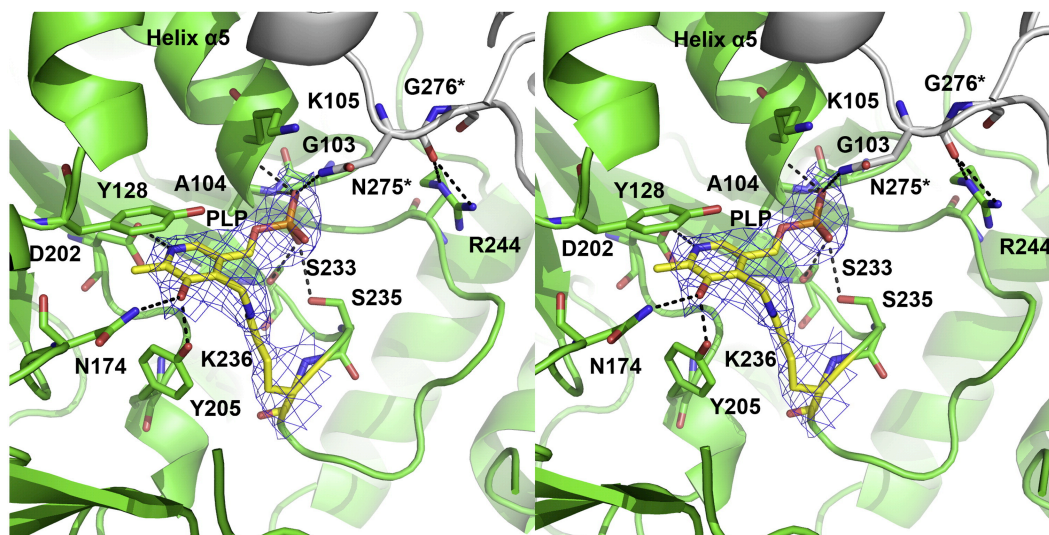


Figure 1-31. Stereo diagram of the structure of the PLP binding site of *Chlamydia* LL-DAP-AT⁴³

As mentioned previously, the substrate specificity for *Chlamydia* LL-DAP-AT is broader than that of the *Arabidopsis* enzyme. Overlap of the structures of the two enzymes reveals a potential reason for this disparity in substrate specificity. Each of the domains are aligned individually, and the superposition of the domain structures between the two enzymes are shown in **Figure 1-32**. By comparison, each of the domains is well conserved in the secondary structural elements.⁴³

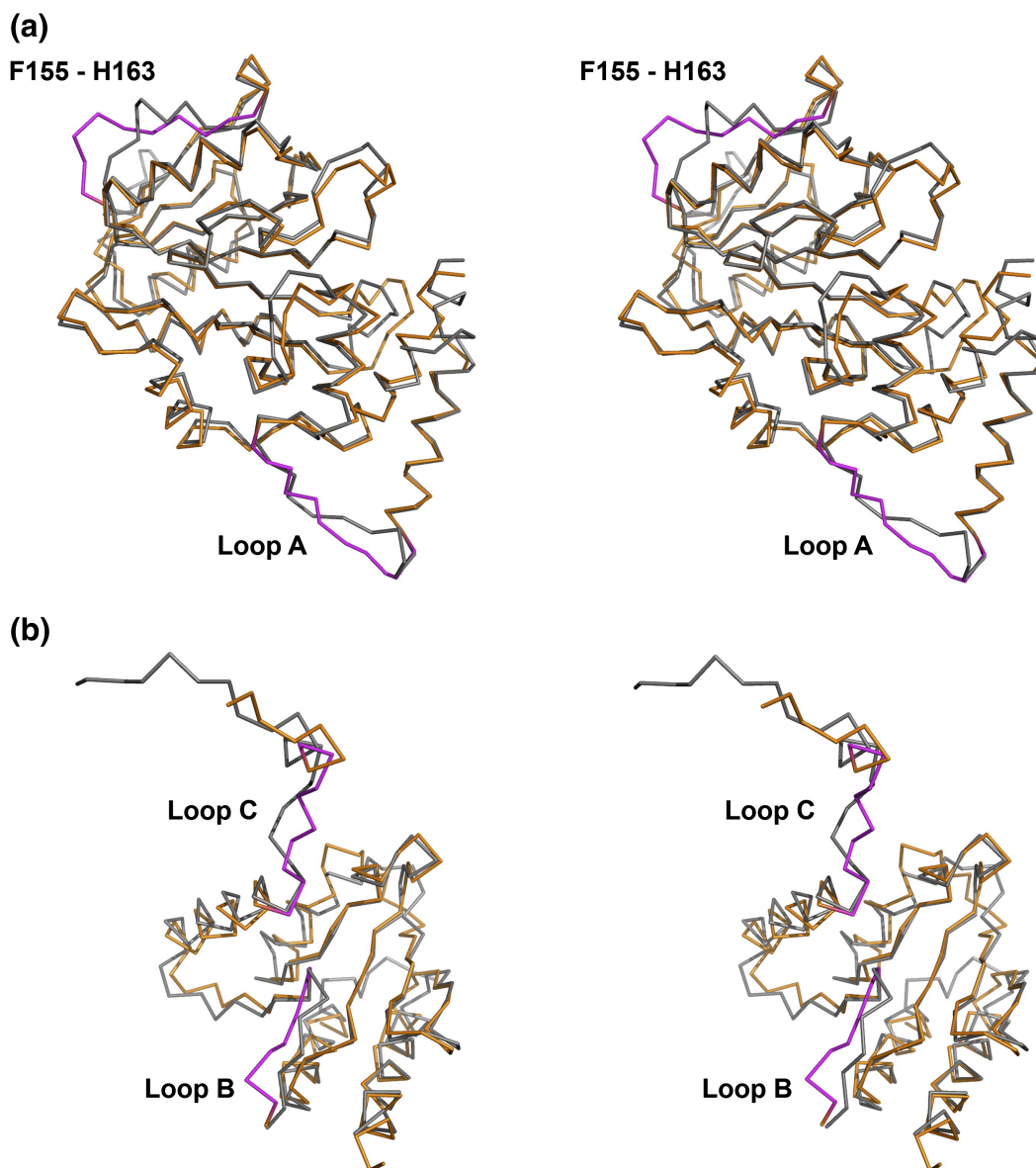


Figure 1-32. The domain alignment structures between *Chlamydia* and *Arabidopsis* LL-DAP-AT. a) Superposition of the large domains (LDs) (*Chlamydia* enzyme in orange; *Arabidopsis* enzyme in grey); b) Superposition of the small domains (SDs) (*Chlamydia* enzyme in orange; *Arabidopsis* enzyme in grey). The flexible loops (A, B, and C) of *Chlamydia* LL-DAP-AT are coloured magenta⁴³

The entire structures of the two enzymes were then aligned to compare the overall geometries of the enzymes. In order to obtain the differences in the

relative positions of each domain, only the large domain (LD) is used for the alignment of the entire enzyme. As shown in **Figure 1-33a**, after the LDs are aligned, there is an average 9.5 Å difference between the small domains (SDs) of the two enzymes. The *Chlamydia* LL-DAP-AT is shifted away from the dimer interface and adopts an open conformation relative to the closed conformation of LL-DAP-AT from *A. thaliana*. This movement of the SD appears to affect the conformation of the active site. As shown in **Figure 1-33b**, the substrate binding residues are well conserved between the two enzymes. However, the residues that coordinate to the α -carboxylate group of the DAP substrate, Asn174 and Arg369, have moved approximately 2.0 Å from the active site. Moreover, Tyr128 and Tyr14 (disordered), which are involved in binding to the distal carboxylate group of DAP show different conformations as well.⁴³

In addition, the open conformation of the overall structure has also caused disorder in the active site loops (loops A, B, and C). Since these loops are directly involved in the substrate binding, any conformational changes are significant with regards to the substrate recognition.⁴³

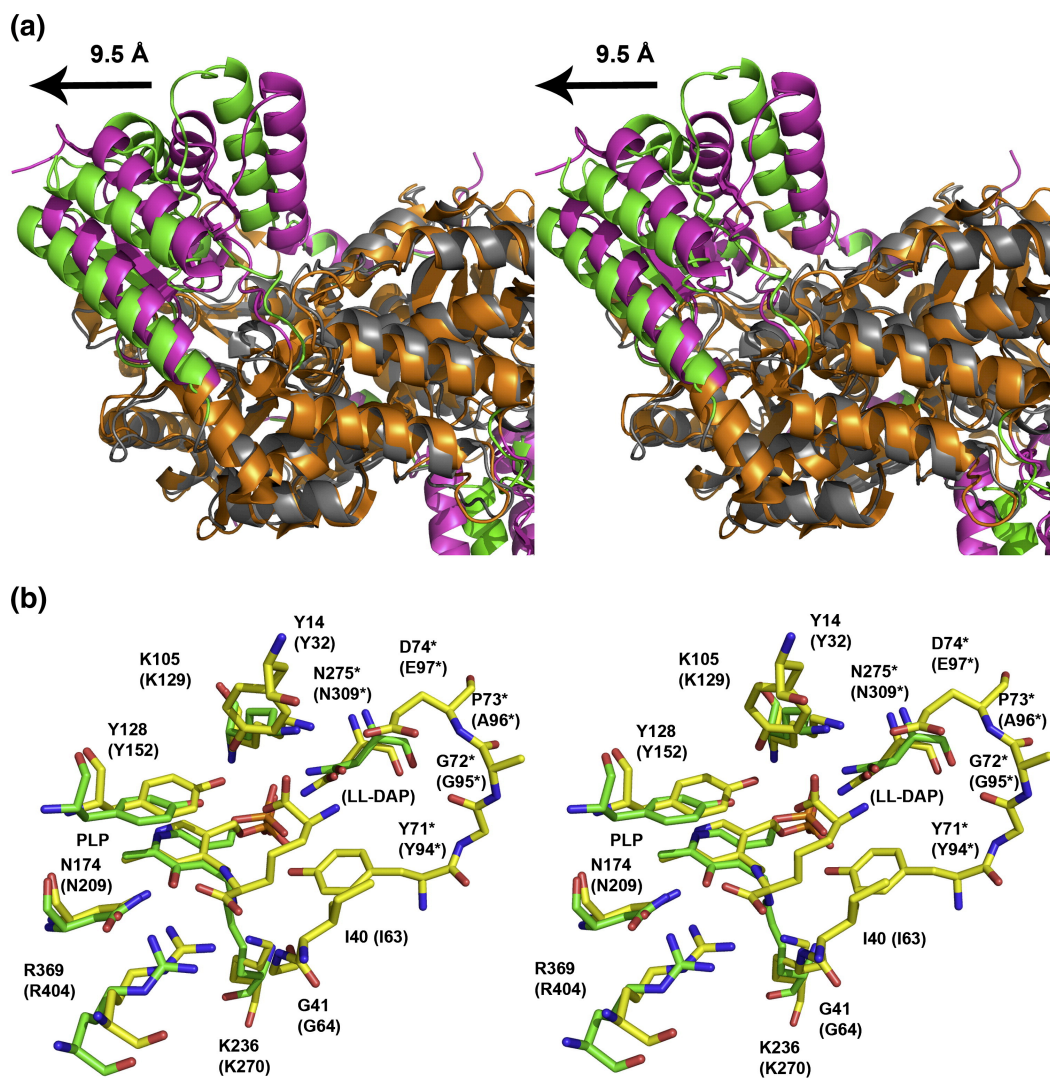


Figure 1-33. The superposition of the structures of LL-DAP-AT from *C. trachomatis* and *A. thaliana*. a) Displacement of the SD (9.5 Å) of LL-DAP-AT from *C. trachomatis* is indicated by the black arrow. The LDs of the *Chlamydia* and *Arabidopsis* enzymes are coloured gray and orange, respectively. The SDs of the *Chlamydia* and *Arabidopsis* enzymes are coloured magenta and green, respectively. b) The overlaid active site structures of *Chlamydia* (green) and *Arabidopsis* (yellow) enzymes. Residue names in brackets are from *Arabidopsis* LL-DAP-AT. Residues from loops A and B of the *Chlamydia* enzyme are not shown, as they are disordered⁴³

Based on this structural evidence, LL-DAP-AT from *C. trachomatis* adopts an open conformation. Upon binding with the substrate, the enzyme undergoes a

significant closing movement. As the SD closes toward the active site, residues such as Asn174 and Arg369 move closer to the substrate and become positioned for the correct coordination to substrates. A similar domain opening/closing mechanism has been observed in several other type I fold PLP-dependent aminotransferases, such as aspartate aminotransferase (AspAT).¹¹³⁻¹¹⁵ Such large movements (9.5 Å) observed in *Chlamydia* LL-DAP-AT are rare when compared to the other similar type I fold PLP-dependent aminotransferase, which move approximately 3.0-4.0 Å.¹¹⁶ This large flexibility can potentially explain the larger substrate specificity of LL-DAP-AT from *C. trachomatis*. In the future, studies of the closed conformation of *Chlamydia* LL-DAP-AT with various substrates, or characterizing the LL-DAP-AT from different species, may provide better understanding of the mechanism of this novel aminotransferase.

1.3.3 High-throughput screening of a 29,201 compound library against LL-DAP-AT

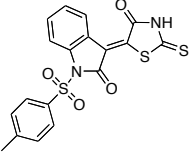
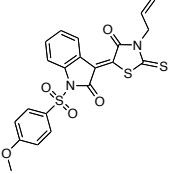
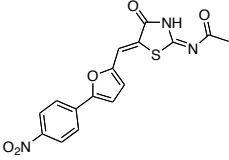
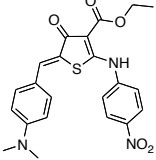
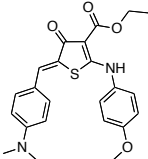
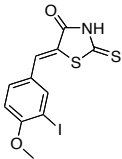
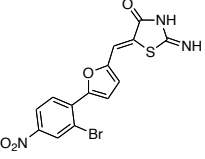
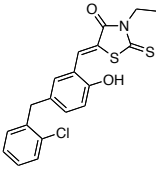
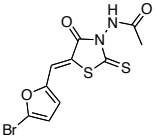
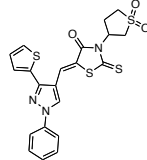
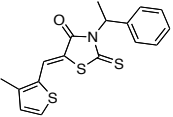
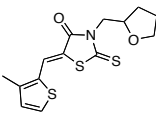
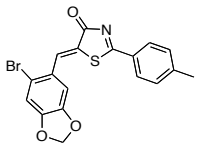
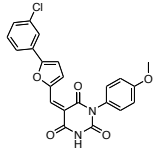
As discussed previously, a high-throughput screening (HTS) approach was initially used for the discovery of new inhibitors of LL-DAP-AT. Our inhibitor screening and structure-activity relationship (SAR) studies are based on LL-DAP-AT from *A. thaliana*. Although the *Chlamydia* enzyme has broader substrate specificity than the *Arabidopsis* enzyme, the plant enzyme still resembles the bacterial enzyme in term of inhibitory studies. Studies on the *Arabidopsis* enzyme may act as a model for the development of novel antibiotics for *Chlamydia*. Furthermore, potent inhibitors against *Arabidopsis* LL-DAP-AT may be used as herbicides.

In this study,⁶⁰ a library of 29,201 accessible drug-like compounds were robotically screened against LL-DAP-AT for inhibition. IC₅₀ determinations have been done for the best 46 inhibitors. Finally, preliminary SAR studies were done based on modification of two lead structures, an arylhydrazide and a rhodanine.

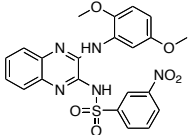
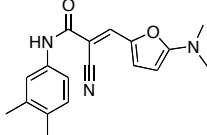
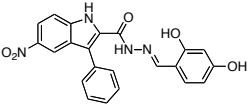
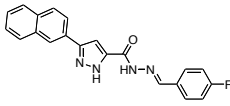
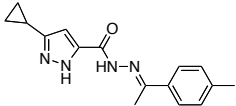
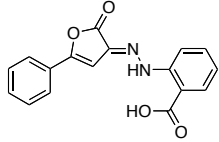
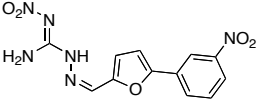
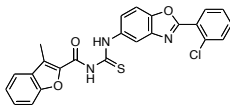
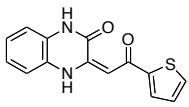
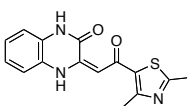
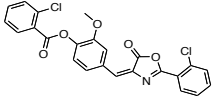
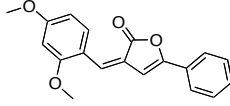
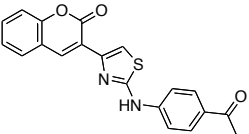
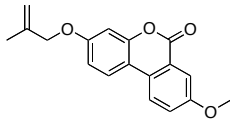
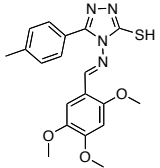
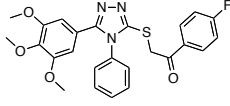
The library of compounds was obtained from ChemBridge Corporation. A known assay based on *o*-aminobenzaldehyde (**80**)²⁴ (**Figure 1-22**) was used for the screening and SAR studies. A brief description of this assay was mentioned in previous sections of this thesis. Detailed experimental procedures are provided in **Chapter 3**. In the robotic screening, the percentage inhibition was determined at a 10 μ M level for all of the compounds in the library (an estimated molecular weight of 500 g/mol was assumed for each compound when calculating the concentration in this screening).

Following the robotic screening of the 29,201 candidates, the top 46 compounds were selected for further manual testing and IC₅₀ determination. These 46 compounds showed inhibition greater than 13% at 10 μ M by both robotic and manual testing. The results of the robotic screening and manual testing of these compounds are presented in **Table 1-1**.

Table 1-1. Inhibition results of the top 46 compounds against LL-DAP-AT from HTS study

Entry	Structure	% Inhibition ^a / IC ₅₀ (μM) ^b	Entry	Structure	% Inhibition ^a / IC ₅₀ (μM) ^b
93		25	94		18
		70			194
95		52	96		19
		78			141
97		22	98		29
		> 200			180
99		13	100		13
		85			46
101		13	102		13
		41 ^c			117
103		13	104		14
		127			> 200
105		13	106		20
		130			42

107		20 45 ^c	108		17 37
109		14 65	110		18 52
111		16 >200	112		13 >200
113		28 99	114		45 33 ^d
115		35 75	116		33 69
117		48 121	118		20 62
119		15 25 ^c	120		16 164
121		17 >200	122		33 5 ^c

123		13	124		14
		153			>200
125		15	126		14
		45			161
127		14	128		16
		>200			39 ^c
129		13	130		19
		>200			83
131		15	132		18
		31			56
133		30	134		14
		81			159
135		16	136		25
		>200			>200
137		18	138		14
		>200			>200

^a Robotic screening at inhibitor concentration of 10 μ M

^b Manually tested for IC₅₀ value

^c Time-independent inhibitor

^d Time-dependent inhibitor

Within these 46 compounds, the best inhibitor was compound **122**, with an IC_{50} value of 5 μ M, which showed time-independent inhibition. In addition, these 46 compounds can be organized into four different groups. The first group (compounds **93 – 105**) contains a rhodanine core structure. Compounds **106 – 113** feature a barbiturate core structure, whereas compounds **114 – 121** are thiobarbiturate derivatives. The remaining compounds do not belong to any of the previous categories, but exhibit reasonable activity against LL-DAP-AT. The large number of rhodanine, barbiturate, and thiobarbiturate structures are suggestive of potential pharmacophores (**Figure 1-34**). For instance, within the 29,201 compounds, approximately 1,000 compounds (~ 3 %) possessed a barbiturate or thiobarbiturate ring, whereas 16 of the top 46 compounds (~ 35 %) contained one of these groups.

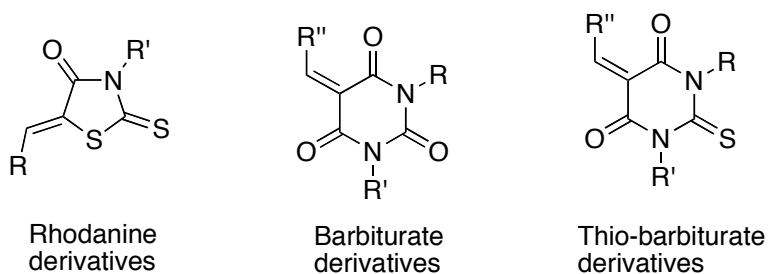


Figure 1-34. The three potential pharmacophore structures identified from the HTS

Following the identification of these potential pharmacophores, one or two compounds were selected from each of the four groups to test the time dependence of inhibition. To distinguish time-dependent from time-independent inhibition, the inhibitors were preincubated with enzyme for varying lengths of

time before adding substrate and measuring activity. Irreversible or slow-binding inhibitors will inactivate enzyme more if they are kept together for a longer time. Rapid reversible inhibitors will inhibit to the same level, regardless of the length of preincubation time. Compound **101**, a rhodanine derivative, showed time-independent inhibition, suggesting that the type of inhibition is one of the following: competitive, uncompetitive, or non-competitive inhibition. Compound **107**, a barbiturate derivative, also showed time-independent inhibition. Compound **114**, a thiobarbiturate derivative, showed time-dependent inhibition, suggesting that the type of inhibition belongs to one of the following categories: affinity label, mechanism-based irreversible inactivation, or slow-binding inhibition. Another thiobarbiturate derivative, compound **119**, showed time-independent inhibition. Within the remaining candidates, compounds **122** and **128** were selected, and both are shown to be time-independent inhibitors.

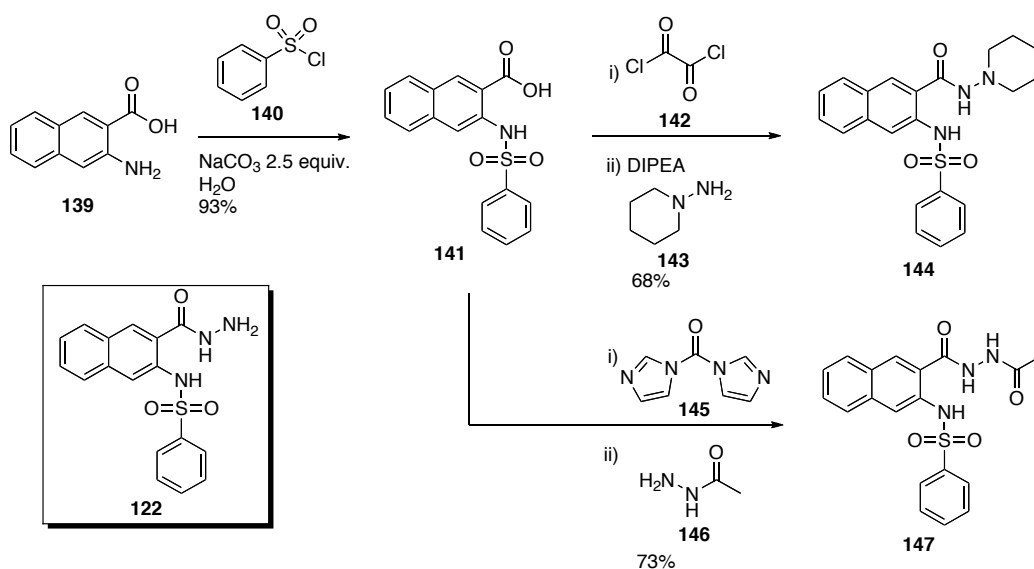
1.3.4 SAR studies on the lead compounds

1.3.4.1 Aryl-hydrazide derivatives as inhibitors of LL-DAP-AT

As mentioned previously compound **122** was found to be active, with an IC_{50} of 5 μ M, and showed reversible inhibition. Subsequent SAR studies on this sulfonamide-arylhydrazide compound were performed. Based on the structure of the lead compound, there are several moieties that may be amenable to modification, including the hydrazide, the main core aryl, and the aryl sulfonamide groups. The modification of each moiety will be described below.

1.3.4.1.1 Modifications of hydrazide moiety of the lead arylhydrazide

The hydrazide moiety is an alkaline nucleophile, which could readily react with the PLP cofactor of LL-DAP-AT. Initially, two analogues were designed and prepared as shown in **Scheme 1-1**. Commercially available 3-amino-2-naphthoic acid (**139**) was used as starting material to prepare the analogues. Reaction with benzenesulfonyl chloride (**140**) yields sulfonamide acid intermediate **141**. The activation of the carboxylic acid with oxalyl chloride (**142**) generates the acid chloride *in situ*, which further reacts with the hydrazine **143** to give analogue **144**. In analogue **144**, the hydrazide moiety was masked by a six-membered ring, which decreases the nucleophilicity while retaining the basicity of the terminal nitrogen atom. Similarly, activation of the carboxylic acid of intermediate **141** with carbonyl diimidazole (**145**) and coupling with acetyl hydrazide yields analogue **147**. In analogue **147**, the acetylated terminal amino group leads to decreased nucleophilicity and basicity at the terminal nitrogen.



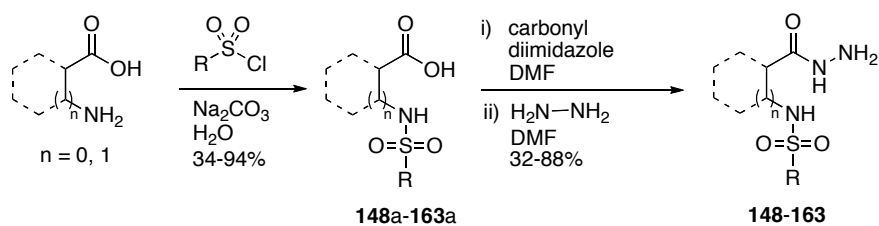
Scheme 1-1. The preparation of hydrazide analogues (**144** and **147**) of the lead arylhydrazide **122**

Upon testing of both analogues (**144** and **147**) against LL-DAP-AT, no enzyme inhibition was observed. These results suggest that the free terminal of the hydrazide moiety may be essential for inhibition of LL-DAP-AT. A preliminary mode of action study has also been done regarding the hydrazide moiety; the results will be discussed in a later section of this thesis.

1.3.4.1.2 Modifications of the naphthalene moiety of the lead arylhydrazide

Next, modifications of the naphthalene moiety of lead compound **122** were explored. This series of analogues were prepared based on the general procedure shown in the **Scheme 1-2**. Similar to the synthesis of analogue **147**, a variety of amino acids were first reacted with sulfonyl chlorides under basic conditions to afford the corresponding sulfonamides (**148a-163a**). Then, the

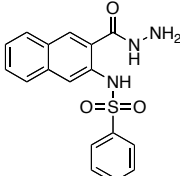
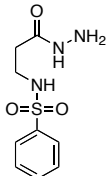
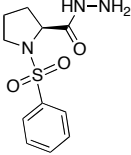
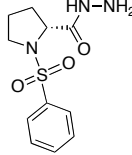
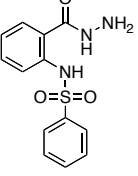
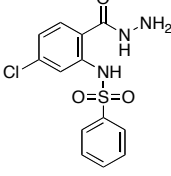
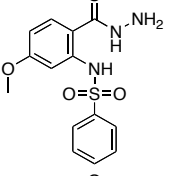
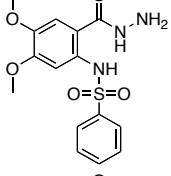
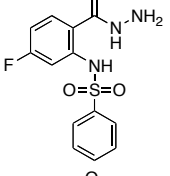
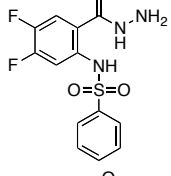
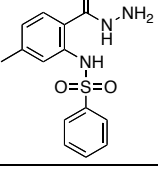
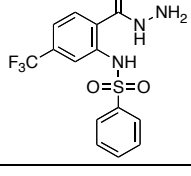
sulfonamide carboxylic acid was coupled with hydrazine using carbonyl diimidazole as a coupling reagent to form the product.



Scheme 1-2. The general synthetic route for preparation of hydrazide analogues

Analogue **148**, lacking the aromatic system, was devoid of inhibitory activity against the enzyme. Furthermore, L- and D-proline derivatives (**149** and **150**) were synthesized, and these showed no inhibition at 200 μM . These results suggest that a β -amino acid-derived aromatic system is necessary for inhibition.

Table 1-2. The inhibitory effects of the aryl-hydrazide analogues obtained from modification of naphthalene moiety against LL-DAP-AT

Entry	Structures	IC ₅₀ /μM	Entry	Structures	IC ₅₀ /μM
122		5	148		No inhibition
149		No inhibition	150		No inhibition
151		13.2	152		4.1
153		4.5	154		20.7
155		2.5	156		5.9
157		7.9	158		3.8

The phenyl ring analogues **151** to **158** were synthesized and tested against the enzyme. Compound **151** showed two-fold worse activity compared to the lead compound **122**, implying that substitution is required on the phenyl ring in order to retain activity. Electronic effects were also considered, and compounds bearing chlorine and methoxy groups *para* to the hydrazide moiety (**152** and **153**) were synthesized. The results showed that these two compounds possessed similar

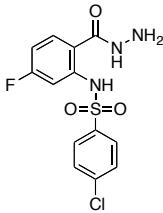
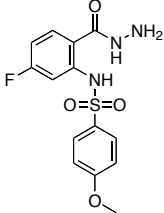
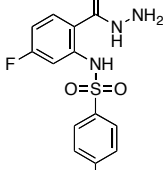
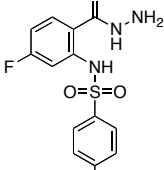
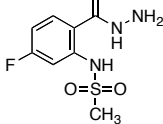
activity against the enzyme, suggesting that electron density in the aromatic ring may not play a significant role in the inhibition. Moreover, these two analogues showed slightly better activity than the lead compound, which supports the hypothesis mentioned above that substitution is required on the phenyl ring. The dimethoxy-substituted analogue **154** showed approximately one magnitude less inhibition than either the lead compound **122** or the mono-methoxy-substituted analogue **153**. The extra methoxy group *para* to the sulfonamide moiety may be hindering enzyme-inhibitor interactions through steric effects. Since substitution is necessary on the phenyl ring and the size of the substituent cannot be too large, monofluoro- and difluoro-substituted analogues **155** and **156** were prepared and evaluated. Difluoro-substituted analogue **156** showed similar inhibition compared to the lead compound **122**, whereas the monofluoro-substituted analogue **155** showed a two-fold improvement with respect to inhibition by the lead compound **122**, and is the best inhibitor prepared in the current study. In addition, *para*-methyl-hydrazide and *para*-trifluoromethyl-hydrazide analogues **157** and **158** were tested. The trifluoromethyl group enhances the activity compared to the methyl analogue, indicating that an electron-withdrawing group on the benzene ring *para* to the hydrazide moiety can be beneficial for the inhibitory activity.

1.3.4.1.3 Modifications of the phenylsulfonamide moiety of the lead arylhydrazide

Since the *para*-fluoro-hydrazide analogue **155** showed the best inhibition in the series of aromatic ring modifications, the SAR studies of the sulfonamide moiety were based on the new lead compound **155** (Table 1-3). At first, *para*-

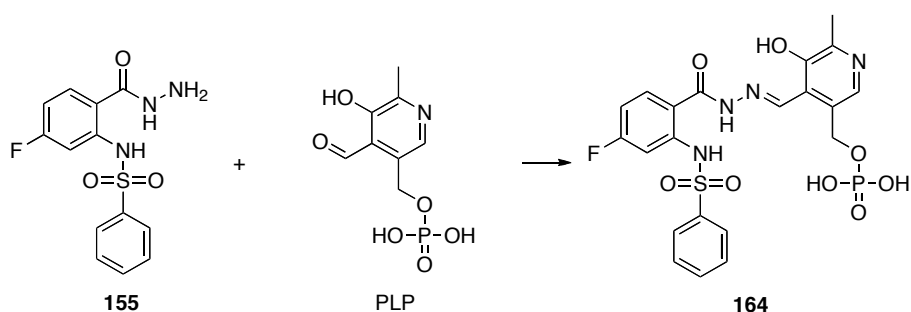
chloro **159** and *para*-methoxy benzenesulfonamide **160** were prepared to examine any electronic effects. Both analogues **159** and **160** showed slightly worse inhibition than compound **155**. An electron-donating group at the *para* position appears to give improved activity of the benzenesulfonamide compared with an electron-withdrawing group. Moreover, *para*-fluorobenzenesulfonamide **161** and *para*-toluenesulfonamide **162** were prepared and tested against the enzyme. Both of these analogues were reasonable inhibitors, but were not as effective as the analogue with an unsubstituted phenyl ring. Finally, the methanesulfonamide analogue **163** was synthesized and tested. Surprisingly, this analogue did not show any inhibition up to 200 μM . This result indicates that an aromatic system connected to the sulfonyl group is necessary for inhibition.

Table 1-3. The inhibitory effects of the aryl-hydrazide analogues obtained from modification of phenylsulfonamide moiety against LL-DAP-AT

Entry	Structures	IC ₅₀ / μM	Entry	Structures	IC ₅₀ / μM
159		5.3	160		3.4
161		7.5	162		5.6
163		No inhibition			

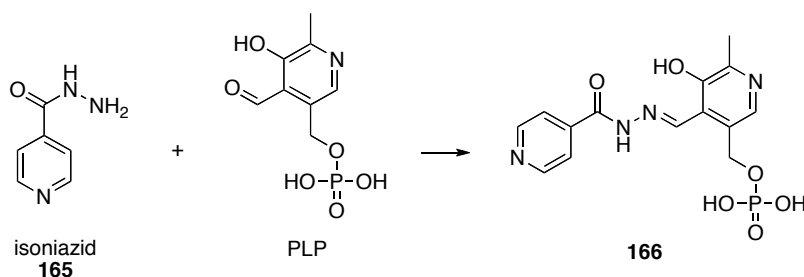
1.3.4.1.4 Preliminary study on the mode of action of the aryl-hydrazide derivatives as inhibitors to LL-DAP-AT

It has been shown that if the terminal amino group of the hydrazide moiety is masked by a ring or an acetyl group, the corresponding analogue loses activity against the enzyme, suggesting that a free hydrazide group is essential for inhibition.⁶⁰ Although the lead compound **122** shows reversible time-independent inhibition, the free hydrazide moiety is a strong nucleophile and could react with the enzyme cofactor, PLP. To determine whether or not the hydrazide inhibitor reacts with PLP, analogue **155** was mixed with one molar equivalent of PLP, in a 1:1 mixture of deuterated water and deuterated methanol at room temperature. ¹H- and ¹³C-NMR characterization of the mixture suggested the presence of the proposed imine adduct **164** (Scheme 1-3). The imine adduct was further isolated, and its identity was confirmed by high-resolution electrospray mass-spectrometry (HR-ESI-MS). These results indicate that, as expected, the hydrazide moiety reacts with PLP to form an imine (hydrazone) adduct.



Scheme 1-3. Hydrazone formation between the hydrazide group of inhibitor **155** and the aldehyde group of PLP

To test whether the free hydrazide is the only requirement for inhibition, a clinically used anti-tuberculosis drug, isoniazid, was tested against LL-DAP-AT for inhibitory activity. Isoniazid shows no inhibition up to 200 μM against LL-DAP-AT. Since isoniazid (**165**) has a hydrazide moiety with a free terminus, the hydrazone adduct is readily formed between isoniazid and PLP in the absence of enzyme (**Scheme 1-4**). If the formation of the PLP-hydrazone adduct or sequestration of the co-factor was the main requirement for enzyme inhibition, then isoniazid should show similar activity against LL-DAP-AT; this is not observed. Similarly, several other hydrazide analogues, such as **148**, **149**, **150** and **163**, did not show inhibition against the enzyme, at concentrations up to 200 μM . The hydrazone adduct may form only after the analogues enter the enzyme active site, which contains PLP bound as an imine to Lys270.⁴⁰ Hydrazone formation is clearly not the only factor required for enzyme inhibition. Additional interactions between the inhibitor and enzyme active site are most likely required. Furthermore, since hydrazone formation is a reversible process by transamination whose rate can be catalyzed by other nucleophilic groups,^{117, 118} active compounds, such as lead compound **122**, act as reversible inhibitors.



Scheme 1-4. Hydrazone formation between the hydrazine group of isoniazid and the aldehyde group of PLP

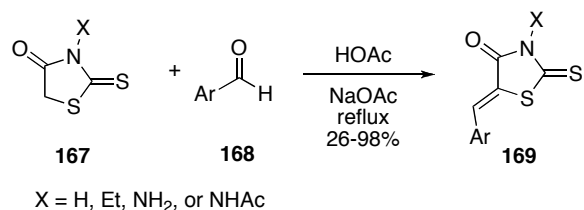
Finally, the preformed adduct **164** was also tested for inhibition against LL-DAP-AT. However, this adduct only showed 40% inhibition at 100 μM . In contrast, the free hydrazide analogue **155** displayed ~98% inhibition at 100 μM . Although it is not possible to fully prevent the hydrolysis of **164** to **155** in the enzyme assay, this preliminary result suggests that cofactor exchange is relatively slow.^{117, 118} The detailed mechanism of inhibition of the hydrazide inhibitors to LL-DAP-AT would be benefit from further study through X-ray crystallography and detailed enzyme kinetics.

1.3.4.2 Rhodanine derivatives as inhibitors of LL-DAP-AT

The initial objective of this study was to find inhibitors that showed time-independent behavior and interacted reversibly with LL-DAP-AT. From the HTS study, a number of inhibitors showed IC_{50} values of 20 – 60 μM , and a significant number of these compounds contained barbiturate or thiobarbiturate moiety. Similar barbiturate-derived compounds have been studied extensively in the past. They have been shown to be good inhibitors of methionine aminopeptidase-1 and have also been used as antidepressant drugs.^{119, 120} However, such unsaturated

barbiturate derivatives are likely to be very good Michael acceptors and may react with enzymes in a non-specific way, potentially leading to mammalian toxicity. From the time-dependence test on the selected inhibitors, one barbiturate-derived compound (**107**) showed time-independent inhibition. Two thiobarbiturate-derived compounds (**114** and **119**) were also tested, with one (**114**) showing time-dependent inhibition, whereas the other (**119**) showed time-independent inhibition. Such a time-dependent inhibitor (**114**) may be reacting with enzyme or may be a slow-binding inhibitor. Thus, we chose to examine the rhodanine-derived compounds, to avoid complications arising from the ability of the barbiturate-based compounds to behave as Michael acceptors.

Of the top 46 hits in the screening study, compounds **93** to **105** are rhodanine-derived inhibitors. There are no obvious functional groups expected to be reactive toward PLP or the enzyme, so these compounds are more likely to be time-independent inhibitors. The inhibitory activity of these compounds is not particularly high and trends in SAR are unclear. Thus, the top two inhibitors, **100** and **101**, with IC_{50} values of 46 and 41 μ M, respectively, were selected for further SAR investigation. The synthesis of analogues followed a general route as shown in **Scheme 1-5**. Various commercially available rhodanine starting materials **167** were reacted with different aromatic aldehydes **168** under refluxing conditions to form analogues **169** through a Knoevenagel condensation.

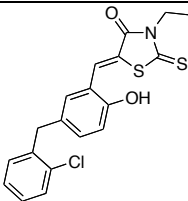
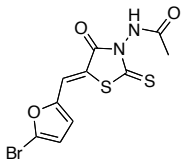
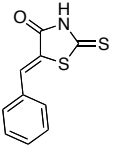
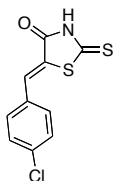
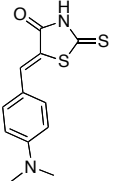
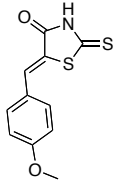
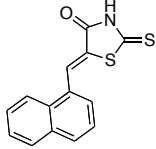
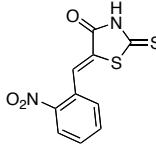
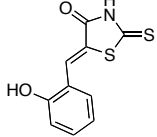


Scheme 1-5. General synthetic route for rhodanine-derived inhibitors for LL-DAP-AT

1.3.4.2.1 Inhibitory studies of rhodanine-based analogues against LL-DAP-AT

The first series of analogues were based on rhodanine analogue **167** where X = H. The inhibitory results are shown in **Table 1-4**. Analogues **170**, **174**, and **175** showed no inhibition up to 1 mM concentration. Compounds **171** and **176** showed weak inhibition with IC₅₀ values higher than 200 μM. Only compounds **172** and **173** displayed reasonable inhibition with IC₅₀ values of 127 and 142 μM, respectively. These results suggest that a substituted aromatic moiety is needed for activity, and an electron-donating substituent is preferred for inhibition.

Table 1-4. Inhibitory effects of *N*-unsubstituted rhodanine analogues against LL-DAP-AT

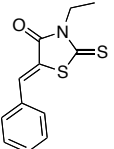
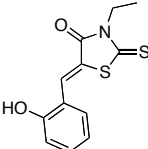
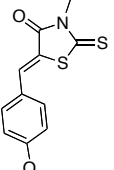
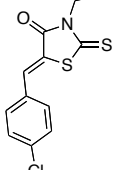
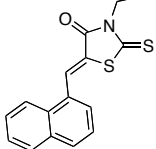
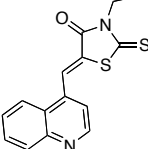
Entry	Structures	IC ₅₀ /μM	Entry	Structures	IC ₅₀ /μM
100		46	101		41
170		No inhibition	171		> 200
172		127	173		142
174		No inhibition	175		No inhibition
176		> 200			

1.3.4.2.2 *N*-Ethyl-rhodanine-based analogues

Six analogues of *N*-ethyl-rhodanine-derived lead compound **100** were synthesized and tested against LL-DAP-AT. The results are shown in **Table 1-5**. In this series, the analogues were not particularly active against LL-DAP-AT. Most of the compounds showed weak inhibition with IC₅₀ values greater than 200 μM, whereas compounds **180** to **182** exhibited IC₅₀ values about 200 μM. Interestingly, comparing analogue **178** with the lead compound **100** reveals the importance of the second aromatic ring bearing a chlorine group. Compounds

lacking a large aromatic substituent on the position *para* to the hydroxyl group on the analogue **178** showed no significant inhibitory activity against LL-DAP-AT, which suggests that an additional aromatic ring is required for inhibition.

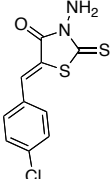
Table 1-5. The inhibitory effect of *N*-ethyl-rhodanine analogues against LL-DAP-AT

Entry	Structures	IC ₅₀ /μM	Entry	Structures	IC ₅₀ /μM
177		> 200	178		> 200
179		> 200	180		~ 200
181		~ 200	182		190

1.3.4.2.3 *N*-Amino-rhodanine-based analogues

Next, *N*-amino-rhodanine was used to prepare another set of analogues. Three analogues were synthesized and tested against the LL-DAP-AT. As shown in **Table 1-6**, only analogue **184**, with an electron-donating group (*i.e.*, methoxy) *para* to the rhodanine moiety, showed inhibitory active against the enzyme with an IC₅₀ value of 155 μM.

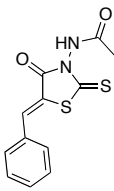
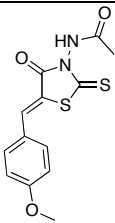
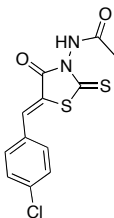
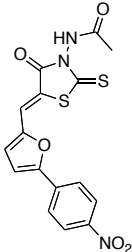
Table 1-6. The inhibitory effects of *N*-amino-rhodanine analogues against LL-DAP-AT

Entry	Structures	IC ₅₀ /μM	Entry	Structures	IC ₅₀ /μM
183		No inhibition	184		155
185		No inhibition			

1.3.4.2.4 *N*-Aminoacetyl-rhodanine based analogues

Finally, analogues of lead compound **101** were prepared and tested against LL-DAP-AT. In the preparation of this series of analogues, an *N*-aminoacetyl-rhodanine was used as starting material. The compounds with either an unsubstituted or substituted phenyl ring next to the rhodanine moiety did not show inhibition, with the exception of compound **187**. Compound **187** contained a methoxy group *para* to the rhodanine moiety, and showed very weak activity with an IC₅₀ value greater than 200 μM. Compound **189** is an analogue of lead compound **101** with a furan ring attached to the rhodanine. Instead of a bromo group on the furan ring, a *para*-nitrophenyl was used. This analogue showed a similar level of inhibition as the lead compound with an IC₅₀ value of 73 μM. These results indicate that the furan ring may play a role in the inhibitory process. Additionally, an electron-withdrawing substituent in the 5-position of the furan ring may enhance the inhibitory activity.

Table 1-7. The inhibitory effects of *N*-aminoacetyl-rhodanine analogues against LL-DAP-AT

Entry	Structures	IC ₅₀ /μM	Entry	Structures	IC ₅₀ /μM
186		No inhibition	187		> 200
188		No inhibition	189		73

1.3.4.2.5 Overall analysis of the SAR studies based on rhodanine-based analogues

Based on this rhodanine-based SAR study, no analogues exhibited better inhibition than the lead compounds. However, several conclusions can be drawn that may prove useful in guiding future studies. Substitution on the nitrogen of the rhodanine ring does not appear to have significant effect on the inhibitory potency of the compounds, as two of the best analogues (**172** and **173**) possessed only a hydrogen atom on the nitrogen. Furthermore, comparison of analogues in which only the substituent on the nitrogen was varied (*e.g.*, [**170**, **177**, **183**, **186**], [**171**, **180**, **185**, **188**], or [**173**, **179**, **184**, **187**]) does not reveal any significant differences. These results imply that the substituent on the rhodanine does not dramatically affect the activity. Comparison of analogues in which the substituent on the nitrogen was kept the same while varying the substituents on the aromatic

ring reveals that an electron-donating group (*e.g.*, methoxy) on the aromatic ring enhanced the activity of the inhibitor. This effect is most pronounced for those analogues in which the nitrogen either bears a hydrogen atom or an amino group (**Table 1-4** and **Table 1-6**). Replacement of the methoxy group with an electron-withdrawing chlorine atom results in a decrease in inhibitory activity in three of the four examples. The location of the substituent also appears to play a role, as an electron-donating group (hydroxyl) added to the *ortho* position (**176**) decreases the inhibition compared to **173**, although it is still better than the unsubstituted ring.

1.4 Conclusion and future direction

In this work, LL-DAP-AT, a PLP-dependent aminotransferase that catalyzes a key transformation in the lysine biosynthetic pathway utilized by plants and some bacteria, has been investigated by X-ray crystallography. With the results from these studies, a better understanding of this enzyme has been gained. This enzyme belongs to the type I fold PLP-dependent aminotransferases and uses glutamate as the amino donor. The mechanism of substrate recognition has been illustrated, and the open form of THDP was found to be the substrate for transamination. Furthermore, both LL-DAP-ATs from *Arabidopsis thaliana* and *Chlamydia trachomatis* have been studied. Essentially, the two enzymes work in a very similar way to catalyze the transamination reaction. However, slight structural differences provide the *Chlamydia* enzyme with a broader substrate specificity. In the future, the substrate analogues bound to *Chlamydia* LL-DAP-AT could be studied and may provide further insights toward a better understanding

of the substrate specificity of this enzyme. In addition, the study of LL-DAP-AT from different species may also provide valuable information to better understand this enzyme, and may furnish new insights towards the development of antibiotics using the enzyme as a target.

Inhibitory studies against LL-DAP-AT have been performed as well. As this enzyme is involved in a key transformation in lysine biosynthesis, which is absent in mammals but present in plants and bacteria, it may represent an ideal target for herbicides and antibiotics. A HTS approach was initially used to identify lead compounds. Three potential pharmacophores (barbiturate, thiobarbiturate, and rhodanine) were identified based on their prevalence in the HTS hits. Using HTS, the best inhibitor was found to be a sulfonamide-arylhydrazide compound **122** which displays time-independent inhibition with an IC_{50} value of 5 μ M. A SAR study based on lead compound **122** has been performed. In total, 18 of inhibitors were developed based on lead compound **122**, five of these analogues showed improved inhibition against LL-DAP-AT. A two-fold better inhibitor, a para-fluoro-phenylhydrazide **155**, was identified with an IC_{50} value of 2.5 μ M. Besides the identification of a better inhibitor, other valuable trends have been observed that provide insights regarding the SAR of the analogues against LL-DAP-AT. Similarly, SAR studies of 20 rhodanine-derived analogues were performed. Although this series of analogues did not show superior inhibition compared to the lead compounds, some useful trends were drawn from this study, which may prove useful for guiding future inhibitor development. In the future, X-ray crystallography could be applied to study the

enzyme-inhibitor complex, which may then provide a better understanding of the inhibitory mechanism and allow for the design of better inhibitors. Similarly, detailed enzyme kinetics will provide information on how the inhibitors interact with the enzyme and can potentially provide new ideas for the design of inhibitors, which may prove crucial in the development of novel antimicrobial or herbicidal agents.

Chapter 2. Investigation of methods for crystallization of small peptides

2.1 Introduction

It is well known that small peptides (< 5 kDa) are difficult to crystallize. Many known bacteriocins are small peptides in the range of 20 to 50 amino acid residues, and only a few of them have been crystallized. For example, mersacidin, a lantibiotic, was crystallized in the early 2000s.¹²¹ This was the first crystal structure of a lantibiotic peptide. A 39-amino acid glucagon-like peptide, glucagon-Cex, a potential drug candidate for metabolic disease (e.g., diabetes and obesity) treatment, was crystallized under standard protein crystallization conditions in 2007.¹²² An example of the 19-amino acid lasso peptide, BI-32169, has also been crystallized in 2010.¹²³ A 47-amino acid antifungal plant defensin, NaD1, was successfully crystallized earlier this year.¹²⁴ There are additional examples of small peptide crystallization examples, but indeed not many. Thus, a general and easy-accessible method for small peptide crystallization is needed for improved structural studies.

2.1.1 Potential approaches for crystallization of small peptides

2.1.1.1 Racemic peptide crystallization

Despite the difficulties in crystallizing small peptides, there are methods that have been used to overcome this issue. For instance, Kent and co-workers have developed a racemic protein crystallization method that has been used to

successfully crystallize small peptides (3-5 kDa).¹²⁵⁻¹²⁸ This method takes advantage of the fact that more space groups are available for racemates to crystallize, than pure enantiomers.^{129, 130} As an example, D- and L-BmBKTx1, a 31-amino acid scorpion toxin, was crystallized using racemic crystallization (**Figure 2-1**). This method involves the preparation of both enantiomers of the peptide of interest, and combining them in a one to one mixture to form a racemate. These racemates are then exposed to crystallization conditions. This method could be useful in bacteriocin crystallization.

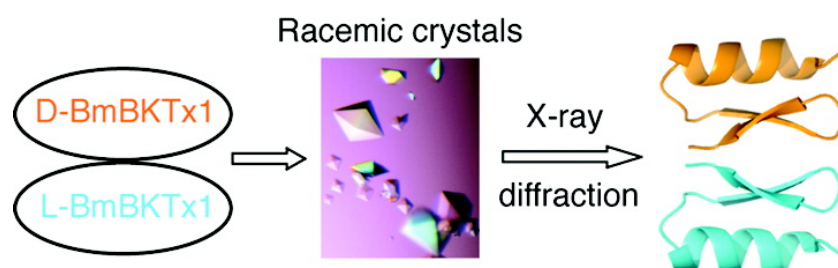


Figure 2-1. D- and L-BmBKTx1 were crystallized by racemic crystallization¹²⁶

2.1.1.2 Co-crystallization method for protein crystallization

There are many examples of co-crystal structures of proteins containing ligand-bound protein complexes. For instance, substrate analogue-bound LL-DAP-AT crystal structures were described in **Chapter 1**. The co-crystallization approach has become a popular method to study biological machinery.

There have been small peptides co-crystallized with large proteins, when the small peptides are bound in the active site of the large proteins. For example, a 21-amino acid interleukin-1 (IL-1) antagonist peptide (AF10874) was co-

crystallized with extracellular domains of IL-1 receptor type 1 (IL-1R1) as shown in **Figure 2-2**.¹³¹ Normally, this approach requires a good inhibitor. In this particular case, the IL-1 antagonist peptide binds to IL-1R1 with a IC_{50} value of 2.6 nM.¹³¹ For many natural peptides, such as bacteriocins, this approach is not available, since many receptor proteins for these peptides are not identified.

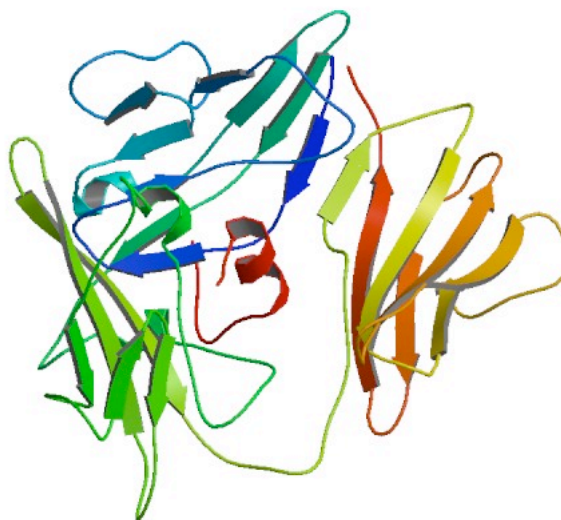


Figure 2-2. The extracellular domains of interleukin-1 receptor type 1 (IL-1R1, in green, blue, and orange) bound to an IL-1 antagonist peptide (AF10847, in red).¹³¹ PDB code: 1G0Y

This approach has also been used in the co-crystallization of a molecule of interest with a readily crystallizable enzyme. In 2008, Christianson and co-workers successfully crystallized a ^{129}Xe -cryptophane biosensor (**190**) complexed with human carbonic anhydrase II (CAII).^{132, 133} In this study, cryptophane¹³⁴ was used as a small molecule host, with xenon bound in the hydrophobic cavity of the cryptophane (**190**). Cryptophane was linked with a benzenesulfonamide, via click

chemistry, with the intention of using the benzenesulfonamide moiety as a well-known inhibitor to the Zn-dependent CAII. In the presence of CAII, benzenesulfonamide coordinates to the zinc cofactor in the active site, and the enzyme complex is then co-crystallized under normal protein crystallization conditions (**Figure 2-3** right).

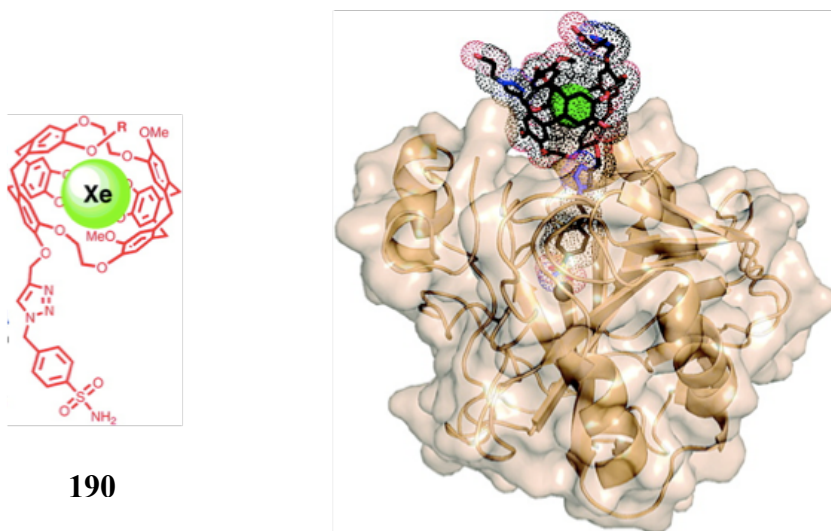


Figure 2-3. ^{129}Xe -cryptophane biosensor (**190**) complexed with CAII. The Xe-cryptophane complex is shown on the left, and the co-crystal structure is shown on the right¹³³

Using this approach to crystallization, a small peptide could be linked to a small molecule inhibitor of a readily crystallizable enzyme. Then, upon mixing, the small peptide may be co-crystallized with the enzyme.

2.1.2 Subtilisin A (SubA) as a target for development of method for crystallization of small peptides

Subtilisin A (SubA, **191**, **Figure 2-4**) is an antimicrobial cyclic bacteriocin that was originally isolated from the Gram-positive, spore-forming soil bacterium *Bacillus subtilis*.¹³⁵ SubA has also recently been found in other *Bacillus* species, such as *B. atrophaeus*¹³⁶ and *B. amyloliquefaciens*.¹³⁷ Through a series of solution multi-dimensional NMR structural elucidation studies,¹³⁸⁻¹⁴⁰ SubA was found to be an *N*- to *C*-terminal linked cyclic peptide that is composed of 35 amino acids. It also has three unusual thioether bridges between the sulfur atom of three cysteine residues and the α -carbon atoms of threonine 28 and two phenylalanine residues 22 and 31 (**Figure 2-4**).

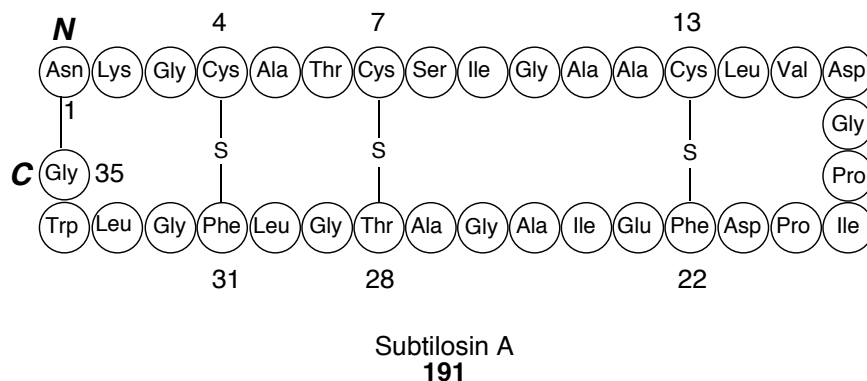


Figure 2-4. Amino acid sequence of subtilisin A showing the three crosslinking thioether bridges

2.1.2.1 Subtilisin A as a bacteriocin

SubA, as a circular bacteriocin, has attracted much attention in the bacteriocin research community since its initial isolation in the mid-1980s.¹³⁵ This

is due to its potent antimicrobial activity against a relatively wide range of bacteria compared to most known bacteriocins¹⁴¹ and also its unique structure features.^{139, 140} These subjects will be discussed in the later sections in this thesis.

2.1.2.2 General background of bacteriocin

Bacteriocins are potent antimicrobial peptides that are produced by bacteria and archaea. These peptides are ribosomally synthesized and often posttranslationally modified. Some bacteriocins are only active against microorganisms closely related to the producer strain.¹⁴² Bacteriocins are the most abundant and diverse bacterial defense weapons,¹⁴³ and it is believed by some that almost all bacteria (99%) produce at least one bacteriocin.¹⁴⁴ Compared to the total number of different bacteriocins existing in nature, the number of isolated ones is very low. Microorganisms spend significant energy producing bacteriocins. However, the evolutionary origins of bacteriocins and the exact physiological mechanisms of these bacterial defense tools are still unclear.^{142, 143}

2.1.2.2.1 Classification of bacteriocins

Bacteriocins can be grouped into several classes. Based on their size, structural features, and modifications. The bacteriocins produced by Gram-negative bacteria are normally large proteins. The mode of action of these large proteinogenic bacteriocins ranges from pore formation to nuclease-type mechanism.¹⁴² For instance, colicins are pore-forming bacteriocins produced by *E. coli* that often have sizes ranging from 449 to 629 amino acid residues.

Nuclease-type bacteriocins have an even broader range of sizes, from 178 to 777 amino acids.¹⁴²

The bacteriocins produced by Gram-positive bacteria have more diversity than those of Gram-negative bacteria. In general, the currently accepted classification separates these bacteriocins into three different classes (**Table 2-1**). However, there are still ongoing revisions.¹⁴⁵⁻¹⁴⁸

Table 2-1. Classification of bacteriocins produced by Gram-positive bacteria

Classes	Sub-classes	Example
Class I Lantibiotics	Type A Elongated and cationic	nisin ¹⁵²
	Type B Globular and neutral/basic	mersacidin ¹⁵³
Class II Non-Lantibiotics	Type IIa ¹⁴⁵ Pediocin-like	pediocin PA-1 ¹⁵⁴
	Type IIb Two-component	lactococcin G ¹⁵⁵
	Type IIc ¹⁴⁸ Circular peptides	subtilosin A ¹³⁹
	Class III Bacteriolysins ¹⁴⁶ Large lytic proteins	lysostaphin ¹⁵⁶

2.1.2.2.2 Application of bacteriocins as antibiotics and food preservative

As mentioned in **Chapter 1**, multi-drug resistant bacterial pathogens have rapidly emerged and spread in recent years. Traditional antibiotics are broad-spectrum drugs, which kill bacteria with very limited selectivity. The high frequency of usage of these antibiotics results in the evolution of antibiotic resistance in both pathogenic and commensal bacteria.¹⁴² Once drug resistance develops, the pathogenic bacteria will acquire the resistance very quickly.¹⁵⁷ One

way to overcome this issue is to find new targets for novel antibiotic development as discussed previously. Alternatively, bacteriocins can be used as antibiotics with a relatively narrower spectrum of action compared to traditional antibiotics; it is a matter of finding a specific bacteriocin for a specific pathogen. This approach may extend the lifespan of the antibiotics since each of the antibiotics is used much less frequently.¹⁴² Due to the limited knowledge of bacteriocins existing in nature, this is an avenue of antibiotic development that can be explored further.

In addition, bacteriocins such as nisin have been previously utilized in food preservation. The only bacteriocins presently used in the food industry are those produced by lactic acid bacteria (LAB). In fact, LAB have been used in food preservation for centuries. However, bacteriocins produced by other kinds of bacteria will likely be useful in the future for food preservation purposes.

2.1.2.3 Structure elucidation of Subtilosin A

Following the isolation of SubA from the wild type strain *B. subtilis* 168,¹³⁵ researchers proposed an incomplete amino acid sequence based upon their knowledge of the blocked *N*- and *C*-terminal residues and few unknown linkages between middle residues. Subsequently, genetic studies have revealed the completed and corrected primary sequence of SubA.^{158, 159} Earlier studies proposed that SubA is a *N*- and *C*-terminal blocked peptide with unusual linkages between the sulfurs of cysteines and other residues; however, the linkages were not identified.

The structural hypothesis was further supported by a ¹H-NMR experiment in the early 2000s.¹³⁸ This circular bacteriocin, SubA, was found to have three

unusual linkages between Cys4, Cys7, Cys13 and Phe31, Thr28, Phe22, respectively, based on this NMR study. However, the authors could not confirm the exact covalent connections between these residues. Interestingly, the authors suggested that sulfur-carbon and sulfur-oxygen linkages could be the unusual connections between the cysteine residues and two phenylalanines and a threonine.

Concurrently, isotopic labeling and multi-dimensional NMR experiments were performed in our research group,^{139, 140} to determine the primary and three-dimensional structure of SubA. In this study, [¹³C, ¹⁵N]-labeled SubA was obtained by fermentation of *B. subtilis* JH642 in the presence of [¹³C, ¹⁵N] peptone derived from cyanobacterium (*Anabaena sp.*) grown in [¹³C]-labeled sodium bicarbonate and [¹⁵N]-labeled sodium nitrate, as previously developed by our research group.^{140, 160} Upon assignment of all proton, carbon, and nitrogen chemical shifts, it was revealed that Phe22, Thr28, and Phe31 were missing α -proton signals. Additionally the α -carbons had higher chemical shifts (~ 10 ppm higher than normal) for these three residues. To further confirm the abnormal chemical shift signals for these α -carbons, [¹³C, ¹⁵N]-labeled L-phenylalanine and L-threonine were used in the fermentation of SubA, resulting in the phenylalanine and threonine residues being predominantly labeled. Upon NMR analysis, the chemical shifts corresponding to the α -carbons of Phe22, Phe31, and Thr28 were found to be 69.4, 69.8, and 72.8 ppm, respectively. Two model molecules (**Figure 2-5**) were synthesized to compare the chemical shift values for the α -carbons. Compound **192**, a racemic phenylalanine derivative, showed a chemical shift of

68.0 ppm for the α -carbon. The threonine derivative **193** showed 74.9 ppm for the α -carbon. Both of the model compounds showed very similar chemical shifts for the fully substituted α -carbons compared to SubA. Based on these results, the authors proposed that the linkage between the three cysteines residues and two phenylalanines and a threonine residue were thioethers, in which the sulfur atom of cysteines were linked to the α -carbons of the phenylalanines and threonine.

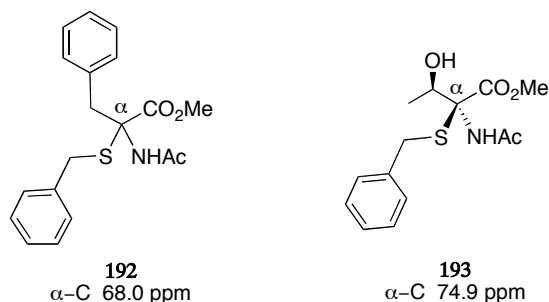


Figure 2-5. Model compounds for the fully substituted phenylalanine and threonine to confirm sulfur-carbon linkage of SubA

This was the first time that such a linkage was observed in bacteriocins. Several more thioether-bridge containing bacteriocins have since been discovered, such as thuricin CD,^{161, 162} a two-component bacteriocin, and thurincin H.¹⁶³ However, thuricin CD and thurincin H are not *C*- and *N*-terminal cyclized bacteriocins. The classification of these thioether-containing bacteriocins is still an ongoing issue.

After the identification of the thioether bridges in SubA, the stereochemistry of the residues was the next issue to be considered. In this regard, the desulfurization of SubA has been performed under nickel boride reduction

conditions to form a circular SubA peptide without the thioether bridges (**Figure 2-6a**).^{139, 140} The resulting circular peptide was hydrolyzed under acidic conditions to give individual amino acids which were subsequently derivatized to the corresponding pentafluoropropanamide isopropyl esters as shown in **Figure 2-6b**.¹⁴⁰ The resulting esters were analyzed by chiral GC-MS. All previously unmodified residues were found to exist in the L-configuration.¹⁴⁰ The derivatized threonine residue was found to be in the L-configuration as well, and the phenylalanines were found to be a mixture of D, L-configuration.¹⁴⁰ Since the desulfurization technique could give a racemic amino acid residue, chiral GC-MS analysis could not confirm the stereochemistry of the modified amino acids present at the sites of the thioether linkages.

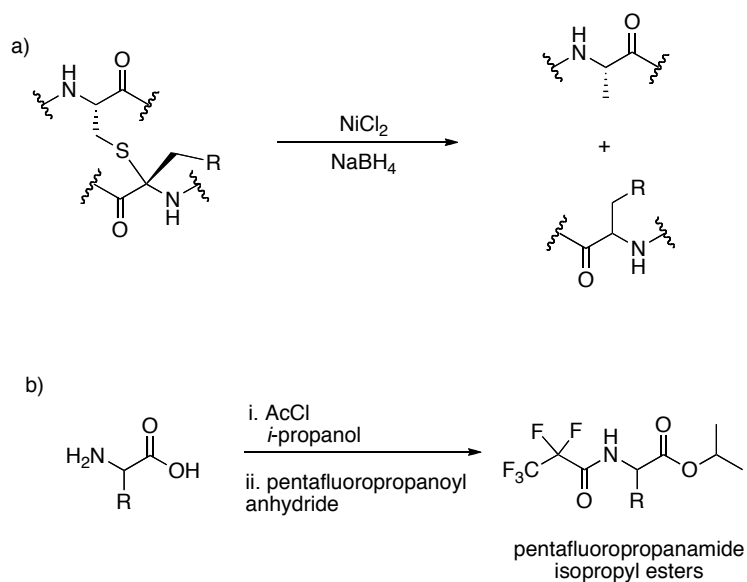


Figure 2-6. a) Desulfurization using nickel boride reduction. b) Conversion between free amino acid to the corresponding pentafluoropropanamide isopropyl esters

Multi-dimensional NMR experiments were then used to study the three-dimensional solution structure of SubA. Through NMR data assignments and energy-minimization calculations,¹⁶⁴ the SubA isomer containing L-Phe22, D-Thr28, and D-Phe31 was found to be the lowest energy isomer.¹⁴⁰ The overall proposed structure of SubA with assigned stereochemistry is shown in **Figure 2-7**.

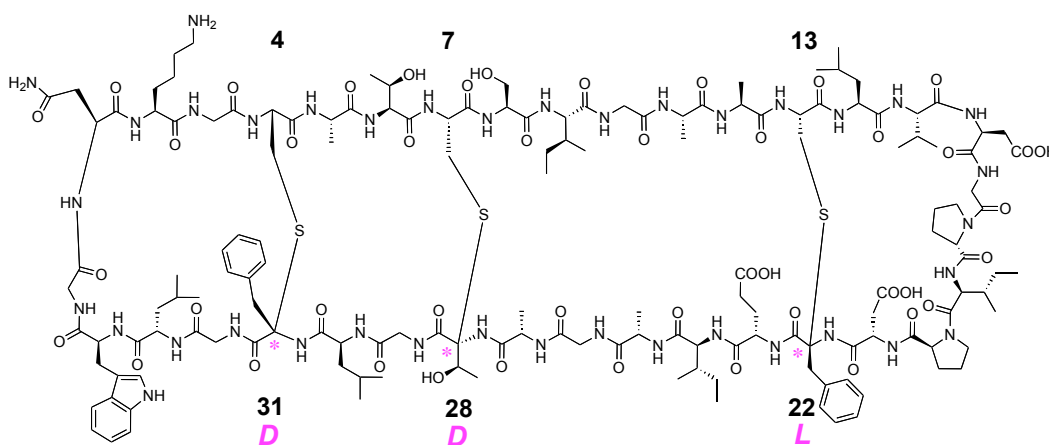


Figure 2-7. Structure of SubA with proposed stereochemistry of sulfur- α -carbon crosslinks labelled in magenta

Through solution NMR studies, a three-dimensional structure of SubA was generated, as shown in **Figure 2-8**. Although the stereochemistries of the modified residues are proposed based on extensive solution NMR studies, it is still desirable to confirm the exact stereochemistry at these three quaternary centres using X-ray crystallography.

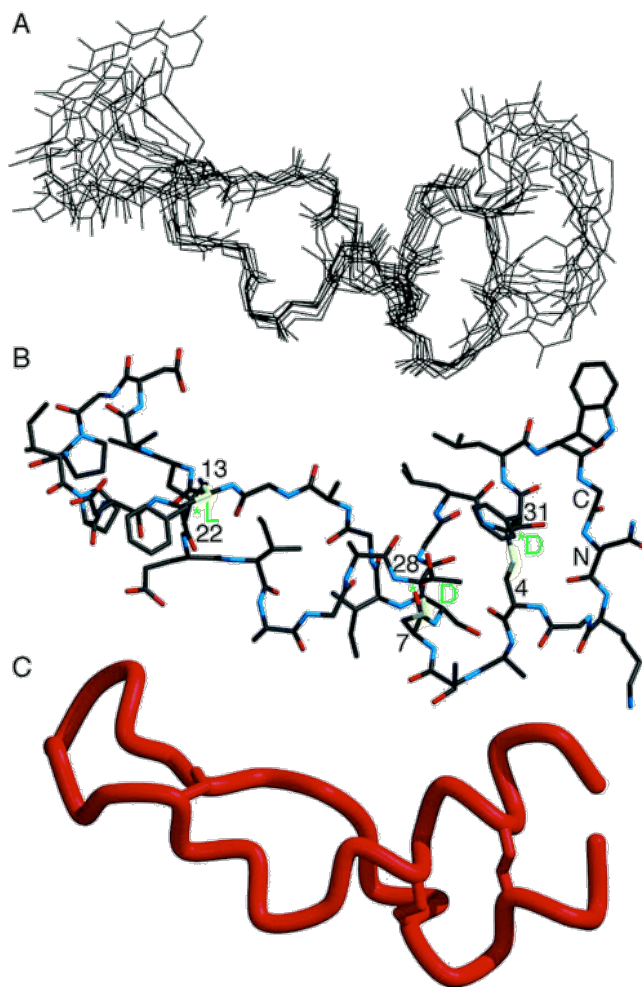


Figure 2-8. A) Superposition of the backbone of residues of the eight lowest energy structures of SubA. B) Representative conformer of SubA with indication of stereochemistry of the modified residues. C) Coil representation of the backbone of SubA, the break shown is at the position of C- and N-terminal cyclization. (This figure adopted Kawulka et al.¹⁴⁰)

2.2 Project goal

In this project, the goal is to develop a general method to crystallize small peptides (e.g., SubA). SubA has not been crystallized by itself despite many attempts in our laboratory. The racemic crystallization is also not suitable for crystallization of SubA, since there is no synthetic method available to generate a

peptide with sulfur- α -carbon crosslinks yet. This makes it impractical to obtain the enantiomer of SubA. It is still unknown whether there are receptor proteins of SubA. Thus, direct co-crystallization of SubA with its receptor was also not a suitable method. In this study, a bioconjugation approach is used to link SubA with various small molecules that are inhibitors of readily crystallizable enzymes, such as lysozyme and CAII. The small molecule inhibitors are chitin derivatives and benzenesulfonamide derivatives for lysozyme and CAII, respectively. The attempts toward the co-crystallization of SubA bioconjugates with enzymes were thus performed.

2.3 Results and discussion

2.3.1 Glucosamine and chitotriose as lysozyme inhibitors

2.3.1.1 Previous crystallographic studies on lysozyme

Lysozyme was initially selected as a readily crystallizable enzyme, with *N*-acetylglucosamine and chitotriose as potential inhibitors. There have been extensive studies on lysozyme. Lysozyme is also known as *N*-acetylmuramide glycanhydrolase, and it was first isolated from hen egg white.¹⁶⁵ Due to its ability to hydrolyse the 1,4- β -linkage between *N*-acetylmuramic acid and *N*-acetyl-D-glucosamine within the peptidoglycan of the bacterial cell wall, lysozyme is one of the first known natural antimicrobial agents.

Lysozyme was also one of the earliest crystallized enzymes. Phillips and co-workers successfully crystallized lysozyme in the mid-1960s.¹⁶⁶ They also studied a lysozyme-inhibitor complex by crystallography.¹⁶⁷ *N*-acetylglucosamine

(GlcNAc, **194**), *N,N'*-diacetylchitobiose (**195**), and 6-iodo- α -methylglucosamine (**196**) were co-crystallized with lysozyme, whereas, glucosamine hydrochloride (**197**) and muramic acid (**198**) were unable to bind into the active site of lysozyme. The authors proposed that the *N*-acetyl groups are essential for the binding; however, the functional groups at the 1 and 6 position of glucosamine are not essential.

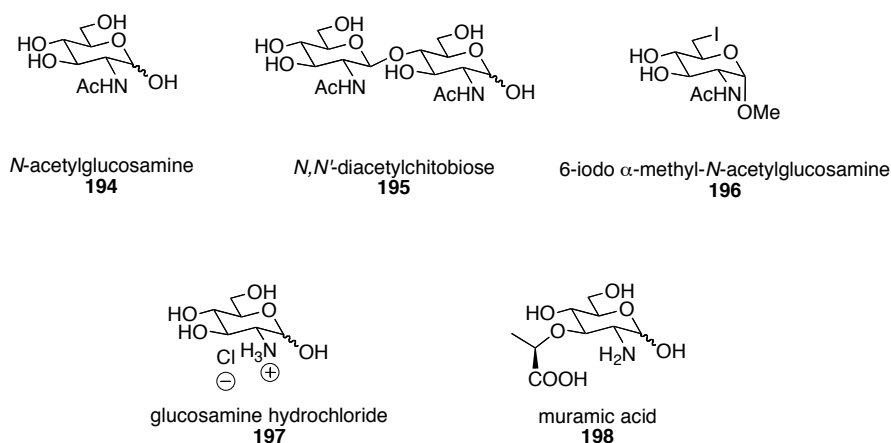


Figure 2-9. Compounds used in the co-crystallography studies of lysozyme by Phillips and co-workers¹⁶⁷

Subsequently, additional crystallography studies of lysozyme have been conducted, and lysozyme became one of the most readily crystallizable proteins. In the late 1990s, two chitin derivatives with fluorogenic groups were co-crystallized with rainbow trout lysozyme.¹⁶⁸ The two saccharides used in this study, 4MeU-(GlcNAc)₃ (**199**) and 4MeU-(GlcNAc)₂ (**200**), are shown in **Figure 2-10**. These types of fluorogenic glycosides have been used for detection of chitinase activity.^{169, 170}

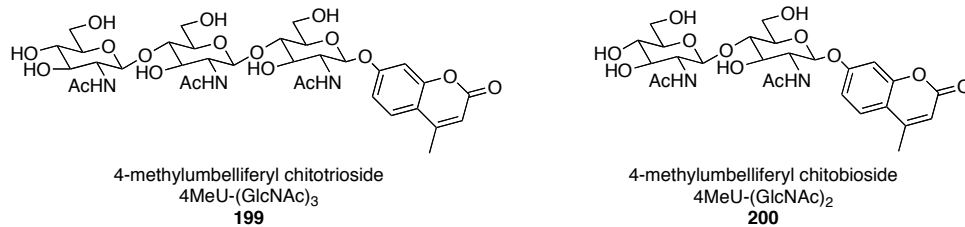


Figure 2-10. 4-Methylumbelliferyl β-glycosides used in the co-crystallization of lysozyme¹⁶⁸

A surface model of the lysozyme-4MeU-(GlcNAc)₃ complex is shown in **Figure 2-11**. Upon analyzing the crystal structure, the *N*-acetyl groups clearly play a role in binding. The *N*-acetyl group at the reducing end of chitotriose is especially important for binding, as it is deeply buried in the active site cavity.¹⁶⁸

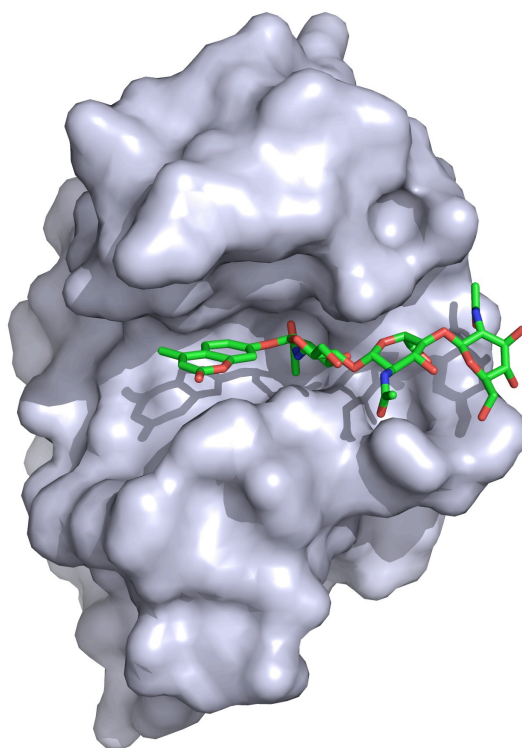


Figure 2-11. Crystal structure of lysozyme complex with 4MeU-(GlcNAc)₃ (199)
PDB code: 1BB6

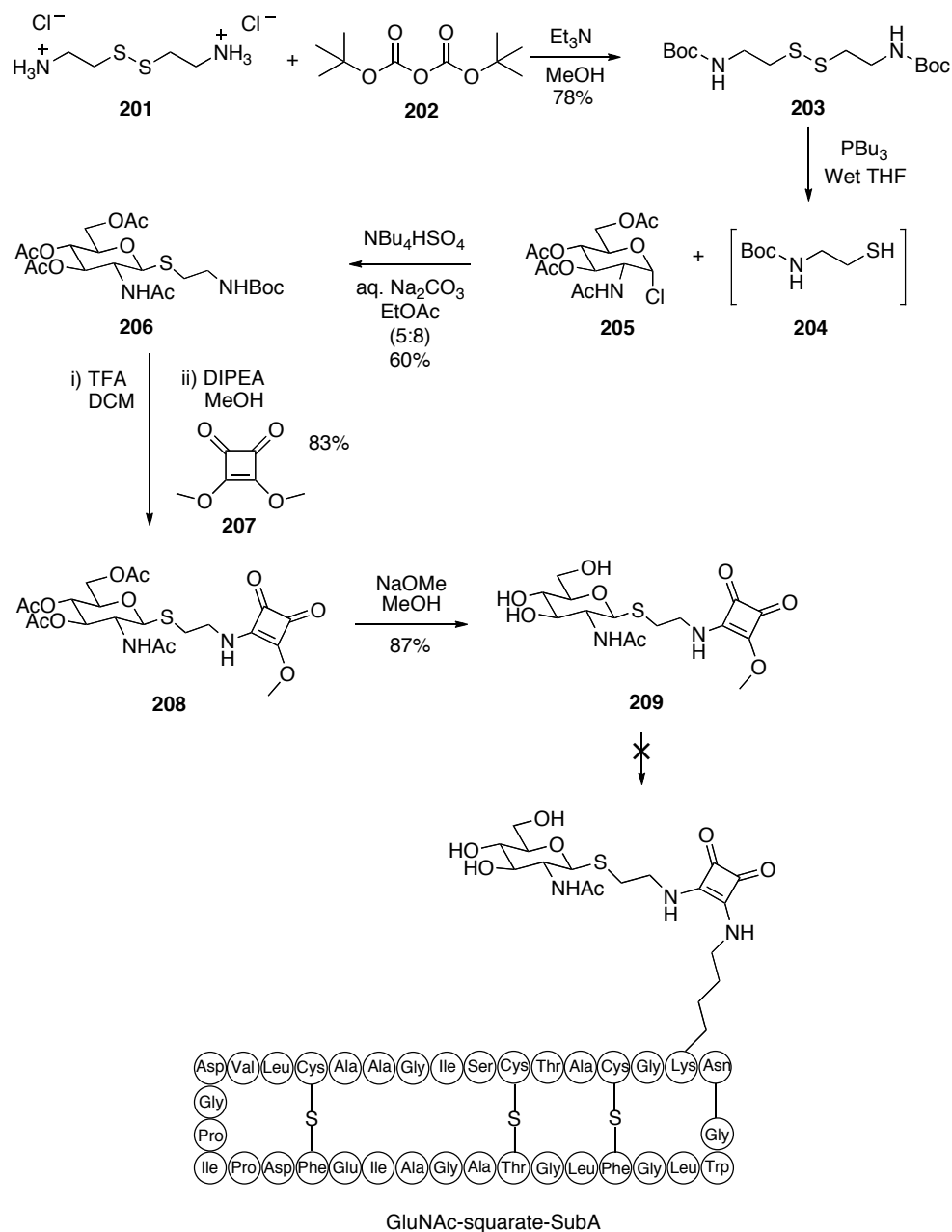
2.3.1.2 Bioconjugation of *N*-acetylglucosamine to SubA

Based on the studies reported above, we initially attempted preparation of a co-crystallizable SubA analogue involved using *N*-acetylglucosamine (GlcNAc, **194**) as the small inhibitor to lysozyme. The bioconjugation of GlcNAc and SubA was explored through two approaches: a squarate linking strategy and click chemistry.

2.3.1.2.1 Squarate as linker in the bioconjugation of *N*-acetylglucosamine to SubA

Squarate was chosen as the linker in the initial bioconjugate preparation. GlcNAc was first linked to squarate by the synthetic route shown in **Scheme 2-1**. Previous studies showed that the 1 and 6 positions of glucosamine do not play a significant role in binding,¹⁶⁷ and since there has been success in modification at position 1,¹⁶⁸ the anomeric position was selected as the linking site.

Commercially available cystamine dihydrochloride (**201**) was first protected with di-*tert*-butyl dicarbonate (Boc anhydride, **202**) as *N*-Boc-cystamine (**203**) under basic conditions. The disulfide bond was then cleaved by tributylphosphine *in situ*, and the resulting thiol **204** was further reacted with commercially available 3,4,6-tri-*O*-acetyl-2-(acetamido)-2-deoxy- α -D-glucopyranosyl chloride (**205**) to form the protected glucosamine derivative **206**. Removal of the Boc protecting group and further nucleophilic reaction with methyl squarate (**207**) yielded the protected glucosamine-squarate adduct **208**. Global deprotection of *O*-acetyl groups under basic conditions gave the GlcNAc-squarate adduct **209**. It was hoped that **209** would react with the ϵ -amino group of the only lysine residue of SubA with the other half of the squarate ester, to form the bioconjugate (GlcNAc-squarate-SubA). Since SubA is not stable under basic conditions, the reaction was done at neutral pH, but this was unsuccessful.



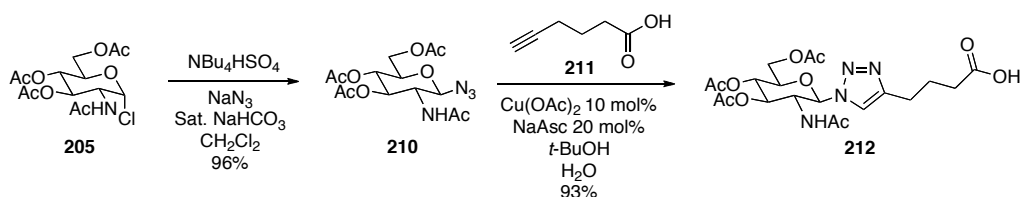
Scheme 2-1. Synthetic approach towards GlcNAc-squarate-SubA bioconjugate

2.3.1.2.2 Preparation of bioconjugate of *N*-acetylglucosamine-SubA via click chemistry

Since the squarate based linking strategy was unsuccessful, a neutral linking approach was required for this study, such as a 1,3-dipolar cycloaddition. The 1,3-dipolar cycloaddition was initially developed by Huisgen.^{171, 172} Subsequently, copper (I) catalyzed 1,3-dipolar cycloaddition has been developed by two individual groups led by Meldal¹⁷³ and Sharpless¹⁷⁴, and is commonly referred to as click chemistry. This reaction has been used widely in bioconjugation research, because of its simplicity, orthogonality to conventional protecting groups, and mild reaction conditions.

2.3.1.2.2.1 Preparation of azido-glucosamine derivative and model study of click chemistry

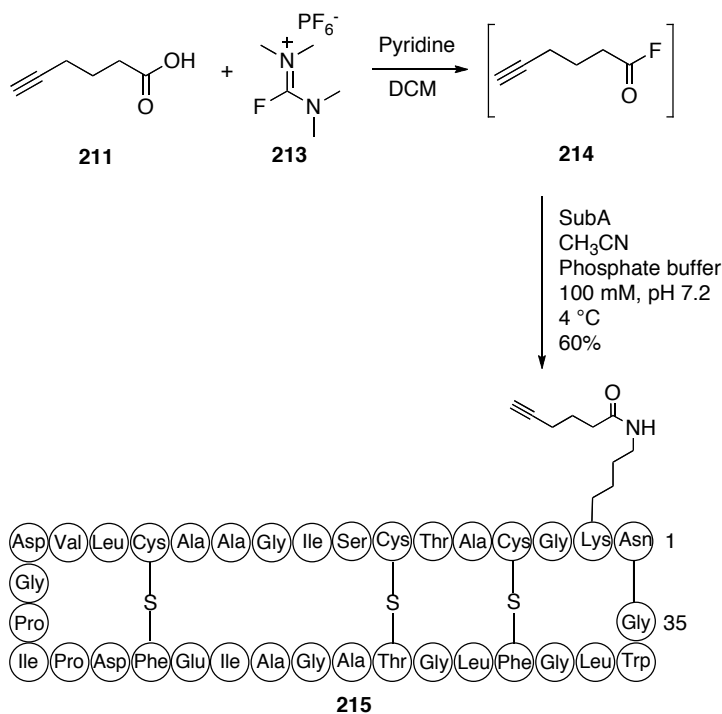
Initially, azido-*N*-acetylglucosamine was prepared under nucleophilic substitution reaction conditions (**Scheme 2-2**). Chlorine was replaced with an azido group to form azido-glucosamine derivative **210**. A model click chemistry reaction was done between 5-hexynoic acid (**211**) and **210**. Copper acetate and sodium ascorbate (NaAsc) were used to generate the copper (I) species, affording the product **212**.



Scheme 2-2. Model click chemistry reaction on glucosamine derivative

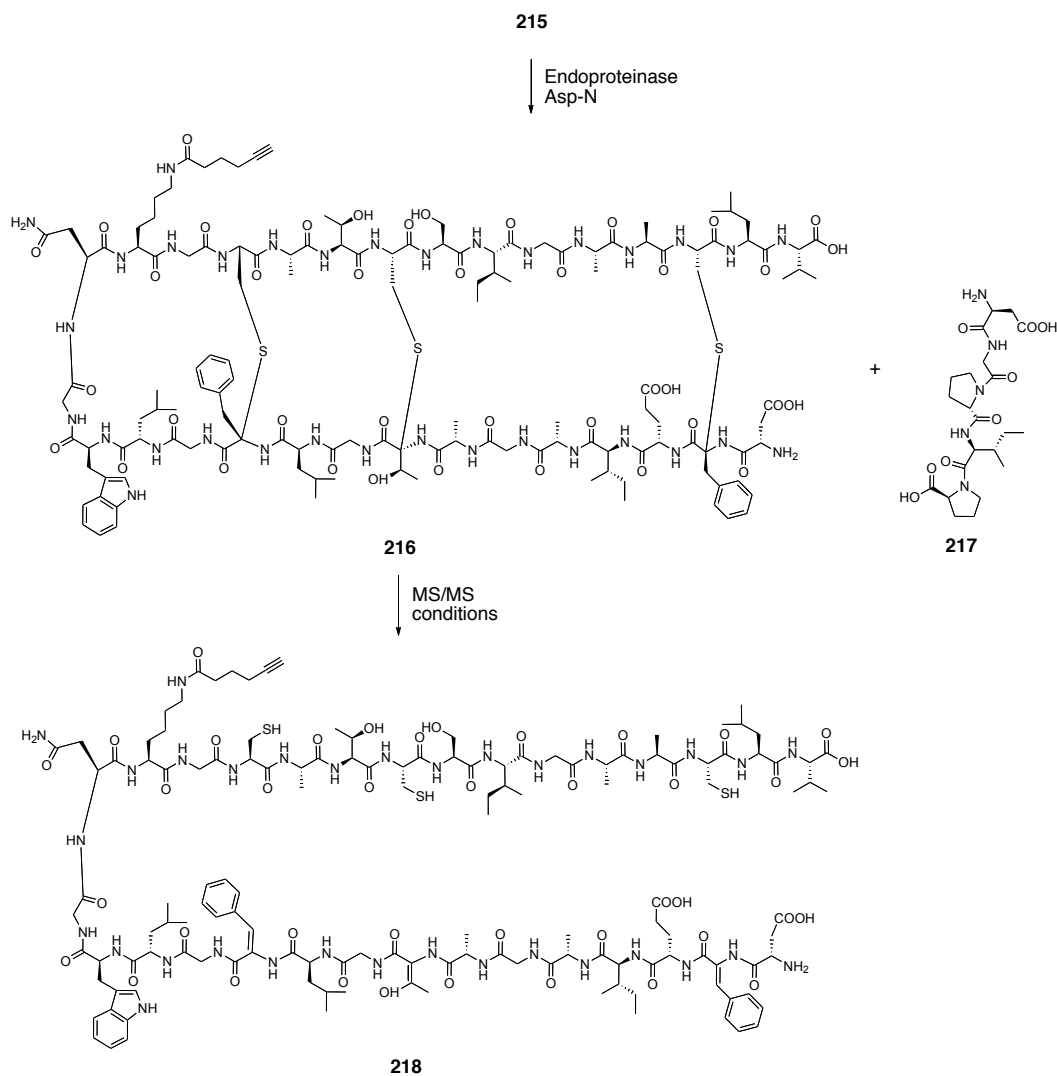
2.3.1.2.2.2 Preparation of the alkynyl-SubA

Since the model reaction was successful, alkynyl-SubA was prepared as shown in **Scheme 2-3**. 5-Hexynoic acid was converted to the corresponding acid fluoride by treatment with tetramethylfluoroformamidinium hexafluoro-phosphate (TFFH, **213**).¹⁷⁵ The resulting acid fluoride **214** was used without purification. SubA was mixed with the acid fluoride (**214**) in a mixture of acetonitrile and aqueous buffer solution at pH 7.2. Upon mixing at 4 °C for two days under argon, alkynyl-SubA (**215**) was purified using high-performance liquid chromatography (HPLC).



Scheme 2-3. Preparation of alkynyl-SubA

Due to the fact that SubA only contains one lysine residue, and thus has only one amino acid containing a free amino group on its side chain, the reaction should take place at the Lys2 position. To confirm reaction occurs at Lys2, MS/MS analysis was performed. Since SubA is not readily degraded under MS/MS conditions, due to its circular structure,¹⁴⁰ enzymatic digestion was applied to SubA. To cleave the circular structure in a controlled fashion, endoproteinase Asp-N was used to digest SubA. After two hours, a small portion of the mixture was analyzed by MALDI-MS. The MS signals suggested that SubA was cleaved into two fragments (**216** and **217**) as shown in **Scheme 2-4**.



Scheme 2-4. Enzymatic digestion of alkynyl-SubA by endoproteinase Asp-N

MS/MS analysis was then applied to the remaining portion of the reaction mixture (**Figure 2-12**), to characterize the larger peptide **216**. The detailed MS/MS analysis is described in **Chapter 3**. The thioether bridges were proposed to be cleaved under the MS/MS conditions to form compound **218** (**Scheme 2-4**). This type of behaviour for such α -linked peptides was subsequently confirmed in analysis of thuricin α and β ,^{161, 162} and thurincin H.¹⁶³ The sequence was

confirmed based upon MS/MS analysis. More importantly, based on the y-ion analysis, it was shown that the lysine residue was successfully modified as 5-hexynamide.

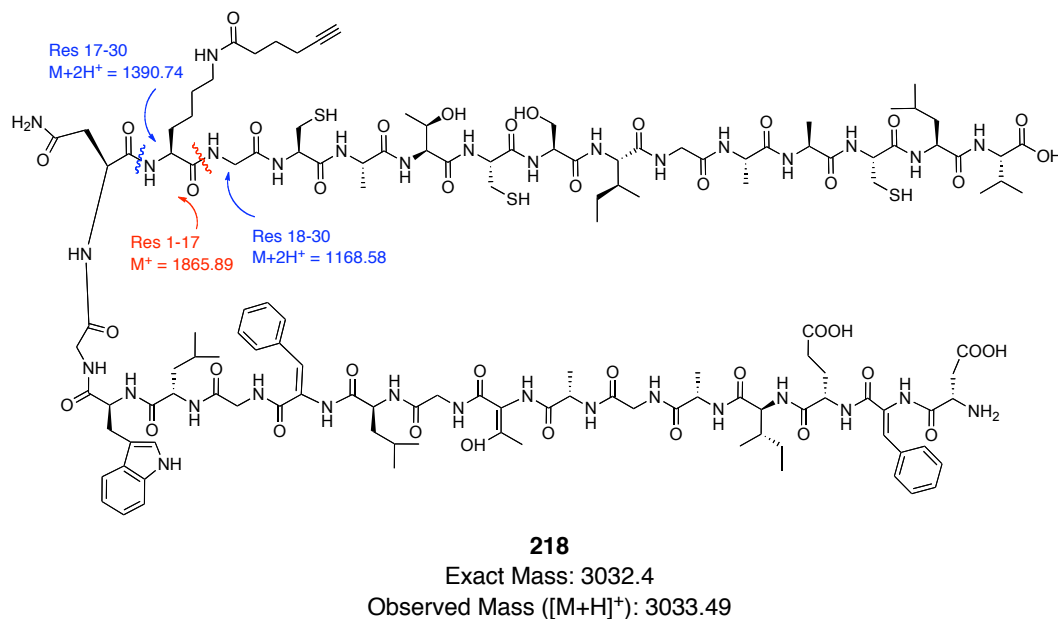


Figure 2-12. MS/MS analysis of enzymatic digested alkynyl-SubA. a) b-ion labeled in red; b) y-ion labeled in blue

2.3.1.2.2.3 Antimicrobial activity testing of the alkynyl-SubA

Alkynyl-SubA has been tested against the indicator organism, *Lactococcus lactis* subsp. *cremoris* HP, for antibacterial activity. As the spot on lawn test results show in **Figure 2-13**, alkynyl-SubA retained a comparable level of antimicrobial activity relative to natural SubA.

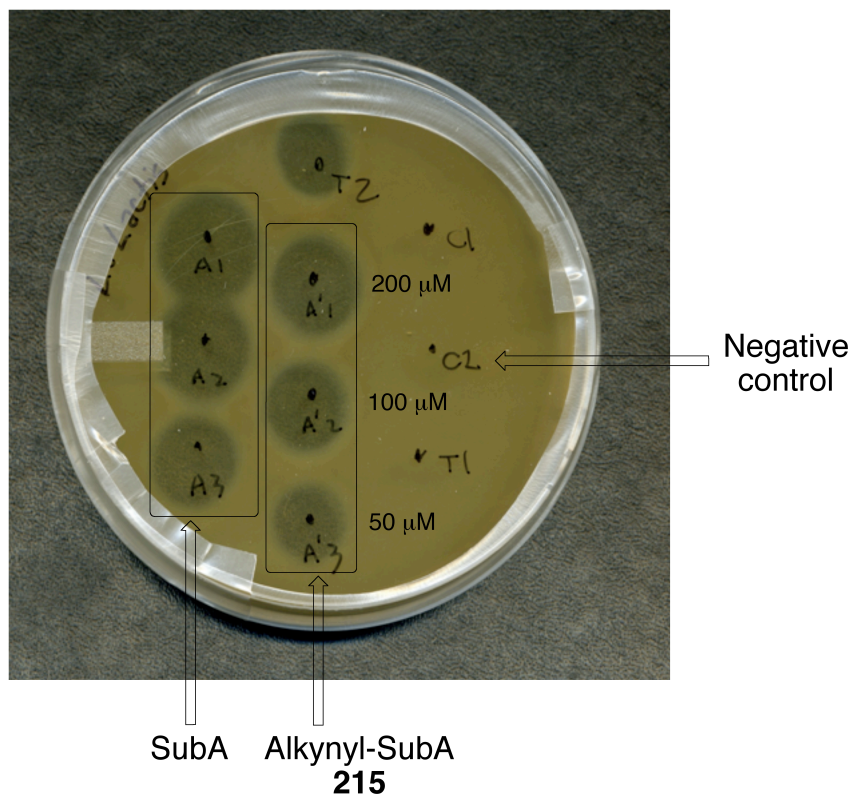


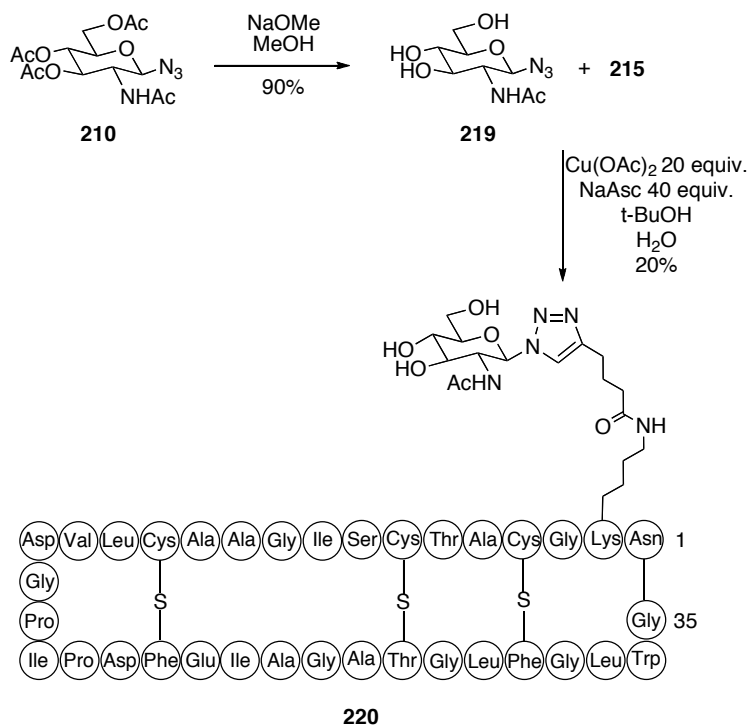
Figure 2-13. Spot on lawn antimicrobial activity testing results of SubA and alkynyl-SubA against *L. lactis* subsp. *cremoris* HP. The spots labelled C1, T1, and T2 were used for a separate study, and should be ignored. The spot labelled C2 was used as a negative control (spotted with 10 μ L of 1:1 mixture of acetonitrile and water). The spots labelled as A1, A2, and A3 correspond to SubA at 200 μ M, 100 μ M, and 50 μ M concentrations, respectively. The spots labelled as A'1, A'2, and A'3 correspond to alkynyl-SubA at 200 μ M, 100 μ M, and 50 μ M concentrations, respectively

These results indicate that the modified lysine residue does not significantly affect the antimicrobial activity. Based on earlier studies,¹⁷⁶ the mode of action of the antimicrobial activity of SubA is derived from membrane permeabilization process, and lysine was thought to interact with the lipid bilayers of the bacterial cell membrane. However, the exact mode of action is still unclear. Based on these current results, it seems that Lys2 is not a key residue with respect to the

antimicrobial activity of SubA. Furthermore, it provides a convenient handle for functionalization of SubA for mode of action studies in the future.

2.3.1.2.2.4 Preparation of *N*-acetylglucosamine-SubA bioconjugate and attempts to co-crystallize with lysozyme

After obtaining alkynyl-SubA (**215**), the bioconjugate of SubA and GlcNAc was then generated by click chemistry as shown in **Scheme 2-5**. The protected azido-glucosamine derivative **210** was deprotected under basic conditions to generate compound **219**. Click chemistry with **215** was performed under standard copper (I) catalyzed conditions to form bioconjugate **220**. It is important to note that 20 equivalents of the copper (I) species were required to afford the product, with low yield.



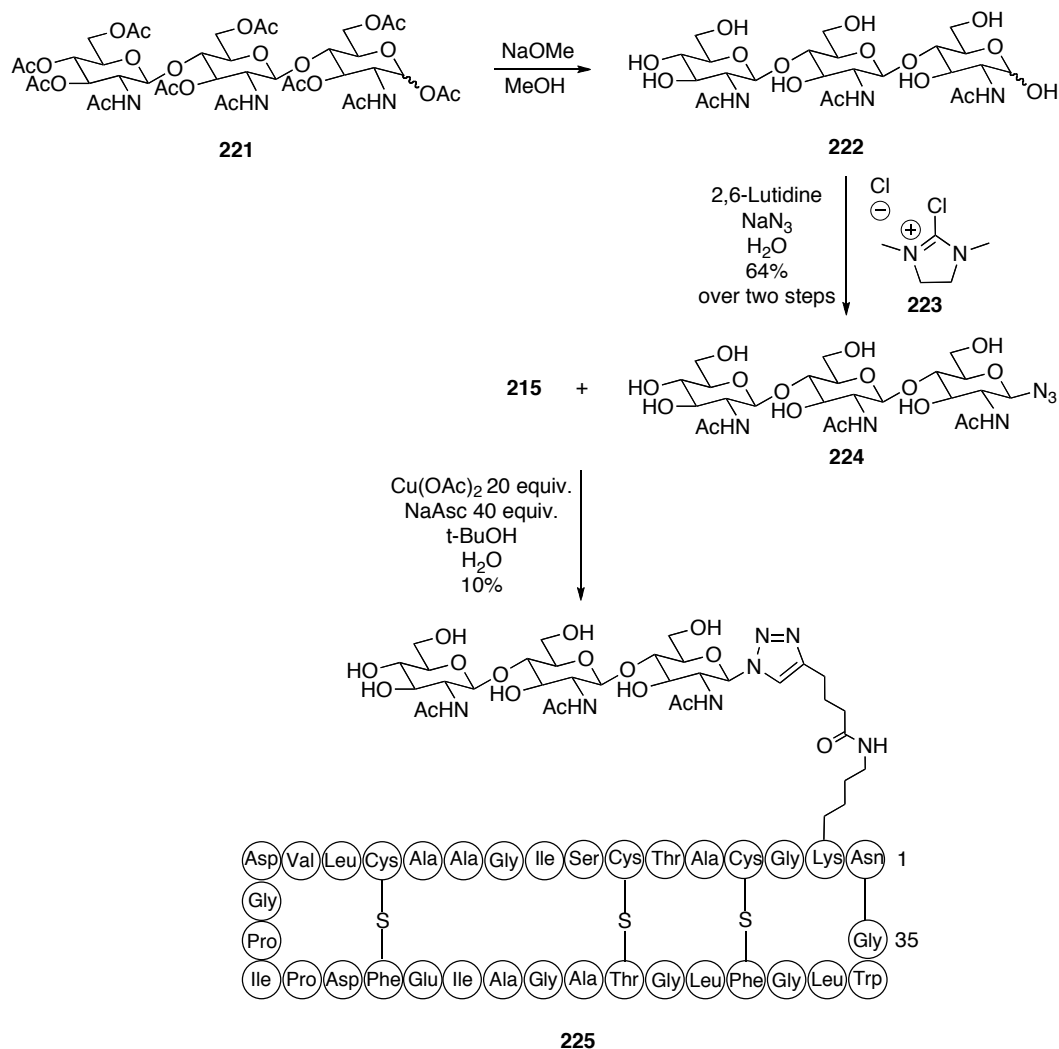
Scheme 2-5. Preparation of GlcNAc-SubA bioconjugate (**220**) using click chemistry

After HPLC purification, adduct **220** was applied to co-crystallization trials with commercially available lysozyme. This was performed in collaboration with Dr. Nobuhiko Watanabe in the Dr. Michael James group in the Department of Biochemistry at the University of Alberta. The co-crystallization studies were unsuccessful, as only crystals of the lysozyme were obtained. There were two potential reasons: the GlcNAc-SubA bioconjugate was too large to fit into the crystal lattice of lysozyme, or more likely, because of the poor solubility of the bioconjugate in aqueous media. Most of the GlcNAc-SubA adduct precipitated upon mixing with lysozyme solution.

2.3.1.3 Bioconjugate of *N,N',N''*-triacetylchitotriose (GlcNAc)₃-SubA

Despite the fact that the monosaccharide-SubA adduct was unable to be co-crystallized with lysozyme, we chose to use chitotriose as a potential inhibitor instead. Since chitotriose is a trisaccharide, the bioconjugate would be more polar, which would improve its water solubility. The (GlcNAc)₃-SubA adduct was prepared by click chemistry in a similar manner as previously done for the GlcNAc-SubA adduct. Again the anomeric position was chosen as the site of modification.

The synthesis of the bioconjugate followed the synthetic route shown in **Scheme 2-6**. First, commercially available peracetylated chitotriose (**221**) was deprotected under basic conditions to give *N,N',N''*-triacetylchitotriose **222**. Anomeric azido-chitotriose was prepared by treatment of **222** with 2-chloro-1,3-dimethylimidazolium chloride (DMC, **223**) and sodium azide under basic conditions.¹⁷⁷ The β-glycosyl azide (**224**) was generated in this one-pot reaction. Upon obtaining the azido-chitotriose (**224**), click chemistry conditions were applied to alkynyl-SubA (**215**) and the azidosaccharide **224**. The resulting adduct **225** was purified by HPLC. Again, a low yield was observed even in the presence of more than 20 equivalents of copper.



Scheme 2-6. Preparation of (GlcNAc)₃-SubA bioconjugate **225** using click chemistry

With the (GlcNAc)₃-SubA adduct in hand, the co-crystallization attempts were then again performed by Dr. Nobuhiko Watanabe in Professor Michael James' laboratory. Again, only pure lysozyme was crystallized, with no (GlcNAc)₃-SubA in the protein crystal. Solubility of the bioconjugate again seems to be the main issue. GlcNAc-SubA (**220**) and (GlcNAc)₃-SubA (**225**) were purified by an identical HPLC method. The (GlcNAc)₃-SubA adduct is indeed

more polar than the GlcNAc-SubA adduct; however, it is still quite hydrophobic. In fact, the solubility of these bioconjugates was the major issue throughout the co-crystallization trials, and will be discussed in the later sections.

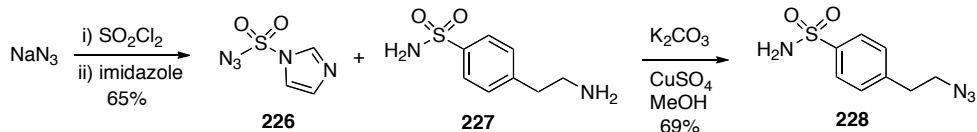
2.3.2 Benzenesulfonamide-SubA bioconjugates as inhibitors of carbonic anhydrase II (CAII).

As mentioned previously, CAII is a readily crystallizable enzyme; many crystal structures of this enzyme are available in the literature. Importantly, a benzenesulfonamide-linked ^{129}Xe -cryptophane biosensor (**190**) has been co-crystallized with CAII.^{132, 133} Based on this knowledge, we decided to use a similar approach to link benzenesulfonamide to SubA. Click chemistry was used as the initial linking strategy.

2.3.2.1 Click chemistry as a linking approach between benzenesulfonamide and SubA

2.3.2.1.1 Copper (I) catalyzed click chemistry between benzenesulfonamide and SubA

Based on Christianson's work,^{132, 133} a SubA-benzenesulfonamide adduct with a short linker was designed. The azido-benzenesulfonamide was prepared as shown in **Scheme 2-7**. The diazotransfer reagent **226** was prepared according to literature procedure,¹⁷⁸ in which sulfuryl chloride was reacted with sodium azide and imidazole in a stepwise process. Commercially available amino-benzenesulfonamide **227** was then reacted with **226** to form adduct **228**, the desired azido-benzenesulfonamide.



Scheme 2-7. Preparation of azido-benzenesulfonamide **228**

Similar copper (I) catalyzed click chemistry was then performed as seen previously (i.e. **220** and **225**). In this case, the reaction did not proceed as expected. In the syntheses of GlcNAc-SubA (**220**) and (GlcNAc)₃-SubA (**225**), the products were formed with relatively low yield and required more than 20 equivalents of copper. In the azido-benzenesulfonamide case, no product was detected by HPLC or MALDI-MS. This unsuccessful reaction, along with the low yield obtained for the other bioconjugates, indicates that copper (I) catalyzed click chemistry may not be the most efficient approach for bioconjugate preparation. One potential explanation is that the sulfur atoms of the three thioether bridges in SubA could coordinate to the copper catalyst and lower the efficiency of copper-catalyzed click chemistry, which resulted in low yields and long reaction times. Recent developments of copper-free click chemistry^{179, 180} caught our attention, and we decided to explore this further.

2.3.2.1.2 Copper-free click chemistry between benzenesulfonamide and SubA

Since click chemistry is used widely in organic synthesis and biological chemistry, this bioconjugate approach has become very popular in the past decade. However, when click chemistry is used in a biological environment, toxicity of the copper catalyst becomes an issue. Because of the cytotoxicity of

copper (I), Bertozzi and co-workers^{179, 180} have developed a copper-free click chemistry method. In their initial study, a strained cyclooctyne compound **229** was examined as the click chemistry substrate. The eight-membered ring is the smallest size capable of containing a carbon-carbon triple bond. The ring strain activates the alkynyl group, and so it is more reactive than a normal alkyne. Thus, click chemistry with a cyclooctyne species can proceed without copper (I) catalysis.¹⁷⁹ Subsequently, a difluorinated cyclooctyne (DIFO, **230**) was developed.¹⁸⁰ The difluoro group further activates the triple bond via an electron-withdrawing effect, making DIFO more reactive than non-fluorinated cyclooctyne compounds. However, one limitation of the application of DIFO in copper-free click chemistry is the complicated preparation, which typically requires more than ten synthetic steps.

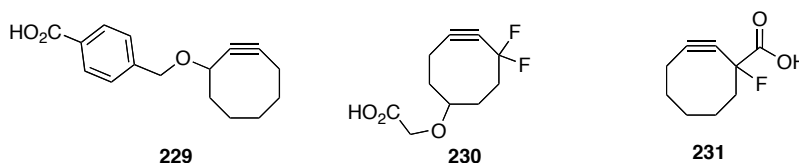


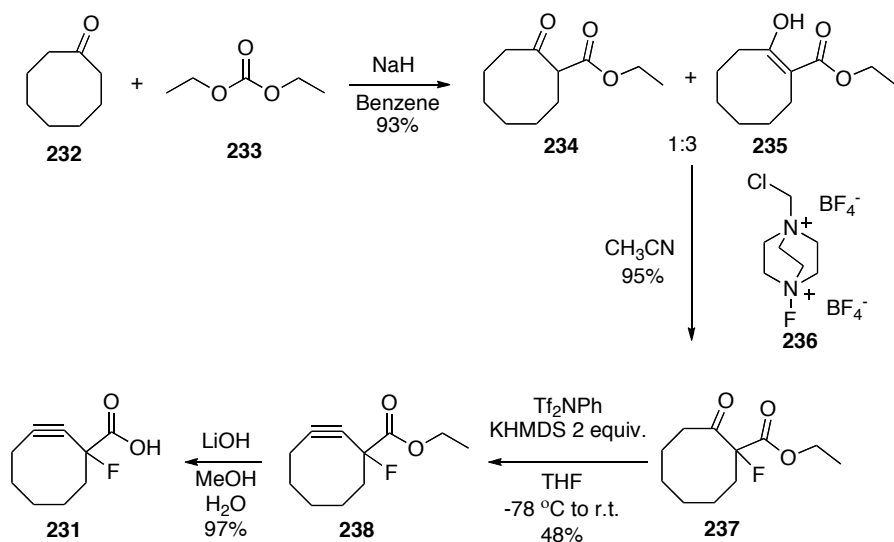
Figure 2-14. Literature examples of cyclooctyne derivatives **229**, **230**, and **231** used in copper-free click chemistry¹⁷⁹⁻¹⁸²

Since the synthesis of DIFO (**230**) is complicated and lengthy, a simpler cyclooctyne derivative (**231**) has recently been developed.¹⁸¹ This compound was found to be very effective toward click chemistry as well. The rate of reaction for this monofluoro-substituted **231** when reacting with benzyl azide was two-fold slower than the reaction with DIFO.^{181, 182} However, the monofluoro-substituted

cyclooctyne reacts about one order of magnitude faster than the compound without fluorine as a substituent (**229**).^{181, 182} The monofluorinated cyclooctyne **231** was selected for the copper-free click chemistry linkage between SubA and the benzenesulfonamide inhibitor in the present study because of the reasonable rate of the reaction and relatively simple synthesis.

2.3.2.1.2.1 Preparation of the monofluorinated cyclooctyne derivative

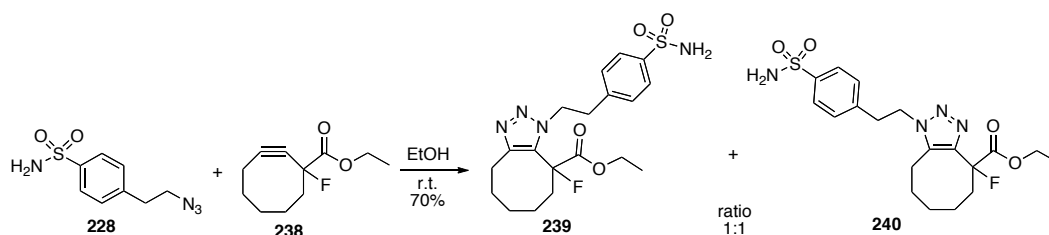
Preparation of the monofluorinated cyclooctyne **231** followed literature procedures¹⁸¹ and is shown in **Scheme 2-8**. Commercially available cyclooctanone (**232**) and diethyl carbonate (**233**) were used to facilitate the formation of **234** and **235**, which were obtained in 1:3 ratio. The mixture was then reacted with Selectfluor[®] (**236**) to form the monofluorinated intermediate **237**. Subsequently, introduction of a triflate leaving group on the corresponding enolate under basic conditions, followed by elimination, afforded acetylene **238**. Saponification gave the desired monofluorinated cyclooctyne derivative **231** with a carboxylic acid substituent as a handle for further linkage to biomolecules.



Scheme 2-8. Preparation of the monofluorinated cyclooctyne **231**

2.3.2.1.2.2 Click chemistry between the monofluorinated cyclooctyne and the azido-benzenesulfonamide derivative

Upon obtaining the monofluorinated cyclooctyne derivative **231**, a test click reaction was done using azido-benzenesulfonamide derivative **228**. The reaction is shown in **Scheme 2-9**. A 1:1 mixture of two regioisomers was formed upon mixing the two substrates. The isomers were separated by column chromatography and characterized by NMR. Furthermore, isomer **239** was crystallized and analyzed by X-ray crystallography. The detailed crystallographic information is included in **Chapter 3**.



Scheme 2-9. Click chemistry with monofluorinated cyclooctyne derivative and azido-benzenesulfonamide derivative affords isomers **239** and **240**

2.3.2.1.2.3 Testing inhibitory activity of the click chemistry adduct against

CAII

After obtaining the click chemistry adducts of azido-benzenesulfonamide and cyclooctyne, the compounds were tested for inhibitory activity against CAII to ensure that they retained activity. The plasmid containing the gene for CAII was obtained from Professor David Christianson, and then the enzyme was transformed and expressed in *E. coli*, and purified by ion exchange chromatography with the help of Dr. Marco J. van Belkum in our laboratory. A detailed purification procedure is described in **Chapter 3**. A literature assay was adopted, using *p*-nitrophenol acetate as a substrate for the esterase activity of the CAII as shown in **Figure 2-15**.¹⁸³ A detailed procedure for assay of the inhibitory activity is described in **Chapter 3**.

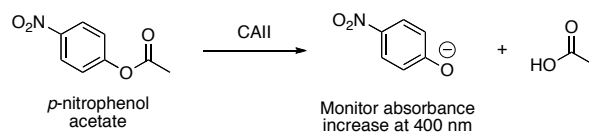


Figure 2-15. *p*-Nitrophenol acetate assay for activity testing of CAII.

The results of testing are shown in **Figure 2-16**. In this preliminary inhibitory study, only IC_{50} values were measured, since the important aspect is whether the adduct retains activity compared to the starting material azidobenzenesulfonamide.¹⁸⁴ In this assay, the inhibitors were shown to have IC_{50} values in the 100 nM range. Based on these results, click chemistry adduct **239** (IC_{50} 176 nM) showed very similar inhibitory activity to the azidobenzenesulfonamide **228** (IC_{50} 171 nM). The regioisomer **240** showed slightly lower inhibitory activity (IC_{50} 250 nM), however, it is still a very effective inhibitor of CAII.

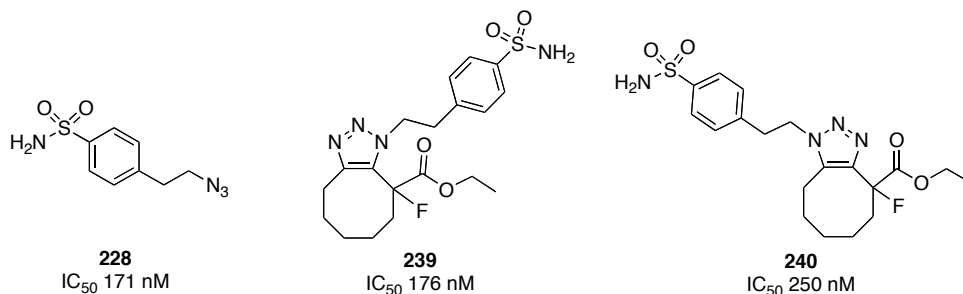


Figure 2-16. Inhibitory activity testing of the sulfonamide inhibitors against CAII as tested using *p*-nitrophenol acetate assay

2.3.2.1.2.4 Attempts towards the bioconjugate of SubA-cyclooctyne-benzenesulfonamide

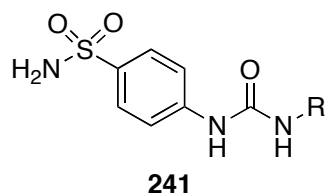
With the adducts of the benzenesulfonamide and cyclooctyne in hand, the next step was to couple the adducts to SubA through formation of an amide bond to the lysine residue. After saponification of compound **238**, **239**, and **240**, the resulting carboxylic acids were activated with TFFH to form the acid fluoride.

However, the coupling reactions between SubA and the generated acid fluorides were unsuccessful for all three cases, potentially due to the sterically hindered nature of the cyclooctyne substrate. This reaction could still be explored further with different coupling conditions.

2.3.2.2 Ureido-containing arylsulfonamide coupled SubA bioconjugate

2.3.2.2.1 Literature precedent for ureido-containing arylsulfonamide inhibitors to CAII

The ultimate goal for this project is to develop a general method for small peptide co-crystallization. At the same time, parallel to the click chemistry strategy, a simpler linking method was also investigated. Since carbonic anhydrases are interesting targets for medicinal chemistry development, new inhibitors of these enzymes frequently appear in the literature. In 2010, a group of ureido-benzenesulfonamide derivatives (**241a-e**, **Figure 2-17**) were reported as inhibitors of CAII.¹⁸⁵ These compounds have potent inhibitory activity against CAII with inhibition constant values in the range of 3.3 to 226 nM. Compound **241c** is especially potent with a K_i of 3.3 nM.



	K_i (nM)
a) R = 4-F-C ₆ H ₄	96 ± 8
b) R = C ₆ F ₅	50 ± 4
c) R = 2-iso-Pr-C ₆ H ₄	3.3 ± 0.07
d) R = 3-NO ₂ -C ₆ H ₄	15 ± 0.8
e) R = cyclopentyl	226 ± 14

Figure 2-17. Examples of ureido-containing arylsulfonamides reported in the literature as inhibitors of CAII¹⁸⁵

In this study, the authors were also able to co-crystallize all five compounds (**241a-e**) with CAII. An overlaid diagram (**Figure 2-18**), taken from the literature,¹⁸⁵ shows the interactions between these five compounds and CAII. The benzenesulfonamide interactions within the active site are well conserved. The sulfonamide, the pharmacophore, is coordinated to the zinc ion in the active site of CAII. Through an ureido linker, the second ring is pointing away from the active site. Based on the co-crystal structures of inhibitor bound CAII, two analogues of these compounds were designed and synthesized.

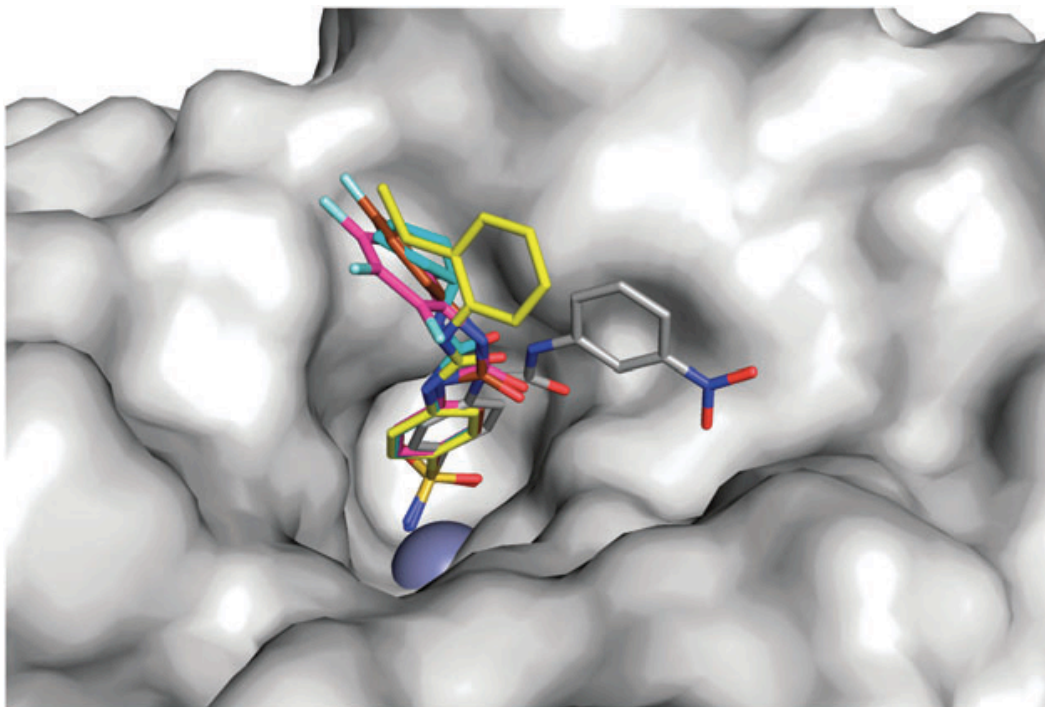


Figure 2-18. Crystal structure of CAII with overlays of various ureido-containing arylsulfonamides, **241a-e**, labeled in orange, pink, yellow, grey, and cyan, respectively¹⁸⁵ Reproduced with permission from Pacchiano et al.¹⁸⁵

2.3.2.2.2 Synthesis of the ureido-containing arylsulfonamide compounds

Since benzenesulfonamides with ureido moieties are well conserved in the active site and appear to be required for binding, this part of the molecule was kept constant. It seems that the inhibitors with higher potency against CAII have aromatic systems at the second ring position, further from sulfonamide moiety. We decided to use coupling reactions to link the benzenesulfonamide inhibitors and SubA through an amide bond. Thus, the second ring of the ureido-containing benzenesulfonamide was designed as 4-carboxy-benzene **242** and 2-methyl-4-carboxy-benzene **243**. The extra methyl group on compound **243** is a homologue

to the compound **241c**. The two carboxyl groups are designed to be the coupling site for linking to Lys2 of SubA.

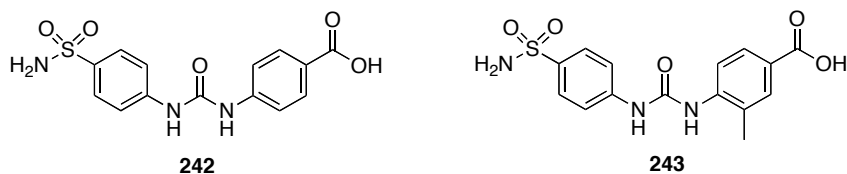
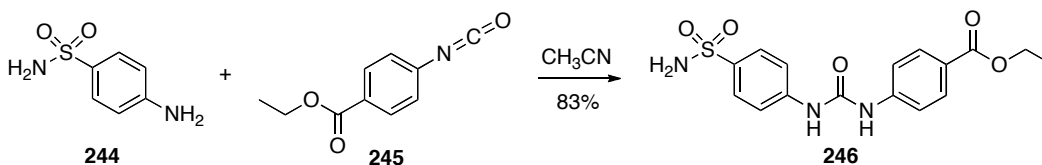


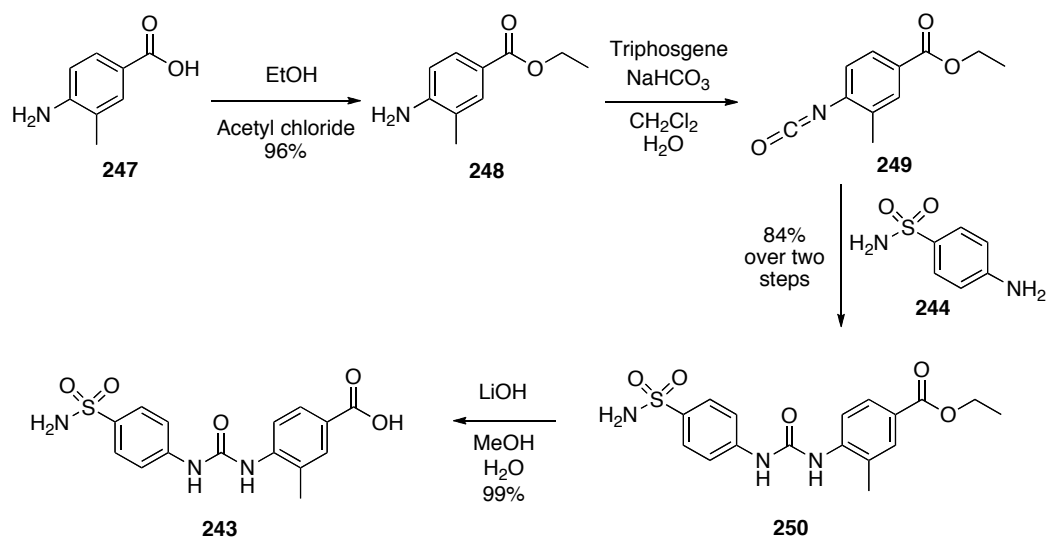
Figure 2-19. Proposed ureido-containing benzenesulfonamide inhibitors to CAII

The ethyl ester of compound **242** was prepared from two commercially available compounds, *p*-aminobenzenesulfonamide (**244**) and ethyl *p*-isocyanatobenzoate (**245**), as shown in **Scheme 2-10**.



Scheme 2-10. Preparation of ureido-containing benzenesulfonamide **246**

The second inhibitor was prepared by the route shown in **Scheme 2-11**. First, 4-amino-3-methylbenzoic acid (**247**) was esterified to form **248**. The amino group was then reacted with triphosgene to yield isocyanate derivative **249**. The isocyanate was then reacted with 4-aminobenzenesulfonamide (**244**) to form the ethyl ester of the ureido-containing benzenesulfonamide inhibitor **250**. Finally, saponification gave the desired inhibitor with a carboxyl group substituent on the second benzene ring.



Scheme 2-11. Preparation of **243**, the second ureido-containing benzenesulfonamide inhibitor

2.3.2.2.3 Inhibitory activity testing of ureido-containing benzenesulfonamide inhibitors against CAII

The ethyl ester forms of the two designed inhibitors were tested against CAII using the *p*-nitrophenyl acetate assay, as described previously. As shown in **Figure 2-20**, the two inhibitors (**246** and **250**) showed nearly identical inhibition against the enzyme and higher potency than the cyclooctyne derivatives (**239** and **240**). Thus, compound **250** with an extra methyl group on the aromatic system was selected for further bioconjugation with SubA.

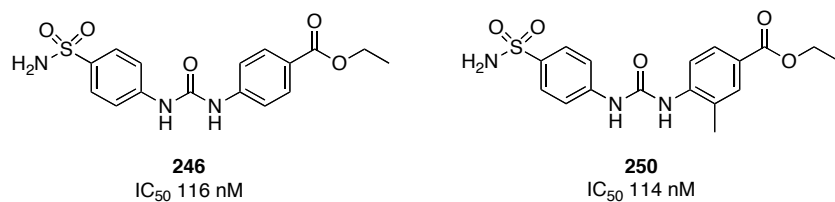
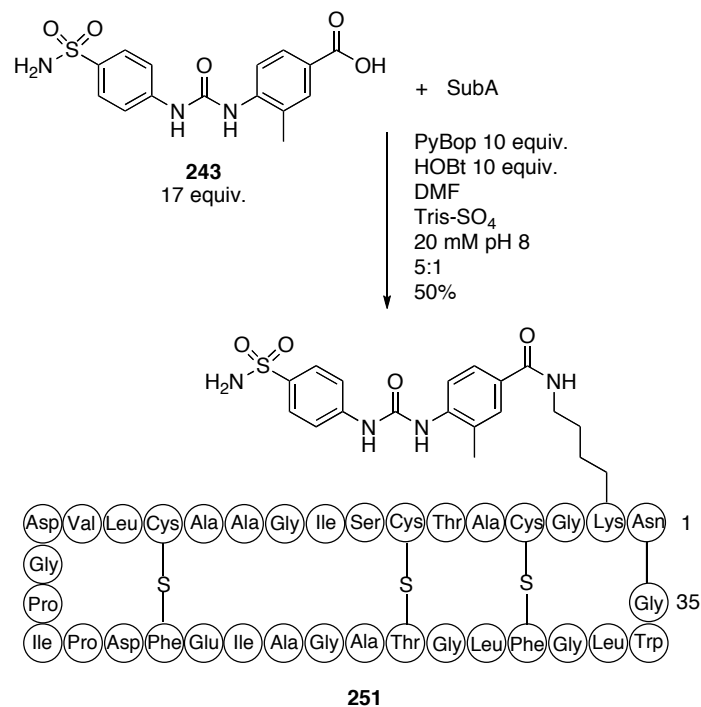


Figure 2-20. Results of activity testing of the ureido-containing benzenesulfonamide inhibitors against CAII

2.3.2.2.4 Coupling between the ureido-containing benzenesulfonamide and

SubA

Upon synthesis of the ureido-containing inhibitors, compound **243** was selected for coupling with SubA. Based on previous experiences of coupling reactions with SubA, the rate of reaction is always slow under neutral conditions. SubA is known to be unstable under basic conditions. To overcome both the stability and rate of reaction issues, slightly basic conditions with a shorter reaction time were applied in this coupling reaction (**Scheme 2-12**), resulting in the successful formation of the bioconjugate product of ureido-benzenesulfonamide and SubA. It is possible that SubA decomposes under basic conditions, in which the thioether bridges are potentially cleaved as observed under MS/MS conditions (**Scheme 2-4**). After purification by HPLC, the bioconjugate was applied to co-crystallization trials with CAII, which are currently in progress and being performed by Dr. Cory Brooks in the group of Dr. Joanne Lemieux.



Scheme 2-12. Preparation of ureido-benzenesulfonamide-SubA bioconjugate

2.4 Conclusion and future directions

During this project, several bioconjugates of SubA with various small molecules were synthesized. Several linking strategies were attempted including using squarate as a linker, click chemistry, copper-free click chemistry, and coupling through an amide linkage. The GlcNAc-SubA and (GlcNAc)₃-SubA adducts were obtained by copper (I) catalyzed click chemistry. An ureido-containing benzenesulfonamide-SubA bioconjugate was prepared through an amide bond linkage.

Although the ultimate goal of this project (a general method for co-crystallization) has not yet been achieved, several conclusions can be drawn from this study. Based on the antimicrobial activity testing of alkynyl-SubA, retention

of the activity indicates that the lysine residue does not play a major role in the antimicrobial mechanism of SubA. This is in contrast to previous hypotheses.¹⁷⁶ In terms of co-crystallization studies, the solubility of SubA bioconjugates appeared to be the major issue due to the hydrophobic nature of SubA.

Since the lysine-modified-SubA retained antimicrobial activity, this provides an opportunity towards mode of action studies of SubA by utilizing the lysine residue as a handle to link various molecules, such as fluorescent probes.

Efforts are still underway towards co-crystallization. A different approach might be required to overcome solubility issues, such as the use of detergents or various organic solvents as co-solvents in the crystallization process. In this regard, the enzyme involved in co-crystallization has to be compatible with the co-solvent. To ensure that enzyme activity is retained, enzymatic testing in different solvent systems is currently in progress.

Chapter 3. Experimental Procedures

3.1 General Information

3.1.1 Reagents, solvents and purifications

All commercially available reagents were purchased from Sigma-Aldrich Canada Ltd., Fisher Scientific Ltd., Alfa Aesar Ltd., AB Chem Inc., ChemBridge Corporation or VWR International and used without further purification. All solvents were of American Chemical Society (ACS) grade and were used without further purification unless otherwise stated. All anhydrous reactions were performed under a positive pressure of argon using flame or oven-dried glassware. Solvents for anhydrous reactions were distilled prior to use: dichloromethane, 1,2-dichloroethane, pyridine, and triethylamine were distilled over calcium hydride, tetrahydrofuran was distilled over sodium with benzophenone as an indicator, and ethyl acetate and methanol were distilled over potassium carbonate. HPLC grade acetonitrile, dimethylformamide, isopropyl alcohol and methanol were used without further purification. Commercially available ACS grade solvents (>99.0% purity) were used for column chromatography without any further purification. Deionized water was obtained from a Milli-Q reagent water system (Millipore Co., Milford, MA). Air sensitive reactions were performed under an atmosphere of argon. All reactions and fractions from column chromatography were monitored by thin layer chromatography (TLC) using glass plates with a UV fluorescent indicator (normal SiO₂, Merck 60 F₂₅₄). One or more of the following methods were used for visualization: UV absorption by fluorescence quenching,

staining with phosphomolybdic acid in ethanol (10 g/100 mL), ninhydrin (ninhydrin : acetic acid : *n*-butanol/ 0.6 g : 6 mL : 200 mL), or *p*-anisaldehyde (*p*-anisaldehyde : acetic acid : 95 % ethanol : conc. H₂SO₄/ 9.2 mL : 3.75 mL : 338 mL : 12.5 mL). Flash chromatography was performed using Merck type 60, 230-400 mesh silica gel. The removal of solvents *in vacuo* was performed via evaporation under reduced pressure at a temperature below 40 °C using a Büchi rotary evaporator followed by evacuation (< 0.1 mm Hg) to a constant sample mass.

Analytical scale high performance liquid chromatography (HPLC) was performed on one or more following systems: Beckman System Gold chromatograph equipped with a model 166 variable wavelength UV detector and a Rheodyne 7725i injector fitted with a 100 µL sample loop; Varian ProStar chromatograph equipped with model 210 pump heads, a model 325 dual wavelength UV detector, and a Rheodyne 7725i injector fitted with a 100 µL sample loop; or a Gilson chromatograph equipped with model 322 pump heads, a model 171 diode array detector, a FC 203B fraction collector, and a Rheodyne 7725i injector fitted with a 500 µL sample loop. Preparative and semi-preparative scale HPLC was performed on one or more following systems: Beckman System Gold chromatograph equipped with a model 125P solvent module, a model 166P variable wavelength UV detector, and a Rheodyne 7725i injector fitted with a 1000 µL sample loop; Gilson chromatograph equipped with model 322 pump heads, a model UV/VIS-156 detector, and a GX-271 liquid handler; Varian ProStar chromatograph equipped with model 210 pump heads, a model 325 dual

wavelength UV detector, and a Rheodyne 7725i injector fitted with a 1000 μ L sample loop. The columns used were Vydac 208TPTM C8 reverse phase (300 \AA , 5 μ m, 4.6 \times 250 mm (analytical) or 10 \times 250 mm (semipreparative)). All HPLC solvents were filtered through a Millipore filtration system under vacuum before use.

3.1.2 Characterization

Nuclear magnetic resonance (NMR) spectra were recorded on a Varian Inova 600, Inova 500, Inova 400, Inova 300 or Unity 500 spectrometers at 27 $^{\circ}$ C. For ^1H (300, 400, 500 or 600 MHz) spectra, δ values were referenced to CDCl_3 (7.26 ppm), CD_3OD (3.30 ppm), $\text{DMSO-}d_6$ (2.50 ppm), or DOH (4.79 ppm) and for ^{13}C (75, 100, 125 or 150 MHz) spectra, δ values were referenced to CDCl_3 (77.0 ppm), CD_3OD (49.0 ppm), or $\text{DMSO-}d_6$ (39.5 ppm). Reported splitting patterns are abbreviated as s = singlet, d = doublet, t = triplet, q = quartet, m = multiplet. When appropriate, a signal splitting pattern is preceded by br to indicate that it is broad.

Infrared spectra (IR) were recorded on either a Nicolet Magna 750 FT-IR spectrometer or a Nic-Plan FT-IR microscope. The term cast refers to the evaporation of a solution on a NaCl plate.

Mass spectra (MS) were recorded on a Agilent Technologies 6220 oaTOF, a Kratos AEIMS-50, an Applied BioSystems Mariner BioSpectrometry Workstation, or a Perspective Biosystems VoyagerTM Elite MALDI-TOF MS using either α -cyano-4-hydroxycinnamic acid (CHCA) or 3,5-dimethoxy-4-

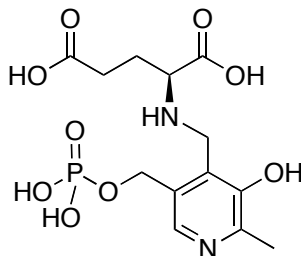
hydroxycinnamic acid (sinapinic acid) as a matrix. MS/MS was performed on a Bruker Ultraflextreme MALDI/TOF/TOF. For MALDI-TOF MS, a typical sample preparation is described as follows. A solution of sample peptide (1 μL) in 0.1% TFA (aq.) is mixed in a 1:1 ratio (vol/vol) with a stock solution of sinapinic acid (10 mg/mL) in 50% acetonitrile containing 0.1% TFA (aq.). To prepare the sample plate, a sinapinic acid layer (0.7 μL ; 10mg/mL sinapinic acid in 3:2 acetone:methanol) is pipetted onto a stainless steel target plate. The solvent is allowed to evaporate, leaving a thin layer of sinapinic acid on the surface of the plate. The sample-matrix solution (0.6 μL) is then spotted onto the dried layer of sinapinic acid and allowed to dry.

Optical rotations were measured on a Perkin Elmer 241 polarimeter with a microcell (10 cm, 1 mL) at ambient temperature and are reported in units of 10^{-1} deg $\text{cm}^2 \text{g}^{-1}$. All reported optical rotations were referenced against air and measured at the sodium D line ($\lambda = 589.3 \text{ nm}$)

3.2 Substrate mimic 88 and 90 into LL-DAP-AT

The substrate mimic and the PLP-Glu and PLP-DAP adducts were synthesized following the procedure published by Dr. Matthew Clay.¹¹²

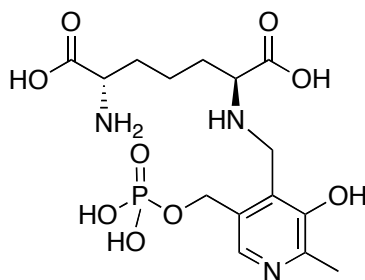
3.2.1 Synthesis of substrate-PLP imine adduct mimic



(S)-2-((3-Hydroxy-2-methyl-5-(phosphonomoxymethyl)pyridin-4-yl)methylamino)pentanedioic acid (88)

Pyridoxal 5'-phosphate (0.100 g, 0.405 mmol) and glutamic acid (0.119 g, 0.809 mmol) were added to water (7 mL) and the pH was adjusted to ~9.3 using 2 M KOH to give a brilliant yellow solution. The mixture was then stirred for 90 minutes at room temperature, after which time solid NaBH₄ (0.062 g, 1.62 mmol) was carefully added in small portions over a period of 3 minutes. The colorless solution was stirred for an additional 15 minutes and then neutralized via the dropwise addition of formic acid. The solution was then concentrated to ~4 mL under reduced pressure to provide 0.390 g of sticky solid which was then loaded onto an anion exchange column (Biorad AG1-X8 resin, 100-200 mesh size, HCO₃⁻ form, column dimensions 1 cm x 40 cm). Elution using a gradient of 0 – 0.5 M NH₄HCO₃ (2 mL/min flow rate) followed by repeated lyophilization then provided pure PLP-Glu (0.110 g, 73%). White solid; IR (microscope): $\nu = 3081$,

2823, 2737, 1603, 1420, 1353, 1178, 1084, 854, 760, 707 cm^{-1} ; ^1H NMR (500 MHz, D_2O) δ 7.77 (s, 1H, Ph-H), 4.94 (d, $J = 7.5$ Hz, 2H, O-CH₂), 4.38 (m, 2H, N-CH₂), 3.72 (m, 1H, N-CH), 2.47-2.51 (m, 5H), 2.13-2.17 (m, 2H); ^{13}C NMR (125 MHz, D_2O) δ 178.5, 173.9, 162.1, 145.3, 134.9, 132.0, 125.7, 62.9, 62.4, 44.5, 31.5, 25.9, 15.7; ESI-HRMS m/z calcd for $\text{C}_{13}\text{H}_{18}\text{N}_2\text{O}_9\text{P}$: 377.0745 [M-H]⁻, found: 377.0745.



(2*S*,6*S*)-2-Amino-6-(2-hydroxy-3-methyl-6-(phosphonooxymethyl)benzylamino)heptanedioic acid (90)

PLP-DAP was prepared analogously to PLP-Glu. Pyridoxal 5'-phosphate (0.0250 g, 0.101 mmol) and LL-DAP (0.0385 g, 0.202 mmol) were added to water (2 mL) and the pH was adjusted to ~9.3 using 2 M KOH to give a brilliant yellow solution. The reaction was then stirred for 90 minutes at room temperature, after which time solid NaBH_4 (0.0153 g, 0.405 mmol) was carefully added in small portions over a period of 3 minutes. The colorless solution was stirred for an additional 15 minutes and then quenched via the dropwise addition of formic acid until the pH was approximately 2. The solution was then neutralized using 2 M KOH and loaded onto an anion exchange column (Biorad AG1-X8 resin, 100-200 mesh size, HCO_3^- form, column dimensions 1 cm x 40 cm). Elution using a

gradient of 0-0.35 M NH_4HCO_3 (2 mL/min flow rate) followed by repeated lyophilization then provided pure PLP-DAP (34 mg, 40%). White solid; IR (microscope): $\nu = 3122, 3036, 2811, 1605, 1404, 1042, 970, 927 \text{ cm}^{-1}$; ^1H NMR (500 MHz, D_2O) δ 7.63 (s, 1H, Ph-H), 4.83-4.84 (m, 2H, O-CH₂), 4.29-4.39 (m, 2H, N-CH₂), 3.69-3.70 (m, 2H), 2.42 (s, 3H, CH₃), 1.84-1.94 (br m, 4H), 1.46-1.48 (br m, 2H); ^{13}C (125 MHz, D_2O) δ 175.5, 174.4, 164.0, 145.4, 134.9, 132.5, 124.1, 62.7, 62.5, 55.3, 44.9, 31.0, 30.0, 21.3, 15.7; ESI-HRMS m/z calcd for $\text{C}_{15}\text{H}_{23}\text{N}_3\text{O}_9\text{P}$: 420.1167 [M-H], found: 420.1168.

3.2.2 Incorporation of PLP-Glu and PLP-DAP into LL-DAP-AT

LL-DAP-AT (3 mg, 9 mg/mL) in a buffer, which contains 200 mM NaCl, 20 mM HEPES-KOH, pH 7.6, 3 mM DTT, was diluted to 2.5 mL using a buffer containing 200 mM NaCl, 200 mM potassium phosphate, pH 7.6, 3 mM DTT. Phenylhydrazine (0.500 mL of a 0.03 M aqueous solution) was then added and the mixture was incubated at 22 °C with occasional gentle mixing. After 1 h the solution was transferred to a dialysis tubing (12-14,000 MWCO) and dialyzed for 2 h at 22 °C against 300 mL of buffer containing 200 mM potassium phosphate, pH 7.6, 200 mM HEPES-KOH, pH 7.6, 3 mM DTT. The dialysis buffer was then changed to a buffer containing 200 mM NaCl, 200 mM HEPES-KOH, pH 7.6, 3 mM DTT. The enzyme solution was supplemented with ~3 mg of the appropriate substrate analogue (PLP-Glu or PLP-DAP). After 2 hours at 22 °C the buffer was exchanged and another 3 mg of compound was added to the enzyme solution. A final buffer exchange was permitted to stir overnight at 22 °C. The following day, the contents of the dialysis bag were transferred to an Amicon Ultra 30,000

MWCO centrifugal filter (Millipore) and the buffer was exchanged for buffer containing 200 mM NaCl, 200 mM HEPES-KOH, pH 7.6, 3 mM DTT, followed by concentration of the solution to ~300 μ L.

3.3 General procedure for high-throughput screening of LL-DAP-AT inhibitors

The screening of a library of 30,000 compounds from ChemBridge Corporation for potential inhibitors of LL-DAP-AT was done in collaboration with Dr. Michael Deyholos (Department of Biological Sciences, University of Alberta). This initial screening was performed by Dr. Matthew Clay of our group. The published 2-aminobenzaldehyde-based assay²⁴ was adapted to reliably work in a 96-well plate (100 μ L volume). Column 1 served as a positive control (no inhibitor) whereas column 12 served as a negative control (no enzyme). Initial and final absorbances were measured and the difference was used as a measure of enzyme activity. Activity was measured relative to the average of column 1 (positive control). The assay consisted of four steps and was performed using a Beckman Coulter Biomek[®] 2000 work station.

Aliquot buffer solution: 420 mg of α -Kg, 280 mg 2-aminobenzaldehyde (OAB), and 480 mg of racemic DAP were dissolved in 280 mL of 100 mM HEPES-KOH, pH 7.6, and 85 μ L of this stock was aliquoted into the 96-well assay plates using an automated protocol on a Beckman Coulter Biomek 2000 Laboratory Automation Workstation. The final concentration of each component in the stock solution was: α -Kg (10 mM); OAB (8.3 mM); LL-DAP (assuming 25% of total

DAP: 2.3 mM). Upon dilution to 100 μ L in the well plate, the final concentrations were: α -Kg (8.5 mM); OAB (7 mM); LL-DAP (2.0 mM).

Preparation of inhibitor working stock: The inhibitor source plates contained 0.25 mg of inhibitor in 25 μ L of DMSO. Inhibitor was present in columns 2-11 of the 96-well plates, and columns 1 and 12 contained pure DMSO. Using an automated protocol on the Biomek 2000, 99 μ L of DMSO was added to each well of a 96-well plate, followed by 1.0 μ L of inhibitor to create the inhibitor working stock. Assuming a molecular weight of 500 g/mol, the final concentration of inhibitor in each well was 200 μ M. The working plates were stored at -20 $^{\circ}$ C.

Addition of inhibitor: A 5 μ L solution of inhibitor working stock was then added to the assay plates containing buffer using an automated protocol on the Biomek 2000. Columns 1 and 12 of the assay plates received pure DMSO as no inhibitor was present in these columns. Assuming a molecular weight of 500 g/mol, the final concentration of inhibitor in each well was 10 μ M. To remove air bubbles, the assay plates were then centrifuged at 2400 rpm for 3 minutes. The absorbance was then recorded at 440 nm in triplicate on a Bio-TEK PowerWave XS Universal Microplate Spectrophotometer.

Addition of enzyme: A 0.043 mg/mL solution of LL-DAP-AT in 100 mM HEPES-KOH, pH 7.6 was prepared and 10 μ L of this was added to each well (with the exception of the wells in column 12, which served as a negative control) using an automated protocol on the Biomek 2000. This resulted in 0.43 μ g of enzyme in each well, or a concentration of 0.0043 mg/mL of LL-DAP-AT. The

assay plates were then allowed to sit at room temperature for 3 hours, at which time a second absorbance reading at 440 nm was taken in triplicate.

3.4 General procedure for determination of IC₅₀ values of inhibitors of LL-DAP-AT

IC₅₀ determinations were done using a Varian Cary 100 Bio UV-Visible spectrophotometer using the Enzyme Kinetic program. The data were then analyzed using Microsoft[®] Excel 2000.

Aliquot buffer solution: 420 mg of α -Kg and 480 mg of racemic DAP (commercial) were dissolved in 280 mL of 100 mM HEPES-KOH, pH 7.6. 7 mL of this solution was used to dissolve 7 mg of 2-aminobenzaldehyde (OAB) and 850 μ L of this stock was added into 8 assay cells (1mL). The final concentration of each component in the stock solution was: α -Kg (10 mM); OAB (8.3 mM); LL-DAP (assuming 25% of total DAP: 2.3 mM). Upon dilution to 1 mL in the assay cells, the final concentrations were: α -Kg (8.5 mM); OAB (7 mM); LL-DAP (2.0 mM).

Preparation of inhibitor working stock: 8 μ mol of inhibitor was dissolved in 2 mL of DMSO, which resulted in a concentration of 4 μ mol/mL. Serial dilutions were performed to prepare 2 μ mol/mL, 1 μ mol/mL, 0.5 μ mol/mL, 0.2 μ mol/mL, and 0.1 μ mol/mL solutions, the final inhibitor concentrations were 200 μ M, 100 μ M, 50 μ M, 25 μ M, 10 μ M, and 5 μ M, respectively.

Addition of inhibitor: 50 μ L of each different concentration of inhibitor solution was added into cell 2 to 7. And 50 μ L of pure DMSO was then added into cell 1

and 8, which act as the negative control. A Varian Cary 100 Bio UV-Visible spectrophotometer was used to measure the absorbance at 440 nm. Using the Enzyme Kinetics program, the absorbance for all the cells was then multi-zeroed.

Addition of enzyme: A 0.043 mg/mL solution of LL-DAP-AT in 100 mM HEPES-KOH pH 7.6 was prepared and 100 μ L of this was added to each cell, excluding the negative control (cell 8). The final concentration of the enzyme was 0.0043 mg/mL. The absorbance was recorded over a period of 120 min with 20 sec/cycle.

Calculation of IC₅₀: The slope of the linear portion (normally 5 – 15 minutes) of each absorbance curve was used to determine the initial rate of the enzymatic conversion. The initial rates were measured for several different inhibitor concentrations, in addition to the positive control, which contained no inhibitor. This allowed for the determination of the percent inhibition for each concentration of the inhibitor. The percent inhibitions were then plotted against the inhibitor concentrations, and the resulting curve was then fitted to a natural logarithm function. Finally, the IC₅₀ value was calculated using this formula.

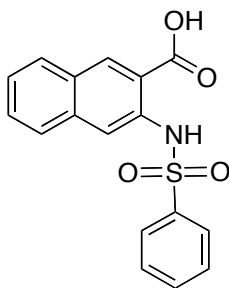
3.5 General procedure for time dependence testing of inhibitors of LL-DAP-AT

The concentration of inhibitor stock was chosen based on the IC₅₀ value. The substrate buffer solution and the enzyme were prepared, as described above. Six portions containing 100 μ L of enzyme and 50 μ L of the inhibitor solution were pre-incubated for different lengths of time prior to addition into the cell, which contains 850 μ L of substrate buffer solution. Cells 1 and 8 served as

positive and negative control, respectively. The absorbance values were recorded as described above. For the time-independent inhibitors, the percentage inhibition did not change with different incubation times. For the time-dependent inhibitors, the percentage inhibition increased with longer pre-incubation times.

3.6 Sulfonamido-arylhydrazide derived inhibitors of LL-DAP-AT

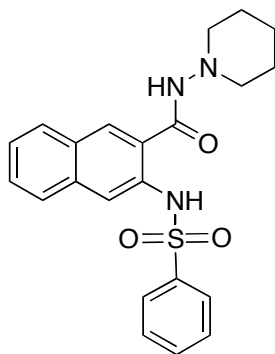
3.6.1 Preparation of the hydrazide-modified analogues (144 and 147)



3-(Phenylsulfonamido)-2-naphthoic acid (141)

3-Amino-2-naphthoic acid (80%, 0.4680g, 2 mmol) and sodium carbonate (0.5148g, 4.8 mmol) were mixed with distilled water (5 mL). The mixture was heated in an oil-bath to ~60 °C. Benzenesulfonyl chloride (0.31 mL, 2.4 mmol) was slowly added into the hot mixture over the course of 15 min. The mixture was then heated to 85 °C for a further 3 h. Norite (~20 mg) was used if the mixture was coloured dark red or brown. The hot mixture was filtered through a pre-heated funnel. The hot filtrate was slowly poured with vigorous swirling into a 50 mL Erlenmeyer flask, which contained 1 mL of 6 N hydrochloride acid. After cooling, the precipitated solid was filtered and washed with 2 mL of 1 N hydrochloride acid. The product was then used in the next step without any further

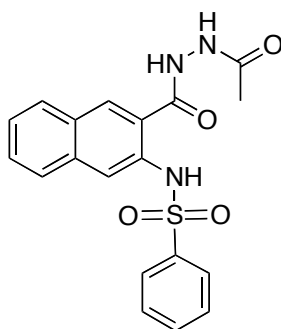
purification. The title compound was obtained as a light red solid; 0.6064g, 93% yield; IR (Microscope) 3221, 3070, 2861 (br), 1676, 1448, 1160 cm^{-1} ; ^1H NMR (400 MHz, $\text{DMSO-}d_6$): δ = 8.59 (s, 1H, Ph-H), 7.97 (d, J = 7.5, 1H, Ph-H), 7.91 (s, 1H, Ph-H), 7.89 (d, J = 7.5, 1H, Ph-H), 7.82 (m, 2H, Ph-H), 7.59 (m, 2H, Ph-H), 7.48 (m, 3H, Ph-H); ^{13}C NMR (100 MHz, $\text{DMSO-}d_6$): δ = 170.3, 139.3, 135.9, 135.7, 134.3, 134.1, 130.2, 130.1, 129.8, 129.2, 127.7, 127.6, 126.6, 118.3, 116.6; ESI-HRMS m/z calcd for $\text{C}_{17}\text{H}_{14}\text{NO}_4\text{S}$: 326.0493 $[\text{M}+\text{H}^+]$, found: 326.0488.



3-(Phenylsulfonamido)-N-(piperidin-1-yl)-2-naphthamide (144)

3-(Phenylsulfonamido)-2-naphthoic acid (**141**, 0.0818 g, 0.250 mmol) was dissolved in dry THF (5 mL). The solution was then cooled in an ice-bath. After 10 minutes, oxalyl chloride (28 μL , 0.32 mmol) was added. Then 2 drops of DMF were added to the mixture. The mixture was stirred for 30 min, and then warmed to 20 $^{\circ}\text{C}$. The mixture was then stirred for another hour. The solvent and excess oxalyl chloride was removed *in vacuo*. Dry THF (5 mL) was then added to the residue. *N,N*-diisopropylethylamine (0.3 mL, 1.7 mmol) was added, followed by the slow addition of 1-aminopiperidine (0.054 mL, 0.50 mmol). The mixture was

stirred for 16 h, and then the solvent was removed *in vacuo*. The residue was dissolved in ethyl acetate (10 mL), and washed with saturated sodium bicarbonate solution (2×15 mL), water (15 mL), and brine (15 mL). The organic layer was dried over sodium sulfate, filtered, and the solvent was removed *in vacuo*. The product was purified by column chromatography (silica gel, EtOAc/hexanes = 2:1), yielding a white solid (0.073 g, 68%); IR (Microscope) 3221, 3070, 2861 (br), 1676, 1448, 1160 cm^{-1} ; ^1H NMR (400 MHz, CDCl_3): δ = 10.42 (br, 1H, $\text{SO}_2\text{-NH}$), 8.04 (s, 1H, Ph-H), 7.94 (br, 1H, CO-NH), 7.89 (d, J = 7.6 Hz, 2H, Ph-H), 7.72 (t, J = 8.0Hz, 2H, Ph-H), 7.50 (t, J = 8.0Hz, 2H, Ph-H), 7.36 (m, 3H, Ph-H), 2.84 (br, 4H), 1.76 (br, 4H), 1.47 (br, 2H); ^{13}C NMR (100 MHz, CDCl_3): δ = 166.9, 139.9, 135.1, 134.4, 132.9, 129.4, 129.1, 128.8, 128.6, 128.5, 127.7, 127.4, 126.3, 122.1, 119.1, 57.0, 25.3, 23.2; ESI-HRMS m/z calcd for $\text{C}_{22}\text{H}_{23}\text{N}_3\text{NaO}_3\text{S}$: 432.1352 [$\text{M}+\text{Na}^+$], found: 432.1348.



***N*-(3-(2-Acetylhydrazinecarbonyl)naphthalen-2-yl)benzenesulfonamide (147)**

3-(Phenylsulfonamido)-2-naphthoic acid (**141**, 0.0818 g, 0.250 mmol) and carbonyl diimidazole (0.0410 g, 0.25 mmol) were dissolved in dry DMF (5 mL). The mixture was then stirred for 4 hours. Acetohydrazide (0.0250 g, 0.3 mL) was dissolved in DMF (1 mL). The activated sulfonamide – carboxylic acid

intermediate was then slowly added to the acetohydrazide solution. The reaction was allowed to stir for 16 h at room temperature. The solvent was removed *in vacuo*, and the residue was purified via column chromatography (silica gel, EtOAc) to yield the title product as a white solid; 0.070 g, 73% yield; IR (Microscope) 3267, 3225, 3020, 1698, 1412, 1156 cm^{-1} ; ^1H NMR (400 MHz, DMSO- d_6): δ = 10.73 (s, 2H, CO-NH), 10.08 (s, 1H, SO₂-NH), 8.28 (s, 1H, Ph-H), 7.84 (m, 5H, Ph-H), 7.53 (m, 5H, Ph-H), 1.99 (s, 3H, CH₃); ^{13}C NMR (100 MHz, DMSO- d_6): δ = 169.4, 168.0, 139.2, 134.9, 134.3, 134.0, 130.5, 130.1, 129.7, 129.2, 129.1, 127.8, 127.7, 126.9, 121.1, 117.0, 21.2; ESI-HRMS m/z calcd for C₁₉H₁₇N₃NaO₄S: 406.0832 [M+Na⁺], found: 406.0827.

3.6.2 Preparation of naphthalene and sulfonamide modified sulfonamide-arylhydrazide analogues

3.6.2.1 General procedure for synthesis of sulfonamide - carboxylic acid intermediate (148a-163a)

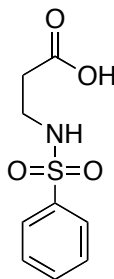
One equivalent of the appropriate amino acid and 2.5 equivalents of sodium carbonate were mixed with distilled water to prepare a 0.4 M amino acid concentration. The mixture was heated in an oil-bath to ~60 °C. An appropriate sulfonyl chloride (1.25 equiv.) was slowly added into the hot mixture over the course of 15 min. The mixture was then heated to 85 °C for a further 3 h. Norite (~20 mg) was used if the mixture was coloured dark red or brown. The hot mixture was filtered through a pre-heated funnel. The hot filtrate was slowly poured with vigorous swirling into a 50 mL Erlenmeyer flask, which contained 1

mL of 6 N hydrochloride acid. After cooling, the precipitated solid was filtered and washed with 2 mL of 1 N hydrochloride acid. The product was then used in the next step without any further purification.

3.6.2.2 General procedure for synthesis of naphthalene and sulfonamide modified sulfonamide – hydrazide analogues (148b-163b) using sulfonamide – carboxylic acid intermediate

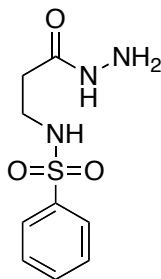
The inhibitor analogues were synthesized from the sulfonamide – carboxylic acid intermediates using the following general procedure unless otherwise stated. One equivalent of the appropriate sulfonamide – carboxylic acid intermediate and 1.2 equivalents of carbonyl diimidazole were dissolved in dry DMF to a substrate concentration of 0.075 M. The mixture was then stirred for 4 hours. The appropriate hydrazine (2 equiv.) was dissolved in dry DMF to a concentration of 0.15 M. The activated sulfonamide – carboxylic acid intermediate was then slowly added to the hydrazine solution. The reaction was allowed to stir for 16 h at room temperature. The solvent was removed *in vacuo*, and the residue was purified via column chromatography to yield the desired sulfonamide–hydrazide analogue.

3.6.2.3 Characterization data of sulfonamide – carboxylic acid intermediates and sulfonamide – hydrazide analogues



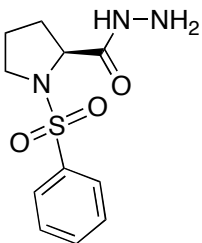
3-(Phenylsulfonamido)propanoic acid (148a)

White solid; 72% yield; IR (Microscope): 3273, 3066, 3150 – 2830 (br), 1701, 1447, 1435, 1413, 1168 cm^{-1} ; ^1H NMR (500 MHz, CD_3OD): δ = 7.85 (m, 2H, Ph-H), 7.63 (m, 1H, Ph-H), 7.56 (m, 2H, Ph-H), 3.10 (t, J = 7.0 Hz, 2 H, NH- CH_2), 2.44 (t, J = 7.0 Hz, 2 H, CO- CH_2); ^{13}C NMR (125 MHz, CD_3OD): δ = 174.8, 141.8, 133.7, 130.3, 128.0, 39.9, 35.4; ESI-HRMS m/z calcd for $\text{C}_9\text{H}_{10}\text{NO}_4\text{S}$: 228.0336 $[\text{M}-\text{H}]^-$, found: 228.0333.



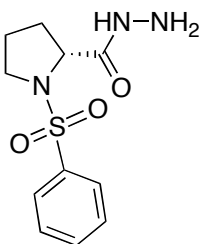
N-(3-Hydrazinyl-3-oxopropyl)benzenesulfonamide (148b)

White solid; 32% yield; IR (KBr pellet): 3417, 3302, 3246, 3194, 3096, 3057, 2914, 2859, 1643, 1534, 1445 cm^{-1} ; ^1H NMR (400 MHz, CD_3OD): δ = 7.85 (m, 2H, Ph-H), 7.57 (m, 3H, Ph-H), 3.11 (t, J = 6.8 Hz, 2H, NH- CH_2), 2.33 (t, J = 6.8 Hz, 2H, CO- CH_2); ^{13}C NMR (100 MHz, CD_3OD): δ = 171.1, 140.3, 132.3, 128.8, 126.6, 39.0, 34.0; ESI-HRMS m/z calcd for $\text{C}_9\text{H}_{13}\text{N}_3\text{NaO}_3\text{S}$: 266.0568 $[\text{M}+\text{Na}]^+$, found: 266.0570.



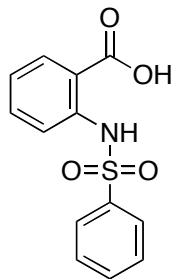
(S)-1-(Phenylsulfonyl)pyrrolidine-2-carbohydrazide (149b)

White solid; 25% yield over two steps; $[\alpha]_D = -130.2$ (c 0.19, CH₃OH); IR (KBr pellet): 3600 – 3120 (br), 3061, 2953, 2926, 2874, 1659, 1512, 1479, 1446 cm⁻¹; ¹H NMR (400 MHz, CD₃OD): $\delta = 7.85$ (m, 2H, Ph-H), 7.66 (m, 3H, Ph-H), 4.10 (dd, $J = 4.0, 8.4$ Hz, 1H, N-CH), 3.55 (m, 1H), 3.23 (td, $J = 7.2, 10.0$ Hz, 1H, N-CH₂), 1.84 (m, 3H), 1.56 (m, 1H); ¹³C NMR (100 MHz, CD₃OD): $\delta = 173.0, 137.6, 134.2, 130.2, 128.5, 62.1, 50.3, 31.4, 25.1$; ESI-HRMS m/z calcd for C₁₁H₁₆N₃O₃S: 270.0907 [M+H]⁺, found: 270.0908.



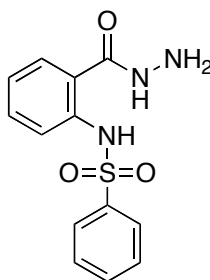
(R)-1-(Phenylsulfonyl)pyrrolidine-2-carbohydrazide (150b)

White solid; 28% yield over two steps; $[\alpha]_D = 144.4$ (c 0.165, CH₃OH); IR (KBr pellet): 3600 – 3050 (br), 3061, 2976, 2921, 2874, 1660, 1515, 1480, 1446 cm⁻¹; ¹H NMR (500 MHz, CD₃OD): $\delta = 7.88$ (m, 2H, Ph-H), 7.68 (m, 1H, Ph-H), 7.60 (m, 2H, Ph-H), 4.11 (dd, $J = 4.0, 9.0$ Hz, 1H, N-CH), 3.55 (ddd, $J = 4.5, 7.0, 10.0$ Hz, 1H, N-CH₂), 3.23 (td, $J = 7.0, 10.0$ Hz, 1H, N-CH₂), 1.84 (m, 3H), 1.54 (m, 1H); ¹³C NMR (125 MHz, CD₃OD): $\delta = 173.4, 137.9, 134.6, 130.6, 128.9, 62.6, 50.7, 32.0, 25.5$; ESI-HRMS m/z calcd for C₁₁H₁₅N₃NaO₃S: 292.0726 [M+Na]⁺, found: 292.0726.



2-(Phenylsulfonamido)benzoic acid (151a)¹⁸⁶

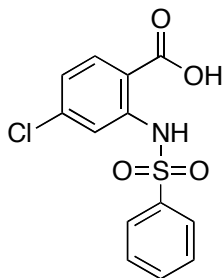
Solid; 68% yield; IR (microscope): 3179, 3100, 3200 – 2850 (br), 2885, 1680, 1600, 1582, 1492, 1448, 1431 cm^{-1} ; ^1H NMR (400 MHz, $\text{DMSO-}d_6$): δ = 7.87 (m, 1H, Ph-H), 7.80 (m, 2H, Ph-H), 7.63 (m, 1H, Ph-H), 7.53 (m, 4H, Ph-H), 7.10 (m, 1H, Ph-H); ^{13}C NMR (100 MHz, $\text{DMSO-}d_6$): δ = 170.4, 140.5, 139.3, 135.2, 134.3, 132.2, 130.2, 127.5, 124.1, 119.2, 117.5; ESI-HRMS m/z calcd for $\text{C}_{13}\text{H}_{11}\text{NO}_4\text{S}$: 276.0336 [M-H]⁻, found: 276.0336.



N-(2-(Hydrazinecarbonyl)phenyl)benzenesulfonamide (151b)

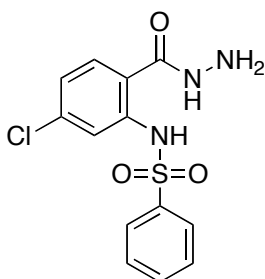
White solid; 76% yield; IR (CH_2Cl_2 cast): 3327, 3400 – 2900 (br), 3064, 1631, 1598, 1518, 1494, 1447 cm^{-1} ; ^1H NMR (500 MHz, CDCl_3): δ = 7.78 (m, 2H, Ph-H), 7.65 (m, 1H, Ph-H), 7.51 (m, 1H, Ph-H), 7.39 (m, 4H, Ph-H), 7.07 (m, 1H, Ph-H); ^{13}C NMR (100 MHz, CDCl_3): δ = 179.2, 139.5, 138.6, 133.2, 129.3, 129.2,

127.4, 126.9, 124.3, 122.0, 120.5; ESI-HRMS m/z calcd for $C_{13}H_{13}N_3NaO_3S$: 314.0570 $[M+Na]^+$, found: 314.0571.



4-Chloro-2-(phenylsulfonamido)benzoic acid (152a)

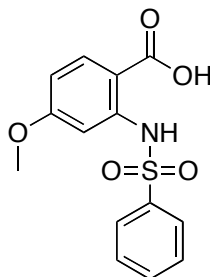
Solid; 85% yield; IR (microscope): 3179, 3106, 3060, 3200 – 2700 (br), 1672, 1597, 1566, 1488, 1449, 1433 cm^{-1} ; 1H NMR (500 MHz, $DMSO-d_6$): δ = 7.88 (d, J = 8.5 Hz, 1H, 2-carboxyl-Ph-H), 7.82 (m, 2H, Ph-H), 7.66 (m, 1H, Ph-H), 7.58 (m, 2H, Ph-H), 7.45 (d, J = 1.5 Hz, 1H, 2-sulfonamide-Ph-H), 7.16 (dd, J = 1.5, 8.5 Hz, 1H, 4-sulfonamide-Ph-H); ^{13}C NMR (125 MHz, $DMSO-d_6$): δ = 168.9, 141.3, 138.6, 138.5, 133.7, 133.2, 129.6, 126.7, 123.1, 117.7, 116.0; ESI-HRMS m/z calcd for $C_{13}H_9ClNO_4S$: 309.9946 $[M-H]^-$, found: 309.9945.



N-(5-Chloro-2-(hydrazinecarbonyl)phenyl)benzenesulfonamide (152b)

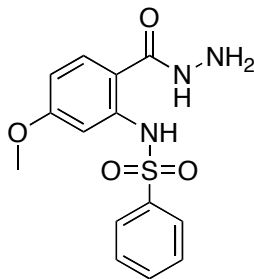
Light yellow solid; 58% yield; IR (CH_2Cl_2 cast): 3328, 3400 – 2900 (br), 3066, 1633, 1593, 1520, 1492, 1447 cm^{-1} ; 1H NMR (500 MHz, CD_3OD): δ = 7.75 (m, 2H, Ph-H), 7.60 (m, 1H, Ph-H), 7.56 (m, 1H, Ph-H), 7.46 (m, 3H, Ph-H), 7.08 (m,

1H, Ph-H); ¹³C NMR (125 MHz, CD₃OD): δ = 168.6, 140.8, 140.2, 139.1, 134.5, 130.3, 130.2, 128.3, 125.2, 122.3, 121.0; ESI-HRMS *m/z* calcd for C₁₃H₁₂ClN₃NaO₃S: 348.0180 [M+Na]⁺, found: 348.0180.



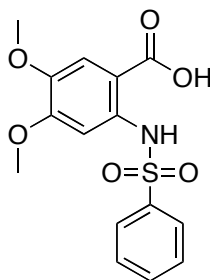
4-Methoxy-2-(phenylsulfonamido)benzoic acid (153a)

Light grey solid; 88% yield; IR (microscope): 3170, 2975, 3200 – 2700 (br), 1637, 1615, 1570, 1510, 1441 cm⁻¹; ¹H NMR (500 MHz, DMSO-*d*₆): δ = 7.83 (m, 3H, Ph-H), 7.65 (m, 1H, Ph-H), 7.57 (m, 2H, Ph-H), 6.97 (d, *J* = 2.5 Hz, 1H, 2-sulfonamide-Ph-H), 6.67 (dd, *J* = 2.5, 9.0 Hz, 1H, 4-sulfonamide-Ph-H), 3.76 (s, 3H, CH₃); ¹³C NMR (125 MHz, DMSO-*d*₆): δ = 169.7, 163.6, 141.8, 138.4, 133.7, 133.5, 129.6, 126.8, 108.9, 108.6, 103.1, 55.6; ESI-HRMS *m/z* calcd for C₁₄H₁₂NO₅S: 306.0442 [M-H]⁻, found: 306.0439.



***N*-(2-(Hydrazinecarbonyl)-5-methoxyphenyl)benzenesulfonamide (153b)**

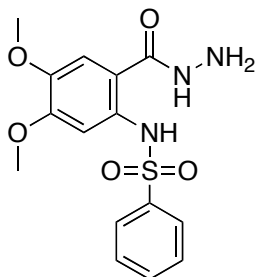
White solid; 74% yield; IR (CH₂Cl₂ cast): 3328, 3400 – 2900 (br), 3065, 3009, 2968, 2843, 1611, 1578, 1503, 1464, 1447 cm⁻¹; ¹H NMR (500 MHz, CD₃OD): δ = 7.75 (m, 2H, Ph-H), 7.53 (m, 1H, Ph-H), 7.45 (m, 3H, Ph-H), 7.13 (d, *J* = 2.5 Hz, 1H, 2-sulfonamide-Ph-H), 6.60 (dd, *J* = 2.5, 9.0 Hz, 1H, 4-sulfonamide-Ph-H), 3.77 (s, 3H, CH₃); ¹³C NMR (125 MHz, CD₃OD): δ = 169.7, 164.1, 141.6, 140.4, 134.3, 130.3, 130.2, 128.4, 114.0, 110.7, 107.2, 56.1; ESI-HRMS *m/z* calcd for C₁₄H₁₅N₃NaO₄S: 344.0675 [M+Na]⁺, found: 344.0680.



4,5-Dimethoxy-2-(phenylsulfonamido)benzoic acid (154a)

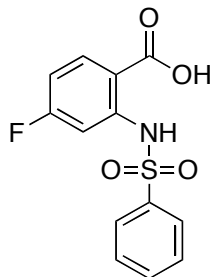
Grey solid; 70% yield; IR (microscope): 3160, 3078, 3030, 2976, 2941, 2843, 3300 – 2700 (br), 1662, 1610, 1587, 1520, 1448, 1417 cm⁻¹; ¹H NMR (500 MHz, DMSO-*d*₆): δ = 7.74 (m, 2H, Ph-H), 7.61 (m, 1H, Ph-H), 7.52 (m, 2H, Ph-H), 7.26 (s, 1H, 2-carboxyl-Ph-H), 7.11 (s, 1H, 3-carboxyl-Ph-H), 3.79 (s, 3H, CH₃), 3.68

(s, 3H, CH_3); ^{13}C NMR (100 MHz, $\text{DMSO}-d_6$): $\delta = 169.9, 153.8, 145.0, 138.8, 135.4, 134.0, 129.9, 127.3, 113.2, 109.2, 103.2, 56.2, 56.0$; ESI-HRMS m/z calcd for $\text{C}_{15}\text{H}_{14}\text{NO}_6\text{S}$: 336.0547 $[\text{M}-\text{H}]^-$, found: 336.0549.



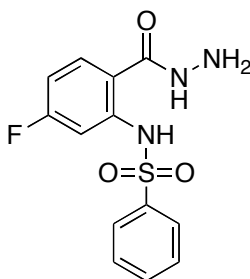
***N*-(2-(Hydrazinecarbonyl)-4,5-dimethoxyphenyl)benzenesulfonamide (154b)**

White solid; 37% yield; IR (CHCl_3 cast): 3335, 3400 – 3250 (br), 3022, 2917, 2849, 1606, 1515, 1465, 1448 cm^{-1} ; ^1H NMR (500 MHz, CDCl_3): $\delta = 7.73$ (m, 2H, Ph-H), 7.52 (m, 1H, Ph-H), 7.41 (m, 2H, Ph-H), 7.25 (s, 1H, 2-carboxyl-Ph-H), 6.77 (s, 1H, 3-carboxyl-Ph-H), 3.92 (s, 3H, CH_3), 3.82 (s, 3H, CH_3); ^{13}C NMR (125 MHz, CDCl_3): $\delta = 168.8, 152.6, 145.8, 139.0, 133.1, 132.9, 128.8, 127.3, 112.9, 108.7, 106.5, 56.3, 56.2$; ESI-HRMS m/z calcd for $\text{C}_{15}\text{H}_{17}\text{N}_3\text{NaO}_5\text{S}$: 374.0781 $[\text{M}+\text{Na}]^+$, found: 374.0781.



4-Fluoro-2-(phenylsulfonamido)benzoic acid (155a)¹⁸⁷

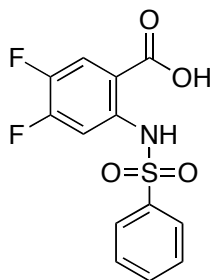
Light yellow solid; 76% yield; IR (microscope): 3490, 3101, 3300 – 2750 (br), 1670, 1613, 1592, 1506, 1448, 1430 cm^{-1} ; ^1H NMR (500 MHz, $\text{DMSO-}d_6$): δ = 7.97 (dd, J = 6.5, 9.0 Hz, 1H, Ph-H), 7.86 (m, 2H, Ph-H), 7.67 (m, 1H, Ph-H), 7.58 (m, 2H, Ph-H), 7.24 (dd, J = 2.5, 11.0 Hz, 1H, Ph-H), 6.97 (m, 1H, Ph-H); ^{13}C NMR (100 MHz, $\text{DMSO-}d_6$): δ = 169.5, 165.4 (d, J = 250.4 Hz), 142.5 (d, J = 11.9 Hz), 138.7, 134.9 (d, J = 10.9 Hz), 134.3, 130.2, 127.3, 113.6 (d, J = 2.9 Hz), 111.0 (d, J = 21.6 Hz), 105.4 (d, J = 27.0 Hz); ^{19}F NMR (380 MHz, $\text{DMSO-}d_6$): δ = -102.2 (ddd, J = 7.2, 7.2, 12.1 Hz); ESI-HRMS m/z calcd for $\text{C}_{13}\text{H}_9\text{FNO}_4\text{S}$: 294.0242 $[\text{M-H}]^-$, found: 294.0245.



***N*-(5-Fluoro-2-(hydrazinecarbonyl)phenyl)benzenesulfonamide (155b)**

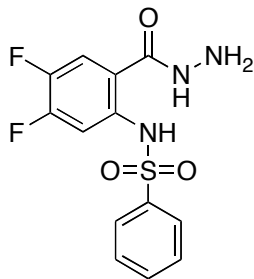
Light yellow solid; 58% yield; IR (CH_2Cl_2 cast): 3334, 3400 – 3250 (br), 3093, 3027, 1631, 1596, 1502, 1448, 1423 cm^{-1} ; ^1H NMR (500 MHz, CDCl_3): δ = 7.85

(m, 2H, Ph-H), 7.56 (m, 1H, Ph-H), 7.46 (m, 2H, Ph-H), 7.41 (m, 2H, Ph-H), 6.75 (m, 1H, Ph-H); ^{13}C NMR (125 MHz, CDCl_3): δ = 168.5, 165.0 (d, J = 252.3 Hz), 141.2 (d, J = 11.8 Hz), 139.1, 133.3, 129.2, 128.7 (d, J = 10.3 Hz), 127.2, 115.2 (d, J = 3.0 Hz), 110.7 (d, J = 22.4 Hz), 107.8 (d, J = 26.4 Hz); ^{19}F NMR (380 MHz, CDCl_3): δ = -103.0 (ddd, J = 7.6, 7.6, 11.0 Hz); ESI-HRMS m/z calcd for $\text{C}_{13}\text{H}_{12}\text{FN}_3\text{NaO}_3\text{S}$: 332.0476 $[\text{M}+\text{Na}]^+$, found: 332.0475.



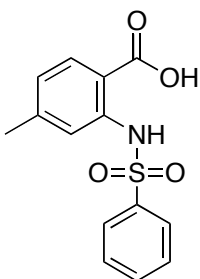
4,5-Difluoro-2-(phenylsulfonamido)benzoic acid (156a)

Solid; 89% yield; IR (microscope): 3161, 3087, 3400 – 2750 (br), 1686, 1604, 1522, 1481, 1449, 1401 cm^{-1} ; ^1H NMR (500 MHz, $\text{DMSO-}d_6$): δ = 7.84 (dd, J = 9.0, 11.0 Hz, 1H, Ph-H), 7.80 (m, 2H, Ph-H), 7.64 (m, 1H, Ph-H), 7.55 (m, 2H, Ph-H), 7.45 (dd, J = 7.0, 12.5 Hz, 1H, Ph-H); ^{13}C NMR (100 MHz, $\text{DMSO-}d_6$): δ = 168.4 (d, J = 1.0 Hz), 153.0 (dd, J = 13.6, 252.0 Hz), 145.6 (dd, J = 12.9, 243.0 Hz), 138.6, 137.7 (dd, J = 2.5, 9.7 Hz), 134.3, 130.1, 127.3, 120.5 (dd, J = 2.1, 19.2 Hz), 115.1 (dd, J = 3.3, 4.7 Hz), 108.8 (d, J = 21.9 Hz); ^{19}F NMR (380 MHz, $\text{DMSO-}d_6$): δ = -127.4 (ddd, J = 9.9, 12.2, 23.2 Hz), -142.9 (ddd, J = 7.2, 11.0, 23.2 Hz); ESI-HRMS m/z calcd for $\text{C}_{13}\text{H}_8\text{F}_2\text{NO}_4\text{S}$: 312.0148 $[\text{M}-\text{H}]^-$, found: 312.0151.



***N*-(4,5-Difluoro-2-(hydrazinecarbonyl)phenyl)benzenesulfonamide (156b)**

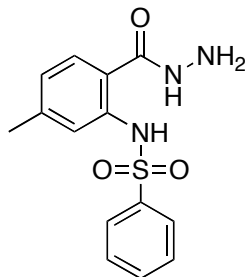
Light yellow solid; 48% yield; IR (microscope): 3345, 3400 – 3250 (br), 3065, 1606, 1509, 1448, 1392 cm^{-1} ; ^1H NMR (500 MHz, CDCl_3): δ = 7.80 (m, 2H, Ph-H), 7.58 (m, 2H, Ph-H), 7.47 (m, 2H, Ph-H), 7.22 (dd, J = 8.5, 10.0 Hz, 1H, Ph-H); ^{13}C NMR (125 MHz, CDCl_3): δ = 167.4, 152.6 (dd, J = 13.1, 254.6 Hz), 146.4 (dd, J = 13.0, 247.3 Hz), 138.8, 135.9 (dd, J = 2.8, 9.3 Hz), 133.4, 129.2, 127.2, 116.4, 115.5 (d, J = 17.8 Hz), 111.5 (d, J = 21.5 Hz); ^{19}F NMR (380 MHz, CDCl_3): δ = -127.3 (ddd, J = 9.5, 11.8, 20.7 Hz), -140.7 (ddd, J = 7.6, 9.9, 22.8 Hz); ESI-HRMS m/z calcd for $\text{C}_{13}\text{H}_{11}\text{F}_2\text{N}_3\text{NaO}_3\text{S}$: 350.0382 $[\text{M}+\text{Na}]^+$, found: 350.0381.



4-Methyl-2-(phenylsulfonamido)benzoic acid (157a)

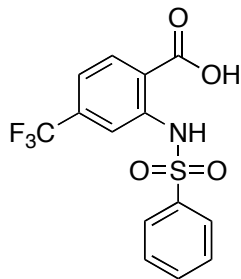
Light grey solid; 93% yield; IR (CHCl_3 cast): 3178, 3071, 3100 – 2750 (br), 2871, 1644, 1568, 1479, 1447 cm^{-1} ; ^1H NMR (500 MHz, $\text{DMSO}-d_6$): δ = 7.79 (m, 2H,

Ph-H), 7.75 (d, $J = 8.0$ Hz, 1H, Ph-H), 7.62 (m, 1H, Ph-H), 7.54 (m, 2H, Ph-H), 7.33 (m, 1H, Ph-H), 6.92 (m, 1H, Ph-H), 2.28 (s, 3H, CH₃); ¹³C NMR (100 MHz, DMSO-*d*₆): $\delta = 170.2, 145.6, 140.3, 139.0, 134.0, 131.9, 130.0, 127.3, 124.7, 119.2, 114.4, 21.9$; ESI-HRMS m/z calcd for C₁₄H₁₃NNaO₄S: 314.0457 [M+Na]⁺, found: 314.0459.



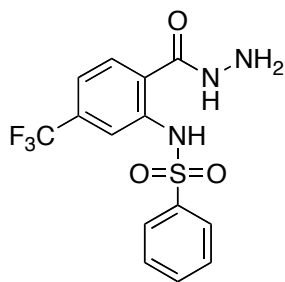
***N*-(2-(Hydrazinecarbonyl)-5-methylphenyl)benzenesulfonamide (157b)**

Light yellow solid; 55% yield; IR (CHCl₃ cast): 3328, 3400 – 3250 (br), 3059, 3028, 2918, 1630, 1523, 1447 cm⁻¹; ¹H NMR (500 MHz, CD₃OD): $\delta = 7.71$ (d, $J = 7.5$ Hz, 2H, Ph-H), 7.54 (m, 1H, Ph-H), 7.43 (m, 3H, Ph-H), 7.37 (d, $J = 8.0$ Hz, 1H, Ph-H), 6.90 (d, $J = 8.0$ Hz, 1H, Ph-H), 2.30 (s, 3H, CH₃); ¹³C NMR (125 MHz, CD₃OD): $\delta = 169.6, 144.4, 140.6, 139.7, 134.1, 130.1, 128.7, 128.3, 125.9, 123.4, 120.1, 21.6$; ESI-HRMS m/z calcd for C₁₄H₁₅N₃NaO₃S: 328.0726 [M+Na]⁺, found: 328.0722.



2-(Phenylsulfonamido)-4-(trifluoromethyl)benzoic acid (158a)¹⁸⁸

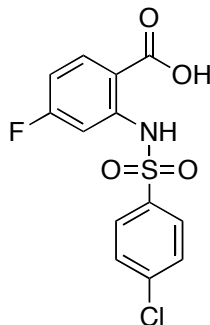
Light orange solid; 94% yield; IR (CHCl₃ cast): 3184, 3300 – 2750 (br), 3105, 3066, 1683, 1584, 1540, 1511, 1449, 1420 cm⁻¹; ¹H NMR (500 MHz, DMSO-*d*₆): δ = 8.05 (d, *J* = 8.0 Hz, 1H, 2-carboxyl-Ph-H), 7.79 (m, 2H, Ph-H), 7.67 (d, *J* = 1.5 Hz, 1H, 2-sulfonamide-Ph-H), 7.62 (m, 1H, Ph-H), 7.55 (m, 2H, Ph-H), 7.39 (dd, *J* = 1.5, 8.0 Hz, 1H, 4-sulfonamide-Ph-H); ¹³C NMR (100 MHz, DMSO-*d*₆): δ = 168.8, 141.3, 139.3, 133.5 (d, *J* = 84.4 Hz), 133.5 (d, *J* = 32.0 Hz), 130.0, 127.7, 127.2, 125.0, 122.2 (d, *J* = 9.2), 119.6 (d, *J* = 3.1 Hz), 115.2 (m); ¹⁹F NMR (380 MHz, DMSO-*d*₆): δ = -62.3; ESI-HRMS *m/z* calcd for C₁₄H₉F₃NO₄S: 344.0210 [M-H]⁻, found: 344.0240.



***N*-(2-(Hydrazinecarbonyl)-5-(trifluoromethyl)phenyl)benzenesulfonamide**

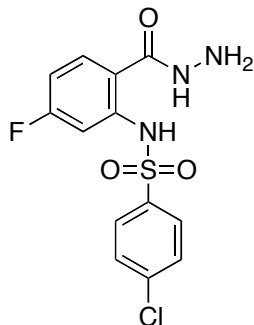
(158b)

Light yellow solid; 36% yield; IR (CHCl₃ cast): 3331, 3400 – 3250 (br), 3069, 1647, 1610, 1521, 1449, 1422 cm⁻¹; ¹H NMR (500 MHz, CD₃OD): δ = 7.84 (d, *J* = 1.5 Hz, 1H, 2-sulfonamide-Ph-H), 7.74 (m, 2H, Ph-H), 7.64 (d, *J* = 8.5 Hz, 1H, 2-carboxyl-Ph-H), 7.57 (m, 1H, Ph-H), 7.47 (m, 2H, Ph-H), 7.37 (dd, *J* = 1.5, 8.5 Hz, 1H, 4-sulfonamide-Ph-H); ¹³C NMR (125 MHz, CD₃OD): δ = 168.1, 139.9 (d, *J* = 23 Hz), 134.6 (q, *J* = 32.8 Hz), 134.6, 130.4, 129.9, 128.3, 126.4, 125.8, 123.6, 121.7 (q, *J* = 3.5 Hz), 119.4 (q, *J* = 3.8 Hz); ¹⁹F NMR (380 MHz, CD₃OD): δ = -65.0; ESI-HRMS *m/z* calcd for C₁₄H₁₂F₃N₃NaO₃S: 382.0444 [M+Na]⁺, found: 382.0440.



2-(4-Chlorophenylsulfonamido)-4-fluorobenzoic acid (159a)

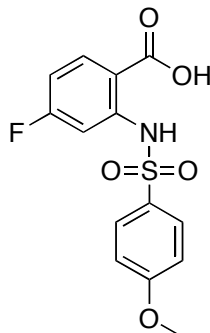
Yellow solid; 37% yield; IR (CHCl₃ cast): 3099, 3300 – 2750 (br), 1662, 1608, 1588, 1501, 1476, 1443, 1424 cm⁻¹; ¹H NMR (500 MHz, DMSO-*d*₆): δ = 7.98 (dd, *J* = 6.5, 9.0 Hz, 1H, 2-carboxyl-Ph-H), 7.87 (m, 2H, Ph-H), 7.66 (m, 2H, Ph-H), 7.23 (dd, *J* = 3.0, 11.0 Hz, 1H, 2-sulfonamide-Ph-H), 7.00 (ddd, *J* = 3.0, 8.5, 9.0 Hz, 1H, 4-sulfonamide-Ph-H); ¹³C NMR (125 MHz, DMSO-*d*₆): δ = 168.9, 164.9 (d, *J* = 250.8 Hz), 141.7 (d, *J* = 11.8 Hz), 138.7, 137.2, 134.5 (d, *J* = 11.0 Hz), 129.8 (d, *J* = 8.0 Hz), 128.8, 113.6 (d, *J* = 2.3 Hz), 110.7 (d, *J* = 21.3 Hz), 105.2 (d, *J* = 27.0 Hz); ¹⁹F NMR (380 MHz, DMSO-*d*₆): δ = -102.2 (q, *J* = 8.7 Hz); ESI-HRMS *m/z* calcd for C₁₃H₈ClFNO₄S: 327.9852 [M-H]⁻, found: 327.9849.



4-Chloro-*N*-(5-fluoro-2-(hydrazinecarbonyl)phenyl)benzenesulfonamide

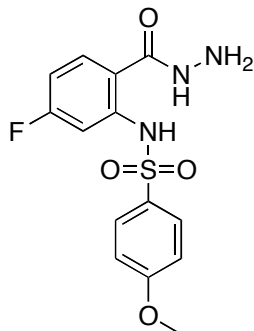
(159b)

Light yellow solid; 40% yield; IR (CHCl₃ cast): 3327, 3400 – 3250 (br), 3093, 2924, 1639, 1594, 1505, 1478, 1423 cm⁻¹; ¹H NMR (500 MHz, CD₃OD): δ = 7.74 (m, 2H, Ph-H), 7.55 (dd, *J* = 6.0, 9.0 Hz, 1H, 2-carboxyl-Ph-H), 7.49 (m, 2H, Ph-H), 7.35 (dd, *J* = 3.0, 11.0 Hz, 1H, 2-sulfonamide-Ph-H), 6.84 (ddd, *J* = 2.5, 8.0, 8.5 Hz, 1H, 4-sulfonamide-Ph-H); ¹³C NMR (125 MHz, CD₃OD): δ = 168.7, 165.9 (d, *J* = 250.3 Hz), 141.7 (d, *J* = 11.4 Hz), 140.8, 139.0, 131.2 (d, *J* = 10.3 Hz), 130.5 (d, *J* = 3.9 Hz), 130.0, 118.6 (d, *J* = 3.1 Hz), 112.1 (d, *J* = 21.9 Hz), 109.3 (d, *J* = 26.5 Hz); ¹⁹F NMR (380 MHz, CD₃OD): δ = -107.2 (ddd, *J* = 7.6, 7.6, 9.9 Hz); ESI-HRMS *m/z* calcd for C₁₃H₁₁ClFN₃NaO₃S: 366.0086 [M+Na]⁺, found: 366.0086.



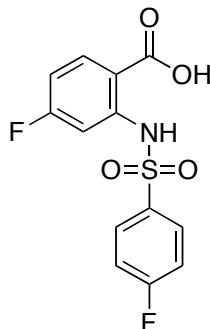
4-Fluoro-2-(4-methoxyphenylsulfonamido)benzoic acid (160a)

Yellow solid; 63% yield; IR (CHCl₃ cast): 3099, 3300 – 2750 (br), 2954, 2923, 2852, 1690, 1672, 1612, 1595, 1500, 1462, 1429 cm⁻¹; ¹H NMR (500 MHz, DMSO-*d*₆): δ = 7.97 (dd, *J* = 6.5, 9.0 Hz, 1H, 2-carboxyl-Ph-H), 7.79 (m, 2H, Ph-H), 7.23 (dd, *J* = 2.5, 11.0 Hz, 1H, 2-sulfonamide-Ph-H), 7.09 (m, 2H, Ph-H), 6.96 (ddd, *J* = 2.5, 8.0, 9.0 Hz, 1H, 4-sulfonamide-Ph-H), 3.80 (s, 3H, CH₃); ¹³C NMR (125 MHz, DMSO-*d*₆): δ = 169.0, 164.9 (d, *J* = 250.4 Hz), 163.1, 142.3 (d, *J* = 12.0 Hz), 134.4 (d, *J* = 11.1 Hz), 129.6, 129.2, 114.8, 112.9, 110.2 (d, *J* = 21.8 Hz), 104.6 (d, *J* = 27.0 Hz), 55.7; ¹⁹F NMR (380 MHz, DMSO-*d*₆): δ = -102.2 (ddd, *J* = 7.6, 7.6, 11.0 Hz); ESI-HRMS *m/z* calcd for C₁₄H₁₁FNO₅S: 324.0347 [M-H]⁻, found: 324.0346.



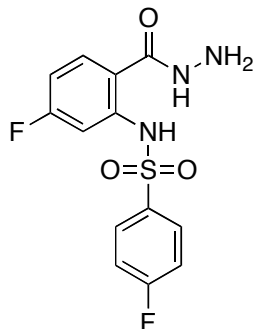
***N*-(5-Fluoro-2-(hydrazinecarbonyl)phenyl)-4-methoxybenzenesulfonamide
(160b)**

Light yellow solid; 58% yield; IR (CHCl₃ cast): 3330, 3400 – 3250 (br), 3099, 3022, 2973, 2946, 2843, 1633, 1596, 1499, 1463, 1440, 1422 cm⁻¹; ¹H NMR (400 MHz, CD₃OD): δ = 7.79 (m, 2H, Ph-H), 7.54 (dd, *J* = 6.0, 8.8 Hz, 1H, 2-carboxyl-Ph-H), 7.33 (dd, *J* = 2.8, 10.8 Hz, 1H, 2-sulfonamide-Ph-H), 6.96 (m, 2H, Ph-H), 6.81 (ddd, *J* = 2.4, 8.0, 8.8 Hz, 1H, 4-sulfonamide-Ph-H), 3.80 (s, 3H, CH₃); ¹³C NMR (100 MHz, CD₃OD): δ = 167.5, 164.5 (d, *J* = 249.0 Hz), 163.6, 140.7 (d, *J* = 11.5 Hz), 130.1, 129.7 (d, *J* = 10.1 Hz), 129.1, 116.9 (d, *J* = 3.1 Hz), 114.0, 110.3 (d, *J* = 22.3 Hz), 107.6 (d, *J* = 26.5 Hz), 54.8; ¹⁹F NMR (380 MHz, CD₃OD): δ = -107.6 (ddd, *J* = 7.6, 7.6, 11.4 Hz); ESI-HRMS *m/z* calcd for C₁₄H₁₄FN₃NaO₄S: 362.0581 [M+Na]⁺, found: 362.0578.



4-Fluoro-2-(4-fluorophenylsulfonamido)benzoic acid (161a)

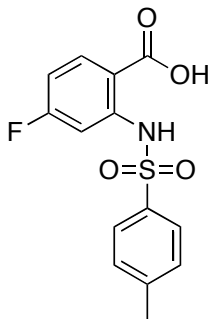
Yellow solid; 53% yield; IR (microscope): 3169, 3106, 3071, 3300 – 2750 (br), 1653, 1611, 1592, 1508, 1498, 1445, 1422 cm^{-1} ; ^1H NMR (600 MHz, CD_3OD): δ = 8.02 (dd, J = 6.6, 9.0 Hz, 1H, 2-carboxyl-Ph-H), 7.89 (m, 2H, Ph-H), 7.39 (dd, J = 2.4, 10.8 Hz, 1H, 2-sulfonamide-Ph-H), 7.25 (m, 2H, Ph-H), 6.84 (ddd, J = 2.4, 8.4, 9.0 Hz, 1H, 4-sulfonamide-Ph-H); ^{13}C NMR (125 MHz, CD_3OD): δ = 170.6, 167.2 (d, J = 251.8 Hz), 166.9 (d, J = 253.0 Hz), 144.0 (d, J = 12.0 Hz), 136.4 (d, J = 3.0 Hz), 135.6 (d, J = 10.8 Hz), 131.4 (d, J = 9.8 Hz), 117.5 (d, J = 23.0 Hz), 114.4 (d, J = 2.9 Hz), 111.6 (d, J = 22.3 Hz), 107.0 (d, J = 27.4 Hz); ^{19}F NMR (380 MHz, CD_3OD): δ = -103.9 (ddd, J = 7.2, 7.2, 11.2 Hz), -106.4 (ddd, J = 4.9, 8.7, 13.7 Hz); ESI-HRMS m/z calcd for $\text{C}_{13}\text{H}_8\text{F}_2\text{NO}_4\text{S}$: 312.0148 [M-H] $^-$, found: 312.0153.



4-Fluoro-N-(5-fluoro-2-(hydrazinecarbonyl)phenyl)benzenesulfonamide

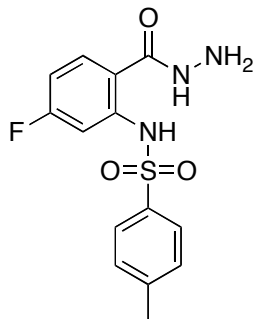
(161b)

White solid; 43% yield; IR (CHCl₃ cast): 3331, 3400 – 3250 (br), 3106, 1637, 1593, 1496, 1423 cm⁻¹; ¹H NMR (500 MHz, CD₃OD): δ = 7.83 (m, 2H, Ph-H), 7.56 (dd, *J* = 8.0, 11.0 Hz, 1H, 2-carboxyl-Ph-H), 7.36 (dd, *J* = 3.5, 13.5 Hz, 1H, 2-sulfonamide-Ph-H), 7.22 (m, 2H, Ph-H), 6.85 (ddd, *J* = 3.0, 10.0, 11.0 Hz, 1H, 4-sulfonamide-Ph-H); ¹³C NMR (125 MHz, CD₃OD): δ = 168.7, 166.8 (d, *J* = 252.5 Hz), 165.8 (d, *J* = 249.4 Hz), 141.8 (d, *J* = 11.4 Hz), 136.4 (d, *J* = 3.0 Hz), 131.3 (d, *J* = 9.8 Hz), 131.2 (d, *J* = 10.3 Hz), 118.7 (d, *J* = 2.6 Hz), 117.4 (d, *J* = 23.0 Hz), 112.1 (d, *J* = 22.0 Hz), 109.4 (d, *J* = 26.4 Hz); ¹⁹F NMR (380 MHz, CD₃OD): δ = -106.7 (ddd, *J* = 4.9, 8.4, 13.3 Hz), -107.3 (ddd, *J* = 7.2, 7.2, 11.0 Hz); ESI-HRMS *m/z* calcd for C₁₃H₁₂F₂N₃O₃S: 328.0562 [M+H]⁺, found: 328.0561.



4-Fluoro-2-(4-methylphenylsulfonamido)benzoic acid (162a)¹⁸⁹

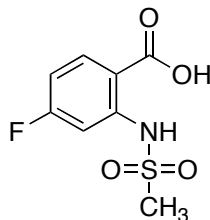
Yellow solid; 34% yield; IR (microscope): 3192, 3103, 3300 – 2750 (br), 2925, 2864, 1681, 1611, 1593, 1504, 1436, 1397 cm^{-1} ; ^1H NMR (500 MHz, CD_3OD): δ = 8.00 (dd, J = 6.5, 9.0 Hz, 1H, 2-carboxyl-Ph-H), 7.71 (d, J = 8.5 Hz, 2H, 3-methyl-Ph-H), 7.37 (dd, J = 2.5, 11.0 Hz, 1H, 2-sulfonamide-Ph-H), 7.31 (d, J = 8.5 Hz, 2H, 2-methyl-Ph-H), 6.80 (ddd, J = 2.5, 8.0, 9.0 Hz, 1H, 4-sulfonamide-Ph-H), 2.36 (s, 3H, CH_3); ^{13}C NMR (125 MHz, CD_3OD): δ = 170.6, 167.2 (d, J = 251.4 Hz), 146.0, 144.3 (d, J = 12.1 Hz), 137.3, 135.6 (d, J = 10.8 Hz), 130.9, 128.4, 114.0 (d, J = 2.8 Hz), 111.2 (d, J = 22.3 Hz), 106.7 (d, J = 27.4 Hz), 21.5; ^{19}F NMR (380 MHz, CD_3OD): δ = -104.2 (ddd, J = 7.2, 7.2, 12.2 Hz); ESI-HRMS m/z calcd for $\text{C}_{14}\text{H}_{11}\text{FNO}_4\text{S}$: 308.0398 $[\text{M}-\text{H}]^-$, found: 308.0404.



***N*-(5-Fluoro-2-(hydrazinecarbonyl)phenyl)-4-methylbenzenesulfonamide**

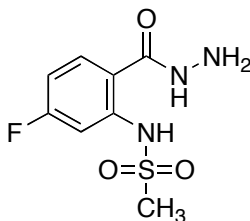
(162b)

Yellow solid; 77% yield; IR (CHCl₃ cast): 3329, 3400 – 3250 (br), 3094, 2926, 1636, 1596, 1503, 1423 cm⁻¹; ¹H NMR (500 MHz, CD₃OD): δ = 7.64 (m, 2H, 3-methyl-Ph-H), 7.54 (dd, *J* = 6.5, 9.0 Hz, 1H, 2-carboxyl-Ph-H), 7.34 (dd, *J* = 2.5, 11.0 Hz, 1H, 2-sulfonamide-Ph-H), 7.28 (m, 2H, 2-methyl-Ph-H), 6.81 (ddd, *J* = 2.5, 8.0, 9.0 Hz, 1H, 4-sulfonamide-Ph-H), 2.36 (s, 3H, CH₃); ¹³C NMR (125 MHz, CD₃OD): δ = 168.8, 165.8 (d, *J* = 250.0 Hz), 145.8, 142.1 (d, *J* = 11.4 Hz), 137.3, 131.1 (d, *J* = 10.3 Hz), 130.8, 128.3, 118.2 (d, *J* = 2.9 Hz), 111.7 (d, *J* = 22.3 Hz), 109.0 (d, *J* = 26.5 Hz), 21.5; ¹⁹F NMR (380 MHz, CD₃OD): δ = -107.4 (ddd, *J* = 7.2, 7.2, 9.9 Hz); ESI-HRMS *m/z* calcd for C₁₄H₁₅FN₃O₃S: 324.0813 [M+H]⁺, found: 324.0813.



4-Fluoro-2-(methylsulfonamido)benzoic acid (163a)

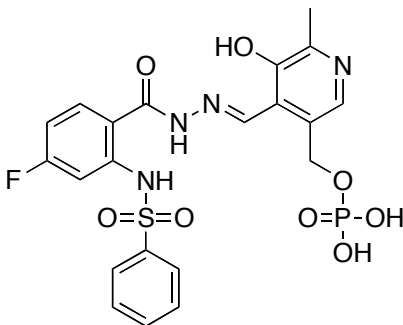
Grey solid; 41% yield; IR (CHCl₃ cast): 3220, 3109, 3300 – 2750 (br), 2931, 2851, 1660, 1623, 1588, 1506, 1430, 1416 cm⁻¹; ¹H NMR (500 MHz, CD₃OD): δ = 8.16 (dd, *J* = 6.5, 9.0 Hz, 1H, 2-carboxyl-Ph-H), 7.44 (dd, *J* = 2.5, 11.0 Hz, 1H, 2-sulfonamide-Ph-H), 6.89 (ddd, *J* = 2.4, 8.0, 8.8 Hz, 1H, 4-sulfonamide-Ph-H), 3.11 (s, 3H, CH₃); ¹³C NMR (125 MHz, CD₃OD): δ = 170.6, 167.5 (d, *J* = 251.1 Hz), 144.7 (d, *J* = 12.0 Hz), 135.8 (d, *J* = 11.0 Hz), 113.5 (d, *J* = 2.5 Hz), 110.8 (d, *J* = 22.4 Hz), 105.8 (d, *J* = 27.8 Hz), 40.2; ¹⁹F NMR (380 MHz, CD₃OD): δ = -103.9 (ddd, *J* = 7.6, 7.6, 11.4 Hz); ESI-HRMS *m/z* calcd for C₈H₇FNO₄S: 232.0085 [M-H]⁻, found: 232.0085.



N-(5-Fluoro-2-(hydrazinecarbonyl)phenyl)methanesulfonamide (163b)

White solid; 88% yield; IR (CHCl₃ cast): 3300, 3400 – 3250 (br), 3093, 3026, 2932, 1641, 1595, 1506, 1426 cm⁻¹; ¹H NMR (500 MHz, CD₃OD): δ = 7.71 (dd, *J* = 6.0, 8.5 Hz, 1H, 2-carboxyl-Ph-H), 7.41 (dd, *J* = 2.5, 11.0 Hz, 1H, 2-sulfonamide-Ph-H), 6.90 (ddd, *J* = 2.5, 8.0, 9.0 Hz, 1H, 4-sulfonamide-Ph-H),

3.06 (s, 3H, CH_3); ^{13}C NMR (125 MHz, CD_3OD): δ = 169.1, 166.2 (d, J = 248.9 Hz), 142.5 (d, J = 11.3 Hz), 131.4 (d, J = 10.3 Hz), 117.5 (d, J = 3.1 Hz), 111.2 (d, J = 22.3 Hz), 107.6 (d, J = 27.1 Hz), 40.0; ^{19}F NMR (380 MHz, CD_3OD): δ = -107.2 (ddd, J = 7.2, 7.2, 11.0 Hz); ESI-HRMS m/z calcd for $\text{C}_8\text{H}_{10}\text{FN}_3\text{NaO}_3\text{S}$: 270.0319 $[\text{M}+\text{Na}]^+$, found: 270.0319.



(E)-4-((2-(4-Fluoro-2-(phenylsulfonamido)benzoyl)hydrazono)methyl)-5-hydroxy-6-methylpyridin-3-yl)methyl dihydrogen phosphate (164)

Compound **155** (7.1 mg, 2.3×10^{-5} mol) and PLP (5.7 mg, 2.3×10^{-5} mol) were mixed in 1 mL of CD_3OD and 1 mL of D_2O . The resulting yellow solution was analyzed by ^1H and ^{13}C NMR. The mixture was dried in *vacuo*, then IR and HRMS data for the solid material was collected. Yellow solid; quantitative yield; IR (CHCl_3 cast): 3500 – 2500 (br), 3062, 2918, 1651, 1605, 1511, 1480, 1447, 1427 cm^{-1} ; ^1H NMR (500 MHz, D_2O): δ = 8.54 (s, 1H, 2-Pyr-H), 7.95 (s, 1H, $\text{CH}=\text{N}$), 7.71 (m, 3H, Ph-H), 7.56 (m, 1H, Ph-H), 7.49 (m, 2H, Ph-H), 7.14 (m, 1H, Ph-H), 6.91 (m, 1H, Ph-H), 5.00 (d, J = 5 Hz, 2H, CH_2), 2.47 (s, 3H, CH_3); ^{13}C NMR (125 MHz, D_2O): δ = 166.8, 165.7, 164.8, 153.5 (d, J = 4.9 Hz), 149.1, 147.7, 142.2 (m), 139.6, 136.6 (m), 134.3, 132.5 (d, J = 10.8 Hz), 131.6 (d, J = 6.1 Hz), 130.4, 127.5 (d, J = 5.1 Hz), 123.4 (d, J = 2.8 Hz), 120.7 (d, J = 3.1 Hz),

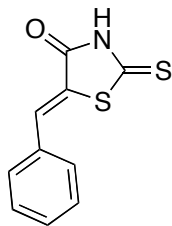
112.4 (m), 62.9 (d, $J = 3.0$ Hz), 18.1; ^{19}F NMR (380 MHz, D_2O): $\delta = -105.0$ (m); ESI-HRMS m/z calcd for $\text{C}_{21}\text{H}_{19}\text{FN}_4\text{O}_8\text{PS}$: 537.0651 $[\text{M-H}]^-$, found: 537.0652.

3.7 Synthesis of Rhodanine derived inhibitors of LL-DAP-AT

3.7.1 General procedure for synthesis of rhodanine-based analogues (170-190)

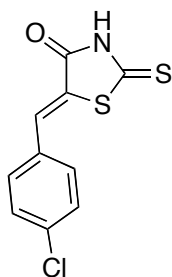
The rhodanine-based analogues were prepared using a Knoevenagel condensation reaction.¹⁹⁰ Acetic acid (10 mL) was heated to ~ 80 °C in an oil-bath. The rhodanine derivative (2.5 mmol) and 10 mmol sodium acetate were then added to the heated acid. The mixture was stirred for 5 min before the addition of 2.5 mmol of the aldehyde. The mixture was then heated to reflux for 16 h, and subsequently cooled to room temperature to give a crystalline product. The mixture was poured into ice-cold water (30 mL) and chilled in an ice bath for an additional 30 min. The solid was filtered under suction. The crude compounds were then purified by recrystallization with ethanol or a multi-solvent method (i.e., ethyl acetate with hexanes). The yields ranged from 37% to quantitative. Compounds were characterized by IR, ^1H NMR, ^{13}C NMR, and high resolution ESI-MS.

3.7.2 Characterization data for rhodanine-based analogues



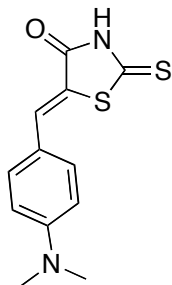
(Z)-5-Benzylidene-2-thioxothiazolidin-4-one (170)^{191, 192}

Yellow crystal; m.p. 196 – 197 °C [Lit. 204 – 205 °C]¹⁹¹; 94% yield; IR (Microscope) 3157, 3064, 2852, 1701, 1445, 1195 cm⁻¹; ¹H NMR (400 MHz, DMSO-*d*₆): δ = 13.81 (br, 1H, NH), 7.63 (s, 1H, C=CH), 7.52 (m, 5H, Ph-H); ¹³C NMR (100 MHz, DMSO-*d*₆): δ = 196.4, 170.1, 133.7, 132.3, 131.4, 131.2, 130.1, 126.2; EI-HRMS *m/z* calcd for C₁₀H₇NOS₂: 220.9969 [M⁺], found: 220.9969.



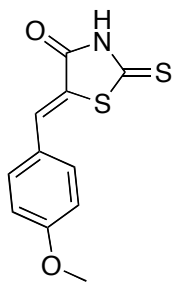
(Z)-5-(4-Chlorobenzylidene)-2-thioxothiazolidin-4-one (171)¹⁹¹

Light yellow crystal; m.p. 220 – 222 °C [Lit. 228 – 229 °C]¹⁹¹; 56% yield: IR (Microscope) 3086, 3015, 2852, 1718, 1488, 1188 cm⁻¹; ¹H NMR (400 MHz, DMSO-*d*₆): δ = 7.61 (s, 1H, C=CH), 7.58 (d, *J* = 2, 4H, Ph-H); ¹³C NMR (100 MHz, DMSO-*d*₆): δ = 196.1, 170.0, 136.0, 132.7, 132.6, 130.9, 130.2, 127.0; EI-HRMS *m/z* calcd for C₁₀H₆ClNOS₂: 254.9579 [M⁺], found: 254.9578.



(Z)-5-(4-(Dimethylamino)benzylidene)-2-thioxothiazolidin-4-one (172)¹⁹¹

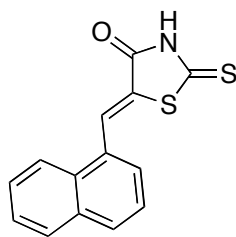
Red crystal; decomposed at 265 °C [Lit. m.p. 247 – 248 °C]¹⁹¹; 61% yield: IR (Microscope) 3139, 3042, 2909, 2853, 1682, 1436, 1180 cm⁻¹; ¹H NMR (400 MHz, DMSO-*d*₆): δ = 13.50 (br, 1H, NH), 7.47 (s, 1H, C=CH), 7.37 (d, *J* = 8.8 Hz, 2H, Ph-H), 6.77 (d, *J* = 8.8 Hz, 2H, Ph-H), 2.99 (s, 6H, 2×CH₃); ¹³C NMR (100 MHz, DMSO-*d*₆): δ = 195.7, 170.1, 152.4, 133.9, 133.6, 120.5, 118.0, 112.9, 40.3; ESI-HRMS *m/z* calcd for C₁₂H₁₂N₂NaOS₂: 287.0283 [M+Na⁺], found: 287.0283.



(Z)-5-(4-Methoxybenzylidene)-2-thioxothiazolidin-4-one (173)¹⁹¹

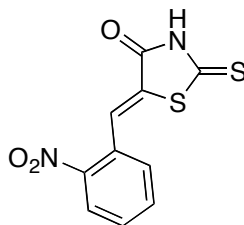
Yellow crystal; m.p. 254 – 255 °C [Lit. decomposed at 247 °C]¹⁹¹; 85% yield: IR (Microscope) 3134, 3017, 2934, 2853, 1687, 1446, 1170 cm⁻¹; ¹H NMR (400 MHz, DMSO-*d*₆): δ = 7.59 (s, 1H, C=CH), 7.55 (d, *J* = 8.8 Hz, 2H, Ph-H), 7.10 (d, *J* = 8.8 Hz, 2H, Ph-H), 3.82 (s, 3H, CH₃); ¹³C NMR (100 MHz, DMSO-*d*₆): δ =

195.5, 169.4, 161.3, 132.7, 131.9, 125.5, 122.2, 115.1, 55.5; ESI-HRMS m/z calcd for $C_{11}H_9NNaO_2S_2$: 273.9967 $[M+Na^+]$, found: 273.9968.



(Z)-5-(Naphthalen-1-ylmethylene)-2-thioxothiazolidin-4-one (174)¹⁹²

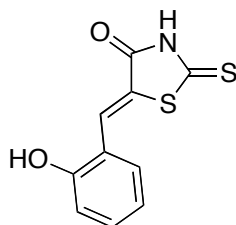
Light yellow crystal; m.p. 222 – 224 °C [Lit. 224 – 225 °C]¹⁹²; 82% yield: IR (Microscope) 3152, 3056, 3017, 2857, 1691, 1437, 1170 cm^{-1} ; 1H NMR (400 MHz, DMSO- d_6): δ = 8.27 (s, 1H, Ph-H), 8.15 (d, J = 8.4 Hz, 1H, Ph-H), 8.07 (dd, J = 6.4Hz, 3.2Hz, 1H, Ph-H), 8.02 (d, J = 8.8Hz, 1H, Ph-H), 7.65 (m, 4H); ^{13}C NMR (100 MHz, DMSO- d_6): δ = 196.8, 169.5, 134.0, 131.8, 131.7, 130.8, 129.6, 129.5, 128.8, 128.2, 127.6, 127.5, 126.4, 124.0; EI-HRMS m/z calcd for $C_{14}H_9NOS_2$: 271.0125 $[M^+]$, found: 271.0123.



(Z)-5-(2-Nitrobenzylidene)-2-thioxothiazolidin-4-one (175)¹⁹³

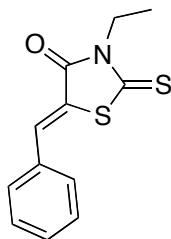
Light green crystal; m.p. 198 – 199 °C [Lit. 204 – 205 °C]¹⁹³; 98% yield: IR (Microscope) 3099, 3033, 2853, 1732, 1533, 1455, 1302, 1200 cm^{-1} ; 1H NMR (400 MHz, DMSO- d_6): δ = 8.16 (dd, J = 10.8Hz, 1.6Hz, 1H, Ph-H), 7.84 (td, J = 10 Hz, 1.6Hz, 1H, Ph-H), 7.82 (s, 1H, C=CH), 7.68 (m, 2H, Ph-H); ^{13}C NMR

(100 MHz, DMSO-*d*₆): δ = 196.5, 169.3, 148.7, 135.3, 131.9, 131.0, 130.1, 129.4, 128.5, 126.2; ESI-HRMS *m/z* calcd for C₁₀H₆N₂NaO₃S₂: 288.9712 [M+Na⁺], found: 288.9716.



(Z)-5-(2-Hydroxybenzylidene)-2-thioxothiazolidin-4-one (176)¹⁹¹

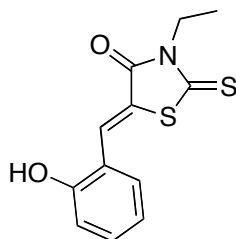
Orange crystal; decomposed at 208 °C [Lit. decomposed at 208 °C]¹⁹¹; 76% yield: IR (Microscope) 3496, 3437, 3096, 2846, 1699, 1450, 1163 cm⁻¹; ¹H NMR (400 MHz, DMSO-*d*₆): δ = 13.66 (br, 1H, NH), 10.62 (s, 1H, OH), 7.83 (s, 1H, C=CH), 7.28 (m, 2H, Ph-H), 6.94 (m, 2H, Ph-H); ¹³C NMR (100 MHz, DMSO-*d*₆): δ = 196.7, 170.2, 158.2, 133.5, 129.9, 128.0, 124.5, 120.6, 120.6, 116.9; ESI-HRMS *m/z* calcd for C₁₀H₇NNaO₂S₂: 259.9810 [M+Na⁺], found: 259.9815.



(Z)-5-Benzylidene-3-ethyl-2-thioxothiazolidin-4-one (177)¹⁹⁴

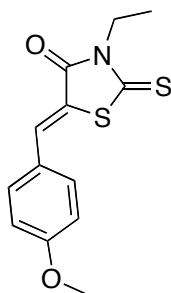
Bright yellow crystal; m.p. 145 – 146 °C [Lit. 148 – 149 °C]¹⁹⁴; 82% yield: IR (dichloromethane cast) 3015, 2982, 2934, 2873, 1705, 1445, 1132 cm⁻¹; ¹H NMR (400 MHz, DMSO-*d*₆): δ = 7.79 (s, 1H, C=CH), 7.61 (dt, *J* = 8 Hz, 1.6 Hz, 2H, Ph-H), 7.52 (m, 3H, Ph-H), 4.04 (q, *J* = 7.2, 2H, CH₂), 1.17 (t, *J* = 7.2, 3H, CH₃); ¹³C

NMR (100 MHz, DMSO-*d*₆): δ = 193.9, 167.4, 133.7, 133.6, 131.6, 131.3, 130.2, 123.3, 40.2, 12.6; ESI-HRMS *m/z* calcd for C₁₂H₁₂NOS₂: 250.0355 [M+H⁺], found: 250.0358.



(Z)-3-Ethyl-5-(2-hydroxybenzylidene)-2-thioxothiazolidin-4-one (178)

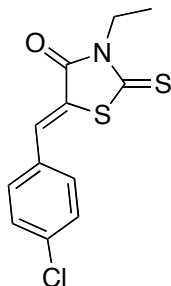
Yellow crystal; m.p. 210 – 212 °C; 56% yield: IR (dichloromethane cast) 3256, 3052, 2980, 2916, 2849, 1678, 1456, 1131 cm⁻¹; ¹H NMR (400 MHz, DMSO-*d*₆): δ = 10.71 (br, 1H, OH), 7.99 (s, 1H, C=CH), 7.34 (m, 2H, Ph-H), 6.96 (m, 2H, Ph-H), 4.06 (q, *J* = 7.2, 2H, CH₂), 1.18 (t, *J* = 7.2, 3H, CH₃); ¹³C NMR (100 MHz, DMSO-*d*₆): δ = 193.5, 166.8, 157.6, 133.0, 129.6, 128.6, 120.8, 120.0, 119.9, 116.3, 40.2, 11.9; ESI-HRMS *m/z* calcd for C₁₂H₁₁NNaO₂S₂: 288.0123 [M+Na⁺], found: 288.0119.



(Z)-3-Ethyl-5-(4-methoxybenzylidene)-2-thioxothiazolidin-4-one (179)¹⁹⁴

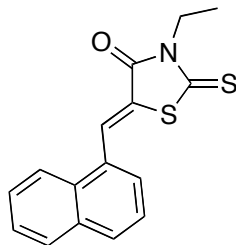
Bright yellow crystal; m.p. 138 – 139 °C [Lit. 133 – 134 °C]¹⁹⁴; 53% yield: IR (dichloromethane cast) 3004, 2983, 2961, 2833, 1703, 1457, 1127 cm⁻¹; ¹H NMR

(400 MHz, DMSO-*d*₆): δ = 7.75 (s, 1H, C=CH), 7.58 (d, *J* = 8.8Hz, 2H, Ph-H), 7.09 (d, *J* = 8.8, 2H, Ph-H), 4.03 (q, *J* = 7.2, 2H, CH₂), 3.82 (s, 3H, O-CH₃), 1.16 (t, *J* = 7.2, 3H, CH₂CH₃); ¹³C NMR (100 MHz, DMSO-*d*₆): δ = 193.7, 167.5, 162.2, 133.8, 133.6, 126.2, 119.9, 115.9, 56.3, 40.2, 12.6; ESI-HRMS *m/z* calcd for C₁₃H₁₄NO₂S₂: 280.0461 [M+H⁺], found: 280.0467.



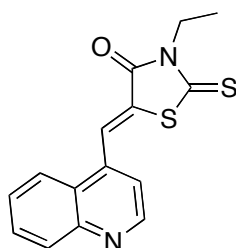
(Z)-5-(4-Chlorobenzylidene)-3-ethyl-2-thioxothiazolidin-4-one (180)¹⁹⁵

Yellow crystal; m.p. 149 – 150 °C; 79% yield: IR (dichloromethane cast) 3004, 2983, 2971, 2872, 1705, 1433, 1137 cm⁻¹; ¹H NMR (400 MHz, DMSO-*d*₆): δ = 7.78 (s, 1H, C=CH), 7.63 (d, *J* = 8.8Hz, 2H, Ph-H), 7.58 (d, *J* = 8.8, 2H, Ph-H), 4.03 (q, *J* = 7.2, 2H, CH₂), 1.16 (t, *J* = 7.2, 3H, CH₃); ¹³C NMR (100 MHz, DMSO-*d*₆): δ = 193.6, 167.3, 133.3, 132.9, 132.6, 132.1, 130.3, 124.0, 40.2, 12.6; EI-HRMS *m/z* calcd for C₁₂H₁₀ClNOS₂: 282.9892 [M⁺], found: 282.9895.



(Z)-3-Ethyl-5-(naphthalen-1-ylmethylene)-2-thioxothiazolidin-4-one (181)¹⁹⁶

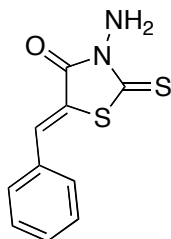
Yellow-brown crystal; m.p. 126 – 127 °C; 31% yield: IR (dichloromethane cast) 3075, 3055, 2974, 2931, 2873, 1704, 1431, 1133 cm^{-1} ; ^1H NMR (400 MHz, CDCl_3): δ = 8.49 (s, 1H, C=CH), 8.16 (d, J = 8.8Hz, 1H, Ph-H), 7.93 (m, 2H, Ph-H), 7.57 (m, 4H, Ph-H), 4.24 (q, J = 7.2, 2H, CH₂), 1.33 (t, J = 7.2, 3H, CH₃); ^{13}C NMR (100 MHz, CDCl_3): δ = 194.0, 167.4, 134.0, 132.1, 131.7, 130.8, 130.0, 129.3, 127.7, 127.3, 127.1, 126.3, 125.6, 123.6, 40.0, 12.6; EI-HRMS m/z calcd for $\text{C}_{16}\text{H}_{13}\text{NOS}_2$: 299.0439 [M^+], found: 299.0440.



(Z)-3-Ethyl-5-(quinolin-5-ylmethylene)-2-thioxothiazolidin-4-one (182)¹⁹⁷

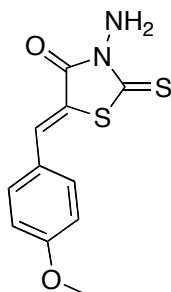
Light yellow crystal; m.p. 172 – 173 °C; 40% yield: IR (dichloromethane cast) 3063, 3042, 2978, 2935, 2876, 1712, 1439, 1134 cm^{-1} ; ^1H NMR (400 MHz, CDCl_3): δ = 9.04 (d, J = 4.4Hz, 1H, Ph-H), 8.38 (s, 1H, C=CH), 8.23 (d, J = 8.4Hz, 1H, Ph-H), 8.16 (d, J = 8.4Hz, 1H, Ph-H), 7.84 (m, 1H, Ph-H), 7.71 (m, 1H, Ph-H), 7.47 (d, J = 4.8Hz, 1H, Ph-H), 4.26 (q, J = 7.2, 2H, CH₂), 1.36 (t, J =

7.2, 3H, $\underline{\text{CH}_3}$); ^{13}C NMR (100 MHz, CDCl_3): $\delta = 192.6, 167.0, 150.0, 148.8, 139.0, 130.7, 130.6, 130.6, 128.1, 126.4, 126.3, 123.5, 119.7, 40.3, 12.5$; ESI-HRMS m/z calcd for $\text{C}_{15}\text{H}_{13}\text{N}_2\text{OS}_2$: 301.0464 $[\text{M}+\text{H}^+]$, found: 301.0464.



(Z)-3-Amino-5-benzylidene-2-thioxothiazolidin-4-one (183)¹⁹⁸

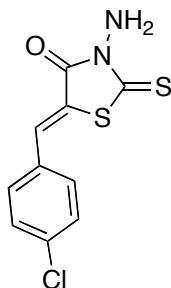
Bright yellow crystal; m.p. 196 – 197 °C [Lit. 192 – 195 °C]¹⁹⁸; 53% yield: IR (dichloromethane cast) 3299, 3225, 3031, 1706, 1448, 1125 cm^{-1} ; ^1H NMR (400 MHz, $\text{DMSO-}d_6$): $\delta = 7.85$ (s, 1H, $\text{C}=\underline{\text{CH}}$), 7.64 (m, 2H, $\text{Ph-}\underline{\text{H}}$), 7.53 (m, 3H, $\text{Ph-}\underline{\text{H}}$), 5.93 (s, 2H, NH_2); ^{13}C NMR (100 MHz, $\text{DMSO-}d_6$): $\delta = 187.7, 163.7, 133.3, 133.0, 131.0, 130.7, 129.5, 120.3$; ESI-HRMS m/z calcd for $\text{C}_{10}\text{H}_8\text{N}_2\text{NaOS}_2$: 258.9970 $[\text{M}+\text{Na}^+]$, found: 258.9975.



(Z)-3-Amino-5-(4-methoxybenzylidene)-2-thioxothiazolidin-4-one (184)¹⁹⁵

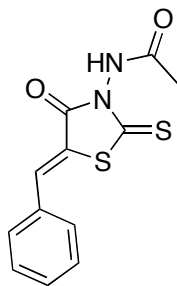
Yellow crystal; m.p. 178 – 179 °C; 26% yield: IR (dichloromethane cast) 3288, 3195, 2942, 2842, 1702, 1509, 1131 cm^{-1} ; ^1H NMR (400 MHz, $\text{DMSO-}d_6$): $\delta = 7.76$ (s, 1H, $\text{C}=\underline{\text{CH}}$), 7.57 (d, $J = 8.8\text{Hz}$, 2H, $\text{Ph-}\underline{\text{H}}$), 7.04 (d, $J = 8.8\text{Hz}$, 2H, $\text{Ph-}\underline{\text{H}}$),

5.90 (s, 2H, NH_2), 3.80 (s, 3H, CH_3); ^{13}C NMR (100 MHz, $\text{DMSO-}d_6$): δ = 187.9, 164.4, 162.3, 134.3, 133.7, 126.2, 117.6, 115.8, 56.3; ESI-HRMS m/z calcd for $\text{C}_{11}\text{H}_{10}\text{N}_2\text{NaO}_2\text{S}_2$: 289.0076 $[\text{M}+\text{Na}^+]$, found: 289.0070.



(Z)-3-Amino-5-(4-chlorobenzylidene)-2-thioxothiazolidin-4-one (185)¹⁹⁵

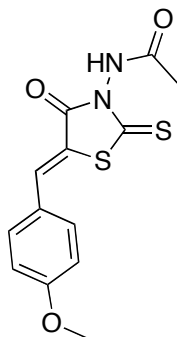
Bright yellow crystal; m.p. 216 – 217 °C; 73% yield: IR (dichloromethane cast) 3299, 3234, 3169, 3071, 1727, 1709, 1493, 1128 cm^{-1} ; ^1H NMR (400 MHz, $\text{DMSO-}d_6$): δ = 7.83 (s, 1H, $\text{C}=\underline{\text{CH}}$), 7.65 (d, J = 8.8Hz, 2H, $\text{Ph-}\underline{\text{H}}$), 7.59 (d, J = 8.8Hz, 2H, $\text{Ph-}\underline{\text{H}}$), 5.92 (s, 2H, NH_2); ^{13}C NMR (100 MHz, $\text{DMSO-}d_6$): δ = 188.2, 164.4, 136.3, 133.0, 132.6, 132.5, 130.3, 121.8; ESI-HRMS m/z calcd for $\text{C}_{10}\text{H}_7\text{ClN}_2\text{NaOS}_2$: 292.9581 $[\text{M}+\text{Na}^+]$, found: 292.9579.



(Z)-N-(5-Benzylidene-4-oxo-2-thioxothiazolidin-3-yl)acetamide (186)¹⁹⁹

Bright yellow crystal; m.p. 206 – 207 °C [Lit. 203 – 205 °C]¹⁹⁹; 88% yield: IR (dichloromethane cast) 3192, 3017, 1737, 1679, 1447, 1125 cm^{-1} ; ^1H NMR (400

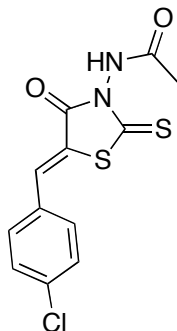
MHz, DMSO-*d*₆): δ = 7.92 (s, 1H, C=CH), 7.68 (m, 2H, Ph-H), 7.56 (m, 3H, Ph-H), 2.07 (s, 3H, CH₃); ¹³C NMR (100 MHz, DMSO-*d*₆): δ = 190.5, 167.7, 163.3, 134.6, 132.7, 131.3, 130.8, 129.5, 119.4, 20.3; ESI-HRMS *m/z* calcd for C₁₂H₁₀N₂NaO₂S₂: 301.0076 [M+Na⁺], found: 301.0071.



(Z)-N-(5-(4-Methoxybenzylidene)-4-oxo-2-thioxothiazolidin-3-yl)acetamide

(187)

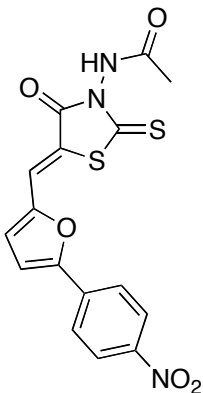
Bright yellow crystal; m.p. 220 – 221 °C; 30% yield: IR (dichloromethane cast) 3194, 3013, 2963, 1729, 1679, 1421, 1134 cm⁻¹; ¹H NMR (400 MHz, DMSO-*d*₆): δ = 11.12 (s, 1H, NH), 7.85 (s, 1H, C=CH), 7.63 (d, *J* = 8.8 Hz, 2H, Ph-H), 7.11 (d, *J* = 8.8 Hz, 2H, Ph-H), 3.83 (s, 3H, O-CH₃), 2.05 (s, 3H, CO-CH₃); ¹³C NMR (100 MHz, DMSO-*d*₆): δ = 191.2, 168.4, 164.1, 162.5, 135.5, 133.9, 126.0, 116.7, 115.9, 56.3, 21.0; ESI-HRMS *m/z* calcd for C₁₃H₁₂N₂NaO₃S₂: 331.0182 [M+Na⁺], found: 331.0182.



(Z)-N-(5-(4-Chlorobenzylidene)-4-oxo-2-thioxothiazolidin-3-yl)acetamide

(188)

Yellow crystal; m.p. 255 – 256 °C; 80% yield: IR (dichloromethane cast) 3199, 3013, 1732, 1680, 1405, 1128 cm^{-1} ; ^1H NMR (400 MHz, $\text{DMSO-}d_6$): δ = 7.92 (s, 1H, C=CH), 7.72 (d, J = 8.5Hz, 2H, Ph-H), 7.63 (d, J = 8.5Hz, 2H, Ph-H), 2.07 (s, 3H, CH₃); ^{13}C NMR (100 MHz, $\text{DMSO-}d_6$): δ = 190.1, 167.6, 163.1, 135.8, 133.1, 132.3, 131.5, 129.5, 120.1, 20.2; ESI-HRMS m/z calcd for $\text{C}_{12}\text{H}_9\text{ClN}_2\text{NaO}_2\text{S}_2$: 334.9686 $[\text{M}+\text{Na}^+]$, found: 334.9682.

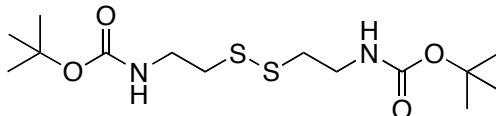


(Z)-N-(5-((5-(4-Nitrophenyl)furan-2-yl)methylene)-4-oxo-2-thioxothiazolidin-3-yl) acetamide (189)

Orange solid; 90% yield: IR (dichloromethane cast) 3239, 3038, 1729, 1678, 1511, 1139 cm^{-1} ; ^1H NMR (400 MHz, $\text{DMSO-}d_6$): δ = 11.14 (s, 1H, NH), 8.37 (d, J = 9.2, 2H, Ph-H), 8.05 (d, J = 9.2, 2H, Ph-H), 7.79 (s, 1H, C=CH), 7.61 (d, J = 4.0Hz, 1H, furan-H), 7.44 (d, J = 4.0Hz, 1H, furan-H), 2.06 (s, 3H, CH₃); ^{13}C NMR (100 MHz, $\text{DMSO-}d_6$): δ = 191.8, 168.4, 163.7, 156.5, 151.5, 147.7, 134.8, 126.0, 125.5, 124.3, 120.1, 118.0, 114.6, 21.0; ESI-HRMS m/z calcd for $\text{C}_{16}\text{H}_{11}\text{N}_3\text{NaO}_5\text{S}_2$: 412.0032 [$\text{M}+\text{Na}^+$], found: 412.0028.

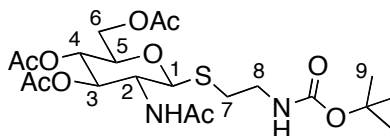
3.8 Preparation of glucosamine linked to SubA

3.8.1 Using squarate as the linker



tert-Butyl 2,2'-disulfanediyldis(ethane-2,1-diyl)dicarbamate (**203**)²⁰⁰

Cystamine dihydrochloride (0.4504 g, 2 mmol) was mixed with 9 mL of MeOH. After adding 1 mL of triethylamine into the mixture, the solid was dissolved. Di-*tert*-butyl dicarbonate (0.92 mL, 4 mmol) was then added into the reaction mixture. The mixture was stirred for three hours. Solvent was removed *in vacuo*. The product was purified by flash column chromatography (silica gel, EtOAc/Hex = 1:1). The title compound was obtained as white solid (0.55 g, 78%). IR (Microscope): 3365, 3346, 2970, 1684 cm⁻¹; ¹H NMR (400 MHz, CDCl₃): δ = 5.00 (br, 2H, NH), 3.45 (m, 4H, NH-CH₂), 2.80 (t, *J* = 6.4 Hz, 4H, S-CH₂), 1.45 (s, 18H, CH₃); ¹³C NMR (100 MHz, CDCl₃): δ = 156.0, 80.0, 39.5, 38.7, 28.6; ESI-HRMS *m/z* calcd for C₁₄H₂₈N₂NaO₄S₂: 375.1383 [M+Na]⁺, found: 375.1383.

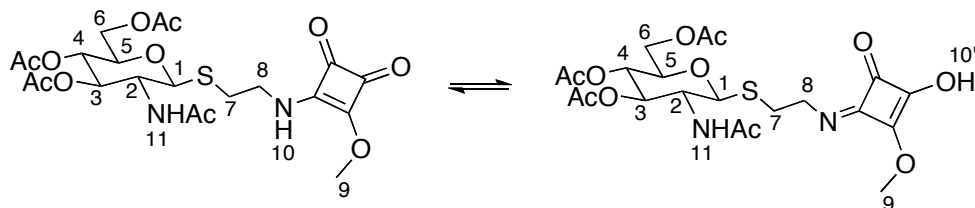


(1*S*,2*R*,3*R*,4*S*,5*R*)-2-Acetamido-5-(acetoxymethyl)-1-(2-(*tert*-butoxycarbonylamino)ethylthio)tetrahydro-2*H*-pyran-3,4-diyl diacetate (**206**)

The protected cystamine **203** (0.3525 g, 1 mmol) was dissolved in 15 mL of THF, to which tributylphosphine (0.37 mL, 1.5 mmol) was added. After half hour of

stirring, 1.5 mL of water was added into the mixture, which was further stirred for 20 hours. THF was then removed *in vacuo*. The residue was dissolved in 20 mL of ethyl acetate and washed with 10% citric acid (2 × 20 mL), water (2 × 20 mL), and brine (20 mL). The organic layer was dried over anhydrous sodium sulfate, the solvent was removed *in vacuo*, and the crude thiol was used directly for the next step. Commercially available 3,4,6-tri-O-acetyl-2-(acetamido)-2-deoxy- α -D-glucopyranosyl chloride (**205**, 0.3657 g, 1 mmol) and tetrabutylammonium hydrogen sulfate (0.3395 g, 1 mmol) were mixed with 5 mL ethyl acetate. The free thiol was mixed with 5 mL of 1.5 M sodium carbonate solution and 3 mL of ethyl acetate, and this mixture was added to the carbohydrate solution. The mixture was clear initially, and the upper layer turned light pink during the reaction. The mixture was stirred vigorously for 16 hours, and monitored by TLC until all of the monosaccharide had reacted. The reaction mixture was diluted with 15 mL of ethyl acetate, and the organic layer was washed with saturated sodium bicarbonate solution (2 × 15 mL), water (2 × 15 mL), and brine (15 mL). The organic layer was dried over anhydrous sodium sulfate and the solvent was removed *in vacuo*. The residue was then purified by column chromatography (silica gel, EtOAc/hexanes = 1:4). The title compound was obtained as a white solid (0.3061 g, 60%). $[\alpha]_D = -21.5$ (*c* 0.78, CHCl₃); IR (Microscope): 3350, 3294, 3088, 2976, 2949, 2886, 1742, 1677, 1662 cm⁻¹; ¹H NMR (400 MHz, CDCl₃): δ = 5.69 (d, *J* = 9.6 Hz, 1H, C-2-N-H), 5.13 (m, 3H, C-8-N-H, H-3, H-4), 4.62 (d, *J* = 10.4 Hz, 1H, H-1), 4.15 (m, 3H, H-2 & H₂-6), 3.71 (ddd, *J* = 2.4, 4.8, 9.6 Hz, 1H, H-5), 3.36 (m, 2H, H₂-8), 2.91 (dt, *J* = 6, 14 Hz,

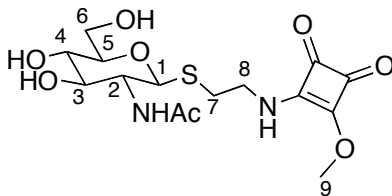
1H, H-7a), 2.71 (m, 1H, H-7b), 2.08 (s, 3H, COCH₃), 2.03 (s, 3H, COCH₃), 2.03 (s, 3H, COCH₃), 1.96 (s, 3H, COCH₃), 1.44 (s, 9H, Boc-CH₃); ¹³C NMR (100 MHz, CDCl₃): δ = 171.3, 170.9, 170.4, 169.5, 156.1, 85.1, 80.0, 76.3, 74.0, 68.5, 62.4, 53.5, 40.8, 31.5, 28.7, 23.5, 20.9, 20.9, 20.8; ESI-HRMS *m/z* calcd for C₂₁H₃₅N₂O₁₀S: 507.2007 [M+H]⁺, found: 507.2007.



(1*S*,2*R*,3*R*,4*S*,5*R*)-2-Acetamido-5-(acetoxymethyl)-1-(2-(2-methoxy-3,4-dioxocyclobut-1-enylamino)ethylthio)tetrahydro-2*H*-pyran-3,4-diyl diacetate and (1*S*,2*R*,3*R*,4*S*,5*R*)-2-acetamido-5-(acetoxymethyl)-1-(2-((*Z*)-3-hydroxy-2-methoxy-4-oxocyclobut-2-enylideneamino)ethylthio)tetrahydro-2*H*-pyran-3,4-diyl diacetate (208)

The Boc protected compound **206** (0.5060 g, 1 mmol) was dissolved in 10 mL of dry CH₂Cl₂, to which was added 10 mL of trifluoroacetic acid. After half an hour, the mixture turned light yellow. After all of the starting material was consumed based on TLC monitoring, the solvent and the excess of TFA were removed *in vacuo*. The residue was dissolved in 4 mL of dry MeOH and mixed with 0.5 mL of diisopropylethylamine. This solution was then added into a dimethyl squarate solution which was prepared by mixing dimethyl squarate (0.1563 g, 1.1 mmol) with 6 mL of dry MeOH and 0.5 mL of diisopropylethylamine. The progress of the reaction was monitored by TLC. After the reaction was complete, the mixture

was concentrated and purified by column chromatography (silica gel, EtOAc). The titled compound was obtained as white solid (0.4281 g, 83%). $[\alpha]_D = -46.6$ (c 0.80, CHCl_3); IR (Microscope): 3291 (br), 3077, 3014, 2956, 2875, 1804, 1748, 1710, 1665, 1610 cm^{-1} ; ^1H NMR (500 MHz, CDCl_3): δ = 6.97 (br, 0.5H, H-10), 6.59 (br, 0.5H, H-10'), 6.28 (m, 1H, H-11), 5.17 (m, 1H, H-3), 5.07 (m, 1H, H-4), 4.69 (m, 1H, H-1), 4.40 (s, 3H, H-9), 4.22 – 4.10 (m, 3H, H₂-6 & H-2), 4.00 – 3.59 (m, 3H, H-5 & H₂-8), 3.04 (dt, J = 5.5, 14.5 Hz, 1H, H-7a), 2.84 (br, 1H, H-7b), 2.07 (s, 3H, COCH_3), 2.02 (s, 3H, COCH_3), 2.02 (s, 3H, COCH_3), 1.96 (s, 3H, COCH_3); ^{13}C NMR (100 MHz, CDCl_3): δ = 188.8, 183.6, 177.6, 172.5, 170.7, 169.3, 84.1, 76.0, 73.5, 68.3, 62.1, 60.6, 52.8, 44.5, 43.7, 31.4, 30.5, 23.2, 20.7, 20.7, 20.6; ESI-HRMS m/z calcd for $\text{C}_{21}\text{H}_{29}\text{N}_2\text{O}_{11}\text{S}$: 517.1487 $[\text{M}+\text{H}]^+$, found: 517.1486.

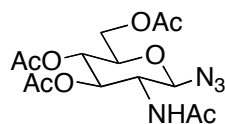


***N*-((1*S*,2*R*,3*R*,4*S*,5*R*)-3,4-Dihydroxy-5-(hydroxymethyl)-1-(2-(2-methoxy-3,4-dioxocyclobut-1-enylamino)ethylthio)tetrahydro-2*H*-pyran-2-yl)acetamide
(209)**

Compound **208** (0.3350 g, 0.65 mmol) was dissolved in 10 mL of dry MeOH. Approximately 1 mL of 1 M sodium methoxide in MeOH was added to adjust the pH to 9. The progress of the reaction was monitored by TLC. Once all of the starting material was converted to product, the mixture was neutralized with

Amberlyst acidic resin, Amberlite[®] IR120. The mixture was filtered and the resin was washed with 2 mL of MeOH. The filtrate was then concentrated and purified by column chromatography (silica gel, 15% MeOH in CH₂Cl₂). The titled compound was obtained as white solid (0.2210 g, 87%). $[\alpha]_D = -23.8$ (*c* 1.10, CH₃OH); IR (Microscope): 3301 (br), 2950, 2881, 1805, 1703, 1609 cm⁻¹; ¹H NMR (300 MHz, CD₃OD): $\delta = 4.51$ (m, 1H, H-1), 4.37 (m, 3H, H-9), 3.94 – 3.54 (m, 5H, H-2, H-3, H-4 & H₂-6), 3.44 (m, 1H, H-5), 3.29 (m, 2H, H-8), 3.01 (m, 1H, H-7a), 2.77 (m, 1H, H-7b), 1.95 (s, 3H, COCH₃); ¹³C NMR (100 MHz, CD₃OD): $\delta = 173.3, 172.8, 172.4, 84.6, 82.7, 81.0, 76.1, 70.8, 61.7, 60.1, 54.9, 44.9, 31.1, 30.5, 21.8$; ESI-HRMS *m/z* calcd for C₁₅H₂₂N₂NaO₈S: 413.0989 [M+Na]⁺, found: 413.0986.

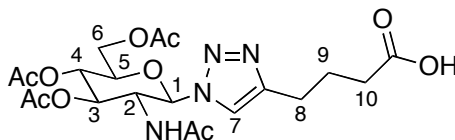
3.8.2 Click chemistry used in linking glucosamine and SubA



(1*R*,2*R*,3*R*,4*S*,5*R*)-2-Acetamido-5-(acetoxymethyl)-1-azidotetrahydro-2*H*-pyran-3,4-diyl diacetate (210)²⁰¹

Compound **205** (1.03 g, 2.7 mmol) was dissolved in 8 mL of CH₂Cl₂. A solution of sodium azide (0.51 g, 7.8 mmol) in 8 mL of saturated sodium bicarbonate was added into the monosaccharide solution, which followed by the addition of tetrabutylammonium hydrogen sulfate (0.89 g, 2.6 mmol). The reaction mixture was stirred for 2 hours before being diluted with 15 mL of CH₂Cl₂. The organic layer was washed with 20 mL of water, followed by 20 mL of brine and dried

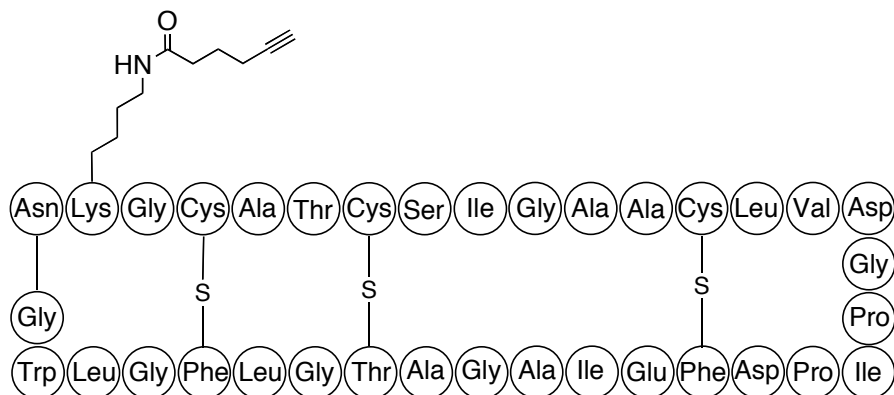
over anhydrous sodium sulfate. The solvent was then removed *in vacuo*. The oil-like crude product was purified by column chromatography (silica gel, EtOAc/hexanes = 2:1). The title compound was obtained as white solid (0.963 g, 96%). $[\alpha]_D = -48.7$ (*c* 0.80, CHCl₃); m.p. 165 – 170 IR (CHCl₃ Cast Microscope): 3286, 3076, 2957, 2119, 1750, 1663 cm⁻¹; ¹H NMR (400 MHz, CDCl₃): δ = 5.58 (d, *J* = 8.8 Hz, 1H, NHAc), 5.24 (m, 1H, H-3), 5.10 (m, 1H, H-4), 4.75 (d, *J* = 9.2 Hz, 1H, H-1), 4.27 (m, 1H, H-6), 4.17 (m, 1H, H-6'), 3.90 (dt, *J* = 9.2, 10.4 Hz, 1H, H-2), 3.78 (ddd, *J* = 2.4, 4.8, 10 Hz, 1H, H-5), 2.10 (s, 3H, COCH₃), 2.04 (s, 3H, COCH₃), 2.03 (s, 3H, COCH₃), 1.98 (s, 3H, COCH₃); ¹³C NMR (125 MHz, CDCl₃): δ = 171.0, 170.6, 170.4, 169.2, 88.4, 74.0, 72.1, 68.1, 61.9, 54.2, 23.2, 20.7, 20.6, 20.5; ESI-HRMS *m/z* calcd for C₁₄H₂₀N₄NaO₈: 395.1173 [M+Na]⁺, found: 395.1178.



4-(1-((2*R*,3*R*,4*R*,5*S*,6*R*)-3-Acetamido-4,5-diacetoxy-6-(acetoxymethyl)tetrahydro-2*H*-pyran-2-yl)-1*H*-1,2,3-triazol-4-yl)butanoic acid (212)

The azido-monosaccharide **210** (0.1860 g, 0.5 mmol) and 5-hexynoic acid (0.055 mL, 0.5 mmol) were mixed with 1 mL of *t*-butanol. Copper acetate (0.0180 g, 0.1 mmol) and sodium L-ascorbate (0.0396 g, 0.2 mmol) were mixed with 1 mL of water. The latter solution, which turned a brown colour, was added into the *t*-butanol solution. The resulting reaction mixture then turned light yellow. After

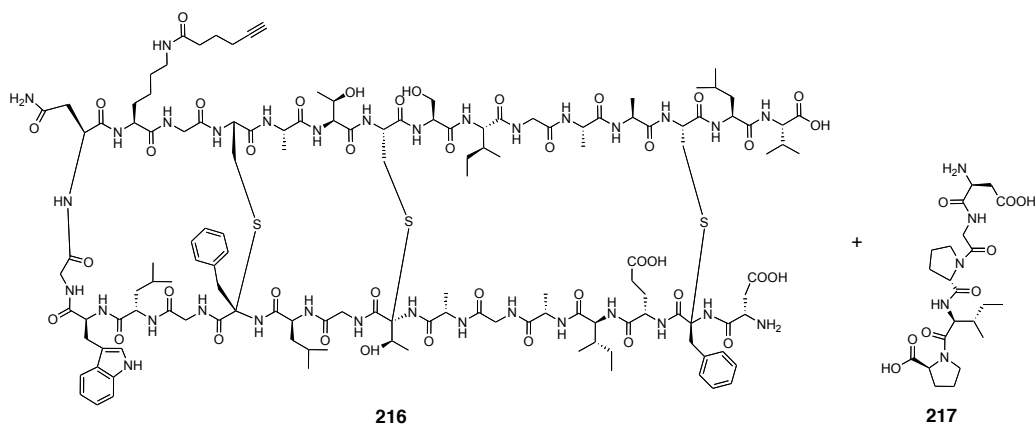
stirring at room temperature for 6 hours, the clear reaction mixture was diluted with 10 mL water. The product was extracted with CH₂Cl₂ (2 × 20 mL). The organic layer was washed with water (20 mL) and brine (20 mL) before being dried over anhydrous sodium sulfate. The solvent was then removed *in vacuo*. The titled compound was obtained as white solid (0.2251 g, 93%). [α]_D = -30.2 (*c* 2.30, CH₃OH); IR (CHCl₃ Cast Microscope): 3275, 3146, 3070, 2941, 1750, 1671, 1558 cm⁻¹; ¹H NMR (400 MHz, CD₃OD): δ = 7.97 (s, 1H, H-7), 6.08 (d, *J* = 9.6 Hz, 1H, H-1), 5.48 (dd, *J* = 9.6 Hz, 1H, H-3), 5.21 (dd, *J* = 9.6 Hz, 1H, H-4), 4.51 (t, *J* = 10.4 Hz, 1H, H-2), 4.31 (dd, *J* = 4.8, 12.8 Hz, 1H, H-6), 4.14 (m, 2H, H-6' & H-5), 2.74 (t, *J* = 7.2 Hz, 2H, H₂-8), 2.26 (m, 2H, H₂-10), 2.04 (m, 6H, 2×COCH₃), 2.00 (s, 3H, COCH₃), 1.95 (m, 2H, H₂-9), 1.71 (s, 3H, COCH₃); ¹³C NMR (100 MHz, CD₃OD): δ = 173.3, 171.2, 171.1, 170.5, 170.0, 154.4, 120.9, 85.6, 74.8, 72.5, 68.5, 61.9, 53.6, 25.8, 22.4, 20.9, 20.6, 20.5, 15.4, 14.4; ESI-HRMS *m/z* calcd for C₂₀H₂₈N₄NaO₁₀: 507.1698 [M+Na]⁺, found: 507.1693.



Subtilosin A-lysine- ϵ -amido-5-hexyne (215)

5-Hexynoic acid (0.11 mL, 1 mmol) and dry pyridine (0.08 mL, 1 mmol) were mixed with 10 mL dry CH₂Cl₂. Fluoro-*N,N,N',N'*-tetramethylformamidinium

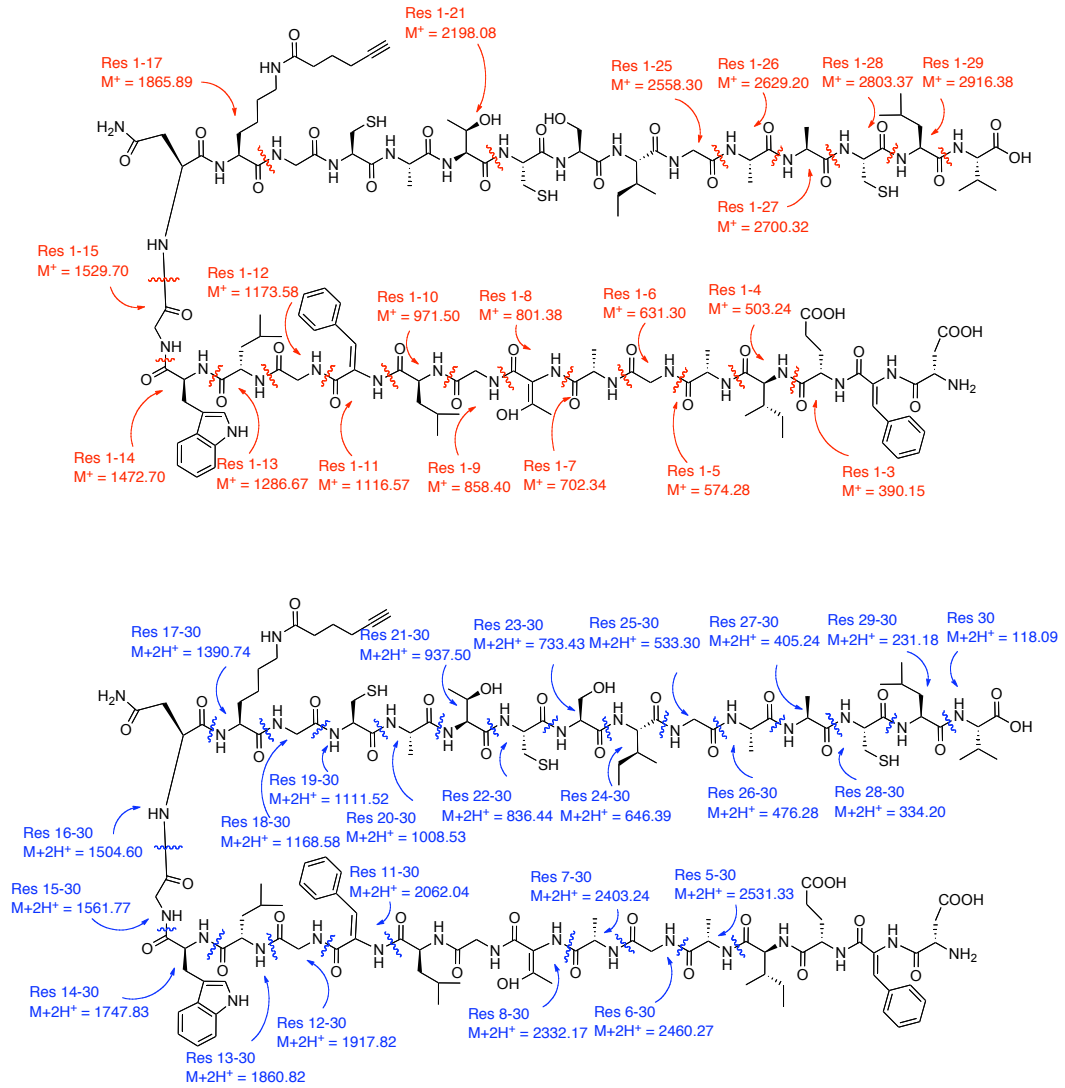
hexafluorophosphate (0.3962 g, 1.5 mmol) was then added into the mixture. The reaction mixture was stirred for 5 hours at room temperature. A white precipitate formed, indicating the formation of insoluble tetramethylurea. The reaction mixture was diluted with 20 mL CH₂Cl₂, and the organic layer was washed with ice-cold water (2 × 15 mL). The CH₂Cl₂ solution was dried over anhydrous sodium sulfate and the solvent was removed *in vacuo*. The crude acid fluoride (0.0512 g, 44%) was used without any further purification. The crude acid fluoride was dissolved in 50 mL of acetonitrile, and 0.5 mL of this solution was mixed with a solution of 3 mg subtilisin A, which was prepared in 1 mL acetonitrile and 1.5 mL 100 mM sodium phosphate buffer pH 7.2. The reaction mixture was stirred at 4 °C for two days, and the product was purified by HPLC. HPLC method: Analytical C8 column, flow rate 1.0 mL/min, detected at 220 nm. Gradient: Starting from 20% MeCN (0.1% TFA) and 80% water (0.1% TFA) for 5 min, ramping up to 80% MeCN over 28 min, keeping 80% MeCN for 5min, ramping down to 20% MeCN over 2 min, then keeping 20% MeCN for 5min. The product (*t_R* = 29.3 minutes) was analyzed by MALDI-TOF-MS *m/z* calcd for C₁₅₈H₂₃₃N₃₈O₄₆S₃: 3494.6 [M+H]⁺, found 3494.5. The white solid material was obtained by lyophilization (1.8 mg, 60%).



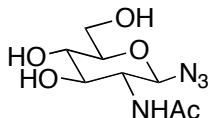
Alkynyl-SubA digestion product (216 & 217) using endoproteinase Asp-N

The alkynyl-SubA **215** (0.6 mg) was dissolved in 150 μL of 1:1 mixture of acetonitrile and water. Endoproteinase Asp-N (2 μg) was dissolved in 28 μL of 200 mM phosphate buffer, pH 7.8. Subsequently, 12 μL of the alkynyl-SubA solution was mixed with the enzyme solution and incubated at 37 $^{\circ}\text{C}$ for two hours. Compound **216** was detected by MALDI-TOF-MS m/z calcd for $\text{C}_{136}\text{H}_{200}\text{N}_{33}\text{O}_{40}\text{S}_3$: 3031.4 $[\text{M}-\text{H}]^-$, found 3031.3.

MS/MS analysis of alkynyl-SubA digestion product (218)

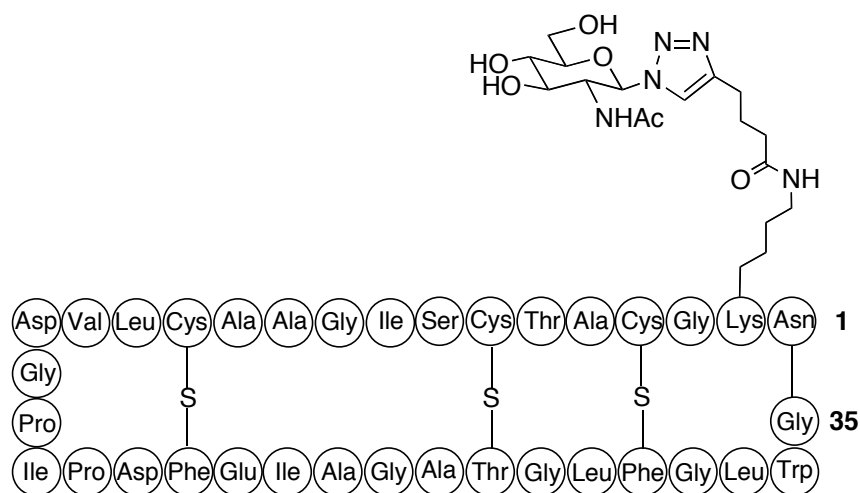


218
 Exact Mass: 3032.4
 Observed Mass ($[M+H]^+$): 3033.49



***N*-((1*R*,2*R*,3*R*,4*S*,5*R*)-1-azido-3,4-dihydroxy-5-(hydroxymethyl)tetrahydro-2*H*-pyran-2-yl)acetamide (**219**)²⁰¹**

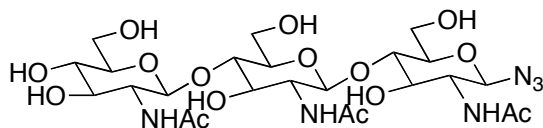
The azido-monosaccharide **210** (0.7210 g, 1.9 mmol) was dissolved in 5 mL dry methanol. Approximately 1 mL of 1 M sodium methoxide in MeOH was added to this solution to adjust the pH to 9. After all of the starting material was converted to product as monitored by TLC, the mixture was neutralized with amberlyst acidic resin, Amberlite[®] IR120. The mixture was filtered and the resin was washed with another 2 mL of MeOH. The filtrate was concentrated and purified by column chromatography (silica gel, EtOAc/hexanes = 9:1). The title compound was obtained as white solid (0.4502 g, 90%). $[\alpha]_D = -27.2$ (*c* 0.36, CH₃OH); IR (Microscope): 3600 – 3100 (br), 2959, 2932, 2911, 2884, 2852, 2118, 2118, 1660, 1560 cm⁻¹; ¹H NMR (400 MHz, CD₃OD): $\delta = 4.50$ (d, *J* = 9.2 Hz, 1H, H-1), 3.89 (dd, *J* = 1.6, 12 Hz, 1H, H-6), 3.68 (m, 2H, H-6' & H-2), 3.45 (dd, *J* = 8.4, 10 Hz, 1H, H-4), 3.35 (m, 2H, H-3 & H-5), 1.98 (s, 3H, COCH₃); ¹³C NMR (100 MHz, CD₃OD): $\delta = 173.8, 90.2, 80.4, 75.8, 71.7, 62.6, 56.7, 22.9$; ESI-HRMS *m/z* calcd for C₈H₁₄N₄NaO₅: 269.0856 [M+Na]⁺, found: 269.0853.



GlcNAc – SubA click chemistry adduct (**220**)

The deprotected azido-monosaccharide **219** (1 mg, 3.8×10^{-6} mol) and the alkynyl-SubA **215** (2 mg, 5.7×10^{-7} mol) were mixed with 1 mL of *t*-butanol. Copper acetate (0.21 mg, 1.1×10^{-5} mol) and sodium L-ascorbate (0.45 mg, 2.3×10^{-5} mol) were mixed with 1 mL of water, resulting in a brown mixture. This brown mixture was added into the *t*-butanol solution, resulting in a light yellow mixture. The progress of the reaction was monitored by HPLC and MALDI-TOF-MS. The product was purified by HPLC with method: Analytical C8 column, flow rate 1.0 mL/min, detected at 220 nm. Gradient: Starting from 20% MeCN (0.1% TFA) and 80% water (0.1% TFA) for 5 min, ramping up to 80% MeCN over 28 min, keeping 80% MeCN for 5min, ramping down to 20% MeCN over 2 min, then keeping 20% MeCN for 5min. The product ($t_R = 27.0$ minutes) was analyzed by MALDI-TOF-MS m/z calcd for $C_{167}H_{249}N_{42}O_{50}S_3$: 3738.7 $[M+H]^+$, found 3738.9. The white solid material was obtained by lyophilization (0.4 mg, 20%).

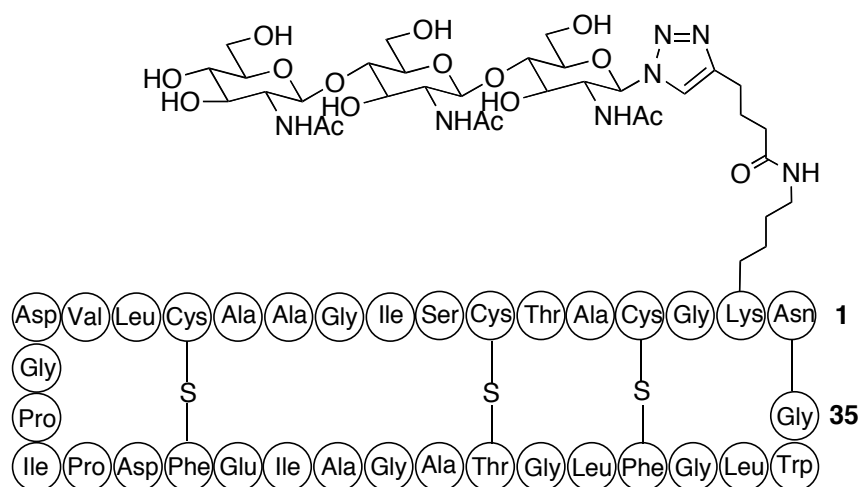
3.9 Click chemistry used in linking chitotriose to SubA



N-((2*S*,3*R*,5*S*,6*R*)-5-((2*S*,3*R*,4*R*,5*S*,6*R*)-3-Acetamido-4,5-dihydroxy-6-(hydroxymethyl)tetrahydro-2*H*-pyran-2-yloxy)-2-((2*R*,3*S*,5*R*,6*R*)-5-acetamido-6-azido-4-hydroxy-2-(hydroxymethyl)tetrahydro-2*H*-pyran-3-yloxy)-4-hydroxy-6-(hydroxymethyl)tetrahydro-2*H*-pyran-3-yl)acetamide (224)¹⁷⁷

Peracetylated chitotriose (0.1020 g, 0.1 mmol) was mixed with 4 mL of dry methanol. Sodium methoxide (1M, 1mL) was then added into the trisaccharide solution. The mixture turned clear after five minutes, and then turned cloudy again after another five minutes. The mixture was stirred for 20 hours at room temperature, followed by the addition of 10 mL of water, resulting in a clear solution once again. The solution was neutralized by adding Amberlite[®] IR120 acidic resin. The resin was removed by filtration, and the filtrate was then concentrated *in vacuo*. Water was removed by lyophilization, and the deprotected chitotriose was used without further purification. This chitotriose was then dissolved in 2 mL of D₂O. 2-Chloro-1,3-dimethylimidazolium chloride (0.1690 g, 1 mmol) and sodium azide (0.3250 g, 5 mmol) were then added to this sugar solution followed by addition of 2,6-lutidine (0.23 mL, 2 mmol). The mixture was stirred for 48 hours, followed by purification by column chromatography (silica gel, 20% MeOH/CHCl₃). The title compound was obtained as white solid (0.0420

g, 64%). $[\alpha]_D = -3.4$ (c 2.00, H_2O); IR (Microscope): 3700 – 3200 (br), 3390, 3299, 3280, 3100 (br), 2939, 2876, 2119, 2042, 1964, 1654, 1560 cm^{-1} ; 1H NMR (500 MHz, D_2O): $\delta = 4.85$ (d, $J = 9.0$ Hz, 1H, H-1), 4.67 (d, $J = 8.5$ Hz, 2H, H-1' & H-1''), 4.01 – 3.91 (m, 3H, H-6^a, H-6'^a & H-6''^a), 3.85 – 3.50 (m, 16H), 2.15 (s, 3H, $COCH_3$), 2.14 (s, 3H, $COCH_3$), 2.13 (s, 3H, $COCH_3$); ^{13}C NMR (125 MHz, D_2O): $\delta = 175.8, 175.6, 175.6, 165.0, 102.4, 102.1, 89.5, 80.1, 79.7, 77.5, 76.9, 75.5, 74.4, 73.2, 73.1, 70.7, 61.5, 61.0, 56.6, 56.0, 55.5, 46.0, 31.9, 23.2$; ESI-HRMS m/z calcd for $C_{24}H_{40}N_6NaO_{15}$: 675.2444 $[M+Na]^+$, found: 675.2437.



(GlcNAc)₃ – SubA click chemistry adduct (225)

The click chemistry was performed by mixing the azido-chitotriose (3 mg, 4.6×10^{-6} mol) and alkynyl-subtilosin A (3 mg, 8.6×10^{-7} mol). Copper acetate (0.62 mg, 3.4×10^{-5} mol) and sodium ascorbate (1.34 mg, 6.8×10^{-5} mol) were added as catalysts. The reaction was performed in a 1:1 mixture of *t*-butanol and water (4 mL). The progress of the reaction was monitored by HPLC and MALDI-TOF-MS. The product was purified by HPLC with the following method: Analytical C8

column, flow rate 1.0 mL/min, detected at 220 nm. Gradient: Starting from 20% MeCN (0.1% TFA) and 80% water (0.1% TFA) for 5 min, ramping up to 80% MeCN over 28 min, keeping 80% MeCN for 5min, ramping down to 20% MeCN over 2 min, then keeping 20% MeCN for 5min. The product ($t_R = 25.2$ minutes) was analyzed by MALDI-TOF-MS m/z calcd for $C_{182}H_{273}N_{44}O_{61}S_3$: 4146.9 $[M+H]^+$, found 4146.4. The white solid material was obtained by lyophilization (0.3 mg, 10%).

3.10 Linking benzenesulfonamides to SubA as CAII inhibitors

3.10.1 Purification of CAII

The plasmid pACA was obtained from the group of Dr. David W. Christianson in the Department of Chemistry at the University of Pennsylvania. The plasmid was transformed into *E. coli* BL21 (DE3) cells, which were plated on LB agar supplemented with ampicillin. After the cells were allowed to grow for 16 hours, a single colony was picked into 5 mL LB media with 0.6 mg/mL of ampicillin. The culture was incubated at 37 °C with shaking at 220 rpm for 16 hours. 1 L of 6×M9 minimal medium was prepared and autoclaved, which contained 20 g tryptone, 10 g yeast extract, 5 g NaCl, 2.2 g Na_2HPO_4 , 1.1 g KH_2PO_4 , 0.2 g NaCl, and 0.4 g NH_4Cl . After autoclaving 20 mL of 20% glucose, 200 μ L of 300 mM $ZnSO_4$, 2 mL of 50 mg/mL ampicillin, and 5 mL of the overnight bacterial culture were added into the 1 L medium. The culture was incubated at 37 °C with shaking at 260 rpm for 5.5 hours. At this point, the OD of the culture was measured to be 0.9 at 600 nm. The culture was induced with 1.5

mL ZnSO₄ (300 mM) and 2.5 mL isopropyl β-D-1-thiogalactopyranoside (IPTG, 100 mM) and was incubated at 30 °C with shaking at 260 rpm for three hours. 2 mL phenylmethanesulfonylfloride (PMSF, 4 mg/mL) was then added into the cell culture. After an additional three hours, the cells were harvested by centrifugation (20 minutes, 6000 xg). The cell pellets were then resuspended in 50 mL of lysis buffer, which contained 50 mM Tris-SO₄, pH 8.0, 50 mM NaCl, 10 mM EDTA, pH 8.0, 0.2 mM ZnSO₄, 1 mM dithiothreitol (DTT), 10 μg/mL PMSF, 1 mM benzamidine, and one tablet of Complete Protease Inhibitor Cocktail Tablets from Roche Applied Science. The cells were lysed with a cell disruptor, and the mixture was centrifuged at 14,000 rpm for 45 minutes. The supernatant was collected, and 8 mL of 10% (w/v) streptomycin-SO₄ was added to the stirred solution in four aliquots over 15 minutes to precipitate nucleic acids. The precipitate was removed by centrifugation at 10,000 rpm for 30 minutes. The supernatant was dialyzed against 4 L 10 mM Tris-SO₄ buffer, supplemented with 0.1 mM ZnSO₄ and 1 mM DTT for 16 hours.

The supernatant was then passed through DEAE Sephacel[™] (GE Healthcare) for anion exchange chromatography. Approximately 100 mL of resin was equilibrated with 2×100 mL Tris-SO₄, pH 8.0 (0.5 – 1.0 M), followed by rinsing with 5×100 mL equilibration buffer (10 mM Tris-SO₄, 0.1 mM ZnSO₄, and 1 mM DTT). The protein solution was then centrifuged, and the supernatant was loaded onto the DEAE Sephacel[™] resin, and shaken for 30 minutes. The mixture was filtered and the resin was washed with 100 mL of equilibration

buffer. The filtrates were combined and dialyzed against 4 L of 10 mM 2-(*N*-morpholino)ethanesulfonic acid (MES), pH 7.0 and 1 mM DTT.

A cation exchange resin, SP Sepharose Fast Flow, from GE Healthcare was then used to further purify the enzyme. Approximately 7 mL of resin was used to prepare a column. The resin was washed with 35 mL water, 35 mL buffer A (10 mM MES, pH 7.0, and 1 mM DTT), and 35 mL buffer B (10 mM MES, 1 mM DTT, and 0.5 M (NH₄)₂SO₄). The resin was then washed again with 35 mL buffer A before loading the protein. After the protein was loaded, the resin was washed with 70 mL of buffer A. The protein was eluted with a 70 mL gradient ranging from 0 – 100% of buffer B. The elution was monitored by UV absorption at 280 nm, and the trace is shown in **Figure 3-1**. Both fractions (peak 1: $t_R = 20 - 30$ min; peak 2: $t_R = 30 - 40$ min) were collected and separately dialyzed against 2 L of 50 mM Tris-SO₄, pH 8.0 for 16 hours.

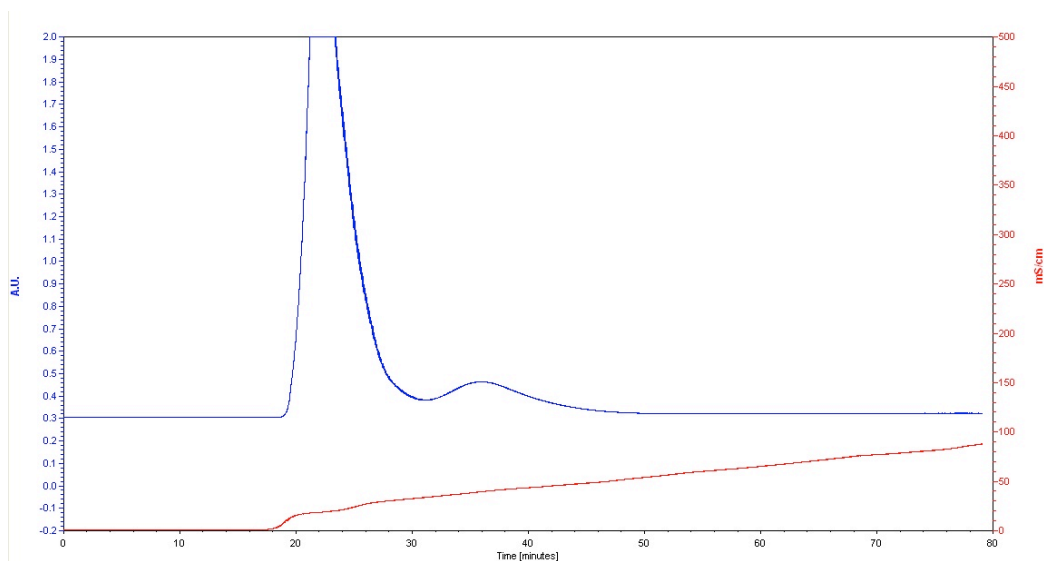


Figure 3-1. Purification of CAII using SP Sepharose Fast Flow resin

The purity of CAII was examined by SDS-PAGE, as shown in **Figure 3-2**. From right to left, lane 1: standard molecular weight markers, lane 2: prior to induction with IPTG, lane 3: three hours after the induction, lane 4: prior to harvesting cells, lane 5: supernatant after cell disruption, lane 6: following removal of nucleic acids, lane 7: following the first dialysis, lane 8: following the anion exchange column, lane 9: peak 1 from the cation exchange column (retention time: 20 – 30 minutes), lane 10: peak 2 from the cation exchange column (retention time: 30 – 40 minutes).

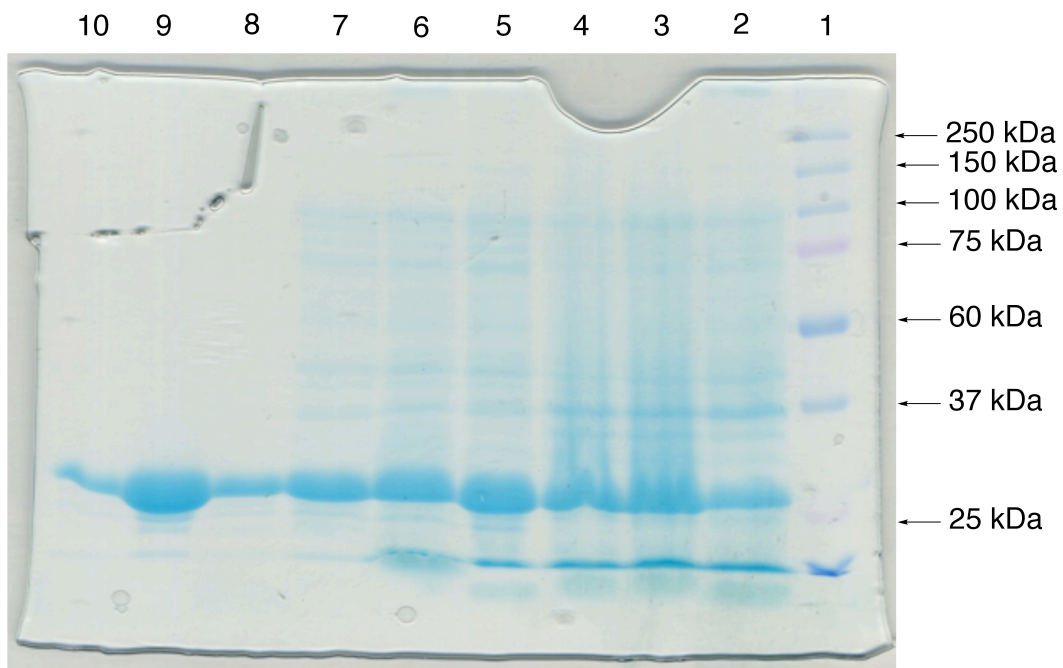


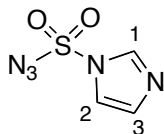
Figure 3-2. SDS-PAGE gel showing the CAII purification. From right to left, lane 1 to lane 10

Finally the enzyme solution was concentrated to 3.36 mg/mL, calculated using a molar absorptivity of $\epsilon^{280} = 54,000 \text{ L/mol/cm}$ at 280 nm.

3.10.2 Inhibitor testing against CAII

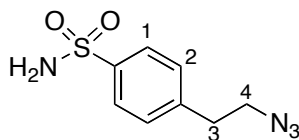
The inhibitor testing was done using a *p*-nitrophenol acetate assay modified from the literature.¹⁸³ A buffer of 20 mM Tris-SO₄, pH 8.3 was used in this assay. The substrate stock solution was 5×10⁻³ M of *p*-nitrophenol acetate in DMSO. The CAII stock was diluted to 0.336 mg/mL (1.12×10⁻⁵ M). Inhibitor stocks were prepared at various concentrations in DMSO. In a 1 mL assay cuvette, 780 μL assay buffer, 10 μL substrate stock solution (or DMSO for the negative control), and 10 μL inhibitor stock solution (or DMSO for the positive control) were added. Then, 200 μL of the CAII stock solution was added, and the change in absorbance at 400 nm was monitored using a Varian Cary 100 Bio UV-Visible spectrophotometer. The data were then analyzed using Microsoft Excel®. The initial rate of increase of the absorbance is proportional to the rate of reaction. By comparing the initial slope of each absorbance curve of the inhibitor assay cell to the control cell, the percentage inhibition was determined and the IC₅₀ value was calculated based on these data according to the method described in section 3.4.

3.10.3 Benzenesulfonamide derivatives – SubA linkage



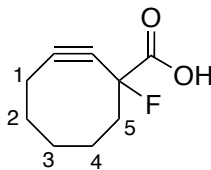
Imidazole-1-sulfonyl azide (226)¹⁷⁸

(**Attention: explosive and small scale only**) Sulfuryl chloride (0.4 mL, 5.0 mmol) was added drop-wise to an ice-cold mixture of sodium azide (0.320 g, 5.0 mmol) in MeCN (5 mL) and the resulting mixture was stirred for 15 hours at room temperature. Imidazole (0.681 g, 10 mmol) was then added to the ice-cold mixture, and the mixture was then stirred for 3 hours at room temperature. The mixture was diluted with EtOAc (10 mL) and water (10 mL). The organic layer was separated and washed with water (10 mL), saturated aqueous sodium bicarbonate (2 × 15 mL), brine (10 mL), dried over anhydrous sodium sulfate and filtered. The filtrate was concentrated and purified by flash column chromatography (silica gel, EtOAc/diethyl ether = 1:3) to give the title compound as a colourless liquid (0.560 g, 65%). IR (Film): 3116, 2170, 1599 cm^{-1} ; ^1H NMR (500 MHz, CDCl_3): δ = 8.02 (dd, J = 1.0, 1.4 Hz, 1H, H-1), 7.41 (dd, J = 1.4, 1.7 Hz, 1H, H-2), 7.23 (dd, J = 1.0, 1.7 Hz, 1H, H-3); ^{13}C NMR (125 MHz, CDCl_3): δ = 117.2, 131.4, 136.2; EI-HRMS m/z calcd for $\text{C}_3\text{H}_3\text{N}_5\text{O}_2\text{S}$: 173.0010 $[\text{M}]^+$, found: 173.0015.



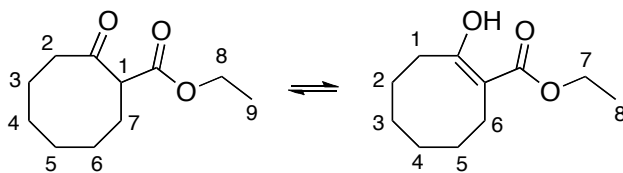
4-(2-Azidoethyl)benzenesulfonamide (**227**)¹³³

Imidazole-1-sulfonyl azide **226** (0.207 g, 1.2 mmol), 4-(2-aminoethyl)benzenesulfonamide (0.203 g, 1.0 mmol), potassium carbonate sesquihydrate (0.248 g, 1.5 mmol), and copper sulfate pentahydrate (2.5 mg, 10 μ mol) were mixed with methanol (5 mL), and the reaction was stirred for 15 hours at room temperature. The solvent was then removed *in vacuo*. The residue was diluted with 15 mL of water, and acidified with 1 M HCl. The mixture was then extracted with EtOAc (3 \times 15 mL). The combined organic layer was washed with water (15 mL), brine (15 mL), dried over anhydrous sodium sulfate, and filtered. The filtrate was then concentrated and purified by flash column chromatography (silica gel, EtOAc/hexanes = 2:1) to give the title compound as a white solid (0.155 g, 69%). IR (solid): 3357, 3259, 3116, 2158, 2115, 1599, 1568 cm^{-1} ; ^1H NMR (500 MHz, CDCl_3): δ = 7.89 (d, J = 8.5 Hz, 2H, H-1), 7.38 (d, J = 8.5 Hz, 2H, H-2), 4.88 (br, 2H, NH), 3.56 (t, J = 7 Hz, 2H, H₂-3), 2.96 (t, J = 7 Hz, 2H, H₂-4); ^{13}C NMR (125 MHz, CDCl_3): δ = 143.6, 140.5, 129.6, 126.9, 51.9, 35.2; EI-HRMS m/z calcd for $\text{C}_8\text{H}_{10}\text{N}_4\text{NaO}_2\text{S}$: 249.0417 $[\text{M}+\text{Na}]^+$, found: 249.0413.



1-Fluorocyclooct-2-ynecarboxylic acid (231)¹⁸¹

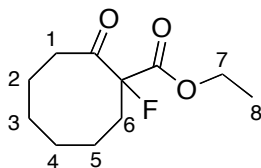
Ethyl 1-fluorocyclooct-2-ynecarboxylate **238** (0.32 g, 1.88 mmol) was mixed with 5 mL 50% aqueous methanol and lithium hydroxide monohydrate (0.158 g, 3.76 mmol) was added into the mixture. The mixture was then heated to 50 °C to dissolve the solid. The mixture was then cooled to room temperature and stirred for an additional two hours. The reaction was cooled to 0 °C and diluted with water (5 mL). The mixture was acidified to pH 2 with 2 M HCl. The mixture was extracted with EtOAc (3 × 20 mL). The combined organic layers were washed with water (20 mL), brine (20 mL), dried over anhydrous sodium sulfate, and filtered. The solvent was then removed *in vacuo* to give the titled compound as a pale yellow liquid (0.3105 g, 97%). IR (Neat): 3500 – 2600, 2933, 2857, 2227, 1733, 1451 cm⁻¹; ¹H NMR (500 MHz, CDCl₃): δ = 10.19 (br, 1H, COOH), 2.49 – 2.30 (m, 4H, H-1 & H-5), 2.12 – 1.88 (m, 4H, H-2 & H-4), 1.80 – 1.72 (m, 1H, H-3a), 1.55 – 1.47 (m, 1H, H-3b); ¹³C NMR (125 MHz, CDCl₃): δ = 173.4 (d, J^2_{C-F} = 29.0 Hz), 109.4 (d, J^3_{C-F} = 10.0 Hz), 91.5 (d, J_{C-F} = 185.9 Hz), 86.1 (d, J^2_{C-F} = 31.5 Hz), 46.3 (d, J^2_{C-F} = 24.9 Hz), 33.8, 29.0, 25.5, 20.5; ESI-HRMS *m/z* calcd for C₉H₁₁FNaO₂: 193.0635 [M+Na]⁺, found: 193.0637.



Ethyl 2-oxocyclooctanecarboxylate and (*Z*)-ethyl 2-hydroxycyclooct-1-enecarboxylate (234 and 235)²⁰²

Sodium hydride (60% in mineral oil, 3.4 g, 85 mmol) and diethyl carbonate (7.26 mL, 60 mmol) were mixed with benzene (40 mL). The mixture was heated to reflux, and a solution of cyclooctanone (3.95 mL, 30 mmol) in benzene (10 mL) was added drop-wise using an additional funnel over the course of three hours. After addition, the mixture was cooled to room temperature and glacial acetic acid (6 mL) was added drop-wise. Ice-cold water (20 mL) was added drop-wise until all solids went into solution. The benzene layer was separated, and the aqueous layer was extracted with benzene (3 × 10 mL). The combined benzene layer was washed with ice-cold water (3 × 10 mL), brine (10 mL), dried over anhydrous sodium sulfate, and filtered. The filtrate was concentrated and purified by column chromatography (silica gel, EtOAc/hexanes = 1:10) to give the title compound as a colourless liquid (5.55 g, 93%). IR (Neat): 2980, 2927, 2856, 1747, 1708, 1644, 1613 cm⁻¹; **Ethyl 2-oxocyclooctanecarboxylate (234)**: ¹H NMR (400 MHz, CDCl₃): δ = 4.14 (q, *J* = 7.2 Hz, 2H, H-8), 3.56 (dd, *J* = 4.4, 11.2 Hz, 1H, H-1), 2.61 (m, 1H, H-2a), 2.47 (m, 1H, H-2b), 2.19 – 2.04 (m, 2H, H-7), 1.96 – 1.83 (m, 2H, H-3), 1.75 – 1.35 (m, 6H, H-4, H-5 & H-6), 1.23 (t, *J* = 7.2 Hz, 3H, H-9); ¹³C NMR (125 MHz, CDCl₃): δ = 212.2, 170.1, 61.1, 57.1, 41.6, 28.9, 27.0, 25.5, 25.3, 24.5, 14.0; **(*Z*)-ethyl 2-hydroxycyclooct-1-enecarboxylate (235)**: ¹H NMR

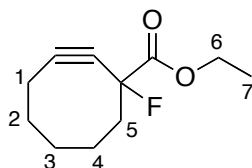
(400 MHz, CDCl₃): δ = 4.21 (q, J = 7.2 Hz, 2H, H-7), 2.39 (m, 2H, H-1), 2.35 (m, 2H, H-6), 1.75 – 1.35 (m, 10H, H-2, H-3, H-4 & H-5), 1.30 (t, J = 7.2 Hz, 3H, H-8); ¹³C NMR (125 MHz, CDCl₃): δ = 176.0, 172.9, 99.2, 60.1, 32.3, 29.9, 28.7, 26.5, 26.0, 23.9, 14.3; ESI-HRMS m/z calcd for C₁₁H₁₈NaO₃: 221.1148 [M+Na]⁺, found: 221.1148.



Ethyl 1-fluoro-2-oxocyclooctanecarboxylate (237)¹⁸¹

Ethyl 2-oxocyclooctanecarboxylate **234** and its tautomer **235** (1.98 g, 10 mmol) was dissolved in dry MeCN (25 mL) and cooled to 0 °C. Selectfluor (4.25 g, 12 mmol) was then added into the solution. The mixture was heated to 55 °C and stirred for 8 hours. After cooling to room temperature, the reaction was quenched with water (20 mL). Following the removal of MeCN under reduced pressure, the residue was extracted with EtOAc (4 × 20 mL). The combined organic layer was washed with water (20 mL), brine (20 mL), dried over anhydrous sodium sulfate, and filtered. The filtrate was concentrated to yield a clear oil which was then dissolved in small amount of CH₂Cl₂ and filtered through a plug of silica gel to give the title compound as clear liquid (2.052 g, 95%). IR (Neat): 2983, 2935, 2862, 1760, 1725 cm⁻¹; ¹H NMR (500 MHz, CDCl₃): δ = 4.26 (q, J = 7.2 Hz, 2H, H-7), 2.74 (ddt, J = 1.0, 4.0, 12.5 Hz, 1H, H-1a), 2.70 – 2.52 (m, 2H, H-1b & H-6a), 2.26 (dddd, J = 3.5, 4.5, 8.0, 16 Hz, 1H, H-6b), 2.06 – 1.96 (m, 1H, H-5a), 1.92 – 1.85 (m, 1H, H-5b), 1.80 – 1.68 (m, 2H, H-2), 1.68 – 1.59 (m, 1H, H-3a),

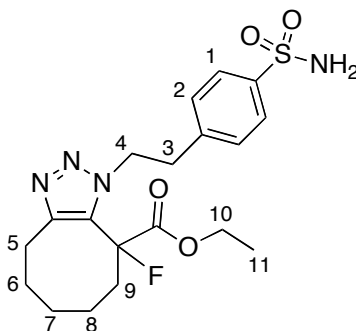
1.55 – 1.36 (m, 3H, H-3b & H-4), 1.31 (t, $J = 7.2$ Hz, 3H, H-8); ^{13}C NMR (125 MHz, CDCl_3): $\delta = 208.7$ (d, $J^2_{\text{C-F}} = 21.6$ Hz), 167.0 (d, $J^2_{\text{C-F}} = 24.7$ Hz), 99.1 (d, $J_{\text{C-F}} = 199.9$ Hz), 62.5, 38.8, 33.3 (d, $J^2_{\text{C-F}} = 22.1$ Hz), 27.5 (d, $J^3_{\text{C-F}} = 2.0$ Hz), 26.5, 24.4, 21.3 (d, $J^3_{\text{C-F}} = 1.4$ Hz), 13.9; ESI-HRMS m/z calcd for $\text{C}_{11}\text{H}_{18}\text{FO}_3$: 217.1234 $[\text{M}+\text{H}]^+$, found: 217.1233.



Ethyl 1-fluorocyclooct-2-ynecarboxylate (238)¹⁸¹

Ethyl 1-fluoro-2-oxocyclooctanecarboxylate **237** (2.12 g, 9.8 mmol) was dissolved in dry THF (125 mL) and stirred at -78 °C. KHMDS (0.5 M, 45 mL) was then added dropwise into the reaction mixture. The reaction mixture was stirred for 30 minutes before the *N*-phenyl-bis(trifluoromethanesulfonimide) (3.90 g, 10.9 mmol) in dry THF (25 mL) was slowly added to the reaction mixture *via* syringe. The reaction was stirred for one additional hour at -78 °C, and was then allowed to warm to room temperature. The reaction mixture was then stirred an additional five hours at room temperature. After quenching the reaction with ethanol, the mixture was concentrated *in vacuo*. The resulting dark red residue was washed with hexanes and filtered. The sticky residue was removed, and the filtrate was concentrated and purified by column chromatography (silica gel, 3% EtOAc in hexanes) to give the title compound as a light red liquid (1.025 g, 48%). IR (Neat): 2930, 2855, 1755 cm^{-1} ; ^1H NMR (500 MHz, CDCl_3): $\delta = 4.28$ (dq, $J = 2.0, 7.0$ Hz, 2H, H-6), 2.41 – 2.23 (m, 4H, H-1 & H-5), 2.04 – 1.85 (m, 4H, H-2 &

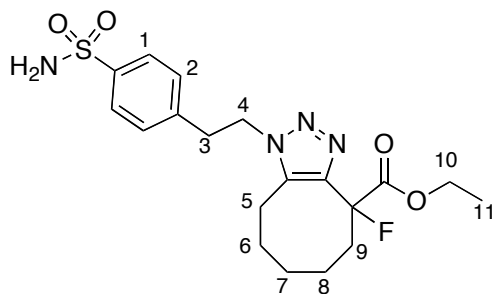
H-4), 1.76 – 1.68 (m, 1H, H-3a), 1.49 – 1.42 (m, 1H, H-3b), 1.33 (t, $J = 7.0$ Hz, 3H, H-7); ^{13}C NMR (125 MHz, CDCl_3): $\delta = 168.7$ (d, $J_{\text{C-F}} = 28.6$ Hz), 108.5 (d, $J_{\text{C-F}} = 10.1$ Hz), 91.8 (d, $J_{\text{C-F}} = 185.6$ Hz), 86.8 (d, $J_{\text{C-F}} = 31.7$ Hz), 62.3, 46.2 (d, $J_{\text{C-F}} = 24.8$ Hz), 33.8, 29.1, 25.4, 20.5, 14.0; ESI-HRMS m/z calcd for $\text{C}_{11}\text{H}_{16}\text{FO}_2$: 199.1128 $[\text{M}+\text{H}]^+$, found: 199.1124.



**Ethyl 9-fluoro-1-(4-sulfamoylphenethyl)-4,5,6,7,8,9-hexahydro-1H-cycloocta-
[d][1,2,3]triazole-9-carboxylate (239)**

4-(2-Azidoethyl)benzenesulfonamide **227** (100 mg, 4.4×10^{-4} mol) and ethyl 1-fluorocyclooct-2-ynecarboxylate (70 mg, 3.5×10^{-4} mol) were mixed in ethanol (3 mL). The resulting mixture was stirred for 5 hours at room temperature, after which the solvent was removed *in vacuo*. The resulting residue was purified by column chromatography (silica gel, EtOAc/hexanes = 1:1) to yield both title compound as white solid and its regioisomer **240** as a colourless liquid (47.5 mg + 55.1 mg, 70%). IR (Microscope): 3250 (br), 3100, 2954, 2931, 2866, 1763, 1598, 1560 cm^{-1} ; ^1H NMR (500 MHz, CD_3OD): $\delta = 7.80$ (d, $J = 8.5$ Hz, 2H, H-1), 7.32 (d, $J = 8.5$ Hz, 2H, H-2), 4.55 (dddd, $J = 7.0, 8.5, 14.0, 41.5$ Hz, 2H, H-4), 4.17 (qdd, $J = 7.5, 11.0, 54.5$ Hz, 2H, H-10), 3.31 (m, 2H, H-3), 3.11 (ddd, $J = 4.5, 6.5, 15.0$ Hz, 1H, H-5a), 2.91 (m, 1H, H-5b), 2.59 (m, 1H, H-9a), 2.41 (m, 1H, H-9b),

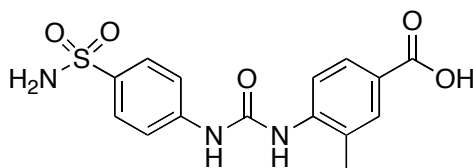
1.85 (m, 1H, H-6a), 1.72 (m, 2H, H-8), 1.58 (m, 1H, H-6b), 1.47 (m, 1H, H-7a), 1.32 (m, 1H, H-7b), 1.17 (t, $J = 7.5$ Hz, 3H, H-11); ^{13}C NMR (125 MHz, CD_3OD): $\delta = 170.2$ (d, $J^2_{\text{C-F}} = 29.1$ Hz), 146.4, 143.5 (d, $J^2_{\text{C-F}} = 40.0$ Hz), 132.2 (d, $J^3_{\text{C-F}} = 23.5$ Hz), 130.6, 127.4, 91.8 (d, $J_{\text{C-F}} = 185.1$ Hz), 64.2, 51.6 (d, $J^3_{\text{C-F}} = 4.1$ Hz), 36.7, 34.6 (d, $J^2_{\text{C-F}} = 22.1$ Hz), 27.4, 25.6, 24.5, 23.4 (d, $J^3_{\text{C-F}} = 3.9$ Hz), 14.2; ESI-HRMS m/z calcd for $\text{C}_{19}\text{H}_{26}\text{FN}_4\text{O}_4\text{S}$: 425.1653 $[\text{M}+\text{H}]^+$, found: 425.1656. The structure was confirmed by X-ray crystallographic studies, a report is included in Appendix.



Ethyl 4-fluoro-1-(4-sulfamoylphenethyl)-4,5,6,7,8,9-hexahydro-1H-cycloocta-[d][1,2,3]triazole-4-carboxylate (240)

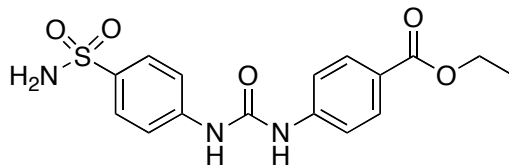
Colourless liquid. IR (Microscope): 3248 (br), 3100, 2949, 2928, 2865, 1760, 1595, 1560 cm^{-1} ; ^1H NMR (500 MHz, CDCl_3): $\delta = 7.78$ (d, $J = 8.5$ Hz, 2H, H-1), 7.15 (d, $J = 8.5$ Hz, 2H, H-2), 4.48 (t, $J = 7.0$ Hz, 2H, H-4), 4.27 (qdd, $J = 7.0$, 10.5, 25.0 Hz, 2H, H-10), 3.28 (t, $J = 7.0$ Hz, 2H, H-3), 2.80 (m, 1H, H-5a), 2.67 (m, 1H, H-5b), 2.33 (m, 2H, H-9), 1.79 (m, 1H, H-8a), 1.61 (m, 1H, H-8b), 1.54 – 1.30 (m, 4H, H-6 & H-7), 1.26 (t, $J = 7.5$ Hz, 3H, H-11); ^{13}C NMR (125 MHz, CDCl_3): $\delta = 170.0$ (d, $J^2_{\text{C-F}} = 27.9$ Hz), 142.2 (d, $J^2_{\text{C-F}} = 25.0$ Hz), 142.1, 141.2, 134.6 (d, $J^3_{\text{C-F}} = 3.1$ Hz), 129.5, 126.8, 91.9 (d, $J_{\text{C-F}} = 185.4$ Hz), 62.2, 48.3, 36.3,

34.0 (d, $J^2_{C-F} = 23.5$ Hz), 25.8, 23.4, 21.7 (d, $J^3_{C-F} = 3.9$ Hz), 20.8, 14.1; ESI-HRMS m/z calcd for $C_{19}H_{25}FN_4NaO_4S$: 447.1473 $[M+Na]^+$, found: 447.1470.



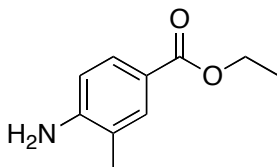
3-methyl-4-(3-(4-sulfamoylphenyl)ureido)benzoic acid (243)

The ethyl ester **250** (68.3 mg, 1.8×10^{-4} mol) was mixed with 50% aqueous methanol (1.2 mL). Lithium hydroxide monohydrate (16.6 mg, 4×10^{-4} mol) was added into the mixture. The mixture was then heated to 50 °C to assist the dissolution of the solid. The mixture was then cooled to room temperature and stirred for an additional two hours. The reaction was cooled to 0 °C and diluted with water (5 mL). The mixture was acidified to pH 2 with 2 M HCl. The title compound then precipitated out and was collected via filtration as a white solid (62.3 mg, 99%). IR (Film): 3500 – 2700, 3377, 3277, 3065, 2981, 1722, 1680, 1611, 1588 cm^{-1} ; 1H NMR (500 MHz, DMSO- d_6): $\delta = 9.63$ (br, 1H, CONH), 8.28 (br, 1H, CONH), 8.11 (d, $J = 8.5$ Hz, 1H, Ph-H), 7.75 (m, 4H, Ph-H), 7.62 (d, $J = 9.5$ Hz, 2H, Ph-H), 7.20 (br, 2H, SO₂NH₂), 2.30 (s, 3H, CH₃); ^{13}C NMR (125 MHz, DMSO- d_6): $\delta = 170.7, 167.1, 152.0, 142.5, 141.5, 137.1, 131.4, 127.9, 126.9, 126.2, 118.9, 117.5, 17.8$; ESI-HRMS m/z calcd for $C_{17}H_{15}F_3N_3O_7S$: 462.0588 $[M+CF_3CO_2]^-$, found: 462.0587.



Ethyl 4-(3-(4-sulfamoylphenyl)ureido)benzoate (246)^{185, 203}

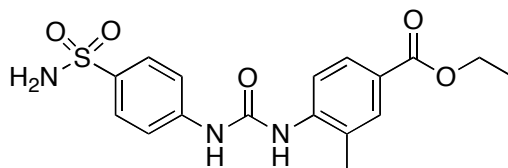
4-Aminobenzenesulfonamide (0.2311 g, 1.3×10^{-3} mol) and ethyl 4-isocyanatobenzoate (0.2561 g, 1.3×10^{-3} mol) were mixed in MeCN (15 mL) and stirred for 16 hours at room temperature. A white precipitate was formed, which was filtered under suction and washed with diethyl ether (15 mL). The titled compound was obtained as white solid (0.406 g, 83%). IR (Film): 3375, 3352, 3331, 3307, 3214, 3074, 2980, 1701, 1594, 1537 cm^{-1} ; ^1H NMR (500 MHz, DMSO- d_6): δ = 9.20 (br, 2H, NHCONH), 7.89 (d, J = 9.0 Hz, 2H, Ph-H), 7.73 (d, J = 9 Hz, 2H, Ph-H), 7.60 (m, 4H, Ph-H), 7.20 (br, 2H, SO_2NH_2), 4.27 (q, J = 7.0 Hz, 2H, OCH_2), 1.30 (t, J = 7.0 Hz, 3H, CH_2CH_3); ^{13}C NMR (125 MHz, DMSO- d_6): δ = 165.3, 151.9, 143.9, 142.4, 137.2, 130.3, 126.8, 123.1, 117.7, 117.5, 60.3, 14.2; ESI-HRMS m/z calcd for $\text{C}_{16}\text{H}_{17}\text{N}_3\text{NaO}_5\text{S}$: 386.0781 $[\text{M}+\text{Na}]^+$, found: 386.0784.



Ethyl 4-amino-3-methylbenzoate (248)²⁰⁴

Acetyl chloride (1.78 mL) was added slowly to ice-cold ethanol (15 mL) in an ice-bath. The mixture was then added into a 4-amino-3-methylbenzoic acid

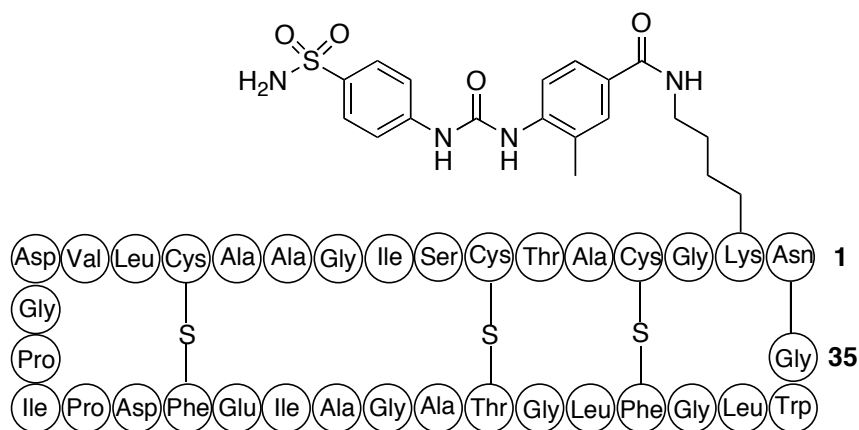
solution in ethanol (15 mL). The mixture was refluxed for two days, after which this dark red mixture was cooled to room temperature. The ethanol was removed *in vacuo*, and the residue was mixed with EtOAc (90 mL). The mixture was then washed with aqueous saturated sodium bicarbonate (70 mL). The separated aqueous layer was extracted one additional time with EtOAc (60 mL). The combined organic layer was then washed with water (60 mL), brine (60 mL), dried over anhydrous sodium sulfate, and filtered. After the solvent was removed, the title compound was obtained as a red solid (1.72 g, 96%). IR (Film): 3479, 3374, 3243, 2980, 2934, 2904, 1693, 1628, 1607, 1579 cm^{-1} ; ^1H NMR (500 MHz, CDCl_3): δ = 7.75 (m, 2H, Ph-H), 6.64 (d, J = 8.0 Hz, 1H, Ph-H), 4.32 (q, J = 7.3 Hz, 2H, OCH_2), 3.98 (br, 2H, NH_2), 2.18 (s, 3H, Ph- CH_3), 1.36 (t, J = 7.3 Hz, 3H, CH_2CH_3); ^{13}C NMR (125 MHz, $\text{DMSO}-d_6$): δ = 166.9, 149.0, 132.2, 129.3, 121.0, 120.1, 113.7, 60.3, 17.2, 14.5; ESI-HRMS m/z calcd for $\text{C}_{10}\text{H}_{13}\text{NNaO}_2$: 202.0838 $[\text{M}+\text{Na}]^+$, found: 202.0841.



Ethyl 3-methyl-4-(3-(4-sulfamoylphenyl)ureido)benzoate (250)^{185, 203, 205}

Ethyl 4-amino-3-methylbenzoate **248** (0.1790 g, 1.0 mmol) and triphosgene (0.2961 g, 1 mmol) were mixed in CH_2Cl_2 (6 mL). A solution of sodium bicarbonate (0.21 g, 2.5 mmol) in water (6 mL) was then added into the ethyl ester solution. The mixture was stirred for 30 minutes, and then poured into water

(5 mL). The separated aqueous layer was extracted with CH_2Cl_2 (2×10 mL). The combined organic layer was then washed with brine (10 mL), dried over anhydrous sodium sulfate, and filtered. After removal of the solvent, the isocyanate was obtained and used without any further purification. The obtained isocyanate was then mixed with 4-aminobenzenesulfonamide (0.1721 g, 1 mmol) in MeCN (10 mL), and stirred for 16 hours at room temperature. A white precipitate was formed, which was filtered under suction and washed with diethyl ether (15 mL). The title compound was obtained as a white solid (0.3167 g, 84%). IR (Film): 3384, 3349, 3217, 2994, 1700, 1681, 1594, 1546 cm^{-1} ; ^1H NMR (500 MHz, $\text{DMSO-}d_6$): δ = 9.59 (br, 1H, CONH), 8.27 (br, 1H, CONH), 8.15 (d, J = 8.5 Hz, 1H, Ph-H), 7.75 (m, 4H, Ph-H), 7.62 (d, J = 8.5 Hz, 2H, Ph-H), 7.21 (br, 2H, SO_2NH_2), 4.27 (q, J = 7.0 Hz, 2H, OCH_2), 2.31 (s, 3H, Ph- CH_3), 1.30 (t, J = 7.0 Hz, 3H, CH_2CH_3); ^{13}C NMR (125 MHz, $\text{DMSO-}d_6$): δ = 165.5, 151.9, 142.4, 141.9, 137.2, 131.2, 127.8, 126.9, 126.3, 123.3, 118.8, 117.5, 60.3, 17.8, 14.2; ESI-HRMS m/z calcd for $\text{C}_{17}\text{H}_{19}\text{N}_3\text{NaO}_5\text{S}$: 400.0938 $[\text{M}+\text{Na}]^+$, found: 400.0934.



Ureido-containing sulfonamide 243– SubA coupling adduct (251)

3-Methyl-4-(3-(4-sulfamoylphenyl)ureido)benzoic acid (7 mg, 2×10^{-5} mol), PyBop (7.8 mg, 1.5×10^{-5} mol), and HOBt (2.1 mg, 1.5×10^{-5} mol) were dissolved in DMF (1 mL), to which was added triethylamine (2.1 μ L, 1.5×10^{-5} mol). The mixture was then stirred for one hour. 250 μ L of the mixture was added to mixture of SubA (1 mg, 3×10^{-7} mol) in an aqueous buffer (20 mM tris-SO₄ pH 8, 50 μ L). The mixture was left on an orbital shaker at 1500 rpm for 16 hours before being quenched with 2 M HCl. The title compound was purified by HPLC, method: Analytical C8 column, flow rate 1.0 mL/min, detected at 220 nm. Gradient: Starting from 5% MeCN (0.1% TFA) and 95% water (0.1% TFA) for 5 min, ramping up to 50% MeCN over 10 min, ramping up to 95% MeCN over other 9 min, keeping 95% MeCN for 4 min, ramping down to 5% MeCN over 3 min, then keeping 5% MeCN for 2min. The product ($t_R = 21.9$ minutes) was analyzed by MALDI-TOF-MS m/z calcd for C₁₆₇H₂₃₉N₄₁NaO₄₉S₄: 3753.6 [M+Na]⁺, found 3753.7. The title compound was obtained as a white solid after lyophilization (0.5 mg, 50%).

Appendix: X-ray crystal structure of compound 239

XCL Code: JCV1101

Date: 5 May 2011

Compound: ethyl 9-fluoro-1-{2-(4-sulfamoylphenyl)ethyl-4,5,6,7,8,9-hexahydro-1*H*-cycloocta[*d*][1,2,3]triazole-9-carboxylate

Formula: C₁₉H₂₅FN₄O₄S

Supervisor: J. C. Vederas
Ferguson

Crystallographer: M. J.

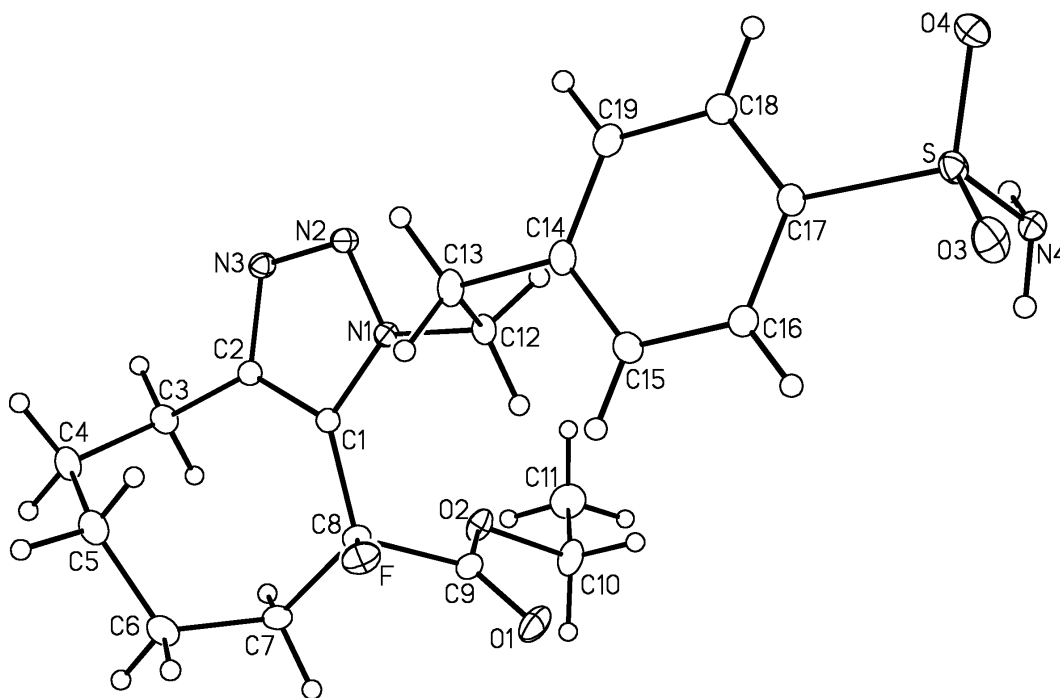
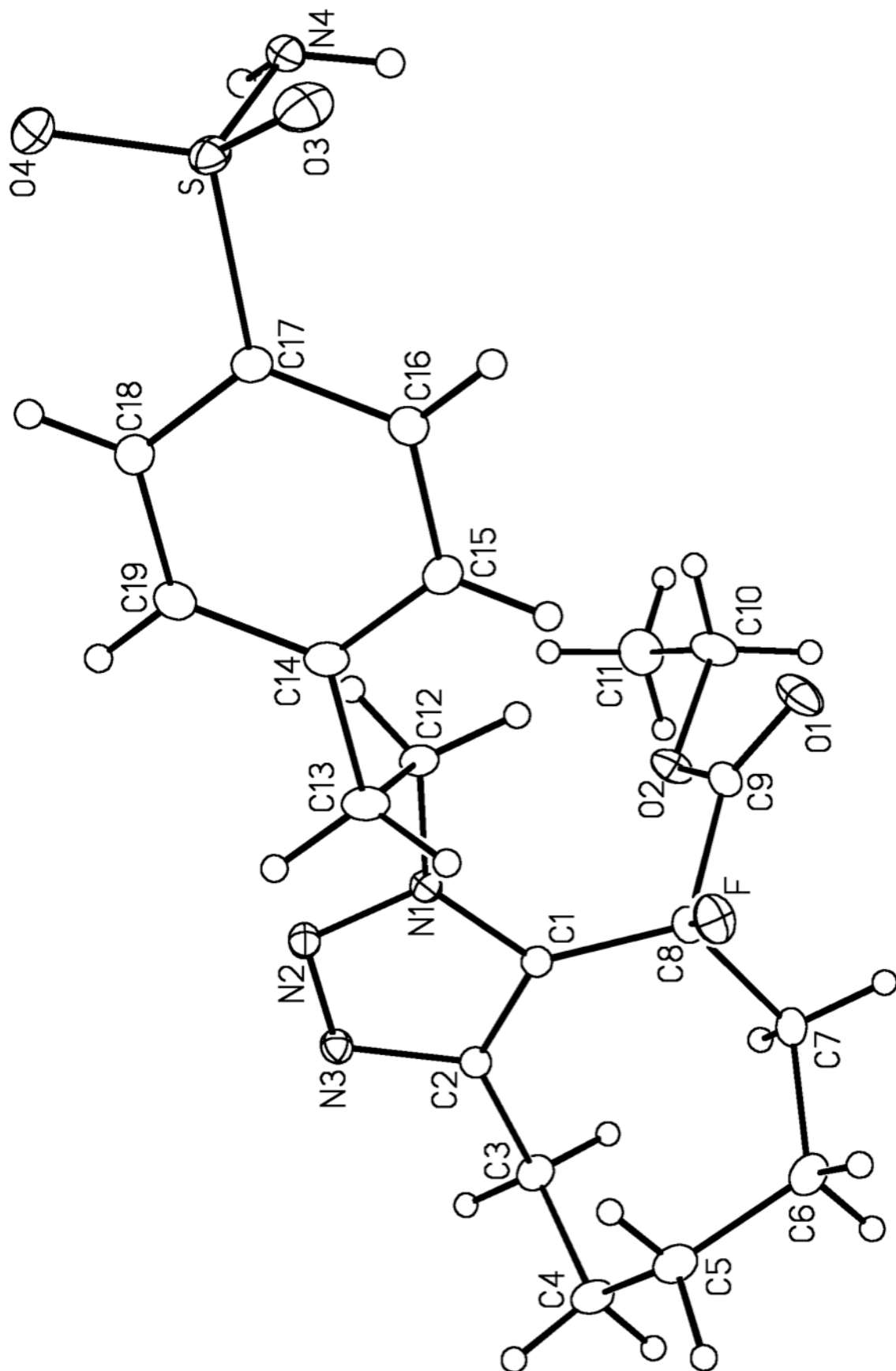
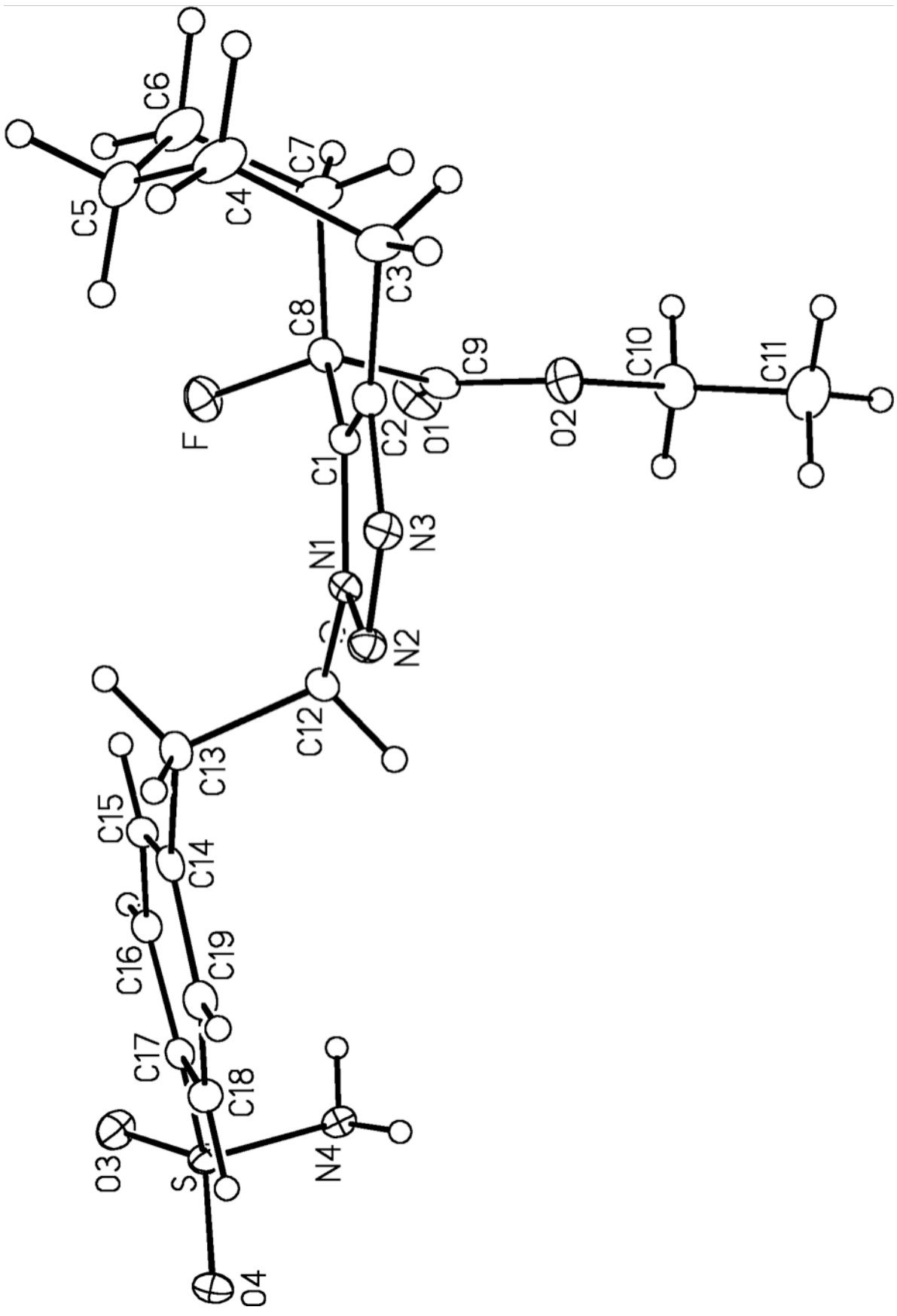


Figure Legends

Figure I. Perspective view of the ethyl 9-fluoro-1-{2-(4-sulfamoylphenyl)ethyl}-4,5,6,7,8,9-hexahydro-1*H*-cycloocta[*d*][1,2,3]triazole-9-carboxylate molecule showing the atom labelling scheme. Non-hydrogen atoms are represented by Gaussian ellipsoids at the 20% probability level. Hydrogen atoms are shown with arbitrarily small thermal parameters.

Figure II. Alternate view of the molecule.





List of Tables

Table I. Crystallographic Experimental Details

Table II. Atomic Coordinates and Equivalent Isotropic Displacement Parameters

Table III. Selected Interatomic Distances

Table IV. Selected Interatomic Angles

Table V. Torsional Angles

Table VI. Hydrogen-Bonded Interactions

Table VII. Anisotropic Displacement Parameters

Table VIII. Derived Atomic Coordinates and Displacement Parameters for Hydrogen Atoms

Table I. Crystallographic Experimental Details*A. Crystal Data*

formula	C ₁₉ H ₂₅ FN ₄ O ₄ S
formula weight	424.49
crystal dimensions (mm)	0.61 × 0.18 × 0.15
crystal system	triclinic
space group	<i>P</i> 1' (No. 2)
unit cell parameters ^a	
<i>a</i> (Å)	8.6519 (4)
<i>b</i> (Å)	8.9370 (4)
<i>c</i> (Å)	13.7359 (6)
α (deg)	82.1623 (5)
β (deg)	81.9087 (5)
γ (deg)	77.5942 (5)
<i>V</i> (Å ³)	1020.76 (8)
<i>Z</i>	2
ρ _{calcd} (g cm ⁻³)	1.381
μ (mm ⁻¹)	0.201

B. Data Collection and Refinement Conditions

diffractometer	Bruker PLATFORM/APEX II CCD ^b
radiation (λ [Å])	graphite-monochromated Mo Kα (0.71073)
temperature (°C)	-100
scan type	ω scans (0.3°) (20 s exposures)
data collection 2θ limit (deg)	53.14
total data collected	8307 (-10 ≤ <i>h</i> ≤ 10, -11 ≤ <i>k</i> ≤ 11, -17 ≤ <i>l</i> ≤ 17)
independent reflections	4226 (<i>R</i> _{int} = 0.0111)
number of observed reflections (<i>NO</i>)	3849 [<i>F</i> _o ² ≥ 2σ(<i>F</i> _o ²)]
structure solution method	direct methods (<i>SHELXD</i> ^c)
refinement method	full-matrix least-squares on <i>F</i> ² (<i>SHELXL-97</i> ^d)
absorption correction method	Gaussian integration (face-indexed)
range of transmission factors	0.9705–0.8865
data/restraints/parameters	4226 / 0 / 270
goodness-of-fit (<i>S</i>) ^e [all data]	1.052
final <i>R</i> indices ^f	
<i>R</i> ₁ [<i>F</i> _o ² ≥ 2σ(<i>F</i> _o ²)]	0.0324
<i>wR</i> ₂ [all data]	0.0897
largest difference peak and hole	0.301 and -0.399 e Å ⁻³

^aObtained from least-squares refinement of 9360 reflections with $4.70^\circ < 2\theta < 53.14^\circ$.

(continued)

Table I. Crystallographic Experimental Details (continued)

^bPrograms for diffractometer operation, data collection, data reduction and absorption correction were those supplied by Bruker.

^cSchneider, T. R.; Sheldrick, G. M. *Acta Crystallogr.* **2002**, *D58*, 1772-1779.

^dSheldrick, G. M. *Acta Crystallogr.* **2008**, *A64*, 112–122.

^e $S = [\sum w(F_o^2 - F_c^2)^2 / (n - p)]^{1/2}$ (n = number of data; p = number of parameters varied; $w = [\sigma^2(F_o^2) + (0.0456P)^2 + 0.3672P]^{-1}$ where $P = [\text{Max}(F_o^2, 0) + 2F_c^2]/3$).

^f $R_1 = \sum ||F_o| - |F_c|| / \sum |F_o|$; $wR_2 = [\sum w(F_o^2 - F_c^2)^2 / \sum w(F_o^4)]^{1/2}$.

Table II. Atomic Coordinates and Equivalent Isotropic Displacement Parameters

Atom	<i>x</i>	<i>y</i>	<i>z</i>	$U_{\text{eq}}, \text{\AA}^2$
S	0.58848(4)	0.26968(4)	0.33533(2)	0.02623(10)*
F	-0.14641(10)	0.27704(10)	0.82236(6)	0.0366(2)*
O1	0.05844(12)	0.02906(14)	0.88166(8)	0.0430(3)*
O2	-0.10521(11)	-0.12480(11)	0.85961(8)	0.0346(2)*
O3	0.66770(13)	0.38229(13)	0.36040(8)	0.0405(3)*
O4	0.57821(12)	0.25757(12)	0.23356(7)	0.0352(2)*
N1	-0.22049(12)	0.12233(12)	0.66622(7)	0.0214(2)*
N2	-0.32060(13)	0.10396(13)	0.60497(8)	0.0253(2)*
N3	-0.45721(13)	0.09291(13)	0.65849(8)	0.0254(2)*
N4	0.67933(13)	0.10271(14)	0.38248(9)	0.0276(2)*
H4NA	0.690(2)	0.105(2)	0.4449(14)	0.038(5)
H4NB	0.631(2)	0.029(2)	0.3737(13)	0.042(5)
C1	-0.29339(14)	0.12525(13)	0.76062(9)	0.0203(2)*
C2	-0.44545(14)	0.10510(14)	0.75452(9)	0.0221(2)*
C3	-0.58550(16)	0.10017(17)	0.83106(10)	0.0317(3)*
C4	-0.66436(18)	0.2593(2)	0.86411(12)	0.0416(4)*
C5	-0.5512(2)	0.36150(18)	0.87750(12)	0.0403(4)*
C6	-0.4378(2)	0.3037(2)	0.95530(12)	0.0431(4)*
C7	-0.31623(17)	0.15263(18)	0.94417(10)	0.0338(3)*
C8	-0.20960(15)	0.14287(15)	0.84553(9)	0.0249(3)*
C9	-0.06644(15)	0.01039(16)	0.86285(9)	0.0278(3)*
C10	0.01443(18)	-0.26110(19)	0.88843(13)	0.0423(4)*
C11	-0.0459(3)	-0.3995(2)	0.87290(15)	0.0562(5)*
C12	-0.06024(14)	0.14252(15)	0.62321(9)	0.0246(3)*
C13	-0.06568(15)	0.30216(15)	0.56587(11)	0.0295(3)*
C14	0.09360(15)	0.30912(14)	0.50556(10)	0.0253(3)*
C15	0.21720(16)	0.34473(15)	0.54703(9)	0.0264(3)*
C16	0.36649(15)	0.34111(15)	0.49330(9)	0.0250(3)*
C17	0.39220(14)	0.29927(14)	0.39760(9)	0.0235(3)*
C18	0.26892(16)	0.26758(15)	0.35372(10)	0.0273(3)*
C19	0.11991(16)	0.27359(15)	0.40809(10)	0.0279(3)*

Anisotropically-refined atoms are marked with an asterisk (*). The form of the anisotropic displacement parameter is: $\exp[-2\pi^2(h^2a^*U_{11} + k^2b^*U_{22} + l^2c^*U_{33} + 2klb^*c^*U_{23} + 2hla^*c^*U_{13} + 2hka^*b^*U_{12})]$.

Table III. Selected Interatomic Distances (Å)

Atom1	Atom2	Distance	Atom1	Atom2	Distance
S	O3	1.4347(10)	C3	C4	1.538(2)
S	O4	1.4332(10)	C4	C5	1.519(2)
S	N4	1.6247(12)	C5	C6	1.517(2)
S	C17	1.7735(12)	C6	C7	1.534(2)
F	C8	1.4023(15)	C7	C8	1.5298(18)
O1	C9	1.1957(16)	C8	C9	1.5390(18)
O2	C9	1.3293(17)	C10	C11	1.492(3)
O2	C10	1.4677(16)	C12	C13	1.5275(17)
N1	N2	1.3375(15)	C13	C14	1.5134(17)
N1	C1	1.3608(15)	C14	C15	1.3916(19)
N1	C12	1.4668(15)	C14	C19	1.3944(19)
N2	N3	1.3164(15)	C15	C16	1.3908(18)
N3	C2	1.3579(16)	C16	C17	1.3903(18)
C1	C2	1.3810(17)	C17	C18	1.3924(18)
C1	C8	1.4993(17)	C18	C19	1.3903(18)
C2	C3	1.4923(17)			

Table IV. Selected Interatomic Angles (deg)

Atom1	Atom2	Atom3	Angle	Atom1	Atom2	Atom3	Angle
O3	S	O4	119.82(6)	F	C8	C1	108.31(10)
O3	S	N4	106.71(7)	F	C8	C7	108.90(11)
O3	S	C17	108.36(6)	F	C8	C9	105.73(10)
O4	S	N4	107.27(6)	C1	C8	C7	114.12(11)
O4	S	C17	107.84(6)	C1	C8	C9	112.71(11)
N4	S	C17	106.06(6)	C7	C8	C9	106.69(10)
C9	O2	C10	115.60(11)	O1	C9	O2	125.83(13)
N2	N1	C1	110.82(10)	O1	C9	C8	123.54(13)
N2	N1	C12	117.82(10)	O2	C9	C8	110.52(10)
C1	N1	C12	131.29(10)	O2	C10	C11	107.31(13)
N1	N2	N3	107.41(10)	N1	C12	C13	110.82(10)
N2	N3	C2	109.38(10)	C12	C13	C14	109.80(10)
N1	C1	C2	104.45(10)	C13	C14	C15	121.00(12)
N1	C1	C8	122.71(11)	C13	C14	C19	119.85(12)
C2	C1	C8	132.82(11)	C15	C14	C19	119.10(12)
N3	C2	C1	107.94(11)	C14	C15	C16	120.74(12)
N3	C2	C3	120.45(11)	C15	C16	C17	119.27(12)
C1	C2	C3	131.58(12)	S	C17	C16	119.17(10)
C2	C3	C4	113.10(12)	S	C17	C18	119.72(10)
C3	C4	C5	115.81(12)	C16	C17	C18	120.87(11)
C4	C5	C6	117.48(14)	C17	C18	C19	119.04(12)
C5	C6	C7	118.65(12)	C14	C19	C18	120.89(12)
C6	C7	C8	116.27(13)				

Table V. Torsional Angles (deg)

Atom1	Atom2	Atom3	Atom4	Angle	Atom1	Atom2	Atom3	Atom4	Angle
O3	S	C17	C16	-37.94(12)	C2	C1	C8	C9	116.54(15)
O3	S	C17	C18	147.58(11)	N3	C2	C3	C4	-104.93(14)
O4	S	C17	C16	-169.02(10)	C1	C2	C3	C4	72.95(19)
O4	S	C17	C18	16.50(12)	C2	C3	C4	C5	-40.67(19)
N4	S	C17	C16	76.32(11)	C3	C4	C5	C6	-61.94(19)
N4	S	C17	C18	-98.16(11)	C4	C5	C6	C7	61.2(2)
C10	O2	C9	O1	4.3(2)	C5	C6	C7	C8	53.9(2)
C10	O2	C9	C8	-171.99(11)	C6	C7	C8	F	48.17(16)
C9	O2	C10	C11	-175.97(13)	C6	C7	C8	C1	-72.97(16)
C1	N1	N2	N3	-0.78(14)	C6	C7	C8	C9	161.86(12)
C12	N1	N2	N3	-178.08(10)	F	C8	C9	O1	20.01(17)
N2	N1	C1	C2	0.87(13)	F	C8	C9	O2	-163.62(10)
N2	N1	C1	C8	179.35(11)	C1	C8	C9	O1	138.15(13)
C12	N1	C1	C2	177.70(12)	C1	C8	C9	O2	-45.48(14)
C12	N1	C1	C8	-3.83(19)	C7	C8	C9	O1	-95.83(15)
N2	N1	C12	C13	72.79(14)	C7	C8	C9	O2	80.54(13)
C1	N1	C12	C13	-103.85(15)	N1	C12	C13	C14	-168.65(11)
N1	N2	N3	C2	0.35(13)	C12	C13	C14	C15	-85.42(15)
N2	N3	C2	C1	0.19(14)	C12	C13	C14	C19	92.04(14)
N2	N3	C2	C3	178.52(11)	C13	C14	C15	C16	175.77(11)
N1	C1	C2	N3	-0.64(13)	C19	C14	C15	C16	-1.71(19)
N1	C1	C2	C3	-178.71(13)	C13	C14	C19	C18	-175.00(12)
C8	C1	C2	N3	-178.89(12)	C15	C14	C19	C18	2.51(19)
C8	C1	C2	C3	3.0(2)	C14	C15	C16	C17	-0.89(19)
N1	C1	C8	F	55.17(15)	C15	C16	C17	S	-171.64(9)
N1	C1	C8	C7	176.64(11)	C15	C16	C17	C18	2.77(19)
N1	C1	C8	C9	-61.45(15)	S	C17	C18	C19	172.39(10)
C2	C1	C8	F	-126.84(14)	C16	C17	C18	C19	-1.99(19)
C2	C1	C8	C7	-5.4(2)	C17	C18	C19	C14	-0.68(19)

Table VI. Hydrogen-Bonded Interactions

D-H...A	D-H (Å)	H...A (Å)	D...A (Å)	∠D-H...A (deg)	Note
N4-H4NA...N2 ¹	0.878(18)	2.186(19)	3.0577(16)	171.4(16)	¹ At 1+x, y, z.
N4-H4NB...N3 ²	0.88(2)	2.16(2)	3.0138(16)	162.8(17)	² At x', y', 1-z.

Table VII. Anisotropic Displacement Parameters (U_{ij} , Å²)

Atom	U_{11}	U_{22}	U_{33}	U_{23}	U_{13}	U_{12}
S	0.02319(16)	0.03036(18)	0.02606(17)	-0.00473(13)	0.00266(12)	-0.00987(13)
F	0.0423(5)	0.0326(4)	0.0419(5)	-0.0022(4)	-0.0122(4)	-0.0188(4)
O1	0.0250(5)	0.0564(7)	0.0488(6)	0.0060(5)	-0.0121(5)	-0.0134(5)
O2	0.0265(5)	0.0303(5)	0.0454(6)	0.0019(4)	-0.0121(4)	-0.0007(4)
O3	0.0352(6)	0.0415(6)	0.0498(6)	-0.0133(5)	0.0074(5)	-0.0215(5)
O4	0.0350(5)	0.0445(6)	0.0245(5)	-0.0013(4)	0.0023(4)	-0.0095(4)
N1	0.0209(5)	0.0225(5)	0.0205(5)	0.0000(4)	-0.0017(4)	-0.0055(4)
N2	0.0266(5)	0.0283(6)	0.0219(5)	-0.0024(4)	-0.0037(4)	-0.0071(4)
N3	0.0244(5)	0.0275(6)	0.0256(5)	-0.0032(4)	-0.0043(4)	-0.0071(4)
N4	0.0219(5)	0.0339(6)	0.0280(6)	-0.0080(5)	-0.0035(4)	-0.0048(5)
C1	0.0213(6)	0.0192(6)	0.0196(5)	-0.0002(4)	-0.0019(4)	-0.0041(4)
C2	0.0219(6)	0.0215(6)	0.0235(6)	-0.0028(5)	-0.0028(5)	-0.0053(5)
C3	0.0239(6)	0.0413(8)	0.0319(7)	-0.0090(6)	0.0042(5)	-0.0123(6)
C4	0.0271(7)	0.0512(10)	0.0455(9)	-0.0196(7)	0.0017(6)	-0.0006(7)
C5	0.0440(9)	0.0314(8)	0.0422(8)	-0.0113(6)	-0.0029(7)	0.0025(6)
C6	0.0436(9)	0.0477(9)	0.0400(8)	-0.0216(7)	-0.0040(7)	-0.0033(7)
C7	0.0324(7)	0.0469(8)	0.0221(6)	-0.0069(6)	-0.0060(5)	-0.0045(6)
C8	0.0257(6)	0.0269(6)	0.0244(6)	-0.0012(5)	-0.0057(5)	-0.0093(5)
C9	0.0226(6)	0.0385(7)	0.0216(6)	0.0027(5)	-0.0033(5)	-0.0076(5)
C10	0.0303(7)	0.0389(8)	0.0497(9)	0.0069(7)	-0.0083(7)	0.0060(6)
C11	0.0680(12)	0.0380(9)	0.0575(11)	-0.0046(8)	-0.0207(9)	0.0087(8)
C12	0.0199(6)	0.0249(6)	0.0263(6)	0.0007(5)	0.0026(5)	-0.0044(5)
C13	0.0230(6)	0.0234(6)	0.0377(7)	0.0022(5)	0.0037(5)	-0.0032(5)
C14	0.0228(6)	0.0180(6)	0.0316(7)	0.0036(5)	0.0010(5)	-0.0027(5)
C15	0.0283(6)	0.0247(6)	0.0239(6)	-0.0007(5)	0.0003(5)	-0.0034(5)
C16	0.0241(6)	0.0238(6)	0.0273(6)	-0.0016(5)	-0.0036(5)	-0.0053(5)
C17	0.0216(6)	0.0216(6)	0.0257(6)	0.0003(5)	0.0006(5)	-0.0049(5)
C18	0.0271(6)	0.0284(7)	0.0267(6)	-0.0037(5)	-0.0026(5)	-0.0061(5)
C19	0.0237(6)	0.0269(7)	0.0340(7)	-0.0013(5)	-0.0050(5)	-0.0073(5)

The form of the anisotropic displacement parameter is:

$$\exp[-2\pi^2(h^2a^2U_{11} + k^2b^2U_{22} + l^2c^2U_{33} + 2klb*c*U_{23} + 2hla*c*U_{13} + 2hka*b*U_{12})]$$

Table VIII. Derived Atomic Coordinates and Displacement Parameters for

Hydrogen Atoms

Atom	<i>x</i>	<i>y</i>	<i>z</i>	$U_{\text{eq}}, \text{\AA}^2$
H3A	-0.5507	0.0296	0.8895	0.038
H3B	-0.6654	0.0577	0.8042	0.038
H4A	-0.7354	0.3147	0.8146	0.050
H4B	-0.7320	0.2438	0.9276	0.050
H5A	-0.4869	0.3799	0.8131	0.048
H5B	-0.6160	0.4624	0.8938	0.048
H6A	-0.5027	0.2916	1.0201	0.052
H6B	-0.3778	0.3855	0.9580	0.052
H7A	-0.2470	0.1359	0.9978	0.041
H7B	-0.3749	0.0670	0.9541	0.041
H10A	0.0302	-0.2643	0.9588	0.051
H10B	0.1176	-0.2580	0.8474	0.051
H11A	0.0330	-0.4928	0.8894	0.067
H11B	-0.0641	-0.3933	0.8035	0.067
H11C	-0.1461	-0.4031	0.9155	0.067
H12A	-0.0138	0.0627	0.5782	0.029
H12B	0.0089	0.1294	0.6766	0.029
H13A	-0.1504	0.3238	0.5214	0.035
H13B	-0.0908	0.3814	0.6126	0.035
H15	0.1994	0.3718	0.6128	0.032
H16	0.4500	0.3669	0.5217	0.030
H18	0.2864	0.2422	0.2876	0.033
H19	0.0349	0.2532	0.3784	0.033

References

1. Vederas, J. C., 2005 Alfred Bader Award Lecture: Diaminopimelate and lysine biosynthesis - An antimicrobial target in bacteria. *Can. J. Chem.* **2006**, *84* (10), 1197-1207.
2. Dairi, T.; Kuzuyama, T.; Nishiyama, M.; Fujii, I., Convergent strategies in biosynthesis. *Nat. Prod. Rep.* **2011**, *28* (6), 1054-1086.
3. Velasco, A. M.; Leguina, J. I.; Lazcano, A., Molecular evolution of the lysine biosynthetic pathways. *J. Mol. Evol.* **2002**, *55* (4), 445-459.
4. Schafer, S.; Paalme, T.; Vilu, R.; Fuchs, G., ¹³C-NMR study of acetate assimilation in *Thermoproteus neutrophilus*. *Eur. J. Biochem.* **1989**, *186* (3), 695-700.
5. Nishiyama, M.; Kukimoto, M.; Beppu, T.; Horinouchi, S., An operon encoding aspartokinase and purine phosphoribosyltransferase in *Thermus flavus*. *Microbiology* **1995**, *141*, 1211-1219.
6. Kosuge, T.; Hoshino, T., Lysine is synthesized through the alpha-aminoadipate pathway in *Thermus thermophilus*. *FEMS Microbiol. Lett.* **1998**, *169* (2), 361-367.
7. Sakai, H.; Vassylyeva, M. N.; Matsuura, T.; Sekine, S.-I.; Gotoh, K.; Nishiyama, M.; Terada, T.; Shirouzu, M.; Kuramitsu, S.; Vassylyev, D.; Yokoyama, S., Crystal structure of a lysine biosynthesis enzyme, lysX, from *Thermus thermophilus* HB8. *J. Mol. Biol.* **2003**, *332* (3), 729-740.

8. Nishida, H.; Nishiyama, M.; Kobashi, N.; Kosuge, T.; Hoshino, T.; Yamane, H., A prokaryotic gene cluster involved in synthesis of lysine through the amino adipate pathway: A key to the evolution of amino acid biosynthesis. *Genome Res.* **1999**, *9* (12), 1175-1183.
9. Miyazaki, J.; Kobashi, N.; Nishiyama, M.; Yamane, H., Functional and evolutionary relationship between arginine biosynthesis and prokaryotic lysine biosynthesis through alpha-amino adipate. *J. Bacteriol.* **2001**, *183* (17), 5067-5073.
10. Miyazaki, J.; Kobashi, N.; Fujii, T.; Nishiyama, M.; Yamane, H., Characterization of a lysK gene as an argE homolog in *Thermus thermophilus* HB27. *FEBS Lett.* **2002**, *512* (1-3), 269-274.
11. Jander, G.; Joshi, V., Recent progress in deciphering the biosynthesis of aspartate-derived amino acids in plants. *Mol. Plant* **2010**, *3* (1), 54-65.
12. Hutton, C. A.; Perugini, M. A.; Gerrard, J. A., Inhibition of lysine biosynthesis: an evolving antibiotic strategy. *Mol. Biosyst.* **2007**, *3* (7), 458-465.
13. Blickling, S.; Renner, C.; Laber, B.; Pohlenz, H. D.; Holak, T. A.; Huber, R., Reaction mechanism of *Escherichia coli* dihydrodipicolinate synthase investigated by X-ray crystallography and NMR spectroscopy. *Biochemistry* **1997**, *36* (1), 24-33.
14. Sundharadas, G.; Gilvarg, C., Biosynthesis of alpha, epsilon-diaminopimelic acid in *Bacillus megaterium*. *J. Biol. Chem.* **1967**, *242* (27), 3983-3984.

15. Scapin, G.; Blanchard, J. S., Enzymology of bacterial lysine biosynthesis. In *Advances in enzymology and related areas of molecular biology: Amino acid metabolism, Part A*, Purich, D. L., Ed. John Wiley & Sons, Inc.: Hoboken, NJ, USA, 1998; Vol. 72, pp 279-324.
16. Pillai, B.; Cherney, M. M.; Diaper, C. M.; Sutherland, A.; Blanchard, J. S.; Vederas, J. C.; James, M. N. G., Structural insights into stereochemical inversion by diaminopimelate epimerase: An antibacterial drug target. *Proc. Natl. Acad. Sci. U.S.A.* **2006**, *103* (23), 8668-8673.
17. Pillai, B.; Cherney, M.; Diaper, C. M.; Sutherland, A.; Blanchard, J. S.; Vederas, J. C.; James, M. N. G., Dynamics of catalysis revealed from the crystal structures of mutants of diaminopimelate epimerase. *Biochem. Biophys. Res. Commun.* **2007**, *363* (3), 547-553.
18. Gokulan, K.; Rupp, B.; Pavelka, M. S.; Jacobs, W. R.; Sacchettini, J. C., Crystal structure of *Mycobacterium tuberculosis* diaminopimelate decarboxylase, an essential enzyme in bacterial lysine biosynthesis. *J. Biol. Chem.* **2003**, *278* (20), 18588-18596.
19. Misono, H.; Togawa, H.; Yamamoto, T.; Soda, K., Occurrence of meso-alpha, epsilon-diaminopimelate dehydrogenase in *Bacillus sphaericus*. *Biochem. Biophys. Res. Commun.* **1976**, *72* (1), 89-93.
20. Misono, H.; Soda, K., Properties of meso-alpha,epsilon-diaminopimelate D-dehydrogenase from *Bacillus sphaericus*. *J. Biol. Chem.* **1980**, *255* (22), 10599-10605.

21. Misono, H.; Togawa, H.; Yamamoto, T.; Soda, K., Meso-alpha,epsilon-diaminopimelate D-dehydrogenase: Distribution and the reaction product. *J. Bacteriol.* **1978**, *137* (1), 22-27.
22. Chatterjee, S. P.; Singh, B. K.; Gilvarg, C., Biosynthesis of lysine in plants: The putative role of meso-diaminopimelate dehydrogenase. *Plant Mol. Biol.* **1994**, *26* (1), 285-290.
23. Hudson, A. O.; Gilvarg, C.; Leustek, T., Biochemical and phylogenetic characterization of a novel diaminopimelate biosynthesis pathway in prokaryotes identifies a diverged form of LL-diaminopimelate aminotransferase. *J. Bacteriol.* **2008**, *190* (9), 3256-3263.
24. Hudson, A. O.; Singh, B. K.; Leustek, T.; Gilvarg, C., An LL-diaminopimelate aminotransferase defines a novel variant of the lysine biosynthesis pathway in plants. *Plant Physiol.* **2006**, *140* (1), 292-301.
25. Watanabe, N.; James, M. N., Structural insights for the substrate recognition mechanism of LL-diaminopimelate aminotransferase. *Biochim. Biophys. Acta* **2011**, *1814* (11), 1528-1533.
26. Vogel, H. J., On biochemical evolution: Lysine formation in higher plants. *Proc. Natl. Acad. Sci. U.S.A.* **1959**, *45* (12), 1717-1721.
27. Glawischnig, E.; Gierl, A.; Tomas, A.; Bacher, A.; Eisenreich, W., Retrobiosynthetic nuclear magnetic resonance analysis of amino acid biosynthesis and intermediary metabolism. Metabolic flux in developing maize kernels. *Plant Physiol.* **2001**, *125* (3), 1178-1186.

28. Hudson, A. O.; Bless, C.; Macedo, P.; Chatterjee, S. P.; Singh, B. K.; Gilvarg, C.; Leustek, T., Biosynthesis of lysine in plants: evidence for a variant of the known bacterial pathways. *Biochim. Biophys. Acta* **2005**, *1721* (1-3), 27-36.
29. Bryan, J. K., Synthesis of the aspartate family and branched-chain amino acids. In *The Biochemistry of Plants* Mifflin, B. J.; Lea, P. J., Eds. Academic Press: New York, 1989; Vol. 5, pp 403-452.
30. Paris, S.; Viemon, C.; Curien, G.; Dumas, R., Mechanism of control of *Arabidopsis thaliana* Asp kinase-homoserine dehydrogenase by threonine. *J. Biol. Chem.* **2003**, *278* (7), 5361-5366.
31. Mazelis, M.; Whatley, F. R.; Whatley, J., The enzymology of lysine biosynthesis in higher plants. The occurrence, characterization and some regulatory properties of dihydrodipicolinate synthase. *FEBS Lett.* **1977**, *84* (2), 236-240.
32. Wallsgrove, R. M.; Mazelis, M., The enzymology of lysine biosynthesis in higher plants: Complete localization of the regulatory enzyme dihydrodipicolinate synthase in the chloroplasts of spinach leaves. *FEBS Lett.* **1980**, *116* (2), 189-192.
33. Tyagi, V. V. S.; Henke, R. R.; Farkas, W. R., Partial purification and characterization of dihydrodipicolinic acid reductase from maize. *Plant Physiol.* **1983**, *73* (3), 687-691.

34. Shimizu, H.; Shikanai, T., Dihydrodipicolinate reductase-like protein, CRR1, is essential for chloroplast NAD(P)H dehydrogenase in *Arabidopsis*. *Plant J.* **2007**, *52* (3), 539-547.
35. Tyagi, V. V. S.; Henke, R. R.; Farkas, W. R., Occurrence of diaminopimelic epimerase in maize. *Biochim. Biophys. Acta* **1982**, *719* (2), 363-369.
36. Shimura, Y.; Vogel, H. J., Diaminopimelate decarboxylase of *Lemna perpusilla*: Partial purification and some properties *Biochim. Biophys. Acta* **1966**, *118* (2), 396-404.
37. Mazelis, M.; Miflin, B. J.; Pratt, H. M., A chloroplast-localized diaminopimelate decarboxylase in higher plants. *FEBS Lett.* **1976**, *64* (1), 197-200.
38. Pillai, B.; Moorthie, V. A.; van Belkum, M. J.; Marcus, S. L.; Cherney, M. M.; Diaper, C. M.; Vederas, J. C.; James, M. N. G., Crystal structure of diaminopimelate epimerase from *Arabidopsis thaliana*, an amino acid racemase critical for L-lysine biosynthesis. *J. Mol. Biol.* **2009**, *385* (2), 580-594.
39. The Arabidopsis Genome Initiative, Analysis of the genome sequence of the flowering plant *Arabidopsis thaliana*. *Nature* **2000**, *408* (6814), 796-815.
40. Watanabe, N.; Cherney, M. M.; van Belkum, M. J.; Marcus, S. L.; Flegel, M. D.; Clay, M. D.; Deyholos, M. K.; Vederas, J. C.; James, M. N., Crystal structure of LL-diaminopimelate aminotransferase from

- Arabidopsis thaliana*: a recently discovered enzyme in the biosynthesis of L-lysine by plants and Chlamydia. *J. Mol. Biol.* **2007**, *371* (3), 685-702.
41. Martin, W.; Rujan, T.; Richly, E.; Hansen, A.; Cornelsen, S.; Lins, T.; Leister, D.; Stoebe, B.; Hasegawa, M.; Penny, D., Evolutionary analysis of *Arabidopsis*, cyanobacterial, and chloroplast genomes reveals plastid phylogeny and thousands of cyanobacterial genes in the nucleus. *Proc. Natl. Acad. Sci. U.S.A.* **2002**, *99* (19), 12246-12251.
42. McCoy, A. J.; Adams, N. E.; Hudson, A. O.; Gilvarg, C.; Leustek, T.; Maurelli, A. T., L,L-diaminopimelate aminotransferase, a trans-kingdom enzyme shared by *Chlamydia* and plants for synthesis of diaminopimelate/lysine. *Proc. Natl. Acad. Sci. U.S.A.* **2006**, *103* (47), 17909-17914.
43. Watanabe, N.; Clay, M. D.; van Belkum, M. J.; Fan, C.; Vederas, J. C.; James, M. N., The structure of LL-diaminopimelate aminotransferase from *Chlamydia trachomatis*: implications for its broad substrate specificity. *J. Mol. Biol.* **2011**, *411* (3), 649-660.
44. Liu, Y.; White, R. H.; Whitman, W. B., Methanococci use the diaminopimelate aminotransferase pathway for lysine biosynthesis. *J. Bacteriol.* **2010**, *192* (13), 3304-3310.
45. Hudson, A. O.; Klartag, A.; Gilvarg, C.; Dobson, R. C.; Marques, F. G.; Leustek, T., Dual diaminopimelate biosynthesis pathways in *Bacteroides fragilis* and *Clostridium thermocellum*. *Biochim. Biophys. Acta* **2011**, *1814* (9), 1162-1168.

46. Mazur, B.; Krebbers, E.; Tingey, S., Gene discovery and product development for grain quality traits. *Science* **1999**, *285* (5426), 372-375.
47. Peters, N. K.; Dixon, D. M.; Holland, S. M.; Fauci, A. S., The research agenda of the national institute of allergy and infectious diseases for antimicrobial resistance. *J. Infect. Dis.* **2008**, *197* (8), 1087-1093.
48. Mandavilli, A., Virtually incurable TB warns of impending disaster. *Nat. Med.* **2007**, *13* (3), 271-271.
49. Somani, J.; Bhullar, V. B.; Workowski, K. A.; Farshy, C. E.; Black, C. M., Multiple drug-resistant *Chlamydia trachomatis* associated with clinical treatment failure. *J. Infect. Dis.* **2000**, *181* (4), 1421-1427.
50. Manavi, K., A review on infection with *Chlamydia trachomatis*. *Best Pract. Res. Clin. Obstet. Gynaecol.* **2006**, *20* (6), 941-951.
51. Belland, R.; Ojcius, D. M.; Byrne, G. I., Disease watch - Focus - Chlamydia. *Nat. Rev. Microbiol.* **2004**, *2* (7), 530-531.
52. Fischbach, M. A.; Walsh, C. T., Antibiotics for emerging pathogens. *Science* **2009**, *325* (5944), 1089-1093.
53. Walsh, C. T., Where will new antibiotics come from? *Nat. Rev. Microbiol.* **2003**, *1* (1), 65-70.
54. Vollmer, W.; Blanot, D.; de Pedro, M. A., Peptidoglycan structure and architecture. *FEMS Microbiol. Rev.* **2008**, *32* (2), 149-167.
55. Vollmer, W.; Bertsche, U., Murein (peptidoglycan) structure, architecture and biosynthesis in *Escherichia coli*. *Biochim. Biophys. Acta* **2008**, *1778* (9), 1714-1734.

56. Cox, R. J.; Sutherland, A.; Vederas, J. C., Bacterial diaminopimelate metabolism as a target for antibiotic design. *Bioorg. Med. Chem.* **2000**, *8* (5), 843-871.
57. Gillner, D.; Armoush, N.; Holz, R. C.; Becker, D. P., Inhibitors of bacterial *N*-succinyl-L,L-diaminopimelic acid desuccinylase (DapE) and demonstration of in vitro antimicrobial activity. *Bioorg. Med. Chem. Lett.* **2009**, *19* (22), 6350-6352.
58. Boughton, B. A.; Dobson, R. C.; Gerrard, J. A.; Hutton, C. A., Conformationally constrained diketopimelic acid analogues as inhibitors of dihydrodipicolinate synthase. *Bioorg. Med. Chem. Lett.* **2008**, *18* (2), 460-463.
59. Boughton, B. A.; Griffin, M. D. W.; O'Donnell, P. A.; Dobson, R. C. J.; Perugini, M. A.; Gerrard, J. A.; Hutton, C. A., Irreversible inhibition of dihydrodipicolinate synthase by 4-oxo-heptenedioic acid analogues. *Bioorg. Med. Chem.* **2008**, *16* (23), 9975-9983.
60. Fan, C.; Clay, M. D.; Deyholos, M. K.; Vederas, J. C., Exploration of inhibitors for diaminopimelate aminotransferase. *Bioorg. Med. Chem.* **2010**, *18* (6), 2141-2151.
61. Kelland, J. G.; Arnold, L. D.; Palcic, M. M.; Pickard, M. A.; Vederas, J. C., Analogs of diaminopimelic acid as inhibitors of meso-diaminopimelate decarboxylase from *Bacillus sphaericus* and wheat germ. *J. Biol. Chem.* **1986**, *261* (28), 13216-13223.

62. Dobson, R. C.; Griffin, M. D.; Devenish, S. R.; Pearce, F. G.; Hutton, C. A.; Gerrard, J. A.; Jameson, G. B.; Perugini, M. A., Conserved main-chain peptide distortions: a proposed role for Ile203 in catalysis by dihydrodipicolinate synthase. *Protein Sci.* **2008**, *17* (12), 2080-2090.
63. Devenish, S. R.; Blunt, J. W.; Gerrard, J. A., NMR studies uncover alternate substrates for dihydrodipicolinate synthase and suggest that dihydrodipicolinate reductase is also a dehydratase. *J. Med. Chem.* **2010**, *53* (12), 4808-4812.
64. Turner, J. J.; Gerrard, J. A.; Hutton, C. A., Heterocyclic inhibitors of dihydrodipicolinate synthase are not competitive. *Bioorg. Med. Chem.* **2005**, *13* (6), 2133-2140.
65. Mitsakos, V.; Dobson, R. C.; Pearce, F. G.; Devenish, S. R.; Evans, G. L.; Burgess, B. R.; Perugini, M. A.; Gerrard, J. A.; Hutton, C. A., Inhibiting dihydrodipicolinate synthase across species: towards specificity for pathogens? *Bioorg. Med. Chem. Lett.* **2008**, *18* (2), 842-844.
66. Turner, J. J.; Healy, J. P.; Dobson, R. C.; Gerrard, J. A.; Hutton, C. A., Two new irreversible inhibitors of dihydrodipicolinate synthase: diethyl (*E,E*)-4-oxo-2,5-heptadienedioate and diethyl (*E*)-4-oxo-2-heptenedioate. *Bioorg. Med. Chem. Lett.* **2005**, *15* (4), 995-998.
67. Paiva, A. M.; Vanderwall, D. E.; Blanchard, J. S.; Kozarich, J. W.; Williamson, J. M.; Kelly, T. M., Inhibitors of dihydrodipicolinate reductase, a key enzyme of the diaminopimelate pathway of

- Mycobacterium tuberculosis*. *Biochim. Biophys. Acta* **2001**, *1545* (1-2), 67-77.
68. Janowski, R.; Kefala, G.; Weiss, M. S., The structure of dihydrodipicolinate reductase (DapB) from *Mycobacterium tuberculosis* in three crystal forms. *Acta Cryst. D* **2010**, *66* (Pt 1), 61-72.
69. Dommaraju, S.; Gorman, M. A.; Dogovski, C.; Pearce, F. G.; Gerrard, J. A.; Dobson, R. C.; Parker, M. W.; Perugini, M. A., Cloning, expression and crystallization of dihydrodipicolinate reductase from methicillin-resistant *Staphylococcus aureus*. *Acta Cryst. F* **2010**, *66* (Pt 1), 57-60.
70. Girilli, M.; Zheng, R.; Scapin, G.; Blanchard, J. S., The three-dimensional structures of the *Mycobacterium tuberculosis* dihydrodipicolinate reductase-NADH-2,6-PDC and NADPH-2,6-PDC complexes. structure and mutagenic analysis of relaxed nucleotide specificity. *Biochemistry* **2003**, *42* (36), 10644-10650.
71. Kefala, G.; Janowski, R.; Panjekar, S.; Mueller-Dieckmann, C.; Weiss, M. S., Cloning, expression, purification, crystallization and preliminary X-ray diffraction analysis of DapB from *M. tuberculosis*. *Acta Cryst. F* **2005**, *61* (Pt 7), 718-721.
72. Ge, X.; Wakim, B.; Sem, D. S., Chemical proteomics-based drug design: Target and antitarget fishing with a catechol-rhodanine privileged scaffold for NAD(P)(H) binding proteins. *J. Med. Chem.* **2008**, *51* (15), 4571-4580.

73. Sem, D. S.; Bertolaet, B.; Baker, B.; Chang, E.; Costache, A. D.; Coutts, S.; Dong, Q.; Hansen, M.; Hong, V.; Huang, X.; Jack, R. M.; Kho, R.; Lang, H.; Ma, C.-T.; Meininger, D.; Pellecchia, M.; Pierre, F.; Villar, H.; Yu, L., System-based design of bi-ligand inhibitors of oxidoreductases: Filling the chemical proteomic toolbox. *Chem. Biol.* **2004**, *11* (2), 185-194.
74. Ge, X.; Olson, A.; Cai, S.; Sem, D. S., Binding synergy and cooperativity in dihydrodipicolinate reductase: Implications for mechanism and the design of biligand inhibitors. *Biochemistry* **2008**, *47* (38), 9966-9980.
75. Schuldt, L.; Weyand, S.; Kefala, G.; Weiss, M. S., The three-dimensional structure of a Mycobacterial DapD provides insights into DapD diversity and reveals unexpected particulars about the enzymatic mechanism. *J. Mol. Biol.* **2009**, *389* (5), 863-879.
76. Nguyen, L.; Kozlov, G.; Gehring, K., Structure of *Escherichia coli* tetrahydrodipicolinate *N*-succinyltransferase reveals the role of a conserved C-terminal helix in cooperative substrate binding. *FEBS Lett.* **2008**, *582* (5), 623-626.
77. Weyand, S.; Kefala, G.; Weiss, M. S., The Three-dimensional structure of *N*-Succinyldiaminopimelate aminotransferase from *Mycobacterium tuberculosis*. *J. Mol. Biol.* **2007**, *367* (3), 825-838.
78. Berges, D. A.; DeWolf, W. E.; Dunn, G. L.; Newman, D. J.; Schmidt, S. J.; Taggart, J. J.; Gilvarg, C., Studies on the active site of succinyl-CoA: Tetrahydrodipicolinate *N*-succinyltransferase. Characterization using

- analogs of tetrahydrodipicolinate. *J. Biol. Chem.* **1986**, *261* (14), 6160-6167.
79. Beaman, T. W.; Blanchard, J. S.; Roderick, S. L., The conformational change and active site structure of tetrahydrodipicolinate *N*-succinyltransferase. *Biochemistry* **1998**, *37* (29), 10363-10369.
80. Beaman, T. W.; Vogel, K. W.; Drueckhammer, D. G.; Blanchard, J. S.; Roderick, S. L., Acyl group specificity at the active site of tetrahydrodipicolinate *N*-succinyltransferase. *Protein Sci.* **2002**, *11* (4), 974-979.
81. Cox, R. J.; Schouten, J. A.; Stentiford, R. A.; Wareing, K. J., Peptide inhibitors of *N*-succinyl diaminopimelic acid aminotransferase (DAP-AT): A novel class of antimicrobial compounds. *Bioorg. Med. Chem. Lett.* **1998**, *8* (8), 945-950.
82. Cox, R. J.; Wang, P. S. H., Synthesis and in vitro enzyme activity of aza, oxa and thia derivatives of bacterial cell wall biosynthesis intermediates. *J. Chem. Soc., Perkin Trans. I* **2001**, (17), 2022-2034.
83. Cox, R. J.; Sherwin, W. A.; Lam, L. K.; Vederas, J. C., Synthesis and evaluation of novel substrates and inhibitors of *N*-succinyl-LL-diaminopimelate-aminotransferase from *Escherichia coli*. *J. Am. Chem. Soc.* **1996**, *118* (32), 7449-7460.
84. Cox, R. J.; Jenkins, H.; Schouten, J. A.; Stentiford, R. A.; Wareing, K. J., Synthesis and in vitro enzyme activity of peptide derivatives of bacterial

- cell wall biosynthesis inhibitors. *J. Chem. Soc., Perkin Trans. 1* **2000**, (13), 2023-2036.
85. Born, T. L.; Zheng, R.; Blanchard, J. S., Hydrolysis of *N*-succinyl-L,L-diaminopimelic acid by the *Haemophilus influenzae* dapE-encoded desuccinylase: Metal activation, solvent isotope effects, and kinetic mechanism. *Biochemistry* **1998**, *37* (29), 10478-10487.
86. Meyers, R. S.; Siu, A., Pharmacotherapy review of chronic pediatric hypertension. *Clin. Ther.* **2011**, *33* (10), 1331-1356.
87. Walshe, J. M., The story of penicillamine: A difficult birth. *Mov. Disord.* **2003**, *18* (8), 853-859.
88. Gerhart, F.; Higgins, W.; Tardif, C.; Ducep, J.-B., 2-(4-amino-4-carboxybutyl)aziridine-2-carboxylic acid. A potent irreversible inhibitor of diaminopimelic acid epimerase. Spontaneous formation from alpha-(halomethyl)diaminopimelic acid. *J. Med. Chem.* **1990**, *33* (8), 2157-2162.
89. Cox, R. J.; Durston, J.; Roper, D., Synthesis and in vitro enzyme activity of an oxa analogue of azi-DAP. *J. Chem. Soc., Perkin Trans. 1* **2002**, (8), 1029-1035.
90. Diaper, C. M.; Sutherland, A.; Pillai, B.; James, M. N.; Semchuk, P.; Blanchard, J. S.; Vederas, J. C., The stereoselective synthesis of aziridine analogues of diaminopimelic acid (DAP) and their interaction with dap epimerase. *Org. Biomol. Chem.* **2005**, *3* (24), 4402-4411.
91. Gelb, M. H.; Lin, Y.; Pickard, M. A.; Song, Y.; Vederas, J. C., Synthesis of 3-fluorodiaminopimelic acid isomers as inhibitors of diaminopimelate

- epimerase: Stereocontrolled enzymatic elimination of hydrogen fluoride. *J. Am. Chem. Soc.* **1990**, *112* (12), 4932-4942.
92. Brunhuber, N. M. W.; Blanchard, J. S., The biochemistry and enzymology of amino acid dehydrogenase. *Crit. Rev. Biochem. Mol. Biol.* **1994**, *29* (6), 415-467.
93. Abbott, S. D.; Lane-Bell, P. M.; Sidhu, K. P. S.; Vederas, J. C., Synthesis and testing of heterocyclic analogues of diaminopimelic acid (DAP) as inhibitors of DAP dehydrogenase and DAP epimerase. *J. Am. Chem. Soc.* **1994**, *116* (15), 6513-6520.
94. Cirilli, M.; Zheng, R.; Scapin, G.; Blanchard, J. S., Structural symmetry: The three-dimensional structure of *Haemophilus influenzae* diaminopimelate epimerase. *Biochemistry* **1998**, *37* (47), 16452-16458.
95. Sutherland, A.; Caplan, J. F.; Vederas, J. C., Unsaturated alpha-aminopimelic acids as potent inhibitors of meso-diaminopimelic acid (DAP) D-dehydrogenase. *Chem. Commun.* **1999**, (6), 555-556.
96. Cirilli, M.; Scapin, G.; Sutherland, A.; Vederas, J. C.; Blanchard, J. S., The three-dimensional structure of the ternary complex of *Corynebacterium glutamicum* diaminopimelate dehydrogenase-NADPH-L-2-amino-6-methylene-pimelate. *Protein Sci.* **2000**, *9* (10), 2034-2037.
97. Caplan, J. F.; Zheng, R.; Blanchard, J. S.; Vederas, J. C., Vinylogous amide analogues of diaminopimelic acid (DAP) as inhibitors of enzymes involved in bacterial lysine biosynthesis. *Org. Lett.* **2000**, *2* (24), 3857-3860.

98. Lam, L. K.; Arnold, L. D.; Kalantar, T. H.; Kelland, J. G.; Lane-Bell, P. M.; Palcic, M. M.; Pickard, M. A.; Vederas, J. C., Analogs of diaminopimelic acid as inhibitors of meso-diaminopimelate dehydrogenase and LL-diaminopimelate epimerase. *J. Biol. Chem.* **1988**, *263* (24), 11814-11819.
99. Steger, M.; Young, D. W., Versatile synthesis of inhibitors of late enzymes in the bacterial pathway of lysine. *Tetrahedron* **1999**, *55* (25), 7935-7956.
100. Hutton, C. A.; Southwood, T. J.; Turner, J. J., Inhibitors of lysine biosynthesis as antibacterial agents. *Mini-Rev. Med. Chem.* **2003**, *3* (2), 115-127.
101. Kelland, J. G.; Palcic, M. M.; Pickard, M. A.; Vederas, J. C., Stereochemistry of lysine formation by meso-diaminopimelate decarboxylase from wheat germ: Use of ^1H - ^{13}C NMR shift correlation to detect stereospecific deuterium labeling. *Biochemistry* **1985**, *24* (13), 3263-3267.
102. Asada, Y.; Tanizawa, K.; Sawada, S.; Suzuki, T.; Misono, H.; Soda, K., Stereochemistry of meso-alpha,epsilon-diaminopimelate decarboxylase reaction: The first evidence for pyridoxal 5'-phosphate dependent decarboxylation with inversion of configuration. *Biochemistry* **1981**, *20* (24), 6881-6886.
103. Kefala, G.; Perry, L. J.; Weiss, M. S., Cloning, expression, purification, crystallization and preliminary X-ray diffraction analysis of LysA

- (Rv1293) from *Mycobacterium tuberculosis*. *Acta Cryst. F* **2005**, *61* (Pt 8), 782-784.
104. Tomioka, H., Development of new antituberculous agents based on new drug targets and structure-activity relationship. *Expert Opin. Drug Discov.* **2008**, *3* (1), 21-49.
105. Girodeau, J.-M.; Agouridas, C.; Masson, M.; Pineau, R.; Le Goffic, F., The lysine pathway as a target for a new genera of synthetic antibacterial antibiotics? *J. Med. Chem.* **1986**, *29* (6), 1023-1030.
106. Song, Y.; Niederer, D.; Lane-Bell, P. M.; Lam, L. K.; Crawley, S.; Palcic, M. M.; Pickard, M. A.; Pruess, D. L.; Vederas, J. C., Stereospecific synthesis of phosphonate analogs of diaminopimelic acid (DAP), their interaction with DAP enzymes, and antibacterial activity of peptide derivatives. *J. Org. Chem.* **1994**, *59* (19), 5784-5793.
107. Dobson, R. C.; Giron, I.; Hudson, A. O., L,L-diaminopimelate aminotransferase from *Chlamydomonas reinhardtii*: a target for algacide development. *PLoS One* **2011**, *6* (5), e20439, 20431-20413.
108. Kumar, R. A.; Clark, D. S., High-throughput screening of biocatalytic activity: Applications in drug discovery. *Curr. Opin. Chem. Biol.* **2006**, *10* (2), 162-168.
109. Eliot, A. C.; Kirsch, J. F., Pyridoxal phosphate enzymes: Mechanistic, structural, and evolutionary considerations. *Annu. Rev. Biochem.* **2004**, *73*, 383-415.

110. Schneider, G.; Kack, H.; Lindqvist, Y., The manifold of vitamin B6 dependent enzymes. *Structure* **2000**, *8* (1), R1-R6.
111. Dubnovitsky, A. P.; Ravelli, R. B. G.; Popov, A. N.; Papageorgiou, A. C., Strain relief at the active site of phosphoserine aminotransferase induced by radiation damage. *Protein Sci.* **2005**, *14* (6), 1498-1507.
112. Watanabe, N.; Clay, M. D.; van Belkum, M. J.; Cherney, M. M.; Vederas, J. C.; James, M. N., Mechanism of substrate recognition and PLP-induced conformational changes in LL-diaminopimelate aminotransferase from *Arabidopsis thaliana*. *J. Mol. Biol.* **2008**, *384* (5), 1314-1329.
113. Islam, M. M.; Goto, M.; Miyahara, I.; Ikushiro, H.; Hirotsu, K.; Hayashi, H., Binding of C5-dicarboxylic substrate to aspartate aminotransferase: Implications for the conformational change at the transaldimination step. *Biochemistry* **2005**, *44* (23), 8218-8229.
114. Jager, J.; Moser, M.; Sauder, U.; Jansonius, J. N., Crystal structures of *Escherichia coli* aspartate aminotransferase in two conformations: Comparison of an unliganded open and two liganded closed forms. *J. Mol. Biol.* **1994**, *239* (2), 285-305.
115. Malashkevich, V. N.; Strokopytov, B. V.; Borisov, V. V.; Dauter, Z.; Wilson, K. S.; Torchinsky, Y. M., Crystal structure of the closed-form of chicken cytosolic aspartate-aminotransferase at 1.9 angstrom resolution. *J. Mol. Biol.* **1995**, *247* (1), 111-124.
116. Okamoto, A.; Higuchi, T.; Hirotsu, K.; Kuramitsu, S.; Kagamiyama, H., X-ray crystallographic study of pyridoxal 5'-phosphate-type aspartate

- aminotransferases from *Escherichia coli* in open and closed-form. *J. Biochem.* **1994**, *116* (1), 95-107.
117. Dirksen, A.; Dirksen, S.; Hackeng, T. M.; Dawson, P. E., Nucleophilic catalysis of hydrazone formation and transamination: Implications for dynamic covalent chemistry. *J. Am. Chem. Soc.* **2006**, *128* (49), 15602-15603.
118. Dirksen, A.; Dawson, P. E., Rapid oxime and hydrazone ligations with aromatic aldehydes for biomolecular labeling. *Bioconj. Chem.* **2008**, *19* (12), 2543-2548.
119. Halder, M. K.; Scott, M. D.; Sule, N.; Srivastava, D. K.; Mallik, S., Synthesis of barbiturate-based methionine aminopeptidase-1 inhibitors. *Bioorg. Med. Chem. Lett.* **2008**, *18* (7), 2373-2376.
120. Mula, M., Anticonvulsants - antidepressants pharmacokinetic drug interactions: the role of the CYP450 system in psychopharmacology. *Curr. Drug Metab.* **2008**, *9* (8), 730-737.
121. Schneider, T. R.; Karcher, J.; Pohl, E.; Lubini, P.; Sheldrick, G. M., Ab initio structure determination of the lantibiotic mersacidin. *Acta Cryst. D* **2000**, *56* (Pt 6), 705-713.
122. Li, P.; Rogers, T.; Smiley, D.; DiMarchi, R. D.; Zhang, F., Design, synthesis and crystallization of a novel glucagon analog as a therapeutic agent. *Acta Cryst. F* **2007**, *63* (Pt 7), 599-601.
123. Nar, H.; Schmid, A.; Puder, C.; Potterat, O., High-resolution crystal structure of a lasso peptide. *ChemMedChem* **2010**, *5* (10), 1689-1692.

124. Lay, F. T.; Mills, G. D.; Hulett, M. D.; Kvansakul, M., Crystallization and preliminary X-ray crystallographic analysis of the plant defensin NaD1. *Acta Cryst. F* **2012**, *68* (Pt 1), 85-88.
125. Pentelute, B.; Gates, Z. P.; Tereshko, V.; Dashnau, J. L.; Vanderkooi, J. M.; Kossiakoff, A. A.; Kent, S. B. H., X-ray structure of snow flea antifreeze protein determined by racemic crystallization of synthetic protein enantiomers. *J. Am. Chem. Soc.* **2008**, *130* (30), 9695-9701.
126. Mandal, K.; Pentelute, B.; Tereshko, V.; Kossiakoff, A. A.; Kent, S. B. H., X-ray structure of native scorpion toxin BmBKTx1 by racemic protein crystallography using direct methods. *J. Am. Chem. Soc.* **2009**, *131* (4), 1362-1363.
127. Mandal, K.; Pentelute, B.; Terada, T.; Thammavongsa, V.; Schneewind, O.; Kossiakoff, A. A.; Kent, S. B. H., Racemic crystallography of synthetic protein enantiomers used to determine the X-ray structure of plectasin by direct methods. *Protein Sci.* **2009**, *18* (6), 1146-1154.
128. Pentelute, B.; Mandal, K.; Gates, Z. P.; Sawaya, M. R.; Yeates, T. O.; Kent, S. B. H., Total chemical synthesis and X-ray structure of kaliotoxin by racemic protein crystallography. *Chem. Commun.* **2010**, *46* (43), 8174-8176.
129. Wukovitz, S. W.; Yeates, T. O., Why protein crystals favor some space groups over others. *Nat. Struct. Biol.* **1995**, *2* (12), 1062-1067.
130. Matthews, B. W., Racemic crystallography-Easy crystals and easy structures: What's not to like? *Protein Sci.* **2009**, *18* (6), 1135-1138.

131. Vigers, G. P. A.; Dripps, D. J.; Edwards III, C. K.; Brandhuber, B. J., X-ray crystal structure of a small antagonist peptide bound to interleukin-1 receptor type 1. *J. Biol. Chem.* **2000**, *275* (47), 36927-36933.
132. Aaron, J. A.; Chambers, J. M.; Jude, K. M.; Costanzo, L. D.; Dmochowski, I. J.; Christianson, D. W., Structure of a (129)Xe-cryptophane biosensor complexed with human carbonic anhydrase II. *J. Am. Chem. Soc.* **2008**, *130* (22), 6942-6943.
133. Chambers, J. M.; Hill, P. A.; Aaron, J. A.; Han, Z.; Christianson, D. W.; Kuzma, N. N.; Dmochowski, I. J., Cryptophane xenon-129 nuclear magnetic resonance biosensors targeting human carbonic anhydrase. *J. Am. Chem. Soc.* **2009**, *131* (2), 563-569.
134. Brotin, T.; Dutasta, J.-P., Cryptophanes and their complexes-present and future. *Chem. Rev.* **2009**, *109* (1), 88-130.
135. Babasaki, K.; Takao, T.; Shimonishi, Y.; Kurahashi, K., Subtilisin A, a new antibiotic peptide produced by *Bacillus subtilis* 168: Isolation, structural analysis, and biogenesis *J. Biochem.* **1985**, *98* (3), 585-603.
136. Stein, T.; Dusterhus, S.; Stroh, A.; Entian, K.-D., Subtilisin production by two *Bacillus subtilis* subspecies and variance of the sbo-alb cluster. *Appl. Environ. Microbiol.* **2004**, *70* (4), 2349-2353.
137. Sutyak, K. E.; Wirawan, R. E.; Aroutcheva, A. A.; Chikindas, M. L., Isolation of the *Bacillus subtilis* antimicrobial peptide subtilisin from the dairy product-derived *Bacillus amyloliquefaciens*. *J. Appl. Microbiol.* **2008**, *104* (4), 1067-1074.

138. Marx, R.; Stein, T.; Entian, K.-D.; Glaser, S. J., Structure of the *Bacillus subtilis* peptide antibiotic subtilosin A determined by ¹H-NMR and matrix assisted laser desorption/ionization time-of-flight mass spectrometry. *J. Protein Chem.* **2001**, *20* (6), 501-506.
139. Kawulka, K.; Sprules, T.; McKay, R. T.; Mercier, P.; Diaper, C. M.; Zuber, P.; Vederas, J. C., Structure of subtilosin A, an antimicrobial peptide from *Bacillus subtilis* with unusual posttranslational modifications linking cysteine sulfurs to alpha-carbons of phenylalanine and threonine. *J. Am. Chem. Soc.* **2003**, *125* (16), 4726-4727.
140. Kawulka, K.; Sprules, T.; Diaper, C. M.; Whittal, R. M.; McKay, R. T.; Mercier, P.; Zuber, P.; Vederas, J. C., Structure of subtilosin A, a cyclic antimicrobial peptide from *Bacillus subtilis* with unusual sulfur to alpha-carbon cross-links: Formation and reduction of alpha-thio-alpha-amino acid derivatives. *Biochemistry* **2004**, *43* (12), 3385-3395.
141. Shelburne, C. E.; An, F. Y.; Dholpe, V.; Ramamoorthy, A.; Lopatin, D. E.; Lantz, M. S., The spectrum of antimicrobial activity of the bacteriocin subtilosin A. *J. Antimicrob. Chemother.* **2007**, *59* (2), 297-300.
142. Riley, M. A.; Wertz, J. E., Bacteriocins: Evolution, ecology, and application. *Annu. Rev. Microbiol.* **2002**, *56*, 117-137.
143. Riley, M. A.; Wertz, J. E., Bacteriocin diversity: Ecological and evolutionary perspectives. *Biochimie* **2002**, *84* (5-6), 357-364.
144. Klaenhammer, T. R., Bacteriocins of lactic acid bacteria. *Biochimie* **1988**, *70* (3), 337-349.

145. Lohans, C. T.; Vederas, J. C., Development of class IIa bacteriocins as therapeutic agents. *Int. J. Microbiol.* **2012**, *2012*, DOI: 10.1155/2012/386410.
146. Cotter, P. D.; Hill, C.; Ross, R. P., Bacteriocins: Developing innate immunity for food. *Nat. Rev. Microbiol.* **2005**, *3* (10), 777-788.
147. Klaenhammer, T. R., Genetics of bacteriocins produced by lactic acid bacteria. *FEMS Microbiol. Rev.* **1993**, *12* (1-3), 39-86.
148. van Belkum, M. J.; Martin-Visscher, L. A.; Vederas, J. C., Structure and genetics of circular bacteriocins. *Trends Microbiol.* **2011**, *19* (8), 411-418.
149. Lee, H.; Kim, H.-Y., Lantibiotics, class I bacteriocins from the genus *Bacillus*. *J. Microbiol. Biotechnol.* **2011**, *21* (3), 229-235.
150. Al-Mahrous, M. M.; Upton, M., Discovery and development of lantibiotics; antimicrobial agents that have significant potential for medical application. *Expert Opin. Drug Discov.* **2011**, *6* (2), 155-170.
151. Ross, A. C.; Vederas, J. C., Fundamental functionality: Recent developments in understanding the structure–activity relationships of lantibiotic peptides. *J. Antibiot.* **2011**, *64* (1), 27-34.
152. Mattick, A. T. R.; Hirsch, A. A., A powerful inhibitory substance produced by group N streptococci. *Nature* **1944**, *154* (3913), 551-551.
153. Chatterjee, S. P.; Chatterjee, D. K.; Jani, R. H.; Blumbach, J.; Ganguli, B. N., Mersacidin, a new antibiotic from *Bacillus*. In vitro and in vivo antibacterial activity. *J. Antibiot.* **1992**, *45* (6), 839-845.

154. Henderson, J. T.; Chopko, A. L.; van Wassenaar, P. D., Purification and primary structure of pediocin PA-1 produced by *Pediococcus acidilactici* PAC-1. *Arch. Biochem. Biophys.* **1992**, *295* (1), 5-12.
155. Nissen-Meyer, J.; Holo, H.; Havarstein, L. S.; Sletten, K.; Nes, I. F., A novel lactococcal bacteriocin whose activity depends on the complementary action of two peptides. *J. Bacteriol.* **1992**, *174* (17), 5686-5692.
156. Schindler, C. A.; Schuhardt, V. T., Lysostaphin: A new bacteriolytic agent for the *Staphylococcus*. *Proc. Natl. Acad. Sci. U.S.A.* **1964**, *51* (3), 414-421.
157. Walker, E. S.; Levy, F., Genetic trends in a population evolving antibiotic resistance. *Evolution* **2001**, *55* (6), 1110-1122.
158. Zheng, G.; Slavik, M. F., Isolation, partial purification and characterization of a bacteriocin produced by a newly isolated *Bacillus subtilis* strain. *Lett. Appl. Microbiol.* **1999**, *28* (5), 363-367.
159. Zheng, G.; Yan, L. Z.; Vederas, J. C.; Zuber, P., Genes of the sbo-alb locus of *Bacillus subtilis* are required for production of the antilisterial bacteriocin subtilisin. *J. Bacteriol.* **1999**, *181* (23), 7346-7355.
160. Sailer, M.; Helms, G. L.; Henkel, T.; Niemczura, W. P.; Stiles, M. E.; Vederas, J. C., Nitrogen-15- and carbon-13-labeled media from *Anabaena* sp. for universal isotopic labeling of bacteriocins: NMR resonance assignments of leucocin A from *Leuconostoc gelidum* and nisin A from *Lactococcus lactis*. *Biochemistry* **1993**, *32* (1), 310-318.

161. Rea, M. C.; Sit, C. S.; Clayton, E.; O'Connor, P. M.; Whittall, R. M.; Zheng, J.; Vederas, J. C.; Ross, R. P.; Hill, C., Thuricin CD, a posttranslationally modified bacteriocin with a narrow spectrum of activity against *Clostridium difficile*. *Proc. Natl. Acad. Sci. U.S.A.* **2010**, *107* (20), 9352-9357.
162. Sit, C. S.; McKay, R. T.; Hill, C.; Ross, R. P.; Vederas, J. C., The 3D structure of thuricin CD, a two-component bacteriocin with cysteine sulfur to α -carbon cross-links. *J. Am. Chem. Soc.* **2011**, *133* (20), 7680-7683.
163. Sit, C. S.; van Belkum, M. J.; McKay, R. T.; Worobo, R. W.; Vederas, J. C., The 3D solution structure of thurincin H, a bacteriocin with four sulfur to alpha-carbon crosslinks. *Angew. Chem. Int. Ed.* **2011**, *50* (37), 8718-8721.
164. Brunger, A. T.; Adams, P. D.; Clore, G. M.; DeLano, W. L.; Gros, P.; Grosse-Kunstleve, R. W.; Jiang, J. S.; Kuszewski, J.; Nilges, M.; Pannu, N. S.; Read, R. J.; Rice, L. M.; Simonson, T.; Warren, G. L., Crystallography & NMR system: A new software suite for macromolecular structure determination. *Acta Cryst. D* **1998**, *54* (Pt 5), 905-921.
165. Fleming, A., On a remarkable bacteriolytic element found in tissues and secretions. *Proc. R. Soc. London, Ser. B* **1922**, *93* (653), 306-317.
166. Blake, C. C. F.; Koenig, D. F.; Mair, G. A.; North, A. C. T.; Phillips, D. C.; Sarma, V. R., Structure of hen egg-white lysozyme. A three-

- dimensional Fourier synthesis at 2 Angstrom resolution. *Nature* **1965**, 206 (4986), 757-761.
167. Johnson, L. N.; Phillips, D. C., Structure of some crystalline lysozyme-inhibitor complexes determined by X-ray analysis at 6 Angstrom resolution. *Nature* **1965**, 206 (4986), 761-763.
168. Vollan, V. B.; Hough, E.; Karlsen, S., Structural studies on the binding of 4-methylumbelliferone glycosides of chitin to rainbow trout lysozyme. *Acta Cryst. D* **1999**, 55 (Pt 1), 60-66.
169. O'Brien, M.; Colwell, R. R., A rapid test for chitinase activity that uses 4-methylumbelliferyl-*N*-acetyl-beta-D-glucosaminide. *Appl. Environ. Microbiol.* **1987**, 53 (7), 1718-1720.
170. Hood, M. A., Comparison of four methods for measuring chitinase activity and the application of the 4-MUF assay in aquatic environments. *J. Microbiol. Methods* **1991**, 13 (2), 151-160.
171. Huisgen, R., 1,3-Dipolar cycloadditions: past and future. *Angew. Chem. Int. Ed.* **1963**, 2 (10), 565-632.
172. Huisgen, R., Kinetics and mechanism of 1,3-dipolar cycloadditions. *Angew. Chem. Int. Ed.* **1963**, 2 (11), 633-696.
173. Tornøe, C. W.; Christensen, C.; Meldal, M., Peptidotriazoles on solid phase: [1,2,3]-triazoles by regioselective copper(I)-catalyzed 1,3-dipolar cycloadditions of terminal alkynes to azides. *J. Org. Chem.* **2002**, 67 (9), 3057-3064.

174. Rostovtsev, V. V.; Green, L. G.; Fokin, V. V.; Sharpless, K. B., A stepwise Huisgen cycloaddition process: copper(I)-catalyzed regioselective "ligation" of azides and terminal alkynes. *Angew. Chem. Int. Ed.* **2002**, *41* (14), 2596.
175. Carpino, L. A.; El-Faham, A., Tetramethylfluoroformamidinium hexafluorophosphate: A rapid-acting peptide coupling reagent for solution and solid phase peptide synthesis. *J. Am. Chem. Soc.* **1995**, *117* (19), 5401-5402.
176. Thennarasu, S.; Lee, D.-K.; Poon, A.; Kawulka, K.; Vederas, J. C.; Ramamoorthy, A., Membrane permeabilization, orientation, and antimicrobial mechanism of subtilisin A. *Chem. Phys. Lipids* **2005**, *137* (1-2), 38-51.
177. Tanaka, T.; Nagai, H.; Noguchi, M.; Kobayashi, A.; Shoda, S.-I., One-step conversion of unprotected sugars to β -glycosyl azides using 2-chloroimidazolium salt in aqueous solution. *Chem. Commun.* **2009**, *23*, 3378-3379.
178. Goddard-Borger, E. D.; Stick, R. V., An efficient, inexpensive, and shelf-stable diazotransfer reagent: imidazole-1-sulfonyl azide hydrochloride. *Org. Lett.* **2007**, *9* (19), 3797-3800.
179. Agard, N. J.; Prescher, J. A.; Bertozzi, C. R., A strain-promoted [3 + 2] azide-alkyne cycloaddition for covalent modification of biomolecules in living systems. *J. Am. Chem. Soc.* **2004**, *126* (46), 15046-15047.

180. Baskin, J. M.; Prescher, J. A.; Laughlin, S. T.; Agard, N. J.; Chang, P. V.; Miller, I. A.; Lo, A.; Codelli, J. A.; Bertozzi, C. R., Copper-free click chemistry for dynamic in vivo imaging. *Proc. Natl. Acad. Sci. U.S.A.* **2007**, *104* (43), 16793-16797.
181. Schultz, M. K.; Parameswarappa, S. G.; Pigge, F. C., Synthesis of a DOTA-biotin conjugate for radionuclide chelation via Cu-free click chemistry. *Org. Lett.* **2010**, *12* (10), 2398-2401.
182. Codelli, J. A.; Baskin, J. M.; Agard, N. J.; Bertozzi, C. R., Second-generation difluorinated cyclooctynes for copper-free click chemistry. *J. Am. Chem. Soc.* **2008**, *130* (34), 11486-11493.
183. Pocker, Y.; Stone, J. T., The catalytic versatility of erythrocyte carbonic anhydrase III. Kinetic studies of the enzyme-catalyzed hydrolysis of *p*-nitrophenyl acetate. *Biochemistry* **1967**, *6* (3), 668-678.
184. Wilkinson, B. L.; Bornaghi, L. F.; Houston, T. A.; Innocenti, A.; Vullo, D.; Supuran, C. T.; Poulsen, S.-A., Carbonic anhydrase inhibitors: inhibition of isozymes I, II, and IX with triazole-linked o-glycosides of benzenesulfonamide. *J. Med. Chem.* **2007**, *50* (7), 1651-1657.
185. Pacchiano, F.; Aggarwal, M.; Avvaru, B. S.; Robbins, A. H.; Scozzafava, A.; McKenna, R.; Supuran, C. T., Selective hydrophobic pocket binding observed within the carbonic anhydrase II active site accommodate different 4-substituted-ureido-benzenesulfonamides and correlate to inhibitor potency. *Chem. Commun.* **2010**, *46* (44), 8371-8373.

186. DeRuiter, J.; Borne, R. F.; Mayfield, C. A., N- and 2-substituted N-(phenylsulfonyl)glycines as inhibitors of rat lens aldose reductase. *J. Med. Chem.* **1989**, *32* (1), 145-151.
187. Richards, I. C.; Wright, B. J.; Parsons, J. H.; Baillie, A. C. Derivatives of 4-fluoroanthranilic acid, their use as fungicides and pesticides, and their preparation. EP 360417 A2, Mar 28, 1990.
188. Comess, K. M.; Erickson, S. A.; Henkin, J.; Kalvin, D. M.; Kawai, M.; H., K. K.; Bamaung, N. Y.; Park, C. H.; Sheppard, G. S.; Vasudevan, A.; Wang, J.; Barnes, D. M.; Fidanze, S. D.; Kolaczowski, L.; Mantei, R. A.; Park, D. C.; Sanders, W. J.; Tedrow, J. S.; Wang, G. T. Preparation of sulfonamides having antiangiogenic and anticancer activity. US 20040167128 A1 Aug 26, 2004.
189. Hunziker, F.; Fischer, R.; Kipfer, P.; Schmutz, J.; Buerki, H. R.; Eichenberger, E.; White, T. G., Seven-membered heterocycles. 28. Neuroleptic piperazinyl derivatives of 10H-thieno[3,2-c][1]benzazepines and 4H-thieno[2,3-c][1]benzazepines. *Eur. J. Med. Chem.* **1981**, *16* (5), 391-398.
190. Khodair, A. I., A convenient synthesis of 2-arylidene-5H-thiazolo[2,3-b]quinazoline-3,5[2H]-diones and their benzoquinazoline derivatives. *J. Heterocyclic Chem.* **2002**, *39* (6), 1153-1160.
191. Brown, F. C.; Bradsher, C. K.; Bond, S. M., Mildew-preventing activity of rhodanine derivatives. Some 5-arylidene derivatives. *Ind. Eng. Chem.* **1953**, *45* (5), 1030-1033.

192. Campaigne, E.; Cline, R. E., preparation and absorption spectra of some beta-aryl-alpha-mercaptoacrylic acids and related disulfides. *J. Org. Chem.* **1956**, *21* (1), 32-38.
193. Allan, F. J.; Allan, G. G.; Thomson, J. B., The condensation of rhodanine with aromatic dialdehydes and some related compounds. *Can. J. Chem.* **1958**, *36* (11), 1579-1583.
194. Behringer, H.; Dillinger, E.; Suter, H.; Kohl, K., Syntheses with vinylogous acid halides. III. Substituted 5-methylenerhodanines from 5-chloromethylenerhodanines. *Chem. Ber.* **1958**, *91* (12), 2773-2783.
195. Powers, J. P.; Piper, D. E.; Li, Y.; Mayorga, V.; Anzola, J.; Chen, J. M.; Jaen, J. C.; Lee, G.; Liu, J.; Peterson, M. G.; Tonn, G. R.; Ye, Q.; Walker, N. P. C.; Wang, Z., SAR and mode of action of novel non-nucleoside inhibitors of hepatitis C NS5b RNA polymerase. *J. Med. Chem.* **2006**, *49* (3), 1034-1046.
196. Allan, F. J.; Allan, G. G.; Crank, G., Fungitoxicity of rhodanine derivatives. *J. Appl. Chem.* **1961**, *11* (2), 68-70.
197. Allan, F. J.; Allan, G. G.; Thomson, J. B., The condensation of rhodanine and derivatives with pyridine and quinoline aldehyde. *Recl. Trav. Chim. Pays-Bas* **1961**, *80* (4), 403-408.
198. Brown, F. C.; Bradsher, C. K.; F., M. B.; Forrester, S., Structure and antimicrobial activity of the 3-aminorhodanines. *J. Org. Chem.* **1959**, *24* (8), 1056-1060.

199. Ueda, H.; Uhta, M., Sulfur-containing heterocyclic compounds. V. 3-Aminorhodanine derivatives. *Nippon Kagaku Zasshi* **1956**, 77 (10), 1520-1525.
200. Moree, W. J.; van Gent, L. C.; van der Marel, G. A.; Liskamp, R. M. J., Synthesis of peptides containing a sulfinamide or a sulfonamide transition-state isostere. *Tetrahedron* **1993**, 49 (5), 1133-1150.
201. Hong, S. Y.; Tobias, G.; Ballesteros, B.; Oualid, F. E.; Errey, J. C.; Doores, K. J.; Kirkland, A. I.; Nellist, P. D.; Green, M. L. H.; Davis, B. G., Atomic-scale detection of organic molecules coupled to single-walled carbon nanotubes. *J. Am. Chem. Soc.* **2007**, 129 (36), 10966-10967.
202. Krapcho, A. P.; Diamanti, J.; Cayen, C.; Bingham, R., 2-Carboxycyclooctanone. *Org. Synth.* **1967**, 47, 20.
203. Pacchiano, F.; Carta, F.; Vullo, D.; Scozzafava, A.; Supuran, C. T., Inhibition of beta-carbonic anhydrases with ureido-substituted benzenesulfonamides. *Bioorg. Med. Chem. Lett.* **2011**, 21 (1), 102-105.
204. Gassman, P. G.; Gruetzmacher, G., ortho-Alkylation of anilines. Ethyl 4-amino-3-methylbenzoate. *Org. Synth.* **1977**, 56, 15-18.
205. Rodriguez, J. M.; Hamilton, A. D., Benzoylurea oligomers: synthetic foldamers that mimic extended α -helices. *Angew. Chem. Int. Ed.* **2007**, 46 (45), 8614-8617.